

DISCOVERY OF APPROVED DRUGS WITH POSSIBLE MULTI-TARGET INHIBITORY ACTIVITIES AGAINST SCHISTOSOMA SPECIES

BY

**FORTUNATUS CHIDOLUE EZEBUO
(201465D7001F)**

**A DISSERTATION SUBMITTED TO THE FACULTY OF
PHARMACEUTICAL SCIENCES, NNAMDI AZIKIWE UNIVERSITY,
AWKA, IN PARTIAL FULFILLMENT OF THE REQUIREMENTS FOR
THE DEGREE OF DOCTOR OF PHILOSOPHY (PhD) IN
PHARMACEUTICAL AND MEDICINAL CHEMISTRY**

AUGUST, 2018

CERTIFICATION

I **FORTUNATUS CHIDOLUE EZEBUO**, a doctoral student with research interest in Computational Chemistry and Drug Design in Department of Pharmaceutical and Medicinal Chemistry, Faculty of Pharmaceutical Sciences, Nnamdi Azikiwe University, Awka with Registration Number **201465D7001F**, hereby certify that the work embodied herein is original and has not been submitted in part or full for any other Diploma or Degree of this or other University.

.....
Fortunatus C. Ezebuo

.....
Date

APPROVAL

The title **discovery of approved drugs with possible multi-target inhibitory activities against schistosoma species** has been approved for **Fortunatus Chidolue Ezebuo**, a doctoral student, with Registration Number **201465D7001F**, of the Department of Pharmaceutical and Medicinal Chemistry, Faculty of Pharmaceutical Sciences, Nnamdi Azikiwe University, Awka.

Prof. Ikemefuna C. Uzochukwu
Supervisor

.....
Date

Dr. Festus B. C Okoye
Head of Department

.....
Date

Prof. Ikemefuna C. Uzochukwu
Dean, Faculty of Pharmaceutical Sciences
Nnamdi Azikiwe University, Awka

.....
Date

Prof. Cyril O. Usifoh
External Examiner

.....
Date

Prof. H. I. Odimegwu
Dean, School of Postgraduate Studies
Nnamdi Azikiwe University, Awka

.....
Date

DEDICATION

This work is dedicated to God Almighty, whose strength and grace made it possible for me to complete this research work.

ACKNOWLEDGEMENT

My unquantifiable gratitude goes to my supervisor and Dean of the Faculty of Pharmaceutical Sciences, Nnamdi Azikiwe University Awka, Professor Ikemefuna Chijioke Uzochukwu who led me through this work. Your encouragements to take part in international workshops, schools and conferences cannot be forgotten. I also appreciate Dr. Chika Abba and Demian N. Abba who made efforts and introduced me to Professor Ikemefuna Chijioke Uzochukwu. I greatly appreciate Dr. Festus B.C Okoye, the Head of Department of Pharmaceutical and Medicinal Chemistry to which I belong. Again, I thank Dr. Kenneth Ngwoke; Dr Obinna Ekwunife; Dr Angus Oli, Dr. C.P Ihekwereme; Dr Ebere Okoye and all the staff and management of Dpartment of Pharmaceutical and Medicinal Chemistry including that of Faculty of Pharmaceutical Sciences.

I also thank Dr. Amos O. Abolaji of Department of Biochemisrty, College of Medicine, University of Ibadan, for basic training on fly biology and provision of *Drosophila melanogaster* (Harwich strain) used in carrying out part of this work. I am also indepted to DrosAfrica for providing more training on use of *D. melanogaster* for research through the funding of International Center for Genetic Engineering and Biotechnology (ICGEB), The Company of Biologist and Cambridge-Africa Alborada Research fund. I want to also thank International Center for Theoretical Physics, Trieste, Italy and Sharif University of Technology, Tehran, Iran for travel grant and support to participate as a PhD student in 5th Workshop on Advanced Techniques for Scientific Programming and Management of Open source Software Packages". Again, I want to thank International Center for Theoretical Physics, Trieste, Italy for travel grant to participate as a PhD student in 'Winter School on Quantitative Systems Biology'. This research was supported in part by the International Centre for Theoretical Sciences (ICTS) during a visit for participating in the program - Winter School on Quantitative Systems Biology (Code: ICTS/Prog-qsb2017/12).

I am very grateful to Dr. Colin B. Lukong, Dr. Jonathan C. Ifemeje and Irene N. Okafor of Department of Biochemistry, Faculty of Natural Sciences, Chukwuemeka Odumegwu Ojukwu University, for encouragements, moral and financial supports. I am also indepted to Dr. Chinwe K Okolie for financial support that led to the success of this work.

I cannot forget Ernest C. Orji; Dr. Arinze Agube; Augustine C. Onyema, and Maxwell C. Onuoha your efforts and encouragements led to the success of this work.

Fortunatus C. Ezebuo

Abstract

Schistosomiasis is a prevalent neglected tropical disease especially in northern Nigeria with high morbidity and mortality. It has shown low activity and resistance in its treatment using praziquantel or oxamniquine. It is important to identify alternative, additional or adjunctive drugs to ensure that praziquantel or oxamniquine resistance does not become a major health concern. Drugs that modulate more than one drug targets are less prone to problem of drug resistance. The aim of the research was to identify approved drugs with possible multi-target inhibitory activities against Schistosoma species. To achieve the aim, the study was designed to: (a) identify schistosoma drug targets using bioinformatic mining; (b) determine binding energies of selected approved drugs against schistosoma drug targets; (c) perform molecular dynamics simulations of targets and target-frontrunner complexes; (d) determine conservation of schistosomal drug targets and human liver enzymes in *Drosophila melanogaster*; (e) determine longevity and survival rates of *D. melanogaster* to some of the predicted drugs. Four schistosomal drug targets were obtained through bioinformatics mining. Six hundred and twelve (612) approved drugs including their isomers were selected based on their Molinspiration® bioscore similarities with reference compounds (praziquantel, oxamniquine, auranofin and propylamino-3-hydroxy-buta-1,4-dionyl]-isoleucylproline). The 3-D coordinates of the selected drugs were obtained from ZINC® database. The drug targets and approved drugs were prepared for docking simulations using Molecular Graphics Laboratory Tools-1.5.6 and University of California San Francisco (UCSF) Chimera 1.9. Molecular docking simulations were performed using AutoDockvina®-1.1.2 while molecular dynamics simulations were performed with GROMACS-4.5.5. The binding energies were calculated from the molecular docking simulations and using g_MMPBSA (Molecular Mechanics Poisson-Boltzmann Surface Area). Conservation of selected drug targets and three human liver enzymes (alkaline phosphatase, alanine aminotransferase and aspartate aminotransferase) in *D. melanogaster* were determined using BLAST search in FlyBase. The use of *D. melanogaster* as a model organism for antischistosomiasis was investigated by studying their longevity and survival rates as percentage of live flies when treated with three identified possible inhibitors. Tolmetin was predicted as potential multi-target antischistosomal drug with binding energies of -231.064 ± 18.55 and -338.636 ± 36.90 KJ/mol for sulfotransferase and thioredoxin glutathione reductase (TGR) respectively. Also diflunisal was predicted as potential multi-target antischistosomal drug with binding energies of -168.641 ± 20.37 and -290.117 ± 43.80 KJ/mol for sulfotransferase and TGR respectively. Schistosomal glutathione s-transferase and sulfotransferase are not conserved in *D. melanogaster*. Also, human liver alkaline phosphatase, alanine aminotransferase and aspartate aminotransferase are conserved in *D. melanogaster*. Longevity and survival rate experiments using *D. melanogaster* showed 100 % survival of the flies in praziquantel, oxytetracycline, haloperidol or vildagliptin within one week of administration. Molecular docking and dynamics simulations indicated that tolmetin and diflunisal are possible inhibitors of schistosomal sulfotransferase and thioredoxin glutathione reductase. Longevity and survival rate experiments using *D. melanogaster* indicate that praziquantel, oxytetracycline, haloperidol or vildagliptin are safe for the flies within one week of administration. Determination of conservation showed that *D. melanogaster* can be used for schistosomiasis studies.

TABLE OF CONTENT

Title page	i
Certification	ii
Approval	iii
Dedication	iv
Acknowledgement	v
Abstract	vi
Table of content	vii
List of tables	xii
List of figures	xiii
List of appendices	xvii
List of abbreviations	xix
Operational definition of terms	xxi
CHAPTER ONE	1
1.0 INTRODUCTION	1
1.1 Background of the study	1
1.2 Problem Statement	2
1.3 Aim	3
1.4 Research objectives	3
1.5 Research hypotheses	4
1.6 Scope of study	4
1.7 Significance of study	4

CHAPTER TWO	6
2.0 LITERATURE REVIEW	6
2.1 Review of empirical studies	6
2.2 Signs and Symptoms of schistosomiasis	6
2.3 Morphological features of schistosome	7
2.4 Diagnosis of schistosomiasis	8
2.5 Treatment of Schistosomiasis	9
2.6 Epidemiology of schistosomiasis infection	12
2.7 Prevalence of schistosomiasis in Africa	13
2.8 Transmission and risk factors for infection	14
2.9 Life-cycle of schistosome	15
2.10 Drug design/discovery	17
2.10.1 Computer aided drug design	18
2.10.2 Homology modeling	19
2.10.3 Molecular docking simulation	20
2.10.4 Molecular dynamics simulation	20
2.10.5 Drug repurposing	22
2.11 Schistosome molecular targets for drug discovery	25
2.11.1 Thioredoxin glutathione reductase	25
2.11.2 Sulfotransferase	26
2.11.3 Glutathione s-transferase	27

2.12 Multi-target therapeutics	27
2.13 Preclinical validation of drug candidates	29
2.13.1 <i>Drosophila</i> as a drug-discovery ‘tool’	30
2.14 Summary of literature review	32
CHAPTER THREE	33
3.0 MATERIALS AND METHODS	33
3.1 Materials	33
3.2 Methods	34
3.2.1 Study site	34
3.2.2 Experimental design	34
3.2.3 <i>In silico</i> investigations	36
3.2.3.1 Creation of in-house database of approved drugs	36
3.2.3.2 Bioinformatics mining of schistosome drug targets	36
3.2.3.3 Examination of selected schistosomal drug targets for missing residues	37
3.2.3.4 Homology modeling of missing residues in sulfotransferase	37
3.2.3.5 Selection of approved drugs using reference compounds	38
3.2.3.6 Validation of molecular docking simulation protocols	39
3.2.3.7 Preparation of selected receptors and approved drugs	40
3.2.3.8 Molecular docking simulations	40
3.2.3.9 Molecular dynamics simulations	40
3.2.3.10 Calculation of binding energy	42
3.2.3.11 <i>Determination of conservation of schistosoma drug targets ...</i>	43

3.2.4 Longevity and survival rate assays using <i>Drosophila melanogaster</i>	43
3.2.4.1 <i>Drosophila melanogaster</i> stock and culture	44
3.2.4.2 Preparation of drosophila feed	44
3.2.4.3 Preparation of doses of tested drugs	44
3.2.4.4 Drug exposure and percentage survival rate analyses	46
3.2.5 Statistical analysis	46
CHAPTER FOUR	48
4.0 RESULTS AND DISCUSSION	48
4.1 Results for selection of schistosome drug targets	48
4.1.1 Results for examination of targets for missing residues	52
4.1.2 Results of homology modeling of missing residues in sulfotransferase	52
4.1.3 Results for selection of approved drugs	54
4.1.4 Results of validation of docking simulation protocols	54
4.1.5 Results of molecular docking simulations	57
4.1.6 Results of molecular dynamics simulations	60
4.1.6.1 Molecular dynamics preparation results	60
4.1.6.2 Energy minimization results	60
4.1.6.3 Positions restrain dynamics results	60
4.1.6.4 Production run results	64
4.1.6.5 Binding energy computation results	123
4.1.7 Molecular descriptors and bioactivities of some predicted drugs	128
4.1.8 Results on conservation of targets and human liver enzymes in drosophila	130
4.1.8.1 Results on conservation of schistosomal targets in drosophila	130
4.1.8.2 Results on conservation of human liver enzymes in drosophila	133

4.1.9 Results on Survival rate and longevity of <i>D. melanogaster</i> in some of the drugs	136
4.1.9.1 Survival and longevity of <i>D. melanogaster</i> on PZQ-treated food	136
4.1.9.2 Survival and longevity of <i>D. melanogaster</i> on oxytetracycline-treated food	139
4.1.9.3 Survival and longevity of <i>D. melanogaster</i> on haloperidol- treated food	142
4.1.9.4 Survival and longevity of <i>D. melanogaster</i> on vildagliptin- treated food	145
4.1.10 Discussions	148
CHAPTER FIVE	159
5.0 SUMMARY, CONCLUSION AND RECOMMENDATION	159
5.1 Summary of findings	159
5.2 Conclusion	160
5.3 Recommendations for further research	161
5.4 Contribution to knowledge	162
5.5 Limitations of the study	162
References	163
Appendices	178

LIST OF TABLES

Table 4.1: Bioinformatic mining of five schistosomal targets	49
Table 4.2: Druggability index and druggable pockets of five schistosomal targets	50
Table 4.3: Summary of schistosomal thioredoxin gluthathione reductase blast search against human proteins	51
Table 4.4: Frontrunners with concurrent Binding affinities for two targets	58
Table 4.5: Binding energies between schistosomal drug targets and some approved drugs	124
Table 4.6: Molecular descriptors and bioactivities of some predicted antischistosomal drugs	129

LIST OF FIGURES

Figure 2.1: Map of the current global distribution of schistosomiasis	13
Figure 2.2: Life cycle of <i>S. mansoni</i> , <i>Sjaponicum</i> and <i>S. hematobium</i>	16
Figure 2.3: Laboratory life cycle of s. mansoni, illustrating the collection points for in vitro chemotherapeutic studies	17
Figure 2.4: Schematic chart of computer aided drug design	19
Figure 2.5: A comparison of traditional de novo drug discovery and development versus drug repositioning	24
Figure 3.1: Experimental design	35
Figure 4.1: Structural alignment of modeled schistosomal sulfotransferase	53
Figure 4.2: Selected approved drugs with activities in the neighborhood reference compounds	55
Figure 4.3: Validation of docking protocols of reference compounds receptor interactions	56
Figure 4.4: Binding Site analysis of the frontrunners	59
Figure 4.5: Solvated and ionized target-fronrunner complex simulation system	61
Figure 4.6: Energy minimization of the molecular systems	62
Figure 4.7: Position restrained molecular dynamics of the molecular systems	63
Figure 4.8: C-alpha root mean square deviation of schistosomal targets	66
Figure 4.9: Root mean square deviation of the ligands	67

Figure 4.10: Total energy of the MD simulated systems	68
Figure 4.11: Radius of gyration of the simulated targets presence of ligands	70
Figure 4.12: Radius of gyration of the ligands	71
Figure 4.13: Root mean square fluctuation of targets in presence of ligands	73
Figure 4.14: Some amino acids associated with reduction in loop flexibility	74
Figure 4.15a: Secondary structure changes in sulfotransferase observed during the 3000 ps MD simulation 1	76
Figure 4.15b: Secondary structure changes in sulfotransferase observed during the 3000 ps MD simulation 2	78
Figure 4.16a: Secondary structure changes in thioredoxin glutathione reductase observed during the 3000 ps MD simulation 1	80
Figure 4.16b: Secondary structure changes in thioredoxin glutathione reductase observed during the 3000 ps MD simulation 2	82
Figure 4.17: The polar contacts/hydrogen bond formation in protein-ligand complex at 0 ps of MD simulation	84
Figure 4.18: The polar contacts/hydrogen bond formation in protein-ligand complex at 480 ps of MD simulation	86
Figure 4.19: The polar contacts/hydrogen bond formation in sulfotransferase-ligand complex at 2800 ps of MD simulation	88
Figure 4.20 Amino acids in sulfotransferase that interacts with the ligands from the MD simulation	89
Figure 4.21: The polar contacts/hydrogen bond formation in thioredoxin glutathione reductase-ligand complex at 0 ps of MD simulation	93
Figure 4.22: The polar contacts/hydrogen bond formation in	

thioredoxin glutathione reductase-ligand complex at 480 ps of MD simulation	97
Figure 4.23: The polar contacts/hydrogen bond formation in thioredoxin glutathione reductase-ligand complex at 2800 ps of MD simulation	100
Figure 4.24 Amino acids in thioredoxin glutathione reductase that interacts with the ligands from the MD simulation	101
Figure 4.25: Distance of hydrogen bonds sulfotransferase-ligand complexes during MD simulations	103
Figure 4.26: The three-dimensional structure of schistosomal thioredoxin glutathione reductase showing the three binding sites for ligands	105
Figure 4.27: Distance of hydrogen bonds at site 1 in ligand bound thioredoxin glutatathione reductase complexes during MD simulations	107
Figure 4.28: Distance of hydrogen bonds at site 2 in ligand bound thioredoxin glutatathione reductase complexes during MD simulations	109
Figure 4.29: Distance of hydrogen bonds at site 3 in ligand bound thioredoxin glutatathione reductase complexes during MD simulations	111
Figure 4.30: Minimum distance between FAD and frontrunners	112
Figure 4.31: Conformational sampling of free and fronrunner bound sulfotransferase and thioredoxin glutathione reductase	114
Figure 4.32: Amino acids remodeling/readjustment due to ligand and sulfotransferase interactions.	116
Figure 4.33: Conformational changes due to ligand and sulfotransferase interactions	117
Figure 4.34: Amino acids remodeling/readjustment due to ligand and thioredoxin glutathione reductase interactions	119
Figure 4.35: Conformational changes due to ligand and thioredoxin glutathione reductase interactions	120
Figure 4.36: Accessible Surface Areas of free and fronrunner	

bound sulfotransferase and thioredoxin glutathione reductase interactions	122
Figure 4.37: Binding energies and their amino acid residues contribution	125
Figure 4.38: Polar and non-polar energies involved in sulfotransferase-fronrunner and thioredoxin glutathione reductase-fronrunner interactions	127
Figure 4.39: Molecular targets (1GTB and 4MUB) of schistosome that are not conserved in <i>drosophila melanogaster</i>	131
Figure 4.40: Molecular targets (3H4K and 3QSD) of schistosome that are conserved in <i>Drosophila melanogaster</i>	132
Figure 4.41: Liver biomarkers (3WZF and 2GLQ) of humans are conserved in <i>Drosophila melanogaster</i> .	134
Figure 4.42: Liver Biomarkers (5F9S) of human is conserved in <i>Drosophila melanogaster</i>	135
Figure 4.43: Survival of male and female <i>D. melanogaster</i> presence of different doses of praziquantel	137
Figure 4.44: Praziquantel reduced survival rates of <i>Drosophila melanogaster</i>	138
Figure 4.45: Survival of male and female <i>D. melanogaster</i> in presence of different doses of oxytetracycline	140
Figure 4.46: Oxytetracycline increased survival rates of <i>Drosophila melanogaster</i>	141
Figure 4.47: Survival of male and female <i>D. melanogaster</i> presence of different doses of haloperidol	143
Figure 4.48: Haloperidol increased survival rates of <i>Drosophila melanogaster</i>	144
Figure 4.49: Survival of male and female <i>D. melanogaster</i> presence of different doses of vildagliptin	146
Figure 4.50: Vildagliptin increased survival rates of <i>Drosophila melanogaster</i>	147

LIST OF APPENDICES

Appendix 1: Morphological features of schistosome	178
Appendix 2: Drugs approved for new indications after being subjected to drug repurposing	179
Appendix 3: Information on drugs used for survival and longevity experiments on <i>D. melanogaster</i>	180
Appendix 4: Configuration files and script used for the validation of docking protocol and the docking simulation	181
Appendix 5: ATB codes for the topologies of drugs used for MD simulation	182
Appendix 6: basic steps in the MD simulations and the molecular dynamics parameter files used	182
Appendix 7: Doses of the drugs used for survival and longevity experiments and their preparations	188
Appendix 8: Administration of the drugs to the <i>Drosophila melanogaster</i>	189
Appendix 9 : Druggability index, Pockets and descriptors schistosome targets	189
Appendix 10: BLAST search results of the schistosome targets against humans	195
Appendix 11: selected drugs with different reference compounds used the molecular docking simulations	203
Appendix 12: amino acids at the binding sites of the docked and wet lab	

experimental complexes	214
------------------------	-----

Appendix 13: Predicted drugs from molecular docking simulations with their binding affinities and previous indications	215
---	-----

Appendix 14: Values of RMSD and Radius of gyration from molecular dynamics simulation	222
--	-----

Appendix 15: Values of total energy from the molecular dynamics simulations	222
---	-----

Appendix 16: Changes in the secondary of sulfotransferase and thioredoxin glutathione reductase due to interaction with the ligands	223
--	-----

Appendix 17: Average bond distances of atoms in the amino acids and atoms in the ligands that show direct interaction	224
--	-----

Appendix 18: Minimum distance of the drugs/frontrunners at different sites from FAD in 3H4K	233
--	-----

Appendix 19: Different conformations of 4mub from the molecular dynamics simulation and their percentages	234
--	-----

Appendix 20: Total, hydrophobic and hydrophilic accessible surface areas of 3H4K and 4MUB	236
--	-----

Appendix 21: Accepted/presented conference/workshop papers from the dissertation	237
--	-----

Appendix 22: Efforts to obtain schistosome	240
--	-----

LIST OF ABBREVIATIONS

GROMACS	Groningen machine for chemical simulation
B3LYP	Becke 3-parameter, Lee-Yang-Parr
PDB	Protein DataBank
VMD	Visual molecular dynamics
MD	Molecular dynamics
FDA	Food and drug administration
FAD	Falvin adinine dinucleotide
PZQ	Praxiqantel
OXA	Oxamniquine
DIF	Diflunisal
DIN	Dinesterol
AUR	Auranofin
OXY	Oxytetracycline
HAL	Haloperidol
VIL	Vildagliptin
GPX	Glutathione peroxidase
TGR	Thioredoxin glutathione reductase
GST	Glutathione s-transferase
SOD	Superoxide dismutase
ALT	Alanine amino transferase
AST	Aspartate amino transferase
SBDD	Structure based drug design
GPCR	G-protein coupled receptor
ICM	Ion channel modulator

PI	Protease inhibitor
RMSF	Root mean square fluctuations
RMSD	Root mean square deviations
Rg	Radius of gyration

OPERATIONAL DEFINITION OF TERMS

Target(s): It is used to refer to sulfotransferase, thioredoxin glutathione reductase, glutathione s-transferase and/or cathepsin B1

Ligand(s): It is used to refer to selected drugs especially praziquantel, oxamnique, auranofin, diflunisal, tolmetin and/or dinesterol

Reference compound: It is used to refer to compounds/drugs used for selecting other drugs for example praziquantel, oxamnique, auranofin

Frontrunner: It means all the selected drugs that showed higher binding affinity than the reference compound

Drug repurposing: Finding new indication for existing/approved drugs

Molecular dynamics: This means movement of molecule.

CHAPTER ONE

1.0 INTRODUCTION

Schistosomiasis is one of the neglected tropical diseases. It is caused by flatworm and occurs mostly in the developing countries. The disease is transmitted through water and children are mostly affected. The treatment for the disease relies on use of one drug known as praziquantel (PZQ). Another drug that could be used to treat the disease is oxamniquine (OXA) and is not readily available in Africa. Other drugs like lucanthone, hycanthone have used in the past but they showed serious side-effects. There are reported cases of treatment failures of schistosomiasis with praziquantel or oxamniquine due to resistance or tolerance (Ismail, 1999; Valentim *et al.*, 2013; da Silva *et al.*, 2017). Drugs bring their pharmacological action by inhibiting drug target(s) and many drugs can inhibit one drug target. Disease like schistosomiasis can be better treated with drugs that can inhibit more than one drug targets and this can help solve the problem of drug resistance (Zimmermann *et al.*, 2007). Discovery of drugs including multi-target drugs can be achieved through computer-aided approach. Different animal models can be used during drug discovery/development process and *Drosophila melanogaster* can serve as non-rodent model for drug testing (Perrimon *et al.*, 2007; Pandey and Nichols, 2011). It is therefore important to identify alternative, drugs especially multi-target drugs to ensure that PZQ and OXA resistance does not become a major health concern. This can be achieved computer-aided and drug repurposing approaches.

1.1 Background of the study

Human schistosomiasis (or synonymously bilharzia) is a family of diseases caused primarily by three major species of the genus Schistosoma of flatworms, *Schistosoma mansoni* and

Schistosoma japonicum that cause intestinal schistosomiasis and *Schistosoma haematobium* that causes urinary schistosomiasis (Chiyaka *et al.*, 2010; Prast-Nielsen *et al.*, 2011; de Moraes, 2012). These infections are transmitted by freshwater snails and humans get infected when they interact with the habitats of these snails. All schistosoma infections follow direct contact with freshwater-harbouring cercariae. Three major factors are responsible for maintaining the transmission of the infection: (1) contamination of fresh water with excreta containing schistosome eggs, (2) the presence of the snail intermediate hosts, and (3) human contact with water-infested with cercariae. Contact with contaminated freshwater, poor sanitation and hygiene are the major risk factor of infection (Grimes *et al.*, 2015). Children, in particular, with their high infection levels, indiscriminate habits of excretion and predilection for playing in water, are very important in propagating the disease (Chiyaka *et al.*, 2010).

Symptoms of schistosomiasis are caused by the body's reaction to the worms' eggs, not by the worms themselves. Intestinal schistosomiasis can result in abdominal pain, diarrhoea, and blood in the stool. The classic sign of urogenital schistosomiasis is haematuria (blood in urine). Fibrosis of the bladder and ureter, and kidney damage are sometimes diagnosed in advanced cases. The economic and health effects of schistosomiasis are considerable. In children, schistosomiasis can cause anaemia, stunting and a reduced ability to learn, although the effects are usually reversible with treatment.

New drugs to treat schistosomiasis are urgently needed because only treatment with a monotherapy (praziquantel - PZQ) is used and effective vaccines are not available (Trainor-Moss and Mutapi, 2016). Oxamniquine (OXA) has an excellent safety record and it is extremely effective against *S. mansoni*, but it is no longer used because unlike PZQ, OXA is ineffective against *Schistosoma haematobium* and *Schistosoma japonicum* (Cioli *et al.*, 1995; Doenhoff *et al.*, 2008; da Silva *et al.*, 2017). Hycanthone, a drug related to OXA, is active against *S. mansoni*, *S.*

haemtobium and inactive against *S. japonicum*, but its unfavorable hepatotoxicity profile precludes use as a therapeutic agent.

Drug ‘repurposing’ is the identification of new therapeutic purposes for already approved drugs and is more affordable and achievable than novel drug discovery (Pessetto *et al.*, 2013). Drug repurposing can provide new therapeutic options for a vast number of diseases where current therapies are failing or are inadequate (Roder and Thomson, 2015). Trainor-Moss and Mutapi (2016) reported that there are no schistosome drug candidates under human clinical trials. The lack of schistosome drugs in the clinical trial pipeline is also of concern and is representative of the drug discovery/development landscape for helminth parasites in general. Drugs or combination of drugs that impact multiple targets simultaneously are better at controlling complex disease systems, less prone to drug resistance and are the standard of care in many important therapeutic areas (Zimmermann *et al.*, 2007).

1.2 Problem Statement

Availability of genomes of three main schistosomiasis agents have shifted traditional drug discovery model from serendipitous testing of compounds to use of knowledge-based approaches (Mafud *et al.*, 2016). Studies have reported computational prediction of schistosome drug targets (Caffrey *et al.*, 2009) and antischistosomal lead compounds (Liu *et al.*, 2013) but no innovative drug have been submitted to relevant clinical trials (Mafud *et al.*, 2016). Praziquantel (PZQ) is the first-line drug chosen for the treatment of schistosomiasis according to the World Health Organization (WHO) treatment guideline (da Silva *et al.*, 2017). Long-term use of PZQ results in decreased efficiency and serious concerns regarding onset of resistance (Greenberg, 2005). Low cure rates of schistosomiasis with PZQ has been reported in Northern Senegal (Greenberg, 2005). Also, *in vitro* and animal studies have demonstrated resistance to PZQ (Ismail, 1999). Given the wide clinical use of PZQ, drug-resistant parasites of clinical concern may evolve. Praziquantel has some problems such as low solubility issues, several side effects, bitter taste

and resistance (da Silva *et al.*, 2017). Again, it is effective against adults of all species of schistosoma but not against the young forms and the reason is still unknown (da Silva *et al.*, 2017). New derivatives of PZQ and oxamniquine (OXA) have not shown significant activity than PZQ or OXA (da Silva *et al.*, 2017). In fact, PZQ and OXA have limitations such as low activity on immature worms of *S. mansoni* and failure of treatment due to resistance or tolerance (da Silva *et al.*, 2017). PZQ's position as the only drug for mass treatment in contemporary African control programmes and the fact that it never achieves 100% cure rates may make it vulnerable. Other drugs are available for the treatment of schistosomiasis, but they are less effective, show unacceptable side effects and/or effective only on one schistosome species (Doenhoff *et al.*, 2008; Prast-Nielsen *et al.*, 2011; da Silva *et al.*, 2017). Trainor-Moss and Mutapi, (2016) reported that there are no new drug candidates under human clinical trials for the treatment of schistosomiasis. It is therefore important to identify alternative, additional or adjunctive drugs to ensure that PZQ and OXA resistance does not become a major health concern. This can be achieved with drug repurposing approaches.

1.3 Aim: The aim of the research is to identify approved drugs with possible multi-target inhibitory activities against schistosoma species.

1.4 Research objectives: To achieve the aim, the study was designed to achieve the following objectives:

- (a) To identify schitosoma druggable target(s) using bioinformatic mining
- (b) To determine binding affinities of selected approved drugs against schitosoma drug targets using molecular docking simulations.
- (c) To perform molecular dynamics simulations of targets and targets-frontrunner complexes
- (d) To determine the conservation of schistosomal drug targets and human liver enzymes in *D. melanogaster*

(e) To determine longevity and survival rates of *D. melanogaster* to some of the predicted drugs.

1.5 Research hypotheses

Following the aim of the research, two research hypotheses (Hypothesis one and two) below were formulated to guide the study.

Hypothesis one (HO): Approved drugs do not have drugs with possible multi-target inhibitory activities against schistosoma species.

Hypothesis two (H1): Approved drugs have drugs with possible multi-target inhibitory activities against schistosoma species.

1.6 Scope of study: The knowledge of the role drugs play in a living organism such as a human body enables one to logically reuse drugs for different indications. Moreover, a drug binds to multiple proteins/targets, themselves involved into multiple biological processes. Therefore a drug can potentially play a multitude of roles, which are accountable for its polypharmacology. Drug repurposing can provide new therapeutic options for a vast number of diseases where current therapies are failing or are inadequate (Roder and Thomson, 2015). The study investigated the binding energies and interactions of selected approved drugs for four schistosomal drug targets using molecular docking simulations, molecular dynamics simulations, conservation of schistosomal drug targets and human liver enzymes in *D. melanogaster*. Also, longevity and survival rates of *D. melanogaster* in some of the predicted drugs against schistosomiasis were carried out. The predicted drugs could be validated for clinical use against schistosomiasis.

1.7 Significance of study: The significance is to discover approved drugs with potential inhibitory activities against schistosomiasis since PZQ and OXA have been reported to have some limitations including failure of treatment due to resistance or tolerance. The study will

identify potential alternative and/or adjunctive drug(s) against schistosomiasis. Validation of the identified drugs in animal and human subjects may provide alternative and/or adjunctive drug(s) against schistosomiasis.

CHAPTER TWO

2.0 LITERATURE REVIEW

2.1 Review of Empirical Studies

Human schistosomiasis (or synonymously bilharzia) is a family of diseases caused primarily by three major species of the genus *Schistosoma* of flatworms, *S. mansoni* and *S. japonicum* that cause intestinal schistosomiasis and *Schistosoma haematobium* that causes urinary schistosomiasis (Chiyaka *et al.*, 2010; Prast-Nielsen *et al.*, 2011; de Moraes, 2012) and *S. mansoni* is the most widely distributed. Schistosomiasis is a neglected disease that remains a considerable public health problem in tropical and subtropical regions of the globe. This parasitic disease is the most important human helminth infection in terms of morbidity and mortality and is a growing concern worldwide (de Moraes, 2012). It affects over 200 million people in developing countries and causes about 280,000 deaths per year in sub-Saharan Africa alone (Angelucci *et al.*, 2009, 2010). It is predominantly a rural disease found in tropical countries, with *S. mansoni* present in parts of South America and the Caribbean, Africa and the Middle East; *S. haematobium* in Africa and the Middle East and *S. japonicum* found in South-east Asia, China and the Philippines (de Moraes, 2012). These infections are transmitted by freshwater snails and humans get infected when they interact with the habitats of these snails. Children, in particular, with their high infection levels, indiscriminate habits of excretion and predilection for playing in water, are very important in propagating the disease (Chiyaka *et al.*, 2010).

2.2 Signs and symptoms of schistosomiasis

Symptoms of schistosomiasis are caused by the body's reaction to the worms' eggs, not by the

worms themselves. Intestinal schistosomiasis can result in abdominal pain, diarrhea, and blood in the stool. Liver enlargement is common in advanced cases, and is frequently associated with an accumulation of fluid in the peritoneal cavity and hypertension of the abdominal blood vessels. In such cases there may also be enlargement of the spleen. The classic sign of urogenital schistosomiasis is haematuria (blood in urine). Fibrosis of the bladder and ureter, and kidney damage are sometimes diagnosed in advanced cases. Bladder cancer is another possible late-stage complication. In women, urogenital schistosomiasis may present a genital lesions, vaginal bleeding, and pain during sexual intercourse including nodules in the vulva. In men, urogenital schistosomiasis can induce pathology of the seminal vesicles, prostate and other organs. It may also have other long-term irreversible consequences, including infertility.

The economic and health effects of schistosomiasis are considerable. In children, schistosomiasis can cause anaemia, stunting and a reduced ability to learn, although the effects are usually reversible with treatment. Chronic schistosomiasis may affect people's ability to work and in some cases can result in death. In sub-Saharan Africa, more than 200 000 deaths per year are due to schistosomiasis.

2.3 Morphological features of schistosome

The morphological features of schistosome are presented in appendix 1. Throughout complex life-cycle of schistosome, they undergo striking morphological and physiological changes with individual life-stages displaying distinct adaptations both to parasitic life, and also to free-living life that permits movement between definitive-vertebrate and intermediate-snail hosts. Such adaptations include cilia or tails for swimming, secretory glands for host penetration, a tegument and glycocalyx for parasite protection/host immuno-modulation, a gynaecophoric canal for sustained pairing between sexes, muscular suckers for attachment/feeding, and highly organized reproductive systems for efficient fertilization and egg production (Walker, 2011).

Unlike other trematodes, schistosomes are dioecious (i.e., they have separate sexes), with the adults having a cylindrical body of 7 to 20 mm in length featuring two terminal suckers, a complex tegument, a blind digestive tract, and reproductive organs. The male's body forms a groove, or gynaecophoric channel, in which it holds the longer and thinner female (McManus and Loukas, 2008).

Cercariae are divided morphologically into the tail region, which propels the organisms through the water, and head region, which, alone, develops into the mature parasite. The rapid switch towards lactate production occurs only in cercarial heads; the tails have little or no hexokinase, and degenerate following separation from the penetrating schistosomula (Skelly *et al.*, 1998). The cercariae of *S. mansoni* have an oval body or head and a long cylindrical tail which is divided into two furculae at the posterior extremity. The most anterior part of the head is provided with triangular slit surrounded by three spiny tegumental folds. The head of *S. mansoni* cercariae is covered with numerous spines which are posteriorly directed. The ventral sucker is well developed and provided with numerous, large and sharp spines directed backwardly. The posterior end of the head is tapered into a spiny collar-like folding over the narrow connection between the head and tail. This area represented the detachment site between the head and tail during penetration. The tail of *S. mansoni* has larger and sharper spines than that of the body. They are concentrated on the dorsal and ventral surface, and they are much fewer on the lateral surface. The ventral surface of the tail furculae has few short and pointed spines. The excretory pore is found on the tip of the tail furculae. The surface topography of *S. mansoni* cercariae exposed to 2 and 3 minutes ultraviolet radiation was more or less similar to those of non-irradiated cercariae and there were no strike differences (Bin Dajem and Mostafa, 2007).

2.4 Diagnosis of schistosomiasis

Schistosomiasis is diagnosed through the detection of parasite eggs in stool or urine specimens (WHO, 2003). Antigens detected in blood or urine samples are also indications of infection. For

urogenital schistosomiasis, a filtration technique using nylon, paper or polycarbonate filters is the standard diagnostic technique. Children with *S. haematobium* almost always have microscopic blood in their urine and this can be detected by chemical reagent strips. The eggs of intestinal schistosomiasis can be detected in faecal specimens through a technique using methylene blue-stained cellophane soaked in glycerine or glass slides, known as the Kato-Katz technique (WHO, 2003). For people from non-endemic or living in low transmission areas, serological and immunological tests may be useful in showing exposure to infection and the need for thorough examination and treatment.

Mantawy *et al.*, (2011) have previously reported the determination of antioxidant enzymes (glutathione peroxidase (GPX), catalase and superoxide dismutase (SOD) in *Schistosoma mansoni* experimental infection in rats. Studies have reported estimation of reduced glutathione, albumin and alanine aminotransferase (ALT) (El-Lakkany *et al.*, 2012), aspartate aminotransferase (AST) (Aziz *et al.*, 2015) in schistosoma infections. Aziz *et al.*, (2015) reported that schistosome induces inflammatory cellular activation and promotes oxidative stress, which leads to lipid peroxidation (LPO), with subsequent increase in inflammatory mediators like malondialdehyde (MDA) and have predicted the involvement of LPO byproducts in schistosomiasis pathogenicity and biomarker for schistosomiasis morbidity. Chauhan and Chauhan, (2016) have estimated levels of malonyldialdehyde (MDA) as marker for oxidative stress in *D. melanogaster*. Study further revealed that MDA correlated with hepatic fibrosis in human *S. mansoni* infection (Aziz *et al.*, 2015).

2.5 Treatment of schistosomiasis

Praziquantel (PZQ) is the generic name for 2-(cyclohexylcarbonyl)-1,2,3,6,7,11b-hexahydro-4H-pyrazino[2,1-a]isoquinoline-4-one. It is a white crystalline powder with a bitter taste. The compound is stable under normal storage conditions, practically insoluble in water, but soluble in some organic solvents. The commercial preparation is a racemate mixture composed of equal parts of 'laevo' and 'dextro' isomers, of which only the former has schistosomicidal activity

either *in vivo* or *in vitro* (Doenhoff *et al.*, 2008). Schistosomiasis can be combated by various methods depending on which part of the parasite life cycle is attacked. Current treatment of schistosomiasis relies exclusively on PZQ, an effective drug that is active against all schistosome species. Study has shown that it is safe and effective at single oral dose of 40–60 mg/kg and can achieve cure rates of 60–90%. One notable failing of PZQ is its reduced efficacy against immature parasites relative to adult worms (da Silva *et al.*, 2017). Although PZQ is effective, reliance on a single drug is a major concern because of the potential clinical development and spread of PZQ-resistant parasites. Even now patients who are not cured by multiple doses of PZQ have been identified from various locales, suggesting that resistance to the drug may already be present in the field (King *et al.*, 2000; Doenhoff *et al.*, 2008; da Silva *et al.*, 2017). Also, *in vitro* and animal model studies have demonstrated resistance to PZQ (Ismail, 1999). Study show that expression or mutagenesis of schistosomal GST by the parasite may confer resistance to PZQ (McTigue *et al.*, 1995). Given the wide clinical use of PZQ, drug-resistant parasites of clinical concern may evolve. Other drugs are available, but they are less effective, have unacceptable side effects and/or are effective on only one schistosome species (da Silva *et al.*, 2017). Therefore, it is imperative to identify alternative drugs to ensure that PZQ resistance does not become a major health concern (Doenhoff *et al.*, 2008; Prast-Nielsen *et al.*, 2011; da Silva *et al.*, 2017).

Alternatives to praziquantel

The major alternative to PZQ is oxamniquine ((\pm)-(7-nitro-2-{{[(propan-2-yl) amino]methyl}-1,2,3,4-tetrahydroquinolin-6-yl)methanol). Artemisinin and its derivatives have also shown promise as antischistosomal agents (da Silva *et al.*, 2017) but proposals for use of artemisinins in areas where Plasmodium spp. and schistosomes coexist will raise concerns about inducing drug-resistance in the former (Doenhoff *et al.*, 2008). Other drugs like lucanthone, hycanthone,

niridazole, stibofen® (sodium and antimony bis-pyrocatechol) etc have been used in the past but they show unacceptable side effects and their use have been discontinued (da Silva *et al.*, 2017).

Oxamniquine is an antischistosomal agent widely used in Brazil. It operates mainly against the specie *S. mansoni* and the adult male worms are more vulnerable to the action of the drug than the female parasites (Cioli *et al.*, 1995). It is easily absorbed orally and intramuscularly; however, its administration by the intramuscular route is not recommended due to intense and prolonged pain (Foster, 1987). After the administration in therapeutic doses, its half life is about 1.5–2 h. According to the World Health Organization, a single OXA oral dose of 15–20 mg/kg is effective in the treatment of schistosomiasis in South America, Caribbean Islands and West Africa, while 30 mg/kg should be used in East Africa, Central Africa and Arabian Peninsula. Doses above 60 mg/kg may also be necessary in Egypt, South Africa and Zimbabwe in order to obtain the desired therapeutic efficacy (WHO, 1989). In the clinic, the side effects most commonly reported by patients undergoing a treatment with oxamniquine were nausea, dizziness, drowsiness, headache and, less often, abdominal discomfort. Vomiting and diarrhea were mild and short-termed. Some authors reported serious adverse effects on the central nervous system after the drug administration (da Silva *et al.*, 2017). It is contraindicated for pregnant women, children under two years of age, patients with hepatic and cardiac decompensations, and in cases of hypertension. Furthermore, it should not be used in people with epilepsy (da Silva *et al.*, 2017).

Oxamniquine resistance evolved in the human blood fluke (*S. mansoni*) in Brazil in the 1970s (Valentim *et al.*, 2013). It has to be activated by a parasite sulfotransferase and resistant/insusceptible schistosomes lack the enzyme. Oxamniquine is effective only against *S. mansoni* and ineffective against the other two main schistosome species (*S. haematobium* and *S. japonicum*) and its use has so far been almost entirely restricted to Brazil and other South American countries (da Silva *et al.*, 2017). The price of oxamniquine has remained much higher

than that of PZQ. For these reasons it is unlikely that oxamniquine will be used much in Africa. Oxamniquine may be particularly prone to the problem of drug resistance, but deserves consideration because it was effective against *S. mansoni* infections in an area in which PZQ yielded unexpectedly low cure rates (Doenhoff *et al.*, 2008). Study has suggested that oxamniquine is converted to a reactive ester by a schistosome enzyme that is missing in drug-resistant parasites (Pica-Mattoccia *et al.*, 2006; da Silva *et al.*, 2017).

2.6 Epidemiology of schistosomiasis infection

Human schistosomiasis is endemic in large areas of the tropics as one can deduce from figure 2.1. It has been estimated that over 700 million people in 74 countries are exposed to the risk of schistosomal infection, and almost 200 million were estimated to be infected in 2003 (Fenwick, 2006), of which 85% in sub-saharan Africa. About 95% of the cases are due to *S. mansoni* and *S. haematobium* infections. *S. haematobium* is endemic in 53 countries, in the Middle East and most of the African continent. Schistosomiasis is largely an infection found in rural areas, but urban schistosomiasis is an increasing problem in many countries. Natural streams, ponds and lakes are typical sources of infection, but over the past few decades, man-made reservoirs and irrigation systems, as well as population growth and migration, have contributed to the spread of schistosomiasis (Gryseels *et al.*, 2006; McManus and Loukas, 2008). Within countries, regions and villages, the distribution of schistosomiasis can be very focal, depending on variations in snail populations and human–water contact behaviour. Also, the distribution of schistosomiasis can be highly uneven across individuals. The majority of the parasites are usually present in a small fraction of the infected individuals.



Figure 2.1: Map of the current global distribution of schistosomiasis. Source: US Centers for Disease Control and Prevention. Source: (Olveda *et al.*, 2013).

2.7 Prevalence of schistosomiasis in Africa

Sub-Saharan Africa accounts for 93% (192 million) of the world estimated 207 million cases of schistosomiasis. The highest prevalence of this infection is seen in Nigeria (29 million), which is closely followed by United Republic of Tanzania (19 million), Ghana, and Democratic Republic of Congo (15 million) making up the top five countries in Africa with schistosomal infection (Kanwai *et al.*, 2011; Adenowo *et al.*, 2015).

On Thursday June 4, 2015, Nigeria's Federal Ministry of Health released comprehensive data on the national distribution of schistosomiasis and intestinal worms. The results showed an overall prevalence rate of 9.5 % for schistosomiasis and 27 % for intestinal worms (Gordon, 2015). Available data from 1994 to 2015 showed that the prevalence of urinary schistosomiasis infestation in Nigeria varied from 2 % to 82.5 % and the pooled prevalence was 34.7% (Abdulkadir *et al.*, 2017). It was also reported that North central, North east, South east, South west, South south have urinary schistosomiasis infestation prevalence range of 20.5–32.6 %,

14.3–44.2 %, 27.9–49.5 %, 17.4–28.0 %, 31.6–58.6 %, 22.5–64.3 % respectively (Abdulkadir *et al.*, 2017). The overall prevalence of schistosomiasis in Kano state, Nigeria was 17.8%, with 8.9% and 8.3% infected with *S. mansoni* and *S. haematobium* respectively, and 0.5% had co-infection of both species (Dawaki *et al.*, 2015).

In Burkina Faso, the overall prevalence of *S. haematobium* infection was 8.76% and that the prevalence of such infection ranged from 0.0 % to 56.3% according to sentinel site. Also, it was reported that *S. mansoni* was only detected in the Hauts Bassins and Centre-Sud regions of Burkina Faso with prevalence of 5 % and 0.31% respectively (Ouedraogo *et al.*, 2016). According to the criteria of the World Health Organization (WHO, 2012) Ouedraogo *et al.*, (2016) reported that Burkina Faso may have eliminated schistosomiasis as a public health problem in eight regions and controlled schistosome-related morbidity in another three regions. In Tanzania, schistosomiasis prevalence has and continues to increase on a national scale and the most recent data estimated countrywide prevalence of 53.3% (Jones, 2015).

2.8 Transmission and risk factors for schistosomiasis infection

Schistosomiasis transmission arises from agricultural practices and water resource manipulation, particularly if there is poor sanitation and substantial water contact. Environmental changes linked to water resource development, population growth, migration, and disease have facilitated the recent spread of schistosomiasis to areas where it is not endemic (McManus and Loukas, 2008). All Schistosoma infections follow direct contact with freshwater-harbouring cercariae. Three major factors are responsible for maintaining the transmission of the infection: (1) contamination of fresh water with excreta containing schistosome eggs, (2) the presence of the snail intermediate hosts, and (3) human contact with water-infested with cercariae. Contact with contaminated freshwater is the major risk factor of infection.

The main risk groups are school-age children, specific occupational groups (fishermen, irrigation workers, farmers), and women and other groups using infested water for domestic purposes.

Many other host-related and environmental risk factors have been identified that may affect the risk of acquiring schistosome infection, and/or influence the distribution, prevalence, intensity of infection, morbidity and mortality of schistosomiasis. Among these are genetic factors, behaviour, household clustering, climate, immune response of the host, and concomitant infections (McManus and Loukas, 2008).

2.9 Life-cycle of schistosome

The schistosome life cycle is depicted in Figure 2.2. The life cycle is complex and begins when eggs are released into freshwater through faeces and urine and consists of an obligatory alternation of sexual and asexual generations. Schistosome eggs produced by the sexual stage leave people via urine or faeces, reach freshwater, shed their shells and hatch a ciliated free-swimming larva called a miracidium. More than 50% of the eggs do not make it into the faecal or urinary stream and become entrapped in adjacent tissues or get carried away by the circulatory or lymphatic system and can become lodged in virtually any organ in the body. A miracidium that locates an appropriate species and genotype snail penetrates and infects it, multiplies asexually through two larval stages into thousands of cercariae that escape the snail and live in water. They swim until they encounter a skin of suitable warmth and smell, and infect humans by direct penetration of the skin. Once the cercariae penetrate the skin, they lose their tails and differentiate into larval forms called schistosomulae. A schistosomulum spends several days in the skin before exiting via blood vessels traversing to the lung, where it undergoes further developmental changes. It then migrates via the systematic circulation to the liver where it settles, reaches sexual maturity and pairs. Only those worm pairs that reach the portal system of the liver mature into adults. Thereafter, worm pairs migrate by the bloodstream to their definitive location; *S. mansoni* and *S. japonicum* to the small and large intestines and *S. haematobium* to the bladder and rectal veins (Chiyaka *et al.*, 2010). The life cycle is completed when the eggs passed in the feces hatch, releasing miracidia that, in turn, infect specific freshwater snails (*S. mansoni* infects *Biomphalaria* sp., *S. haematobium* and *S. intercalatum* infect *Bulinus* sp., *S.*

japonicum infects *Oncomelania* sp., and *S. mekongi* infects *Neotricula* sp.). After two generations of primary and then daughter sporocysts within the snail, asexually produced cercariae are released (McManus and Loukas, 2008).

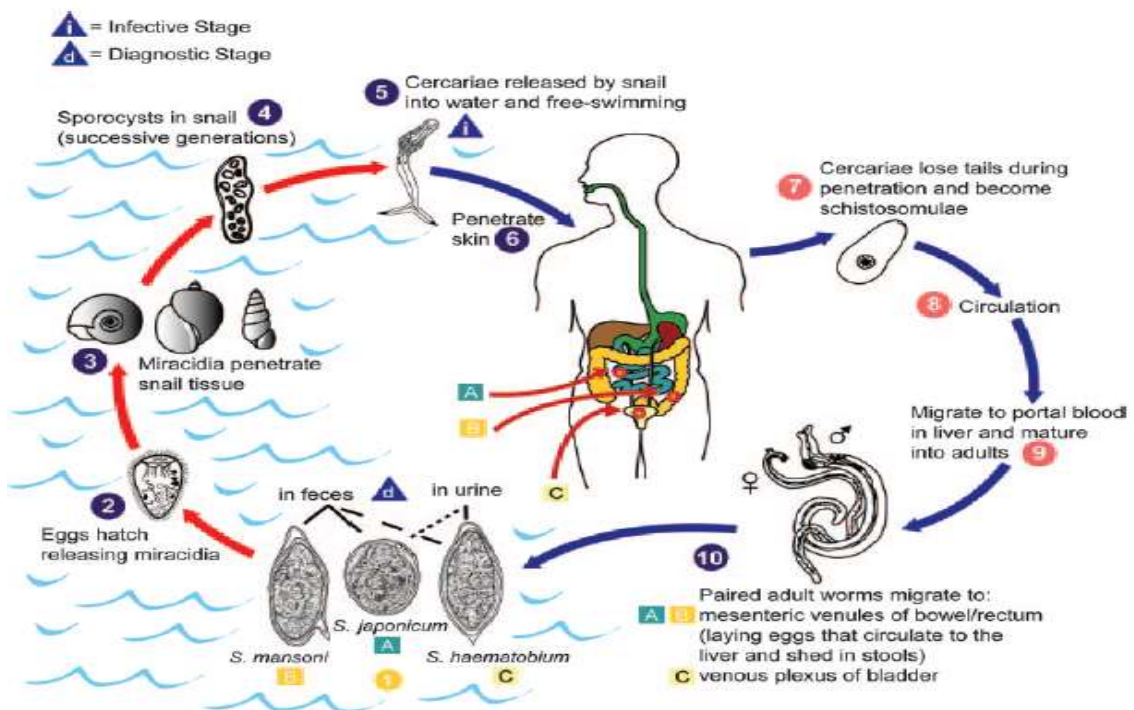


Figure 2.2: Life cycle of *S. mansoni*, *Sjaponicum* and *S. hematobium* (McManus and Loukas, 2008)

Parasite culture system

In vitro studies with schistosomula, juvenile and adult worms of *S. mansoni* are frequently used in screening strategies for the discovery of new antischistosomal drugs (Abdulla *et al.*, 2009; Keiser, 2010; Mølgaard *et al.*, 2001; Peak *et al.*, 2010; Ramirez *et al.*, 2007; Smout *et al.*, 2010; Yousif *et al.*, 2007). Parasites at different stages might show differences with regard to drug sensitivity. The *in vitro* methods currently utilized have recently been reviewed, and following the establishment of the *S. mansoni* life cycle in the laboratory, *in vitro* parasite culture techniques were developed (Keiser, 2010; Ramirez *et al.*, 2007). For *in vitro* trials, parasites of different ages are used, such as 3-h-old and 1-, 3-, 5- and 7-day-old schistosomula, 21 day-old juveniles, and 42- to 56-day-old adults. Figure 2 shows the life cycle of *S. mansoni* in the

laboratory, illustrating the collection points for *in vitro* chemotherapeutic studies. (de Moraes 2012).

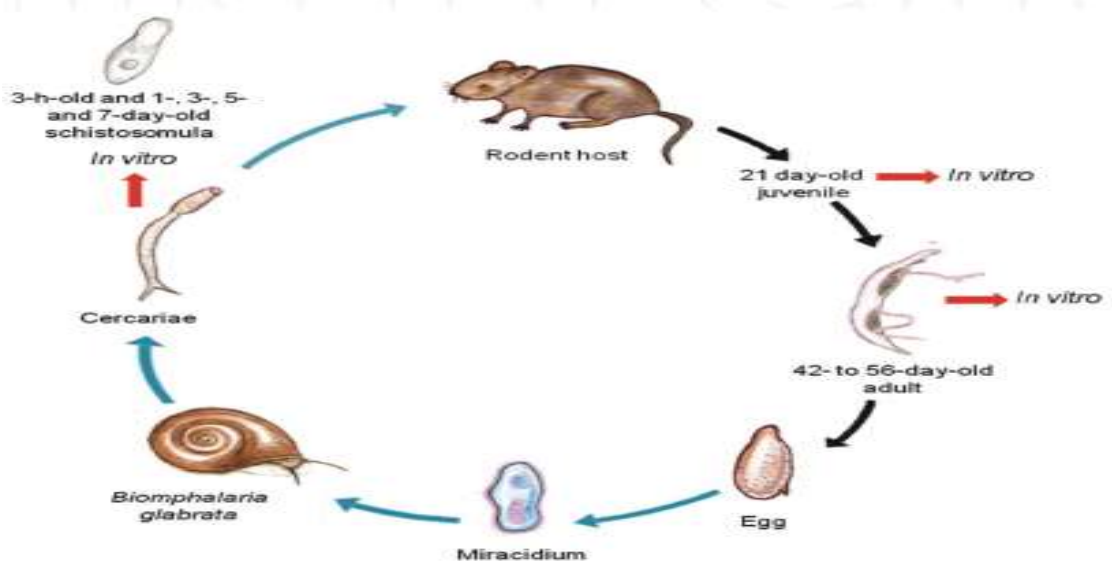


Figure 2.3: Laboratory life cycle of *s. mansoni*, illustrating the collection points for *in vitro* chemotherapeutic studies. Black arrow: maturation of parasite within final host. Blue arrow: aquatic phase (de Moraes, 2012).

2.10 Drug design/discovery

Drug discovery can take the form of traditional approach which has been historically based on phenotypic readouts on the organism level, such as the effect of herbs or other natural remedies on humans. It can take the form of computer-aided approaches which can be ligand-based or structure-based drug discovery approaches. The computer-aided approaches can complement the traditional approach.

Drug discovery has explored the ‘Magic bullets’ concept which state that drugs exert their activities by modulating one target of particular relevance to a disease, the famous idea of one ‘key’ (or ligand) modifying each ‘lock’ (or protein) (Koutsoukas *et al.*, 2011). This paradigm has guided the pharmaceutical industry throughout approximately the last three decades. However, in recent years, there is mounting evidence offering a significant challenge to this hypothesis as it has become increasingly obvious that many drugs elicit their therapeutic activities by modulating multiple targets. Recently, it has been estimated that each drug on the market possesses

bioactivity against, on average; six experimentally confirmed protein targets (Koutsoukas *et al.*, 2011). The fact is that the multi-target interactions of drugs are either largely unknown or insufficiently understood in most cases (Koutsoukas *et al.*, 2011).

2.10.1 Computer aided drug design

Modern methods of computer-aided drug design fall into two major categories: ligand-based and receptor-based methods/approaches. The former methods, which include quantitative structure activity relationship (QSAR), various pharmacophore assignment methods, and database searching or mining, are based entirely on experimental structure–activity relationships for receptor ligands or enzyme inhibitors. Their application in the last three or four decades led to several drugs currently on the market. The structure-based design methods, which include docking and advanced molecular simulations, require structural information about the receptor or enzyme that is available from X-ray crystallography, nuclear magnetic resonance (NMR) techniques, or protein homology model building. Also the structural information can be obtained through homology modeling of the drug target.

The ultimate goal of molecular modeling as a pharmacological and medicinal chemistry tool is to predict, in advance of any laboratory testing, novel biologically active compounds. Molecular modeling research starts from the analysis of experimental observables of drug–receptor interaction. This interaction leads to the formation of the ligand–receptor complex followed by the conformational change of the receptor, which constitutes the putative mechanism of signal transduction. The interaction between ligands and their receptors is clearly a dynamic process. Once the static model of ligand–receptor interaction has been obtained, the stability of ligand–receptor complexes should be evaluated by means of molecular dynamics simulations. The schematic representation of structure-based drug design is presented in figure 2.4.

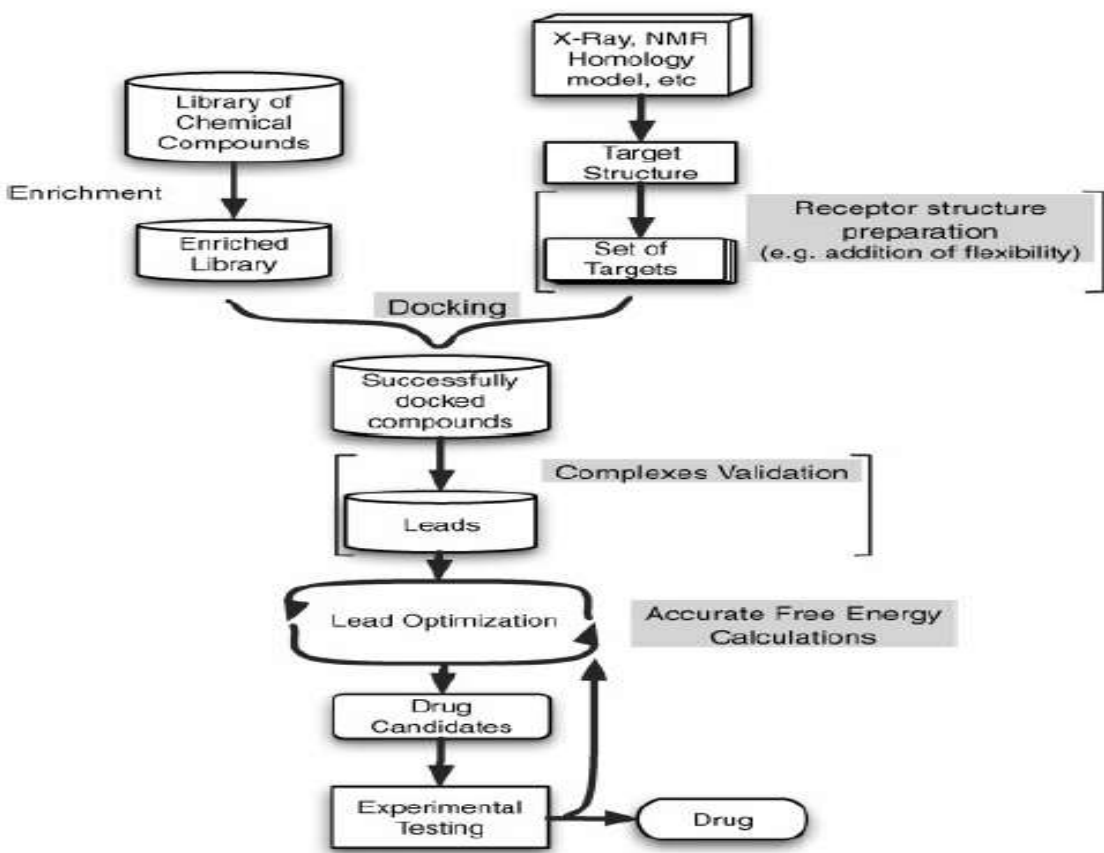


Figure 2.4: Schematic chart of computer aided drug design. Source: Alonso *et al.*, (2006)

2.10.2 Homology modeling

Comparative protein structure modeling is a computational approach to build three-dimensional structural models for proteins using experimental structures of related protein family members as templates. Regular blind assessments of modeling accuracy have demonstrated that comparative protein structure modeling is currently the most reliable technique to model protein structures. Homology models are often sufficiently accurate to substitute for experimental structures in a wide variety of applications. Since the usefulness of a model for specific application is determined by its accuracy, model quality estimation is an essential component of protein structure prediction (Bordoli and Schwede, 2012). Models of the modeled proteins can be ranked according to their sequence identity with their respective templates. The models can be considered sufficiently reliable when there is more than 50 % sequence identity between the template and the targets proteins (Arnold *et al.*, 2006).

2.10.3 Molecular docking simulation

Molecular docking methodologies are of great importance in the planning and design of new drugs. These methods aim to predict the experimental binding mode and affinity of a small molecule within the binding site of the target of interest (Gude *et al.*, 2014). Molecular docking algorithms execute quantitative predictions of binding energetics, providing rankings of docked compounds based on the binding affinity of ligand-receptor complexes (Ferreira *et al.*, 2015). Following the development of the first algorithms in the 1980s, molecular docking became an essential tool in drug discovery (López-Vallejo *et al.*, 2011). Docking studies are used at different stages in drug discovery such as in prediction of the docked structure of a ligand-receptor complex and also to rank ligand molecules based upon their binding energy. Docking protocols aid in elucidation of the most energetically favorable binding pose of a ligand to its receptor (Iman *et al.*, 2015). The most popular docking programs include AutoDockVina®, DOCK, AutoDock FlexX, GOLD, and GLIDE among others (Alonso *et al.*, 2006).

2.10.4 Molecular dynamics simulation

Molecular dynamics (MD) studies is the time-dependent evolution of coordinates of complex molecular systems as a function of time. It has become a major technique in the arsenal of tools to design novel bioactive molecules and can help to rationally comprehend their mode of action and improve chemical structures with regard to biological effect (Mortier *et al.*, 2015). Their main advantage is in explicitly treating structural flexibility and entropic effects. This allows a more accurate estimate of the thermodynamics and kinetics associated with drug–target recognition and binding, as better algorithms and hardware architectures increases their use. Classical MD simulations nowadays allow implementation of structure-based drug design (SBDD) strategies that fully account for structural flexibility of the overall drug–target model system (Durrant and McCammon, 2011; Harvey and De Fabritiis, 2012) Indeed, it is now widely accepted that the two major drug-binding paradigms (induced-fit and conformational selection)

have superseded Emil Fischer's rigid lock-and-key binding paradigm (Boehr *et al.*, 2009; Changeux and Edelstein, 2011; Vogt and Di Cera, 2012). Researchers have recently demonstrated the power of these methods for studying protein–ligand binding and estimating the associated free energy and kinetics (Durrant and McCammon, 2011; Harvey and De Fabritiis, 2012). Receptor and ligand flexibility are crucial for correctly predicting drug binding and related thermodynamic and kinetic properties (Fischer *et al.*, 2014). As a result, classical and/or QM/MM MD simulations is no longer considered prohibitive for effective drug design. Instead, it is pushing the frontiers of computationally driven drug discovery in both academia and industry (Borhani and Shaw, 2012; Mortier *et al.*, 2015).

Advantages of Molecular Dynamics Simulation

MD simulations are usually performed at normal temperature (300 K), relatively low energy barriers, on the order of 0.6 kcal can be easily overcome. Thus if the starting configuration of the drug–receptor complex resulting from docking is separated from the more stable configuration by such a low barrier, molecular dynamics will take the system over the barrier. Molecular simulations may identify more stable, therefore more realistic, conformational states of ligand–receptor complexes (Mortier *et al.*, 2015). Furthermore, they may provide unique information about conformational changes of the receptor due to ligand binding; shed light on the intimate mechanisms of receptor activation that currently cannot be studied by any other technique. Finally, molecular simulations frequently incorporate solvent and thus allow the inclusion of solvent effects in the consideration. Recent studies have shown the importance of MD simulation to investigate the biomolecular flexibility associated with ligand recognition (Nair *et al.*, 2011; Nair *et al.*, 2012; Nair and Miners, 2014). Studying the flexibility of the target receptor would thus permit the improved design of drugs over the simplistic lock and key conceptualization of the static receptor.

Combined Docking and MD Simulations

Fast and inexpensive docking protocols can be combined with accurate but more costly MD techniques to predict more reliable protein–ligand complexes. The strength of this combination lies in their complementary strengths and weaknesses. On the other hand, docking techniques are used to explore the vast conformational space of ligands in a short time, allowing the scrutiny of large libraries of drug-like compounds at a reasonable cost. The major drawbacks are the lack, or poor flexibility of the protein, which is not permitted to adjust its conformation upon ligand binding, and the absence of a unique and widely applicable scoring function, necessary to generate a reliable ranking of the final complexes. On the other hand, MD simulations can treat both ligand and protein in a flexible way, allowing for an induced fit of the receptor-binding site around the newly introduced ligand. In addition, the effect of explicit water molecules can be studied directly, and very accurate binding free energies can be obtained. However, the main problems with MD simulations are that they are time-consuming and that the system can get trapped in local minima. Therefore, the combination of the two techniques in a protocol where docking is used for the fast screening of large libraries and MD simulations are then applied to explore conformations of the target, optimize the structures of the final complexes, and calculate accurate energies, is a logical approach to improving the drug-design process.

2.10.5 Drug repurposing

Molecular docking and dynamics simulations can be used for screening of approved drugs with the aim of predicting new indication(s) for them. The predicted drugs can be validated and brought to the clinic for the new indication. Drug repurposing (also referred as drug repositioning, re-profiling, therapeutic switching and drug re-tasking) is the identification of new therapeutic indications for known drugs (Croset, 2014) or strategy by which new or additional value is generated from a drug by targeting diseases other than those for which it was originally intended (Corbett *et al.*, 2013). These drugs can either be approved and marketed compounds used daily in a clinical setting, or they can be drugs that have been shelved", namely molecules

that did not succeed in clinical trials or for which projects have been discontinued for various reasons. In one sentence, drug repositioning can be defined as renewing failed drugs and expanding successful ones (Croset, 2014). There are two main approaches to drug repositioning. The first, more straightforward approach is to investigate drugs within the mechanism of action for which they are already licensed, the most common example being the repositioning of sildenafil, previously used to treat angina, for use in erectile dysfunction. The second, more innovative approach aims to identify novel targets for existing drugs. Despite being more complex this second approach has the potential to identify more novel compounds (Corbett *et al.*, 2013). Drug repurposing may save time and costs associated with the discovery phase2. Drug repurposing certainly comes with some distinct advantages and the efforts have been driven by several important factors including: the access to increasing amounts of experimental data, better understanding of compound polypharmacology, biological data mining, and regulatory impetus from Food and Drug Administration (FDA) and national institute of health (NIH). The repurposing of existing drugs offers major advantages over the creation of new ones, mainly as it relates to efficiency. This is because a drug already approved for the market by the US Food and Drug Administration (FDA) has already been proven safe for human use, which means that a drug company looking to explore alternative uses can quickly leapfrog one crucial and expensive stage of drug testing. For the company, this means welcome savings in money. And for people who so urgently need better treatments, it may mean savings in time. Therefore, effective antischistosomal drugs could be identified and validated through drug repurposing approach. The total cost of bringing a new drug to market was recently calculated at a staggering \$2.558 billion. Some have argued that this is a gross over-estimation, and a more ‘conservative’ value is \$1.778 billion (Naylor and Schonfeld, 2014). The average time required from drug discovery to launch remains at an eye-watering 12-15 years (Ashburn and Thor, 2004; Naylor and Schonfeld, 2014) as depicted in Figure 2.5.

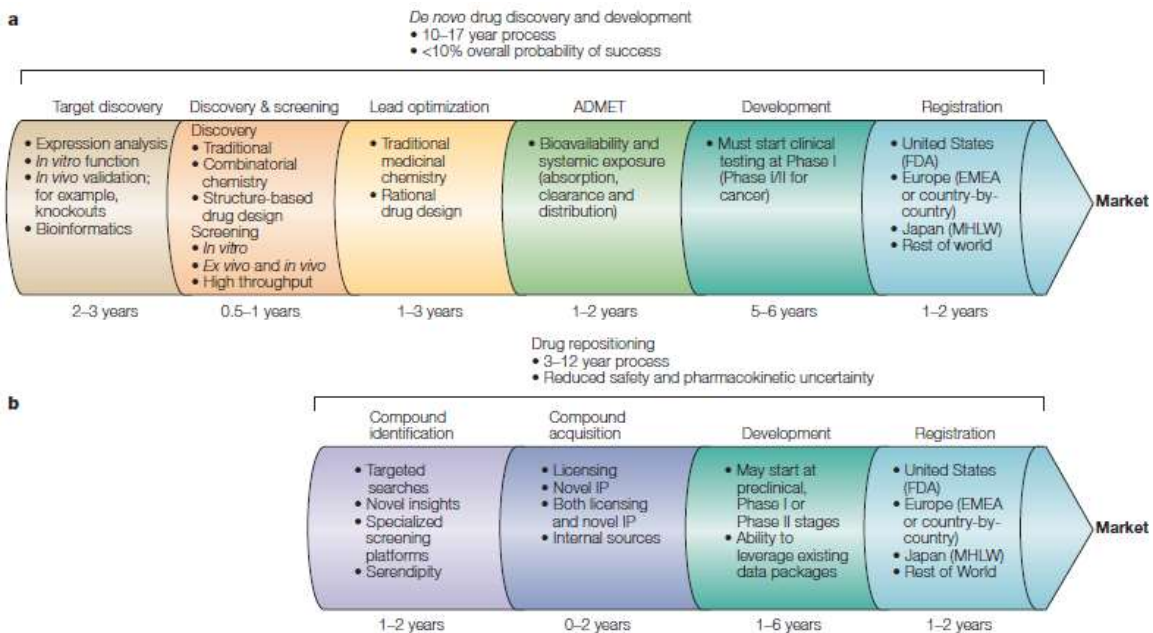


Figure 2.5: A comparison of traditional *de novo* drug discovery and development versus drug repositioning. (a) It is well known that *de novo* drug discovery and development is a 10–17 year process from idea to marketed drug. The probability of success is lower than 10%. (b) Drug repositioning offers the possibility of reduced time and risk as several phases common to *de novo* drug discovery and development can be bypassed because repositioning candidates have frequently been through several phases of development for their original indication. Source: Ashburn and Thor, (2004).

Successes of drug repurposing

Studies have shown that sildenafil was successfully repurposed from its previous indication of angina to its new indication for erectile dysfunction (Ashburn and Thor, 2004; Croset, 2014).

Sildenafil repurposing clearly illustrated that drugs can be repurposed from its clinical side-effects ones (Croset, 2014). The successful repurposing of thalidomide from its previous indication of sedative, sleep inducing agent to its new indication of treatment of *Erythema nodosum leprosum* clearly illustrated how a drug can surprisingly come back from being a hazardous drug retracted from the market into a novel and unique therapeutic agent. Study has shown that the original indication of raloxifene during preclinical developments was breast

cancer (Ashburn and Thor, 2004). Eventually, the molecule successfully passed clinical trials in 1999, with osteoporosis as a unique indication. However, the polypharmacology of the drug, particularly its action against breast cancer, was still under investigation. Finally, in 2007, the FDA approved raloxifene as a preventive agent for breast cancer in post-menopausal women; therefore extending the line of application of the drug back to it's originally thought indication (Croset, 2014). More examples of repurposed drugs are presented in appendix 2.

2.11 Schistosome molecular targets for drug discovery

To date, there have been numerous candidate molecules that were proposed as potential chemotherapeutic targets for treating schistosomiasis. These molecules are involved in a variety of survival related machineries of the worm, including redox metabolism (e.g. thioredoxin glutathione reductase) (Song *et al.*, 2012; Ross *et al.*, 2012; Prast-Nielsen *et al.*, 2012), ion channels (e.g. calcium channel subunits) (Salvador-Recatalà and Greenberg, 2012). Recently, sulfotransferase was identified as the target of oxamniquine action in *S. mansoni* (Taylor *et al.*, 2015). Also, glutathione s-transferase (GST), an essential detoxification enzyme in parasitic helminths, has been implicated as a major vaccine target and attractive drug target against schistosomiasis and other helminthic diseases (McTigue *et al.*, 1995). Also, McTigue *et al.*, (1995) reported glutathione s-transferase as drug target for praziquantel. Again, 3-hydroxy-3-methyl-glutaryl-coenzyme A reductase, histone deacetylase (HDACs), have been validated as drug targets in *S. mansoni* (Mafud *et al.*, 2016).

2.11.1 Thioredoxin glutathione reductase

Differences in redox pathways between mammals and helminths (Salinas *et al.*, 2004) as well as biochemical differences between host and parasite pyridine nucleotide disulfide oxidoreductases suggest that chemotherapy for flatworm infections based on selective inhibition of worm Thioredoxin glutathione reductase (TGR) is feasible. TGR is a natural chimeric flavo-enzyme whose structure results from the fusion of a thioredoxin (TR) domain with a glutaredoxin (GR)

domain. The redox activity of the enzyme relies on at least three redox sites communicating with one another: (i) the FAD site, composed by the isoalloxazine ring of the flavin and the Cys154–Cys159 (Cys-Val-Asn-Val-Gly-Cys) couple (characteristic of all the enzymes of the TR/GR family); (ii) the C terminus, constituted by the Gly-Cys-Sec-Gly sequence shared with the majority of TRs but not with GRs; and (iii) the glutaredoxin redox site represented by Cys28–Cys31 at the N-terminal portion of the protein (Angelucci *et al.*, 2009; 2010, Prast-Nielsen *et al.*, 2011). The schistosomal antioxidant system lacks the typical mammalian TR and GR enzymes, which are both replaced by TGR; this peculiarity revealed that TGR may be a target of choice for the development of new antischistosomal drugs (Kuntz *et al.*, 2007; Angelucci *et al.*, 2010). The schistosomal enzyme has been exploited for discovery of new schistosomicidal drugs (Angelucci *et al.*, 2009). Several studies have demonstrated that furoxan derivatives are capable of inhibiting TGR (da Silva *et al.*, 2017). Study has demonstrated that TGR activity is inhibited by two schistosomicidal drugs (antimonyl potassium tartrate and oltipraz) used in the past to fight the infection, suggesting that the enzyme is the main target of these compounds (Salinas *et al.*, 2004; Angelucci *et al.*, 2009). However, these drugs are obsolete today due to severe adverse side effects (Prast-Nielsen *et al.*, 2011; da Silva *et al.*, 2017). Nevertheless, high throughput screening, establishment of structure activity relationships and lead optimization in order to develop highly specific inhibitors for TGR has great potential for improving treatment of schistosome infections.

2.11.2 Sulfotransferase

Study has identified sulfotransferase as target for rational design of oxamniquine derivatives for treatment of schistosomiasis infection (Valentim *et al.*, 2013). Recently, sulfotransferase was identified as the target of oxamniquine action in *S. mansoni* (Taylor *et al.*, 2015) and OXA bound sulfotransferase provides platform for OXA-based drug design efforts (Taylor *et al.*, 2015) against schistosomiasis. Study shows that molecular dynamics simulation can be used to predict

sulfotransferase flexibility, activity and extract structuraly diverse conformations of protein (Mortier *et al.*, 2015).

2.11.3 Glutathione s-transferase

Glutathione s-transferase (GST), an essential detoxification enzyme in parasitic helminths, is a major vaccine target and an attractive drug target against schistosomiasis and other helminthic diseases (McTigue *et al.*, 1995). GST is a multifunctional enzyme that catalyzes the nucleophilic addition of reduced thiol of glutathione to a variety of electrophiles (Lim *et al.*, 1994). They are important enzymes involved in the metabolism of potentially toxic alkylatinagg agents. Cytosolic GSTs of the genus schistosoma participate in the immunogenicity to the vertebrate host and have been suggested as potential components of a vaccine against schistosomiasis (Capron *et al.*, 1987; Sher *et al.*, 1989). Study has established a protein target for PZQ, identifies GST non-substrate ligand transport site, and implicates PZQ in steric inhibition of schistosomal GST catalytic and transport for ligands. Differences in the xenobiotic binding region between parasitic and mammalian GSTs reveal a distinct substrate repertoire for schistosomal GST and provide basis for design of novel antischistosomal drugs (McTigue *et al.*, 1995).

2.12 Multi-target therapeutics

Recent developments in biological systems and overall clinical experience have revealed that the single-target drugs may not always induce the desired effect to the entire biological system even if they successfully inhibit or activate a specific target (Lu *et al.*, 2012). One reason is that organisms can affect effectiveness through compensatory ways. The development of diseases, particularly the complex ones, involves several aspects. Thus, scientists have recently proposed the multi-target drug design concept (Csermely *et al.*, 2005; Petrelli and Giordano, 2008; Boran and Iyengar, 2010). Drug development strategies have been influenced profoundly by the wealth of potential targets offered by genome projects. At present, the goal is to: (i) find a target of suitable function; (ii) identify the ‘best-binder’ by high throughput screening of large combinatorial libraries and/or by rational drug design based on the three-dimensional structure of

the target; (iii) provide a set of proof-of-principle experiments; and (iv) develop a technology platform projecting to potential clinical applications (Csermely *et al.*, 2005).

Drug combinations are the standard of care for treatment of many diseases (Zimmermann *et al.*, 2007; Zheng *et al.*, 2014). Combination drugs that impact multiple targets simultaneously are better at controlling complex disease systems, are less prone to drug resistance and are the standard of care in many important therapeutic areas. The combination drugs currently employed are primarily of rational design, but the increased efficacy they provide justifies discovery efforts for identifying novel multi-target mechanisms.

There are several categories of multi-target therapeutics that can be defined on the basis of target relationship as reported elsewhere (Zimmermann *et al.*, 2007) and summarized in (i) to (iii) below: (i) Components impact separate targets to create a combination effect. The targets can reside in the same or separate pathways within an individual cell, or in separate tissues. Here, the therapeutic effect occurs at separate molecular targets that can reside within individual signaling pathways, between pathways within a cell or at separate tissues in the body. (ii) One component alters the ability of another to reach its target. In this type of combination one agent can alter the metabolism of the pharmaceutically active component, or one agent can block an efflux pump or other resistance mechanism (e.g. β -lactamase) to increase the activity of the other. Here, modulation of one target facilitates action at a second target, for example by altering compound metabolism, inhibiting efflux pumps or blocking other resistance mechanisms (iii) The components bind separate sites on the same target to create a combination effect and increase the pharmacological action. For example, the components of the combination SynercidW bind two separate sites on the prokaryotic ribosome. Here, a coordinated action at multiple sites on a single target or macromolecular complex (e.g. prokaryotic ribosome) yields the therapeutic effect.

The targets in each of the three cases can be modulated either by a mixture of separate chemical entities or by a single compound designed to have multiple actions. Multi-target action can be

achieved in several ways. It is the coordinated effect at the set of targets that results in the biological and, hopefully, therapeutic effect (Kubinyi, 2003). It is interesting to note that to the best of the knowledge of the researcher, multi-target drugs have not been reported for schistosomiasis as at the time of this investigation. Study showed that some selective inhibitors of *S. mansoni* histone deacetylase 8 have been identified and that some benzohydroxamates showed significant dose-dependent killing of schistosome larvae and markedly impaired egg-laying of adult worm pairs in culture (Heimburg *et al.*, 2016).

Several highly efficient drugs like non-steroidal anti-inflammatory drugs (NSAIDs), salicylate, metformin or Gleevec™ affect many targets simultaneously. Furthermore, combinatorial therapy, which represents another form of multi-target drugs, is used increasingly to treat many types of diseases, such as AIDS, cancer and atherosclerosis (Csermely *et al.*, 2005). The favorable efficacy of existing combination therapeutics shows that searches specifically designed to identify multi-target mechanisms can provide a new path forward in drug discovery. Most multi-target therapeutics will be developed as a mixture of agents with selectivity for individual targets, but in some cases it might be possible to build multi-target action into a single chemical entity (Zimmermann *et al.*, 2007).

2.13 Preclinical validation of drug candidates

Preclinical phase - A laboratory test of a new drug or a new invasive medical device on animal model(s); conducted to gather evidence justifying a clinical trial (Chandramouli *et al.*, 2010).

During preclinical investigations, series of questions concerning the toxicity, pharmacokinetic parameters, safety assessment, and formulation optimization etc need to be answered. In any drug discovery and development effort, once a number of critical steps to arrive at a compound that is safe and efficacious, and also exhibits the complex array of desired drug-like behaviors that warrants advancement to the clinic have been taken. One may proceed to preclinical testing which involves animal testing. Researchers make every effort to use as few animals as possible and to ensure their humane and proper care. Generally, two or more species (one rodent, one

non-rodent) are tested because a drug may affect one species differently from another. Animal testing is used to measure how much of a drug is absorbed into the blood, how it is broken down chemically in the body, the toxicity of the drug and its breakdown products (metabolites), and how quickly the drug and its metabolites are excreted from the body.

2.13.1 *Drosophila* as a drug-discovery ‘tool’

D. melanogaster (fruit fly) can be used as a non-rodent animal for preclinical testing. As a tool for drug discovery, Drosophila has two major advantages over other animals: (i) it is easy to manipulate genetic material both *in vivo* through traditional techniques and in cell culture through RNAi; and (ii) reduced redundancy of the Drosophila genome compared to mammalian systems (Perrimon *et al.*, 2007). Drosophila remains a powerful system for studying the biological effects of existing drugs with known, highly conserved targets (e.g. rapamycin) (Perrimon *et al.*, 2007). Major signaling pathways have distinct, visible phenotypes. There have been several published reports in which *D. melanogaster* were used for both primary screens and secondary validation of biologically active compounds for therapeutic discovery for a wide range of human diseases, ranging from neurodegeneration to cancer (Pandey and Nichols, 2011), alzheimer’s disease (Prüßing *et al.*, 2013), cardiovascular diseases (Bryantsev and Cripps, 2009; Reim and Frasch, 2010), inflammation and Infectious Diseases (Hirth, 2010). The fly has been used as a primary screening platform to probe a drug library of 2000 FDA approved compounds (Pandey and Nichols, 2011). More than 65-70% of human disease genes are present in *D. melanogaster* (Reiter *et al.*, 2001; Pandey and Nichols, 2011; Poddighe *et al.*, 2013), making it an important model to understand not only how the genes induce diseases, but also the discovery of the relation of such genes to diseases (Fortini *et al.*, 2000; Fortini and Bonini, 2000). Compared with other models, *D. melanogaster* offers rapid generation time, ease of use, and easy to maintain in the laboratory in a large quantity due to its tiny body size and short lifespan. The fly has sophisticated innate immune system which enables it to combat bacterial and fungal pathogens but does not have an adaptive immune system. Therefore, a potentially significant

limitation is that the fly is not an appropriate model for the study of antibody and lymphocyte-dependent adaptive immune defenses (Pandey and Nichols, 2011). With respect to drug discovery, a key consideration to take into account are potential differences in the pharmacokinetics and pharmacodynamics of small molecules, which may produce significant discrepancies in drug levels and tissue distribution profiles between mammal and fly. For example, there may be blood-brain permeability differences by neurotherapeutic agent (Stork *et al.*, 2008; Mayer *et al.*, 2009). Another important issue is toxicity. Because of metabolic differences, some drugs may be toxic in flies that are not in humans and vice versa but there seems to be a strong correlation of toxicity between the two species (Pandey and Nichols, 2011).

Routes of drug administration in fly

Studies have pointed out several routes of drug administration to the flies to include vapor (e.g., ethanol and cocaine), sucrose/drug-saturated filter paper, and injection into the abdomen, injection or dropping directly onto the exposed nerve cord of decapitated flies (Pandey and Nichols, 2011; Abolaji *et al.*, 2013). Potential issues determining route of administration include the taste of a drug. The most high-throughput method is to dissolve drug either in normal food substrate, or agarose-sucrose and aliquot into wells of a high-density plate that will contain individual animals. Physiologically effective concentrations can vary from 0.01 to 100 mM in the feeding substrate, although most studies examining the effects of drugs are in the range of 1 to 10 mM. It must be emphasized that these are concentrations in the food; actual physiological concentrations will be much lower, and it may be necessary to examine *in vivo* concentrations using high-performance liquid chromatography or mass spectrometry (Makos *et al.*, 2009; Kuklinski *et al.*, 2010). It is recommended that pilot studies be performed examining three different concentrations of a known effective drug at log dilutions in the feeding substrate (0.03, 0.3, and 3.0 mM) for efficacy in a particular assay and to choose an appropriate concentration based on those results for the full screen (Pandey and Nichols, 2011).

2.14 Summary of literature review

The following summary were drawn from the literature review:

- 1) There is an unmet need for discovery of next generation or alternative drug(s) for treatment of schistosomiasis infection.
- 2) There are reported cases of treatment failures of schistosomiasis with praziquantel or oxamniquine due to resistance or tolerance
- 3) Disease like schistosomiasis can be better treated with drugs that can inhibit more than one drug targets (i.e multi-target drugs).
- 4) Discovery of drugs including multi-target drugs can be achieved through computer-aided approach. This can take the form of predicting new indications for approved drugs which can lead to validation and clinical use.
- 5) *D. melanogaster* can be used as non-rodent model for preclinical testing of compounds for the purpose of drug discovery

CHAPTER THREE

3.0 MATERIALS AND METHODS

3.1 Materials

Software

The following computer software were used for the *in silico* investigations part of the study: Linux operating system (Ubuntu 12.04), AutoDock Vina® AutoDockTools (MGLTools-1.5.6), UCSF Chimera-1.9, Visual molecular dynamics (VMD), GROMACS-4.5.5, Pymol-1.4.1, Openbabel, Grace (xmgrace), g_MMPBSA etc.

Hardware

Computer hardware used for the work was Dell laptop (Intel core i7 with 1 TB of hard disk and 8 GB RAM).

Database/online tools

The following databases/online tools were used for the study: Protein data bank (PDB), ZINC database, Molinspiration online tool, SWISS MODEL, Basic Local Alignment Search Tool (BLAST), Flybase, Drug bank etc.

Reagents/drugs

Nipagin, Agar-agar (High strength gel, Fluka Chemie GMBH). The approved drugs (praziquantel, haloperidol and vildagliptin) used in the study were commercially sourced from pharmacy in Onitsha while oxytetracycline was sourced from a pharmacy in Awka, Nigeria. Information about the drugs is presented in Appendix 3.

Animal

D. melanogaster (Harwich strain) was a gift from Dr. A.O Abolaji from Drosophila Laboratory, Molecular Drug metabolism and Toxicology, Department of Biochemistry, College of Medicine, University of Ibadan, Ibadan, Nigeria.

3.2 Methods

3.2.1 Study site

The study was conducted at Faculty of Pharmaceutical Sciences, Nnamdi Azikiwe University, Awka, Nigeria.

3.2.2 Experimental design

The study was designed to include creation of database of Food and Drug Administration (FDA) of US approved drugs, bioinformatics mining of schistosomal drug targets, molecular docking and dynamics simulations, determination of conservation of schistosomal drug targets and human liver enzymes in *D. melanogaster* including survival rates and longevity of *D. melanogaster* fed with some of the predicted approved drugs (Figure 3.1).

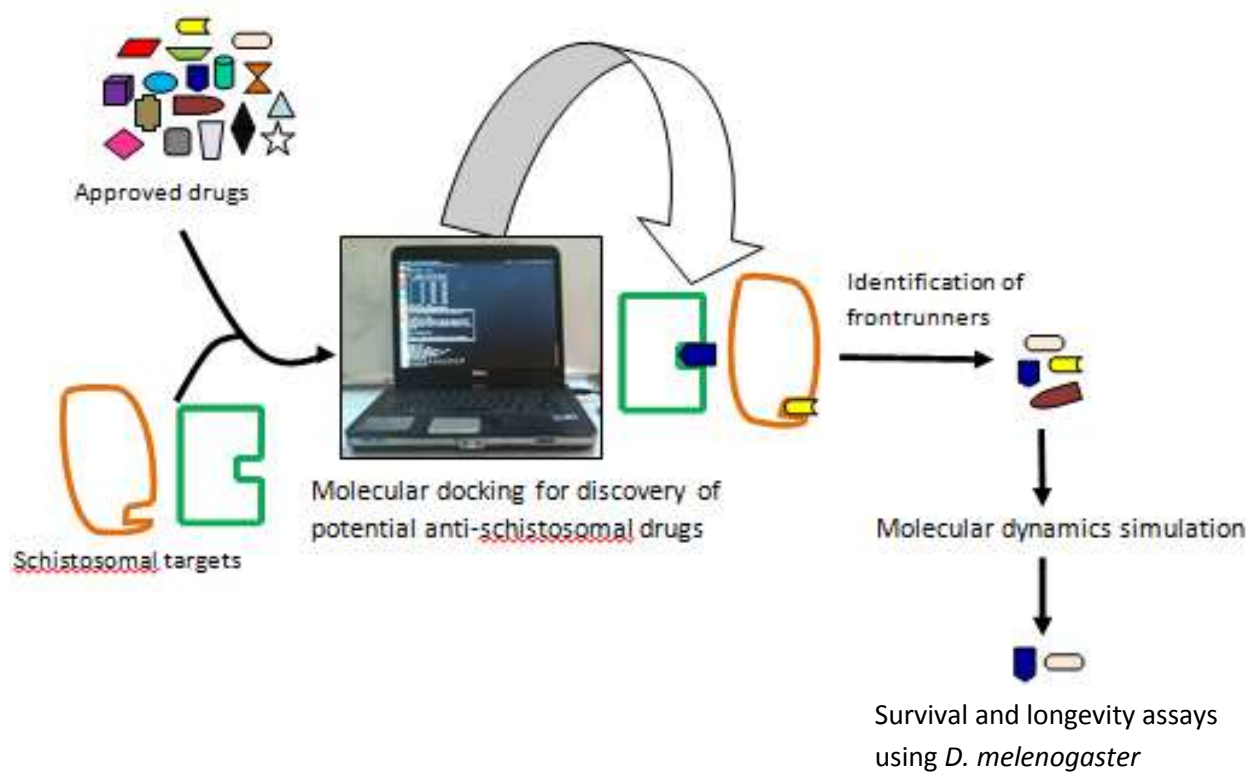


Figure 3.1: Experimental design

3.2.3 *In silico* investigations

Several *in silico* techniques such as bioinformatics mining, molecular docking simulations, molecular dynamics simulations, binding energy computations with g_MMPBSA algorithm e.t.c were implemented on Linux machine (Dell, Intel core i7 with 1.0 TB hard disk and 8 GB RAM) as presented below:

3.2.3.1 Creation of in-house database of approved drugs

An in-house database of approved drugs was created using DrugBank available at <http://www.drugbank.ca>, Zinc® Database available (Irwin *et al.*, 2012) and molinspiration online software available at <http://www.molinspiration.com>. Briefly, DrugBank was queried for all drugs and filtered for all approved drugs. Physicochemical parameters [molecular weight (Mw), topological polar surface area (tPSA), octanol water partition coefficient (xLogP)] of the drugs at pH 7.0 were obtained from ZINC® database. Bioactivities (G-protein coupled receptor (GPCR) ligand, ion channel modulator (ICM), nuclear receptor ligand (NRL), kinase inhibitor (KI), protease inhibitor (PI) and enzyme inhibitor (EI)) of the drugs were predicted with SMILES using molinspiration online tools (www.molinspiration.com).

3.2.3.2 Bioinformatics mining of schistosome drug targets

Schistosomal thioredoxin glutathione reductase and four other proteins were identified as potential drug targets for schistosomiasis through bioinformatic mining of tropical diseases research (tdr) database available at www.tdrtargets.org. Briefly, the database was filtered for all *S. mansoni* targets, followed by another filtration on the essentiality of the targets and then protein databank crystal structures as no record was found on the druggability index of the targets. The druggability indexes of the five essential targets were calculated as described elsewhere (Volkamer *et al.*, 2012) on <http://dogssite.zbh.uni-hamburg.de> because they were not available in www.tdrtargets.org as at the time of the investigation. Three of the five essential targets (Thioredoxin glutathione reductase, Hexokinase and Eukaryotic translation initiation

factor 4e) from druggability index calculation were compared with similar proteins in humans using National Center for Biotechnology Information (NCBI) Basic Local Alignment Search Tool (BLAST). Briefly, the amino acid sequences of the three targets were retrieved in FASTA format from Research Collaboratory for Structural Bioinformatics (RCSB) protein data bank (PDB) database. The retrieved sequences were used as query sequences and were BLAST against *Homo sapiens* (Human) sequences using blastp available at BLAST NCBI after setting the BLAST parameters. The selected drug target from BLAST search and three other drug targets for schistosomiasis used in this work were identified through bioinformatic mining of RCSB protein data bank using standard drugs for treatment of schistosomiasis (praziquantel and oxamniquine) or schistosome as keywords. The 3-D coordinates of the four identified schistosomal drug targets were obtained from RCSB protein DataBank and used for the *in silico* investigations.

3.2.3.3 Examination of selected schistosomal drug targets for missing residues

The suitability of the selected targets for computational studies was examined by checking for missing residues or missing atoms in residues using less command of Linux systems. Crystal structures that have missing residues between the N- and C- terminals of the coordinates were subjected to homology modeling using SWISS-MODEL online tool while those that had missing atoms in a residue were corrected by manual structure editing.

3.2.3.4 Homology modeling of missing residues in sulfotransferase

Homology modeling of missing residues (Pro65, Pro66, and Pro67) in schistosomal sulfotransferase (4MUB) was achieved with SWISS-MODEL online tool (Guex and Peitsch 1997, Arnold *et al.*, 2006; Bordoli *et al.*, 2009) using automatic mode. Template search with Blast and HHblits was performed against the SWISS-MODEL template library. The target sequence was searched with BLAST (Altschul *et al.*, 1997) against the primary amino acid sequence contained in the SMTL. An initial HHblits profile was built using the procedure outlined in Remmert *et al.*, (2011), followed by 1 iteration of HHblits against NR20 and the

obtained profile was searched against all profiles of the SMTL and templates were selected. Template's quality was predicted from features of the target-template alignment and the template with highest quality was selected for modeling the missing residues. The model was built based on the target-template alignment using ProMod3 and coordinates which are conserved between the target and the template are copied from the template to the model. Insertions and deletions were remodeled using a fragment library while side chains are rebuilt. Finally, the geometry of the resulting model was regularized by using a force field. The global and per-residue model quality was assessed using QMEAN scoring function (Benkert *et al.*, 2011). The results were generated and ranked according to their sequence identity with the template. The model was considered sufficiently reliable when there is more than 50 % sequence identity between the template and the targets proteins (Arnold *et al.*, 2006).

3.2.3.5 Selection of approved drugs using reference compounds

Bioactivities of four (4) reference compounds/drugs (praziquantel, oxamniquine, auranofin (ridaura) and [propylamino-3-hydroxy-buta-1,4-dionyl]-isoleucylproline were used for selection of approved drugs from an in-house database of approved drugs using correlation graphing techniques. It is important to note that the bioactivities of [Propylamino-3-hydroxy-buta-1,4-dionyl]-isoleucylproline which was not previously in the in-house database was calculated with molinspiration online tool before its use in the selection of the approved drugs. This was achieved by extraction of its 3-D coordinate from cathepsin B1 (3QSD). The extracted structure was then subjected to 1000 steps of steepest descent and 100 steps of conjugate gradient energy minimization/geometry optimizaton at step size of 0.02 after addition of hydrogens and AM1-BCC charges using UCSF Chimera-1.9 (Pettersen *et al.*, 2004). Then, the geometrically optimized structure was converted to SMILES format using openbabel-2.3.0 (O'Boyle *et al.*, 2011) and was used for prediction of its bioactivities and molecular properties on Molinspiration® online tool.

The best two bioactivities of the reference compounds were used to query the in-house database of approved drugs in order to select about 100 drugs in the neighborhood of the bioactivities of the reference compounds. For example, GPCR ligand and protease inhibitor; GPCR ligand and Ion channel modulator; Enzyme inhibitor and GPCR ligand and protease inhibitor and GPCR ligand bioactivities were used for selection of approved drugs for praziquantel, oxamniquine, auranofin and [Propylamino-3-hydroxy-buta-1,4-dionyl]-isoleucylproline respectively. Also, negative controls with bioactivities of between -3 to -4.15 were selected using the two best bioactivities of the reference compounds.

3.2.3.6 Validation of molecular docking simulation protocols

In order to validate the molecular docking simulations protocol, the experimental complexes of the reference compounds (praziquantel, oxamniquine, auranofin and [propylamino-3-hydroxy-buta-1,4-dionyl]-isoleucylproline) with their respective targets were reproduced *in silico*. Briefly, the drug targets in complex with their reference compounds were obtained from the RCSB Protein DataBank (Berman *et al.*, 2000) using bioinformatics mining and prepared for molecular docking simulations. To this end, the reference compounds and all hetero-molecules in the targets were deleted with Chimera-1.9 (Pettersen *et al.*, 2004); polar hydrogen, Kollman charges, grid box sizes and centers at grid space of 1.0 Å (Appendix 4) were determined with MGLTools-1.5.6 (Michel, 1999; Morris *et al.*, 2009). Then reference compounds coordinates except propylamino-3-hydroxy-buta-1,4-dionyl]-isoleucylproline were obtained from ZINC® database (Irwin *et al.*, 2012). Propylamino-3-hydroxy-buta-1,4-dionyl]-isoleucylproline was extracted from its receptor and subjected to 1000 steps of steepest decent and 100 steps of conjugate gradient energy minimization at step size of 0.02 using Chimera-1.9. All the reference compounds were prepared for molecular docking simulations using MGLTools-1.5.6 (Michel, 1999; Morris *et al.*, 2009). Briefly, all hydrogen were added, roots were detected; torsions and all rotatable bonds were allowed in their natural states. Then outputs were generated in pdbqt extension. Molecular docking simulations were implemented locally using AutoDockVina®

(Trott and Olson, 2010) on a Linux platform using configuration file and script (Appendix 4).

Docked conformations were visualized in PyMol-1.4.1 and docked poses were compared with the experimental crystal structures of the reference compounds.

3.2.3.7 Preparation of selected receptors and approved drugs

Four schistosome targets [Glutathione s-Transferase (1gtb), thioredoxin glutathione reductase (3h4k), cathepsin B1 (3qsd), sulfotransferase (4mub)] were obtained from RCSB protein DataBank (Berman *et al.*, 2000) using bioinformatics mining. They were prepared for molecular docking simulations using MGLTools-1.5.6 (Michel, 1999; Morris *et al.*, 2009) and UCSF Chimera-1.9 as reported in the validation of docking simulation protocol section. Approved drugs were selected by querying of an in-house database of approved drugs using four different probes (praziquantel, oxamniquine, auranofin and propylamino-3-hydroxy-buta-1,4-dionyl]-isoleucylproline) and correlation graphing techniques. The 3-D coordinates of the selected approved drugs (612) including their isomers were obtained from ZINC® database (Irwin *et al.*, 2012) and prepared for docking simulation using MGLTools-1.5.6 (Michel, 1999; Morris *et al.*, 2009 as reported in the validation of docking simulation protocol section. The prepared receptors and drugs were used for molecular docking simulations after validation of the docking protocols.

3.2.3.8 Molecular Docking simulations

The prepared selected drugs were docked into their respective targets using AutoDockvina® (Trott and Olson 2010) and the molecular docking simulations were done in quadruplet on a Linux platform using configuration file and script presented in Appendix 4.

3.2.3.9 Molecular dynamics simulations

In order to incorporate biomolecular dynamics in our investigation, molecular dynamics (MD) simulations were performed on representative coordinates of the free and target-frontrunner

complexes using Groningen Machine for Chemical Simuations (GROMACS) simulation package (Pronk *et al.*, 2013; Hess *et al.*, 2008). Gromos53a6 (Oostenbrink *et al.*, 2004) simulation parameters generation involving, geometry optimization at the Becke 3-parameter, Lee-Yang-Parr (B3LYP) quantum mechanics level were performed for different conformations of the frontrunners (diflunisal, tolmetin and dinesterol) and reference compounds (oxamniquine and auranofin) using the Automatic Topology Builder (ATB) (Malde *et al.*, 2011) or PRODRG (Schüttelkopf and van Aalten, 2004). The ATB codes for the generated topologies are presented in Appendix 5. The crystal structure coordinates of the targets (thioredoxin glutathione reductase (3h4k), and sulfotransferase (4mub)]) obtained from RCSB Protein Databank (Berman *et al.*, 2000) and their complexes with best poses from molecular docking simulations were considered for the MD simulations of free targets and target-fronrunner complexes respectively. Before the dynamics simulations, FAD present in TGR was stripped off and subjected to 100 steps of steepest decent and 10 steps of conjugate gradient energy minimization at the step size of 0.002 using UCSF Chimera-1.9. Topology of the FAD was generated with PRODRG online tool and used for the molecular dynamics simulations. Both free and fronrunner bound complexes of the target were inserted into a simulation box with minimum distance of 15 Å between the box edge (Weber *et al.*, 2000). The boundaries were treated with periodic boundary condition involving the immersion of the simulation unit in periodic images of itself in the x, y and z directions. The setups were subjected to 100 - 200 steps of *in vacuo* energy minimization using steepest descent algorithm. Then the systems were solvated using pre-equilibrated coordinates of the SPC explicit water model (Berendsen *et al.*, 1981). Sodium and chloride ions (Na^+ and Cl^-) were added to neutralize the system and to model physiological salt concentration of 154 mM. The systems were further minimized using 200 to 300 steps of steepest descent algorithm followed by 50 ps of position restrained dynamics where targets and target-fronrunner complexes were kept fixed by adding restraining forces, but water molecules were allowed to move. The P-LINCS (Hess, 2007) algorithm was used to constrain bond lengths, allowing the

use of 2 fs time steps. Short-range non-bounded interactions were truncated at 12 Å and employed the Particle-Mesh Ewald (PME) method (Darden *et al.*, 1993; Essmann *et al.*, 1995) in computing the long-range electrostatic interactions. Final production MD simulations were performed in the isothermal isobaric (NPT) ensemble at 300 K, using v-rescale (Bussi *et al.*, 2007) as external bath with a coupling constant of 0.1 ps. Pressure was kept constant (1 bar) by using the time-constant for pressure coupling of 0.5 ps and Parrinello-rahmanbarostat (Bussi *et al.*, 2007) for pressure coupling. Both free targets and their complexes with frontrunners were subjected to 3000 ps (3.0 ns) of molecular dynamics simulations and conformations generated during the simulations were stored every 2 and 4 ps for simulations involving free and ligand bound sulfotransferase and TGR respectively. Some basic steps in the MD simulations and the molecular dynamics parameter files used are presented in appendix 6. Cluster analysis was performed using the algorithm reported elsewhere (Daura *et al.*, 1999) with a clustering cutoff of 1.5 Å and cluster groups were identified for free and fronrunner bound complexes. The Daura method involves pooling all sampled conformations and counting the number of neighbors within a preselected cutoff radius. The conformation with the highest number of neighbors together with its neighbors constituting a cluster is eliminated from the pool; the process is repeated until all sampled conformations have been assigned to clusters.

3.2.3.10 Calculation of binding energy

The binding energy was calculated using g_MMPSA (Kumari *et al.*, 2014) algorithm. The energy components E_{MM} , G_{polar} , and $G_{nonpolar}$ of sulfotransferase-fronrunner complexes were calculated for 700 snapshots extracted every 2 ps from the production trajectories from 900 to 2300 ps while that of thioredoxin glutathione reductase fronrunner complexes were calculated for 550 snapshots extracted every 4 ps from the production trajectories from 200 to 2400 ps. E_{MM} was calculated using the Leonard Jones (LJ) and Coulomb potential. To calculate G_{polar} , a box was generated using the extreme coordinates of the molecular complex in each dimension. The box was then expanded in each dimension by 2-fold to obtain a coarse-grid box ($cfac = 2$). A

finer grid-box was then placed within the coarse grid-box extending 20 Å ($fadd = 20$) from the complex's extreme coordinates in each direction. An ionic strength of 0.154 M NaCl with radii of 0.95 and 1.81 Å for sodium and chloride ions respectively was used during all G_{polar} calculations. The values for the vacuum (v_{die}) and solvent (s_{die}) dielectric constants were taken as 1 and 80 respectively. The linear PB equation was solved using APBS. G_{nonpolar} was calculated using different nonpolar model parameters reported elsewhere (Kumari *et al.*, 2014).

3.2.3.11 Determination of conservation of schistosoma drug targets and human liver enzymes in drosophila

Determination of conservation of the schistosoma drug targets and human liver enzymes in drosophila was achieved with BLASTp in FlyBase online tool (Altschul *et al.*, 1997). Briefly, blast search of the schistosomal targets [glutathione s-transferase (1gtb), thioredoxin glutathione reductase (3h4k), cathepsin B1 (3qsd), sulfotransferase (4mub)] and human liver enzymes [aspartate aminotransferase (3WZF), alkaline phosphatase (2GLQ) and alanine:glyoxylate aminotransferase (5F9S)] were performed against *D. melanogaster* after retrieval from protein data bank in fasta format using blastp and BLOSUM62 matrix.

3.2.4 Longevity and survival rate assays using *D. melanogaster*

D. melanogaster was used as a non-rodent model for survival rates and longevity testing of three of the predicted approved drugs with possible inhibitory activities against schistosoma species. Twenty (20) *D. melanogaster* (Harwich strain) of 1 to 3 days old were separated according to their sexes after immobilization on ice and maintained on 5.0 g feed treated with different doses (0 – 0.6 mg) of praziquantel, oxytetracycline, haloperidol or vildagliptin at 25 °C, and 12 h dark/light cycle. The longevity and survival rates were expressed as percentage of live flies. The longevity and survival rate assays were achieved as described in section 3.2.4 .1 to 3.2.4.4 below.

3.2.4.1 *Drosophila melanogaster* stock and culture

D. melanogaster (Harwich strain) was a gift from Dr. A.O Abolaji, Drosophila Laboratory, Molecular Drug metabolism and Toxicology, Department of Biochemistry, College of Medicine, University of Ibadan, Ibadan, Nigeria. The flies were maintained and reared on cornmeal medium prepared as described in preparation of drosophila feed section at constant temperature and humidity (25 °C; 60 % relative humidity, respectively) under 12 h dark/light cycle conditions. All the experiments were carried out with the same *D. melanogaster* strain.

3.2.4.2 Preparation of drosophila feed

Eight hundred and fifty milliliter (850 ml) of water was measured and 250 ml of the water was used to dissolve 52 g of cornmeal. The remaining 600 ml was boiled for 10 minutes and 100 ml of the boiling water was used to dissolve 10 g of yeast. Exactly 7.9 g of agar-agar was added to the remaining 500 ml of boiling water and boiled for 10 min with constant stirring. The cornmeal slurry was added and allowed to boil for 10 min with constant stirring. Then, the yeast was added and allowed to boil for another 10 min. The set-up was allowed to cool to about 50 to 60 °C and nipagin (1.0 g/2ml absolute ethanol) was added and thoroughly mixed. The feed was dispensed into the vials and allowed to solidify.

3.2.4.3 Preparation of doses of tested drugs

Different doses of praziquantel, oxytetracycline, haloperidol and vildagliptin were prepared as described below and used for the longevity and survival rates experiments.

Praziquantel

Stock solution of praziquantel (1.0 mg/ml) was prepared by dissolving 600 mg of PZQ with some quantity of distilled water. The dissolved PZQ was made up to 30 ml with distilled water to give 20 mg/ml solution of PZQ. The 20 mg/ml solution was further subjected to 1:20 dilution to obtain a working PZQ solution of 1.0 mg/ml. Since the dose of PZQ in human is 60 mg/kg body weight for three times a day and our interest is to maintain the flies in 5.0 g feed. Therefore,

different doses of PZQ (0.0 – 0.6 mg) were obtained from the 1.0 mg/ml PZQ stock solution and incorporated into the 5.0 g fly feed. See Appendix 7.

Oxytetracycline

Stock solution of oxytetracycline (10 mg/ml) was prepared by dissolving 250 mg of oxytetracycline with some quantity of distilled water. The dissolved oxytetracycline was made up to 25 ml with distilled water to give 10 mg/ml solution of oxytetracycline. The 10 mg/ml solution was further subjected to 1:10 dilution to obtain a first working oxytetracycline solution of 1.0 mg/ml. Also, part of the first working oxytetracycline solution of 1.0 mg/ml was further subjected to 1:10 dilution to obtain second working oxytetracycline solution of 0.1 mg/ml. Since the dose of oxytetracycline in human is 50 mg/kg body weight and our interest is to maintain the flies in 5.0 g feed. Therefore, different doses of oxytetracycline (0.0 – 0.5 mg) were obtained from the 1.0 mg/ml and 0.1 mg/ml oxytetracycline working solutions and incorporated into the 5.0 g fly feed (See Appendix 7).

Haloperidol

Stock solution of haloperidol (0.1 mg/ml) was prepared by dissolving 5 mg of haloperidol with some quantity of distilled water. The dissolved haloperidol was made up to 50 ml with distilled water to give 0.1 mg/ml solution of haloperidol. The 0.1 mg/ml solution was further subjected to 1:10 dilution to obtain a first working oxytetracycline solution of 0.01 mg/ml. Also, part of the first working haloperidol solution of 0.01 mg/ml was further subjected to 1:10 dilution to obtain second working haloperidol solution of 0.001 mg/ml. Since the dose of haloperidol in human is 1.5 mg – 3.0 mg for two or three times daily, 3.0 mg – 5.0 mg for two or three times daily, or 30 mg/day and our interest is to maintain the flies in 5 g (5.0 g) feed. Therefore, different doses of haloperidol (0.0 – 0.002 mg) were obtained from the 0.001 mg/ml and 0.01 mg/ml haloperidol stock solutions and incorporated into the 5.0 g fly feed (See Appendix 7).

Vildagliptin

Stock solution of vildagliptin (1.0 mg/ml) was prepared by dissolving 50 mg of vildagliptin with some quantity of distilled water. The dissolved vildagliptin was made up to 50 ml with distilled water to give 1.0 mg/ml solution of vildagliptin. The 1.0 mg/ml solution was further subjected to 1:10 dilution to obtain a first working vildagliptin solution of 0.1 mg/ml. Also, part of the first working vildagliptin solution of 0.1 mg/ml was further subjected to 1:10 dilution to obtain second working haloperidol solution of 0.01 mg/ml. Since the dose of vildagliptin in human is 100mg/day in two divided doses (i.e 50 mg in the morning and 50 mg in the evening) and our interest is to maintain the flies in 5 g (5.0 g) feed. Therefore, different doses of vildagliptin (0.0 – 0.014 mg) were obtained from the 0.1 mg/ml and 0.01 mg/ml vildagliptin stock solutions and incorporated into the 5.0 g fly feed (See Appendix 7).

3.2.4.4 Drug exposure and percentage survival rate analyses

D. melanogaster of 1 to 3 days old were separated according to sex after immobilization on ice. The separated flies were divided into groups of 20 flies each: In order to determine the doses of drugs (praziquantel, oxytetracycline, haloperidol and vildagliptin) and the duration of exposure to be used in the experiment, longevity assays were carried out. The assay consist of 5 to 6 independent experiments with each containing three replicates of each of the doses of the drugs that were tested, in vials containing 20 flies each with change of diet for every four days. See Appendix 8. The survival rate was determined across the doses, by recording the number of live and dead flies daily. At the end of the experiments, the data was analyzed and plotted as percentage of live flies as reported by Abolaji *et al.*, (2014).

3.2.5 Statistical analysis

The binding affinities from molecular docking simulations were calculated and reported as mean ± SD. The drugs were ranked according to their binding affinities for their respective receptors and compared with the probe compounds. The drugs with concurrent high binding affinities were

identified with Microsoft excel. Docked poses were visualized with Pymol-1.4.1 and best poses were selected based on compound intactness, presence inside the binding pockets of the receptors and binding energy values.

All the MD simulation analyses were carried out using the available trajectory analysis tools of GROMACS packages. Visualization was performed with VMD-1.9 (Humphery *et al.*, 1996) or PyMol-1.4.1 while graphs from MD simulation trajectories were plotted and formatted with Grace plotting program. The longevity and survival rates of *D. melanogaster* were expressed as percentage of live flies and plotted with GraphPad Prism-5.0 GraphPad Software, San Diego California USA, www.graphpad.com and SigmaPlot-11.0. Side chain of amino acid residues and functional groups in diflunisal and tolmetin involved in interaction were generated with ChemDraw Ultra-12.0

CHAPTER FOUR

4.0 RESULTS AND DISCUSSION

4.1 Results for selection of schistosome drug targets

Bioinformatic mining of tropical disease research (tdr) database showed a total of 13331 targets for *S. mansoni* as at 14th February, 2014. Only 3375 of the targets are essential for the parasite and only five (5) of the essential targets had their structures available in protein data bank (Table 4.1). Since the five targets had no record for druggability index in TDR database, their druggability index, druggable pockets, sub-pockets properties were calculated with DoGSiteScorer online tool and the result is presented in Table 4.2 and Appendix 9. The five targets (Table 4.1) were also subjected to BLASTp search against human proteins using NCBI BLAST online tool and the result is presented in Table 4.3 and appendix 10. At the end of the BLASTp search, thioredoxin glutathione reductase (3H4K) was selected from the five targets (Table 4.3). Also schistosomal glutathione s-transferase (1GTB), thioredoxin glutathione reductase (3H4K), cathepsin B1 (3QSD) and sulfotransferase (4MUB) were identified and obtained from protein data bank using bioinformatic mining as described in material and method section. They showed good resolutions. The four schistosomal targets were used for further investigations.

Table 4.1: Bioinformatic mining of five schistosomal targets

Organism	Name	Ortholog group	Target	Pdb code
<i>S. mansoni</i>	Smp_001500	OG4_10783	Eukaryotic translation initiation factor 4e, putative	3HXG, 3HXI
<i>S. mansoni</i>	Smp_008070	OG4_10080	Thioredoxin, putative	2XBI
<i>S. mansoni</i>	Smp_043030	OG4_10257	Hexokinase	1BDG
<i>S. mansoni</i>	Smp_048430	OG4_10249	Thioredoxin glutathione reductase	3H4K, 2X8G, 2X8H, 2X99, 2X8C
<i>S. mansoni</i>	Smp_058690	OG4_10219	Glutathione peroxidase	2V1M

Table 4.2: Druggability index and druggable pockets of five schistosomal targets

Target	Pdb code	Highest druggability index	Pocket(s)
Eukaryotic translation initiation factor 4e, putative	3HXG	0.85	Po
	3HXI	0.76	Po
Thioredoxin, putative	2XBI	0.53	Po
Hexokinase	1BDG	0.79	Po
Thioredoxin glutathione reductuase	3H4K	0.81	Po
	2X8G	0.82	P1
	2X8H	0.81	Po
	2X99	0.81	Po
	2X8C	0.86	P2
Glutathione peroxidase	2V1M	0.54	P1 and P2

Table 4.3: Summary of schistosomal thioredoxin glutathione reductase blast search against human proteins

Sequence id (in a database)	Score (bits)	E value	Identities (%)	Positives (%)	Gaps (%)
Pdb 3H8Q A	58.9	3e-09	28	57	1
Pdb 2HT9 A	62	4e-10	30	54	0
Emb CAA3836.1	68.2	9e-12	27	48	13
Pdb 2CFY A	597	0.0	61	75	1
Gb AAD25167.1 AF044212_1	510	6e-174	53	70	2
Pdb 2J3N A	600	0.0	61	76	1
Pdb 2ZZ0 A	601	0.0	61	76	1
Gb AAD39929.1 AF133519_1	609	0.0	54	70	1
Gb AAD51325.1 AF171055_1	612	0.0	54	70	1
Gb AAL15432.1	635	0.0	55	71	2
Gb EAW97743.1	640	0.0	55	71	2

4.1.1 Results for examination of targets for missing residues

All the targets do not show missing residues in between N- and C- terminals except sulfotransferase which showed Pro65, Pro66 and Pro67 to be missing between its N- and C- terminals.

4.1.2 Results of homology modeling of missing residues in sulfotransferase

Missing amino acid residues (Pro65, Pro66 and Pro67) in schistosomal sulfotransferase were successfully modeled from the starting structure as can be seen in Figure 4.1. The model was sufficiently reliable because sequence identity of 98.8 % with its template.

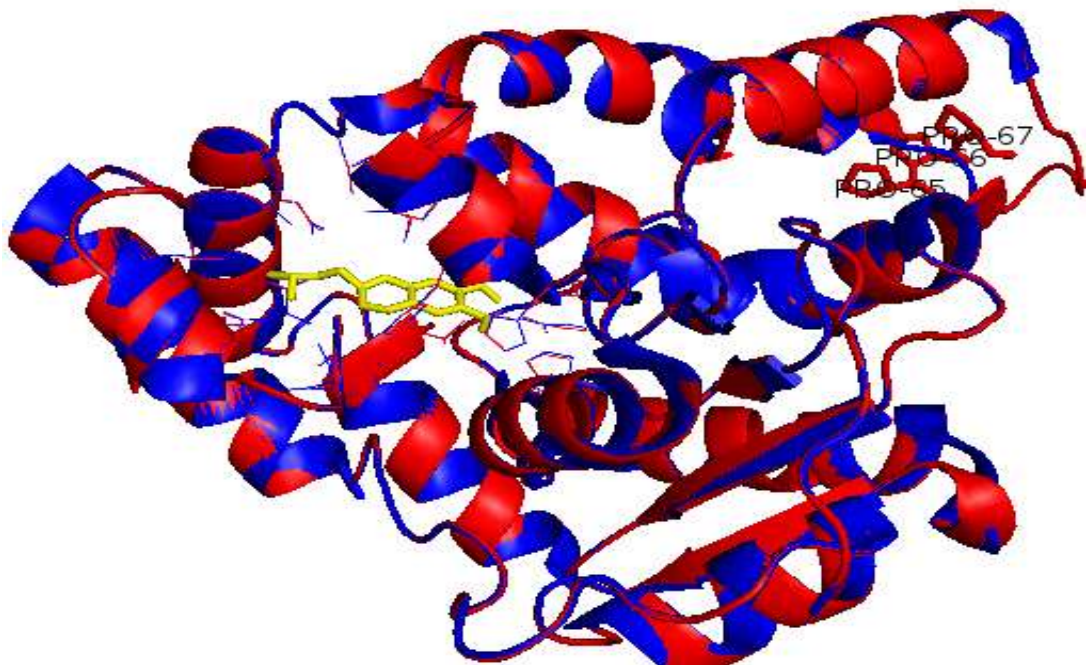


Figure 4.1: Structural alignment of modeled schistosomal sulfotransferase and its template showing modeled amino acid residues (Pro65, Pro66 and Pro67). Yellow stick representation is oxamniquine.

4.1.3 Results for selection of approved drugs

A total of six hundred and twelve (612) drugs including their isomers and derivatives were selected with four (4) reference compounds (probes). Selections with praziquantel, oxamniquine, auranofin and propylamino-3-hydroxy-buta-1,4-dionyl]-isoleucylproline afforded two hundred and twenty five (225), one hundred and forty six (146), one hundred and twenty (120), and one hundred and twenty one (121) compounds respectively. The compounds were selected using the two highest bioactivities of the reference compounds and the selected drugs are shown in Figure 4.2 and Appendix 11.

4.1.4 Results of validation of docking simulation protocols

In order to prove that our docking simulation protocol is able to successfully predict anti-schistosomal activities of tested approved drugs, validation of molecular docking simulation protocols were carried out first. The ability of the protocol to reproduce wet laboratory binding of the reference compounds to the receptors was successfully implemented *in silico*. The reference compounds were found to sit in the expected binding pocket/site of the targets (Figure 4.3) and the amino acids at the binding sites of the docked and wet laboratory experimental complexes are presented in Appendix 12.

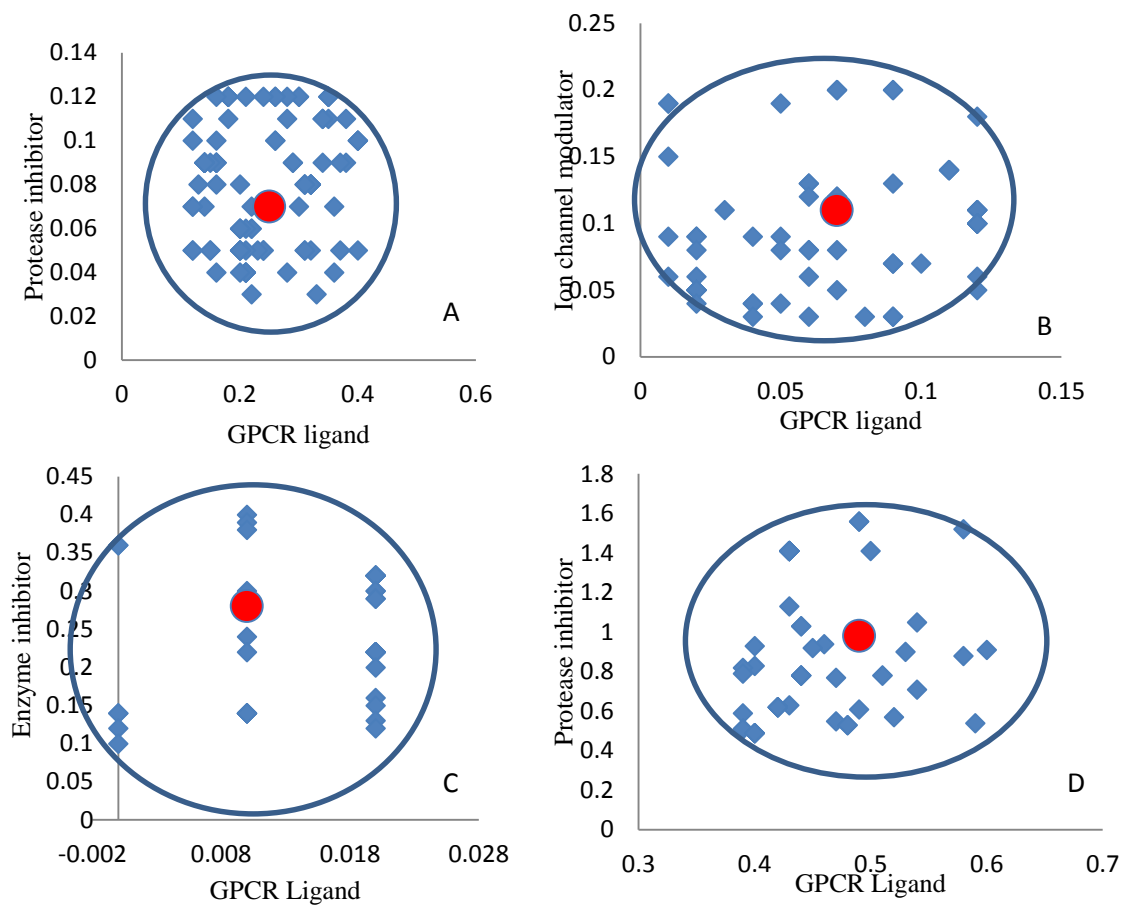


Figure 4.2: Selected approved drugs with activities in the neighborhood reference compounds
 (A) praziquantel (B) oxamniquine (C) propylamino-3-hydroxy-buta-1,4-dionyl]-isoleucylproline
 and (D) auranofin. Red circular spots are the reference compounds while blue square spots are
 approved drugs.

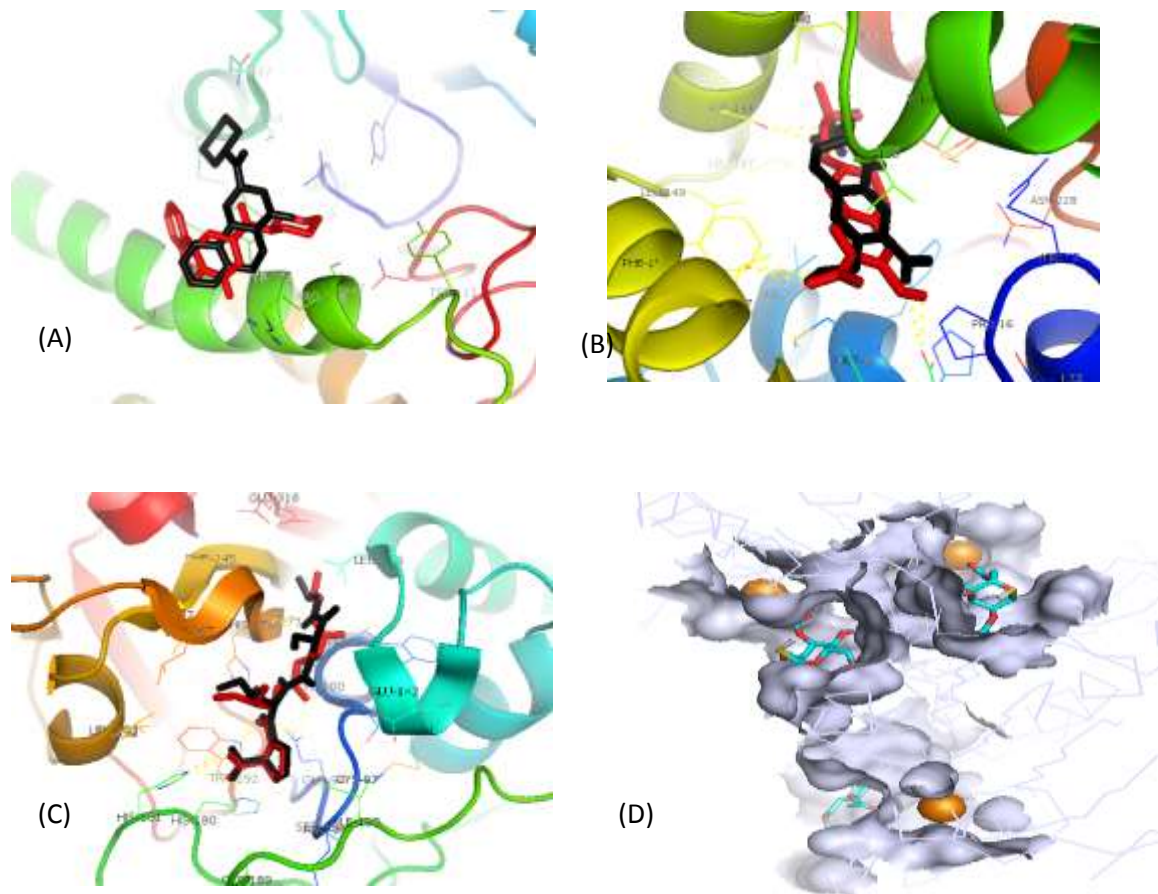


Figure 4.3: Validation of molecular docking simulation protocols of reference compounds and target interactions: (A) Praziquantel and GST (B) Oxamniquine and sulfotransferase (C) Auranofin and TGR (D) Propylamino-3-hydroxy-buta-1,4-dionyl]-isoleucylproline and cathepsin B1. In (A), (B) and (C) experimental complexes of the reference compounds are represented with black sticks color while the docked reference compounds are shown as red colour. In (D) yellow spheres are gold molecules from auranofin in the experimental complex while the stick representations are the docked auranofin molecules.

4.1.5 Results of molecular docking simulations

The results of molecular docking simulations experiments are presented in Table 4.4, Figure 4.4, and Appendix 13 with their previous indications. It is evident from Figure 4.4 that uni and multi-targets approved drugs with possible anti-schistosomal activities have been identified (Appendix 13). The uni and multi-targets approved drugs are exploiting the same binding pockets as the reference compounds in their respective targets (Figure 4.4). Three approved drugs with possible multi-target inhibitory activities against schistosoma species were identified and their binding affinities ranged from -7.7250 ± 0.813 kcal/mol to -8.575 ± 0.0177 kcal/mol (Table 4.4).

Molecular docking simulations results showed that the frontrunners including tolmetin, diflunisal and dinesterol bind and exploit the same binding sites on sulfotransferase and thioredoxin glutathione reductase (Figure 4.4). Molecular docking simulation showed that diflunisal, tolmetin and dinesterol are possible multi-target inhibitors of schistosomal sulfotransferase and TGR.

Table 4.4: Frontrunners with concurrent binding affinities for two targets

Drugs	Zinc code	Affinity (kcal/mol)	Affinity (kcal/mol)	Average affinity (kcal/mol)
		(TGR)	(sulfotransferase)	
Diflunisal	20243	-8.600	-8.575	-8.5875±0.0177
Tolmetin	2191	-7.425	-8.100	-7.7625±0.477
Dienestrol	1283	-7.150	-8.300	-7.7250±0.813

The average binding affinities for praziquantel and oxamniquine for their respective targets (GST and sulfotransferase) are -6.50 ± 0.0 kcal/mol and -7.50 ± 0.0 kcal/mol respectively

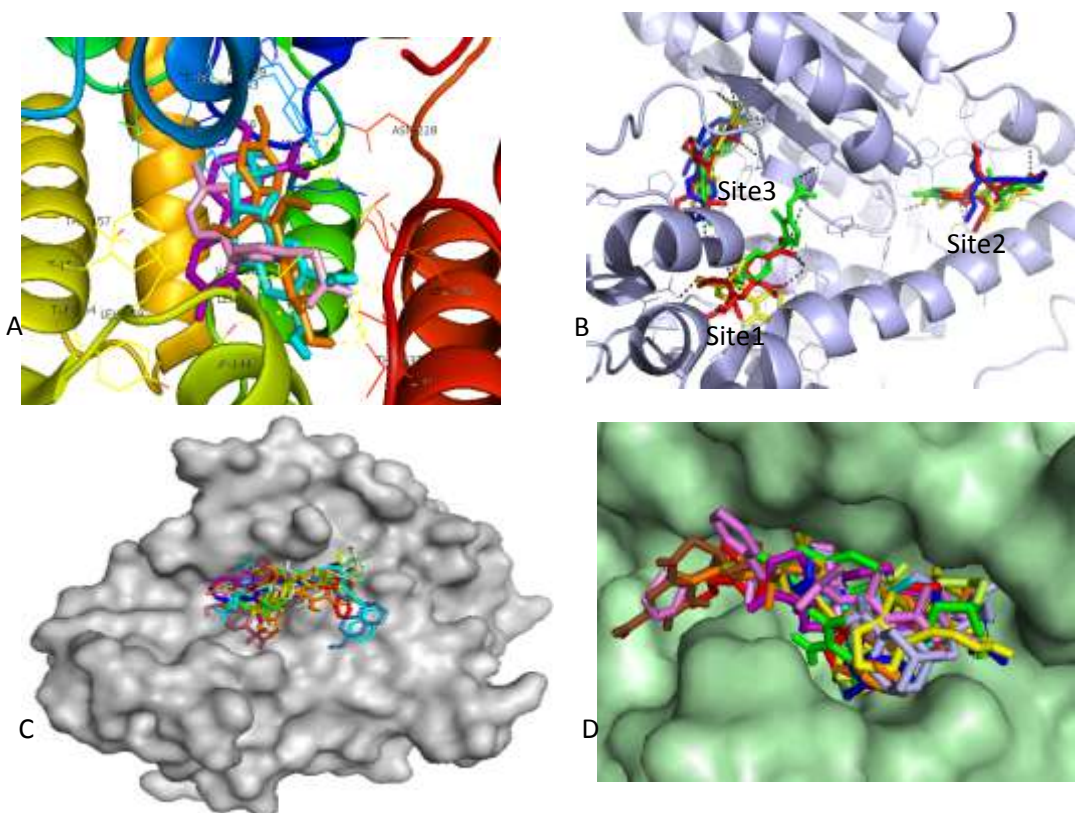


Figure 4.4: Binding site analysis of the frontrunners for (A) sulfotransferase (4mub): Frontrunners are represented in sticks. Dinesterol is colored brown, Diflunisal is colored pink, Tolmetin is colored light blue color, while oxamniquine is colored purple (B) Thioredoxin glutathione reductase (3H4K): diflunisal, auranofin, dienestrol and tolmetin are shown as yellow, red, blue and green stick color respectively while black dots represents polar contacts. (C) and (D) are sulfotransferase and TGR respectively showing that uni and multi-target drugs are exploiting the same binding pockets in the targets.

4.1.6 Results of molecular dynamics simulations

Results from molecular dynamics preparations, trajectories of energy minimizations, position restrained dynamics and productions runs were analyzed and presented below:

4.1.6.1 Molecular dynamics simulations preparation results

The molecular systems (targets or target-fronrunner complexes) were well solvated with simple point-charge (SPC) explicit water molecules to model the physiological system of about 70 % water and neutralized with sodium and chloride ions (Na^+ and Cl^-) to model the physiological system of salt concentration of 154 mM and neutral pH (Figure 4.5).

4.1.6.2 Energy minimization results

The *in vacuo* energy minimization of the molecular systems (Figure 4.6 A and C) followed by that of solvated molecular systems (Figure 4.6 B and D) indicate successful removal of restraining forces in the starting molecular coordinates and systems at global energy minima (Figure 4.6). This means that the geometry of the targets (sulfotransferase and TGR) and their bound ligands (auranofin, oxamniquine, diflunisal, tolmetin or dinesterol) were optimized and brought to global energy minima (Figure 4.6) prior to the postion restrained steps.

4.1.6.3 Position restraints dynamics results

The 50 ps position restrain molecular dynamics simulations of the molecular systems (target, and its ligand bound complexes) showed well soaked systems by adding restraining forces on the targets or target- fronrunner complexes and allowing water molecules to move (Figure 4.7) which allowed for the production MD simulations.

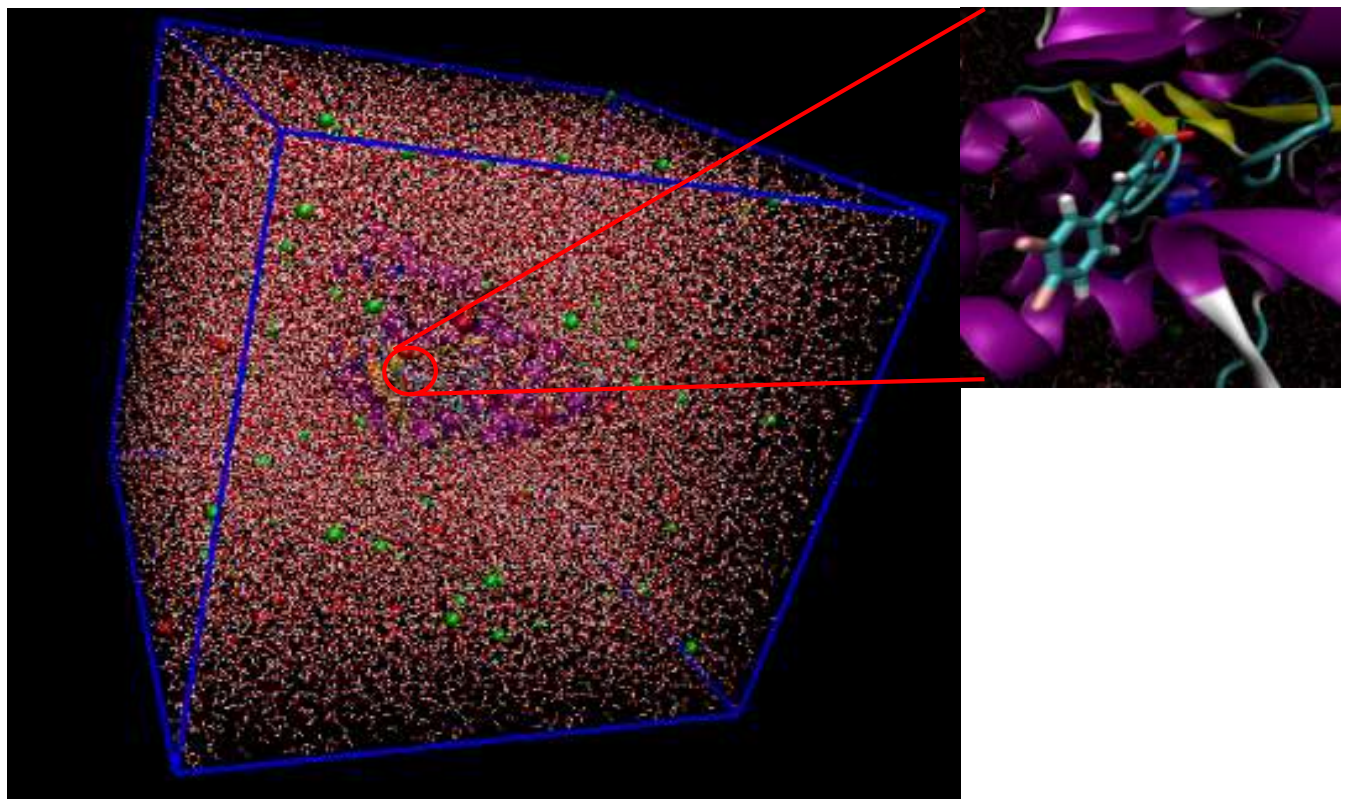


Figure 4.5: Solvated and ionized target-fronrunner complex simulation system. Schistosomal target is represented in new cartoon while fronrunner is representation in stick. Lines are SPC water model; green spheres are chlorine ions while red spheres are sodium ions. Blue solid line is the simulation box

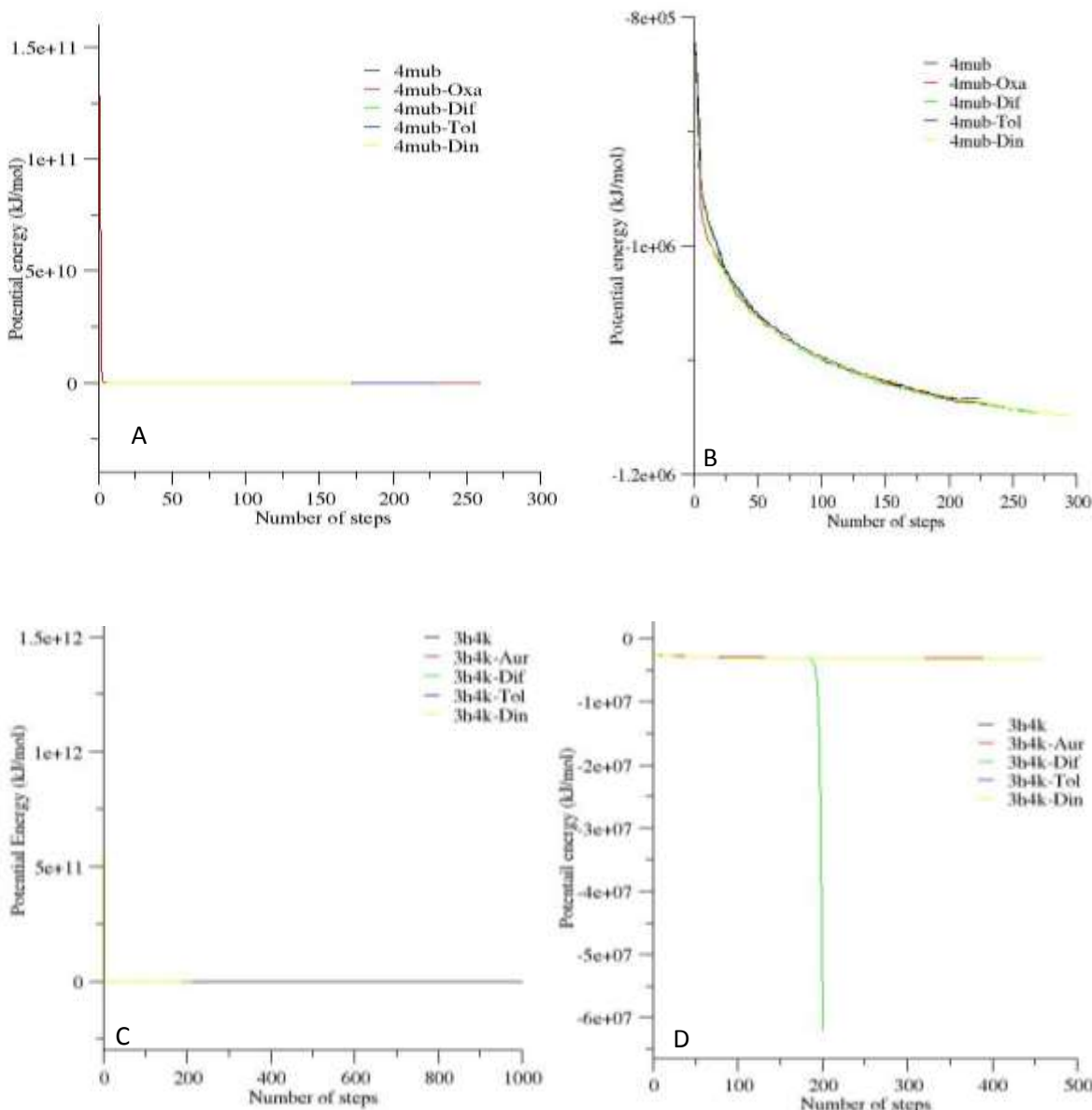


Figure 4.6: Energy minimization of the molecular systems (target, target-frontrunner complexes). A and B is the *in vacuo* energy minimization and energy minimization after solvation and neutralization for sulfotransferase (4mub) respectively while C and D is for thioredoxin glutathione reductase (3h4k). AUR = auranofin, OXA=oxamniquine, DIF=diflunisal, DIN=dinesterol and TOL=tolmetin.

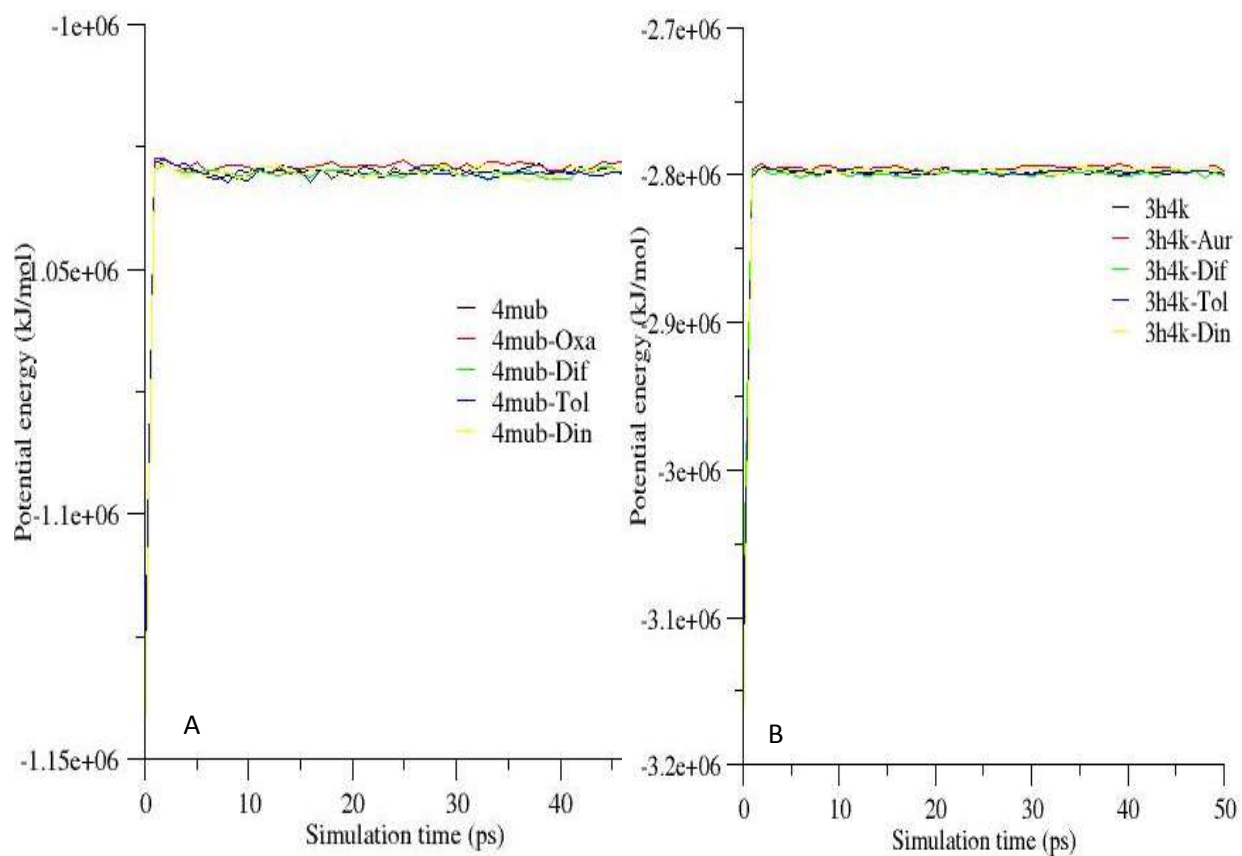


Figure 4.7: Position restrain molecular dynamics of the molecular systems (target, target-fronrunner complexes). Presented in A and B is the position restrain molecular dynamics simulations for sulfotransferase (4MUB) and thioredoxin glutathione reductase (3H4K) respectively. AUR = auranofin, OXA=oxamniquine, DIF=diflunisal, DIN=dinesterol and TOL=tolmetin.

4.1.6.4 Production run results

Different results from the production run MD simulations were computed from the production run trajectories and presented figure 4.8 to 4.38. The results include but not limited to stability profile, structure compactness profile, flexibility profile, secondary structural changes, hydrogen bonds/interaction profile, conformational sampling etc.

Stability Profile Analysis

Figure 4.8 illustrates protein-ligand complex stability in terms of RMSD and total energy. The C_α RMSD of the simulated protein over time is a reliable parameter to analyze the stability of the system. As evident from Figure 4.8, the first 200 ps and 450 ps were considered as equilibration phase where slight structural re-organization takes place for simulations involving thioredoxin glutathione reductase and sulfotransferase respectively. Then C_α RMSD was averaged over the last 3000 ps of the simulations. The C_α RMSD ranged between $0.217006693 \pm 0.031973524$ to $0.310072955 \pm 0.059648152$ nm and $0.188255739 \pm 0.018454807$ to $0.255235308 \pm 0.043743036$ nm for thioredoxin glutathione reductase and sulfotransferase respectively as can be seen in Appendix 14.

The RMSD of ligands show different degrees of fluctuations with unstable structural transitions occurring in diflunisal during diflunisal bound sulfotransferase simulation between 300 to 600 ps of the simulation and from 1250 ps during diflunisal bound TGR simulations (Figure 4.9). Also, dinesterol showed an unstable structural transition from about 2225 ps during sulfotransferase simulation (Figure 4.9, Appendix 14).

Notwithstanding differences/flutuations in the ligand bound targets, frontrunners or reference compounds RMSD, all simulations exhibited stable total energy trajectories between $-2.31383 \times 10^6 \pm 68$ to $-2.317769 \times 10^6 \pm 96$ KJ/mol during thioredoxin glutathione reductase and its ligand bound complexes simulations and between -852766 ± 49 to -853656 ± 23 KJ/mol during sulfotransferase and its ligand bound complexes simulations (Figure 4.10 and Appendix 15).

More fluctuations in total energies were observed during simulations involving sulfotransferase and its ligand bound complexes compared to TGR and its ligand bound complexes (Figure 4.10).

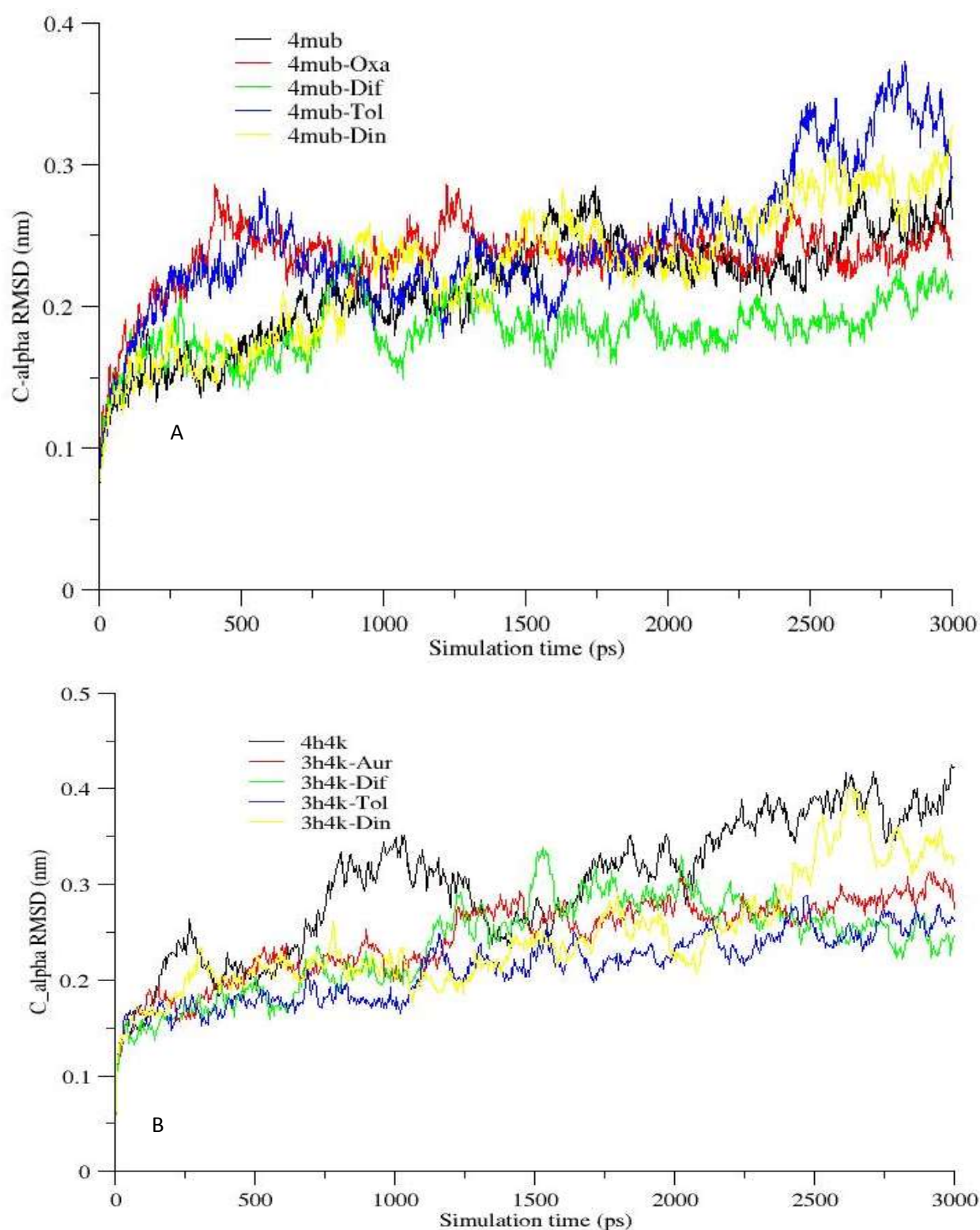


Figure 4.8: C-alpha root mean square deviation of schistosomal targets: (A) sulfotransferase and ligand bound sulfotransferase. (B) thioredoxin glutathione reductase and ligand bound thioredoxin glutathione reductase. AUR = auranofin, OXA=oxamniquine, DIF=diflunisal, DIN=dinesterol and TOL=tolmetin.

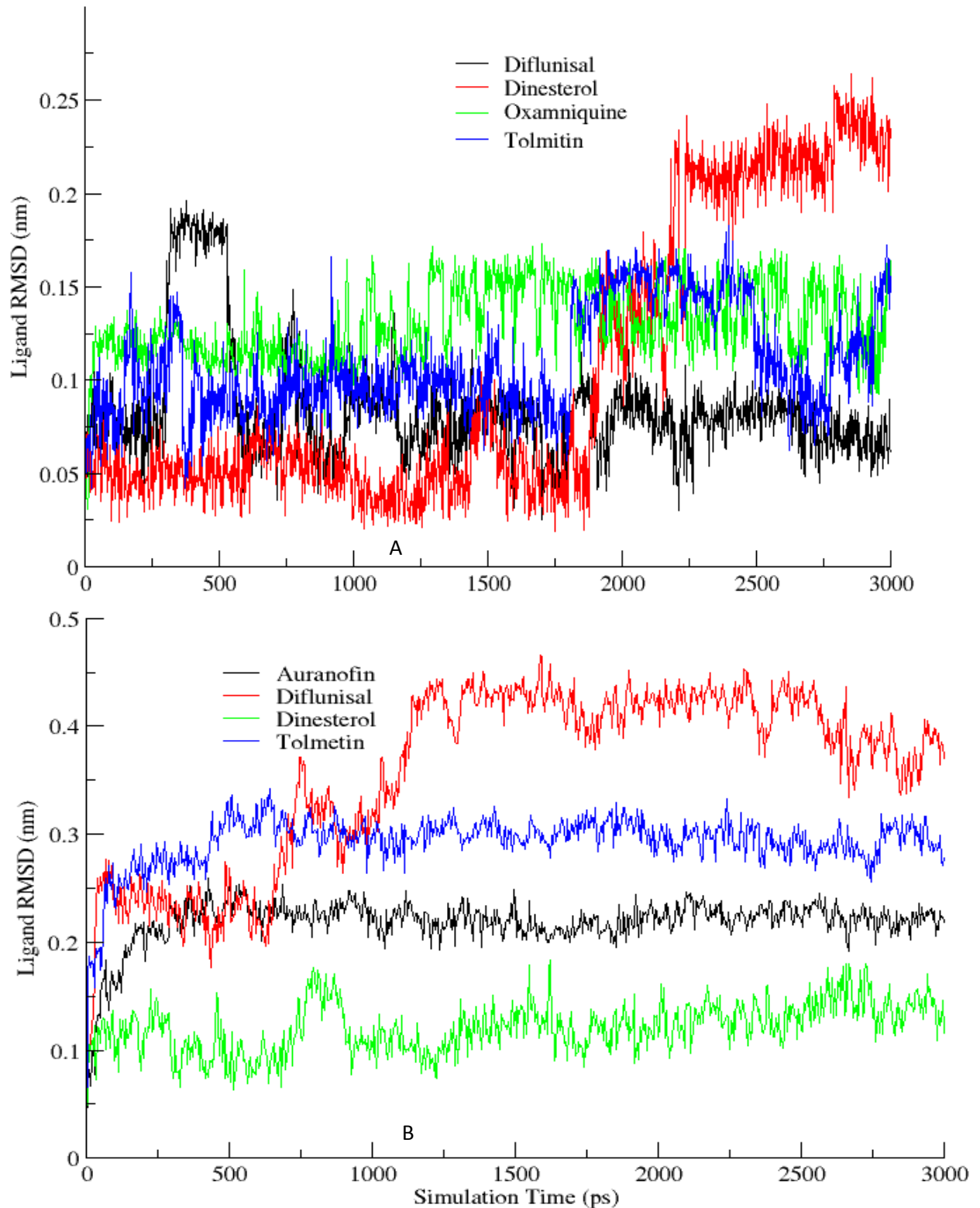


Figure 4.9: Root mean square deviation of ligands in (A) sulfotransferase simulations (B) thioredoxin glutathione reductase simulations.

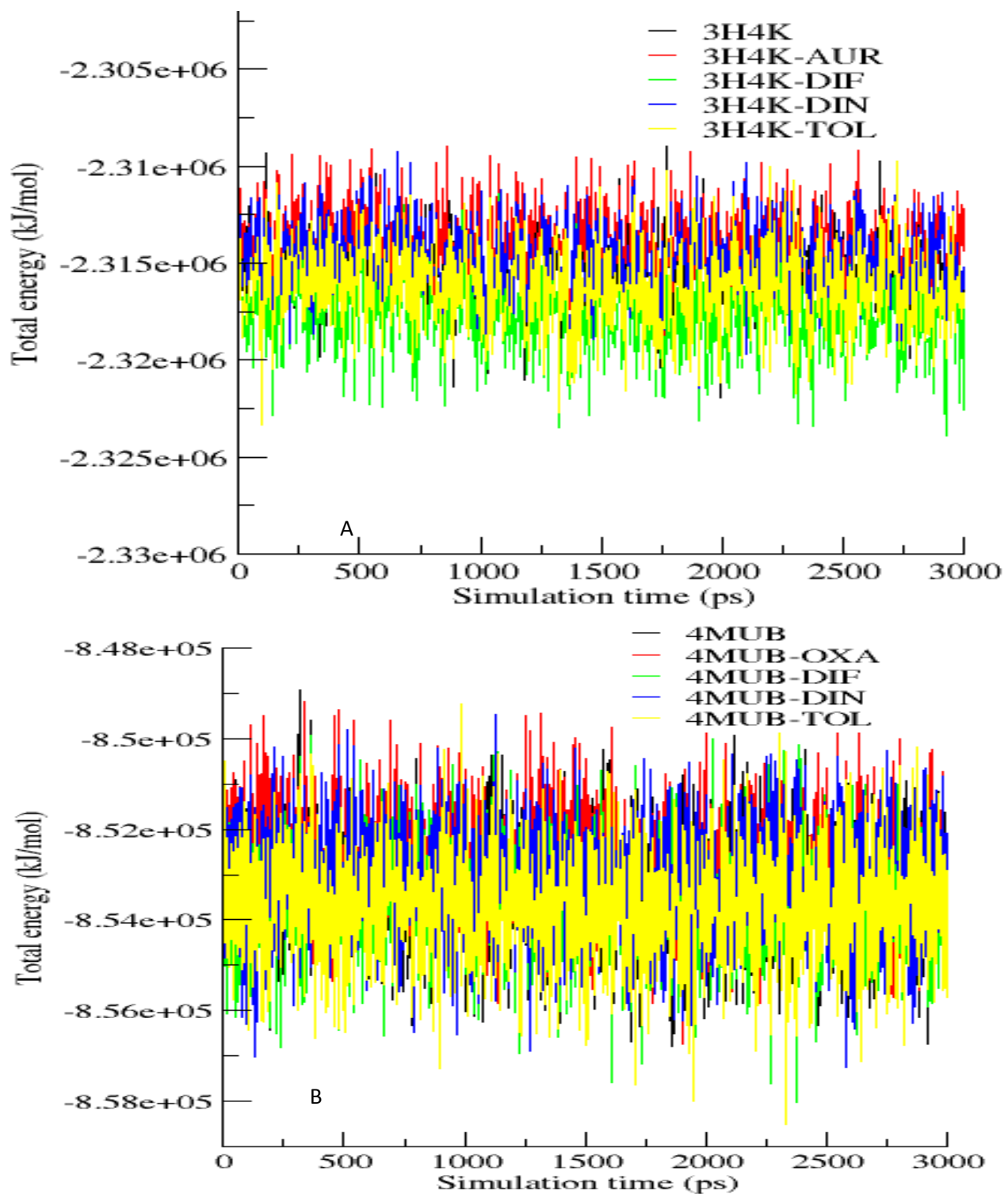


Figure 4.10: Total energy of the MD simulated systems for (A) sulfotransferase (4MUB) and its ligand bound simulations and (B) thioredoxin glutathione reductase (3H4K) and its ligand bound simulations. AUR = auranofin, OXA=oxamniquine, DIF=diflunisal, DIN=dinesterol and TOL=tolmetin.

Structure compactness profile

The radius of gyration of the targets was averaged over the last 3000 ps of the simulations after the equilibration phase. It ranged between $2.80361729 \pm 0.014827062$ to $2.87129903 \pm 0.015824005$ nm and $1.84842529 \pm 0.008945636$ to $1.884123056 \pm 0.008682234$ nm for MD simulations involving sulfotransferase and thioredoxin glutathione reductase and their ligand bound complexes respectively as can be seen in figure 4.11 and appendix 14.

The radius of gyration of the ligands showed various degrees of fluctuations (Figure 4.12, and appendix 14). The unstable structure of diflunisal during sulfotransferase simulation between 300 to 600 ps of the simulations (Figure 4.9) maintained same degree of compactness throughout the simulation (Figure 4.12 A) but such was not observed during thioredoxin glutathione reductase simulations (Figure 4.12 B). Also, it was observed that the unstable structure of the dinesterol during sulfotransferase simulation (Figure 4.9) was more compacted (Figure 4.12 A). The compacted and unstable structures are responsible for the fluctuations and/or stability in C_{α} RMSD of the ligand bound targets relative to unliganded targets (Figure 4.8).

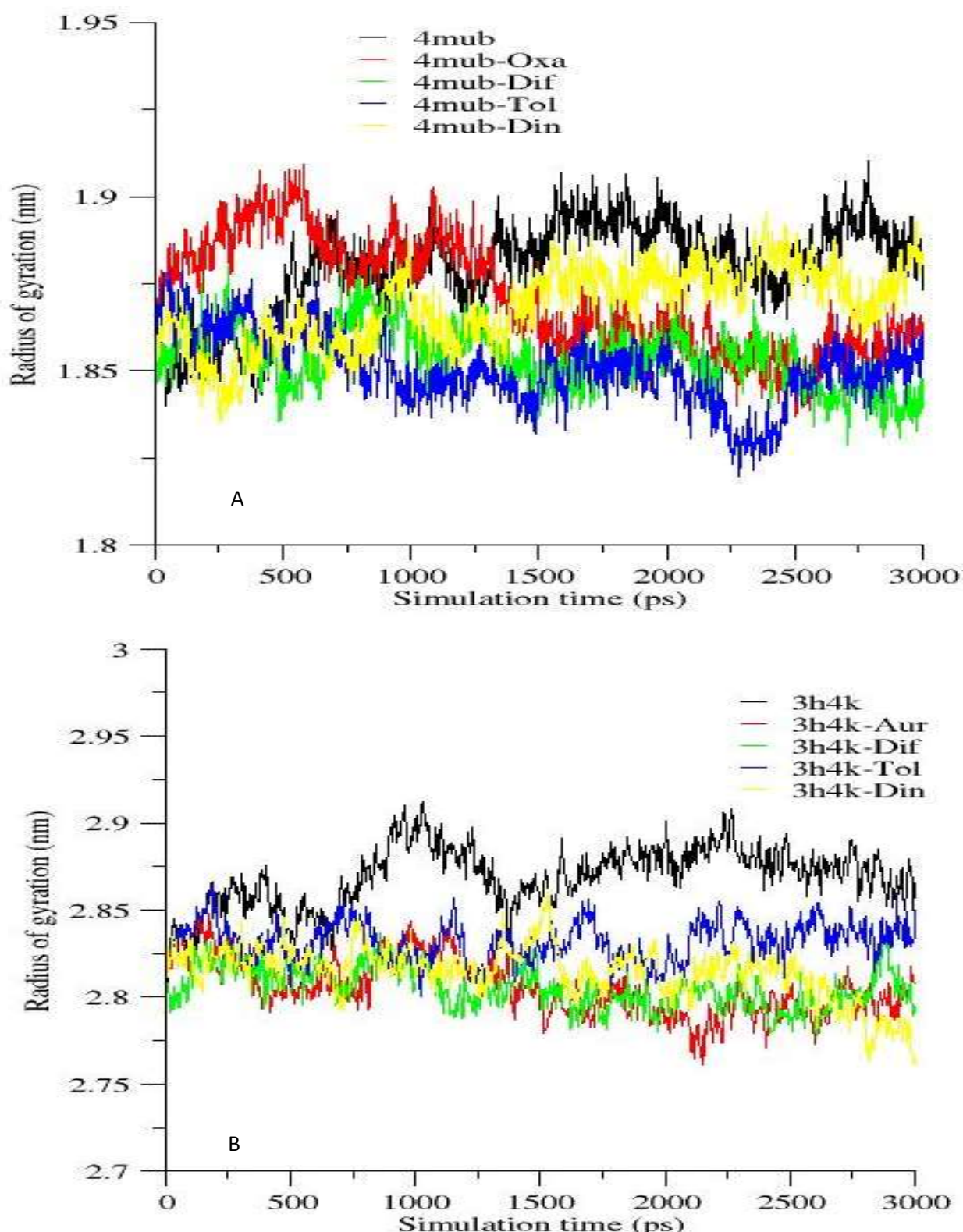


Figure 4.11: Radius of gyration of the simulated targets presence of ligands. (A) Sulfotransferase and its ligand bound complexes. (B) Thioredoxin glutathione reductase and ligand bound complexes. AUR = auranofin, OXA=oxamniquine, DIF=diflunisal, DIN=dinesterol and TOL=tolmetin.

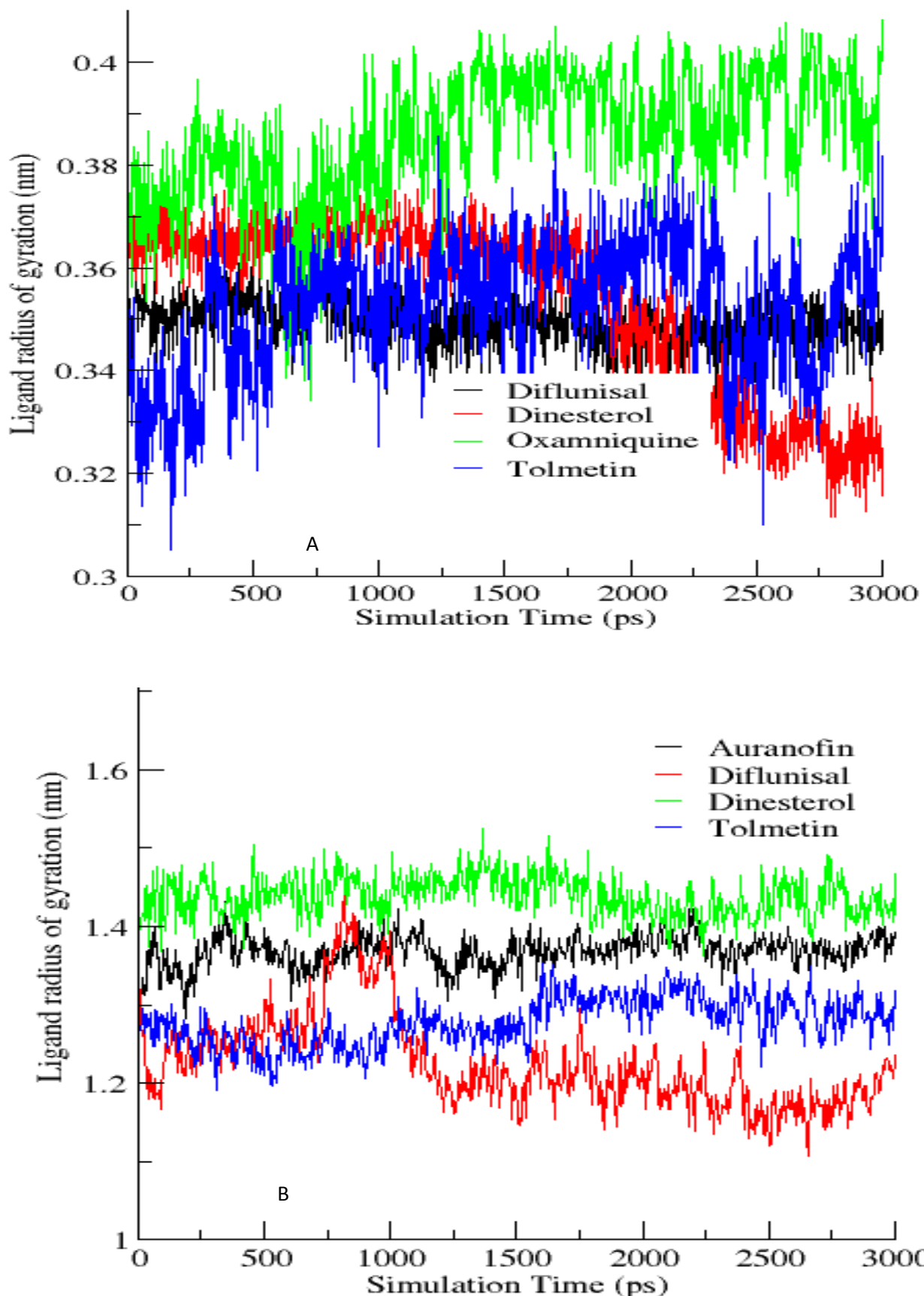


Figure 4.12: Radius of gyration of the ligands during (A) sulfotransferase simulations and (B) thioredoxin glutathione reductase simulations.

Target flexibility profile

Residues contributing to structural fluctuations in the targets can be assessed by root mean square fluctuations (RMSFs) of each residue. Analysis of the RMSF values shows differences in the target flexibilities due to ligand interaction. For example, these were observed at residue ids 71 to 76 and 91 to 93 in ligand bound sulfotransferase MD simulations and 436 to 440 and 181 to 191 in ligand bound TGR MD simulations (Figure 4.13). Reductions in flexiblites were observed at different residue id or ranges of residue ids (Figure 4.13) because vibrations around the equilibrium are not random but depend on local structure flexibilities. Figure 4.13 show the sequence ids of the amino acid residues and their corresponding flexibility during the molecular dynamics simulations.

It was observed that the ligands modulated sulfotransferase flexibility. Generally, reduction in flexibility of sulfotransferase loops was observed at Tyr91-Ile92-Ala93 and Pro70-Pro71-Pro72-Leu73-Thr74-Thr75-Lys76 while that of TGR simulations was observed at Ala436-Gly437-Lys438-Pro439-Gln440 and Phe181-Gly182-Trp183-Ser184-Leu185-Asp186-Arg187-Ser188-Lys189-Ile190-Ser191 (Figure 4.13 and 4.14). These amino acids are found at the loops of the targets (Figure 4.14).

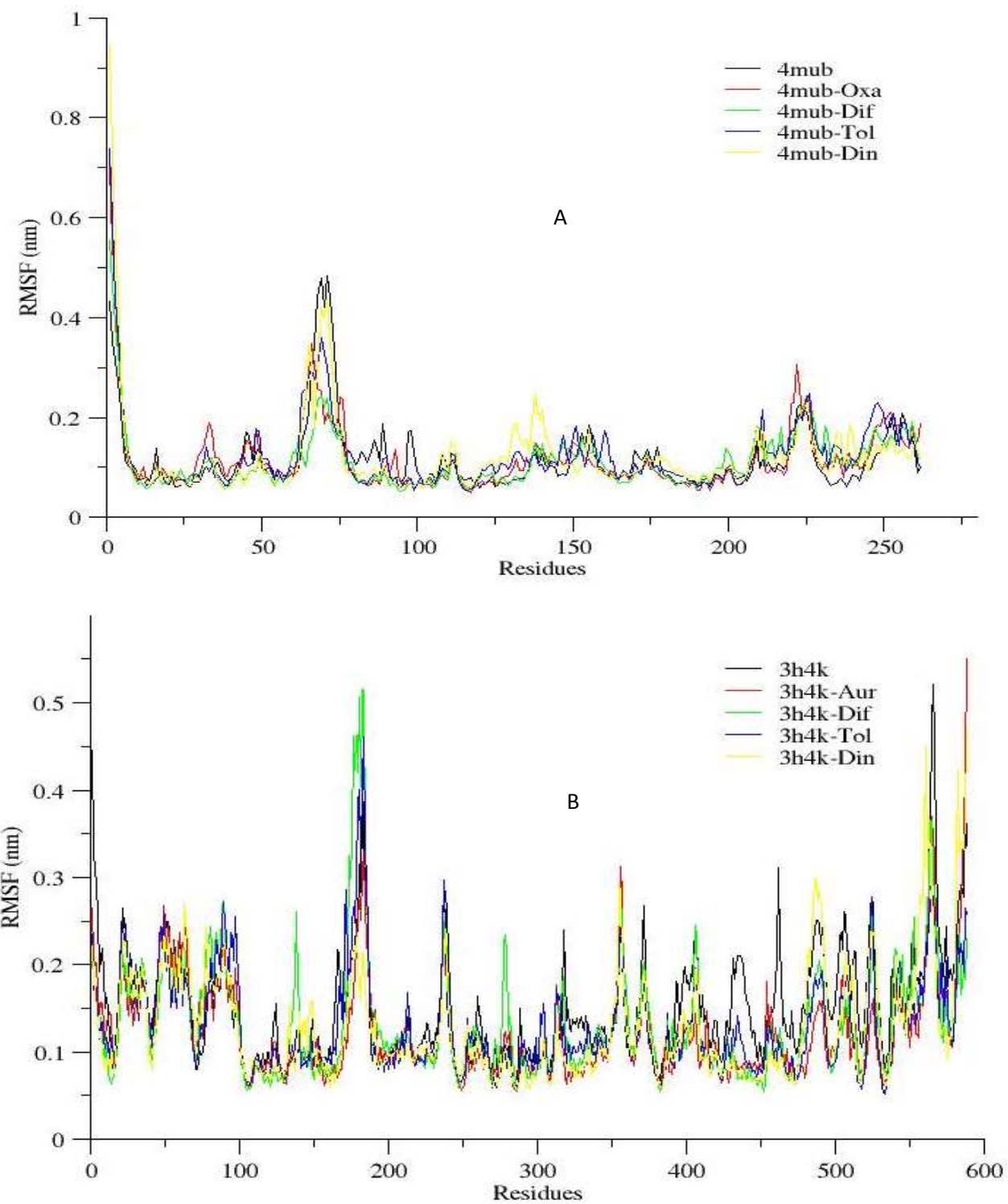


Figure 4.13: Root mean square fluctuation of targets in presence of ligands. (A) Sulfotransferase and ligand bound sulfotransferase. (B) Thioredoxin glutathione reductase and ligand bound thioredoxin glutathione reductase. AUR = auranofin, OXA=oxamniquine, DIF=diflunisal, DIN=dinesterol and TOL=tolmetin.

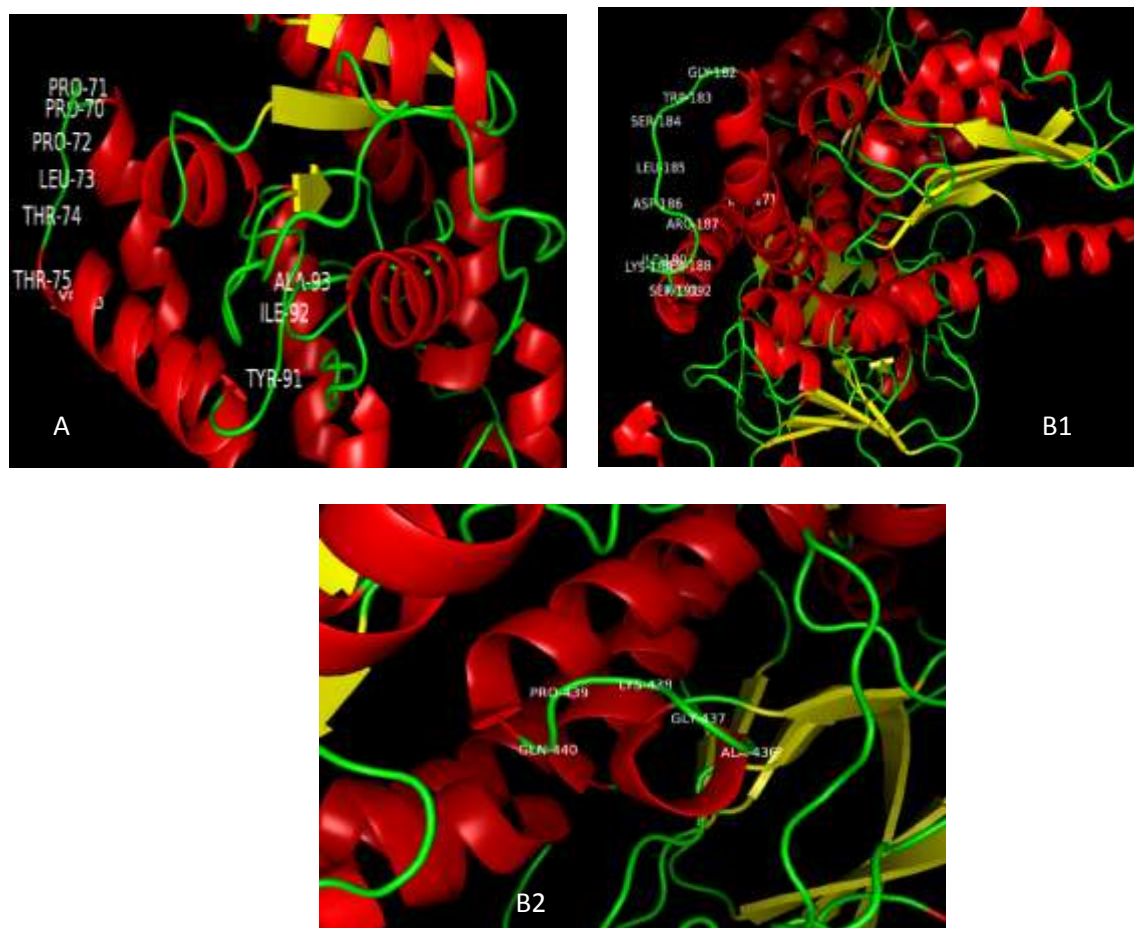


Figure 4.14: Some amino acids associated with reduction in loop flexibility due to interaction with the ligands. (A) Sulfotransferase (B1 and B2) Thioredoxin glutathione reductase. The targets are represented as cartoon. Red represents helix; yellow represents beta-sheet while green represents loops.

Target secondary structure profile

Protein functionality is affected by the tertiary structure formed by the secondary structures. The conformational changes of protein secondary structures for each time frame can be computed by the DSSP program. Changes in the secondary structures of the targets when diflunisal, tolmetin, dinesterol, oxamniquine or auranofin are bound to sulfotransferase and thioredoxin glutathione reductase were calculated and presented in figure 4.15 to 4.16 and Appendix 16.

The number of residues in schistosomal sulfotransferase adopting different conformations as a function of time is presented in figure 4.15a. It can be observed that the alpha-helix compositions of sulfotransferase showed decreasing trend in presence of diflunisal, oxamniquine and dinesterol but not with tolmetin as can be seen in appendix 16. Sulfotransferase showed the smallest α -helix composition in the presence of diflunisal (46.9539391 %) when compared with that in the absence of ligand (51.06799 %). The composition of beta-sheets in sulfotransferase ranged from 6.6032314 % to 7.10366117 % in the presence of the ligands compared with 6.284869 % in absence of the ligands (Appendix 16).

Again, 5-helix composition of 0.003814 % observed in the absence of ligands disappeared due to influence of the ligands (Figure 4.15a and appendix 16). Also, 3-helix compositions of sulfotransferase ranged from 1.475098 % to 2.310419008 % due to influence of ligands as against a value of 0.777853 % in absence of ligands (appendix 16). Finally, increase in the composition of turns due to ligand interactions were observed but not with oxamniquine (Appendix 16). Other changes in secondary structure of sulfotransferase are presented in figure 4.15a, figure 4.15b and appendix 16. All the structural changes in sulfotransferase were due to different number of residues adopting different conformations at different time points in the MD simulations (Figure 4.15a and 4.15b).

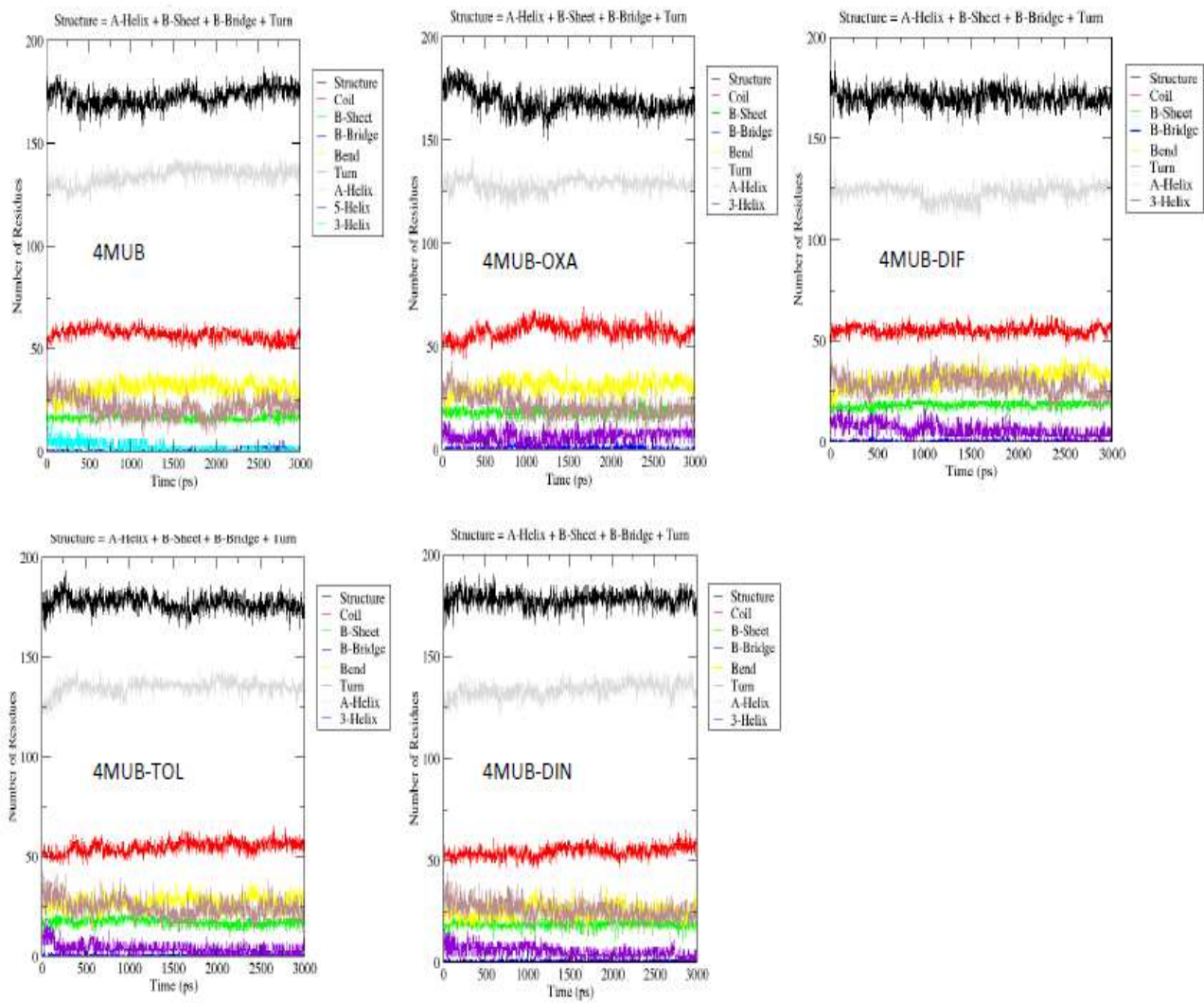


Figure 4.15a: Secondary structure changes observed during the 3000 ps MD simulation of sulfotransferase (4MUB i.e absence of ligands) and its ligand complexes. AUR = auranofin, OXA=oxamniquine, DIF=diflunisal, DIN=dinesterol and TOL=tolmetin.

Figure 4.15b shows that 5-helix which was present in sulfotransferase disappeared as a result of interaction with oxamniquine, diflunisal, tolmetin, or dinesterol but not in their absence. Asn233 was in coil conformation both in presence and absence of oxamniquine, diflunisal, tolmetin, or dinesterol (Figure 4.15b). It can be observed that amino acids in sulfotransferase with residue id between 1 to 10 (which corresponds to Gly1, Ala2, Met3, Ile4, Glu5, Ser6, Ser7, Thr8, Thr9 and Ile10) are predominately in coil conformation from 0.0 ps to 1150 ps in absence of oxamniquine, diflunisal, tolmetin, or dinesterol before adopting bend conformation for the rest of the simulation (Figure 4.15b). They remained in coil conformation in the presence of oxamniquine, diflunisal, tolmetin, or dinesterol. However, bend conformations were observed in presence of oxamniquine and dinesterol at different time points (Figure 4.15b). Again, Asp260 in sulfotransferase was predominately in turn conformation in the presence of tolmetin compared with alternating turn, $\alpha - helix$ and bend conformations observed in presence of oxamniquine, diflunisal or dinesterol (Figure 4.15b). Reduction in beta-sheet conformations due to residue 120 (Arg120) in presence of diflunisal, tolmetin, or dinesterol was observed but such reduction was not observed in presence of oxamniquine (Figure 4.15b). Also, residue ids 65 to 75 (Pro65, Pro66, Pro67, Thr68, Thr69, Pro70, Pro71, Pro72, Leu73, Thr74, and Thr75) are predominately in bend conformation in presence of oxamniquine and diflunisal compared with its conformations in their absence (Figure 4.15b). However, they are predominately in $\alpha - helix$ conformations with traces of turn and bend in the presence of tolmetin and dinesterol (Figure 4.15b).

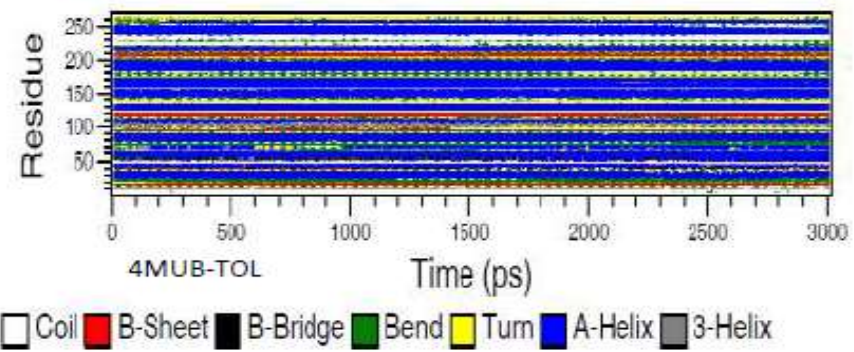
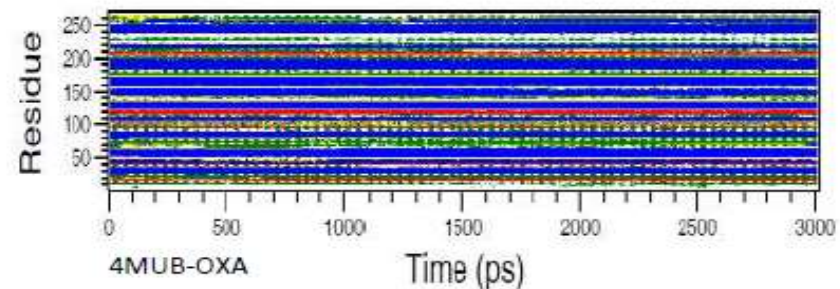
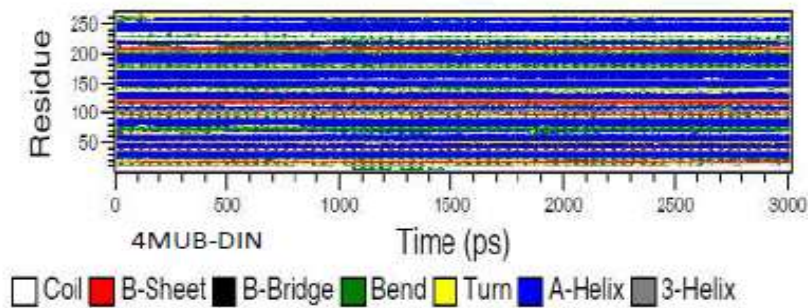
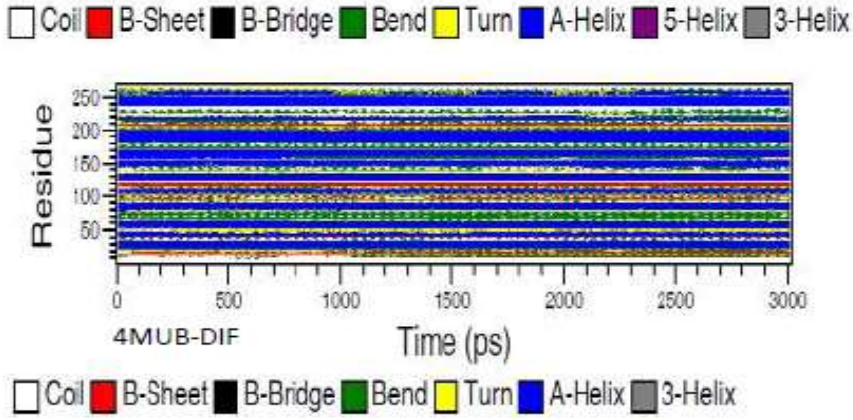
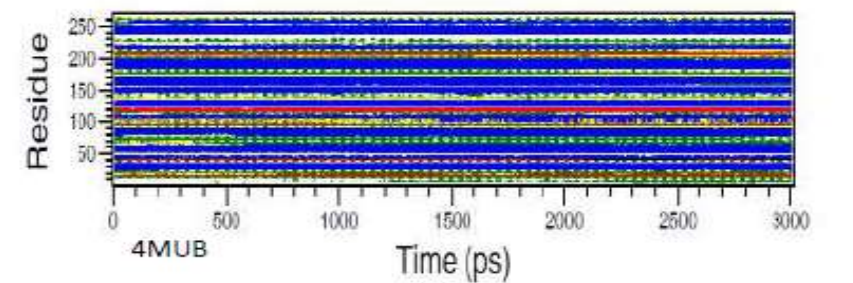


Figure 4.15b: Secondary structure changes in sulfotransferase observed during the 3000 ps MD simulations of sulfotransferase (4MUB i.e in absence of ligand) and its ligand complexes. OXA=oxamniquine, DIF=diflunisal, DIN=dinesterol and TOL=tolmetin.

The number of residues in schistosomal thioredoxin glutathione reductase adopting different conformations as a function of time is presented in figure 4.16a. The alpha-helix compositions of thioredoxin glutathione reductase ranged from 30.363597 % to 31.06945841 % due to influence of the ligands when compared with 29.55945 % in the absence of ligands (Appendix 16).

The composition of beta-sheets in thioredoxin glutathione reductase ranged from 22.018261 % to 22.46234046 % due to influence of ligands when compared with 23.07218 % in absence of ligands (Appendix 16). Again, 5-helix compositions of thioredoxin glutathione reductase were 0.294618513 %, 0.63701912 %, 0.542360753 % and 0.7767421 % in the presence of auranofin, diflunisal, dinesterol, and tolmetin respectively compared with a value of 0.663514 % in the absence of ligands (Appendix 16).

Also, 3-helix compositions of thioredoxin glutathione reductase were 1.204289972 % 1.10895224 %, 0.915106389 % and 1.2149334 % in the presence of auranofin, diflunisal, dinesterol, and tolmetin respectively compared with a value of 1.194326 % in the absence of ligands (Appendix 16). Other changes in secondary structure of thioredoxin glutathione reductase are presented in figure 4.16a, figure 4.16b and appendix 16.

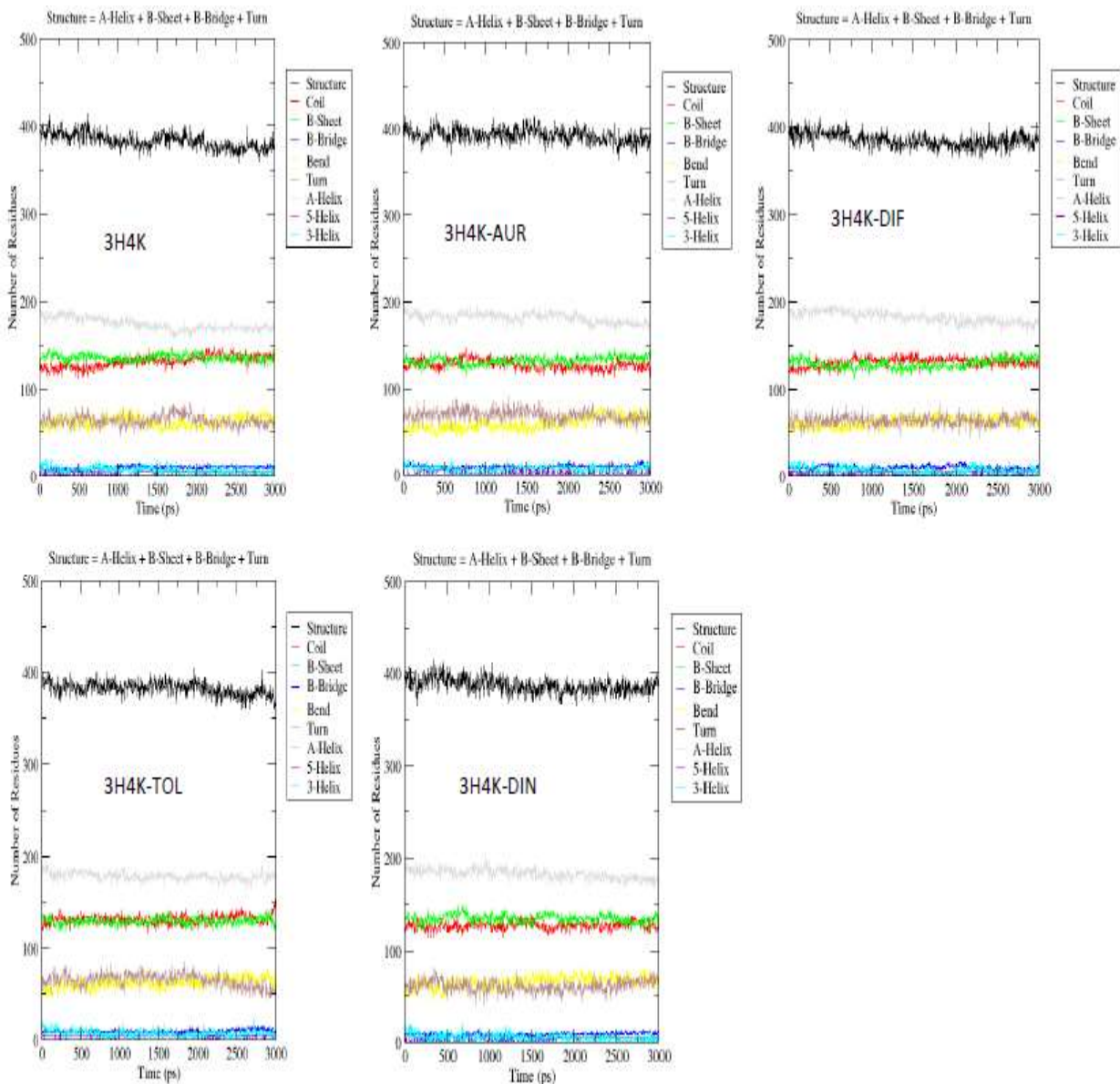


Figure 4.16a: Secondary structure changes in thioredoxin glutathione reductase observed during the 3000 ps MD simulation of thioredoxin glutation reductase (3H4K) and its ligand complexes. AUR = auranofin, DIF=diflunisal, DIN=dinesterol and TOL=tolmetin.

Figure 4.16b showed that more $\alpha - helix$ conformations occurred between residues 380 to 400 in TGR due to influence of auranofin, diflunisal, tolmetin or dinesterol when compared to their absence. Residues id (180 to 182) corresponding to His180, Phe181 and Gly182 are predominately in turn conformation in presence of tolmetin especially between 1100 ps to 3000 ps when compared with that in the presence of auranofin, diflunisal or dinesterol which showed alternating conformations of bend and turn throughout the simulation (Figure 4.16b). Again, residue 460 (Arg460) was predominately in coil conformation especially from 520 ps to 3000 ps in absence of auranofin, diflunisal, tolmetin or dinesterol when compared with its conformation in their presence (Figure 4.16b). Also, residue 580 (Thr580) was more in $\beta - sheet$ conformation in absence of auranofin, diflunisal, tolmetin or dinesterol at the beginning of the simulation when compared with its conformations in the presence of auranofin, diflunisal, tolmetin or dinesterol (Figure 4.16b).

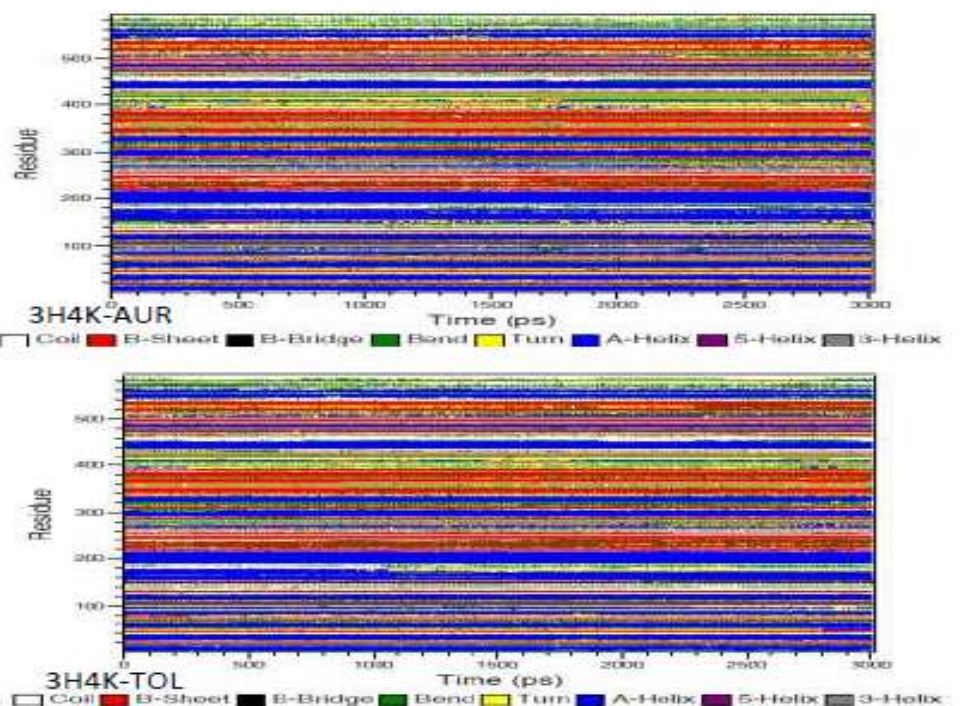
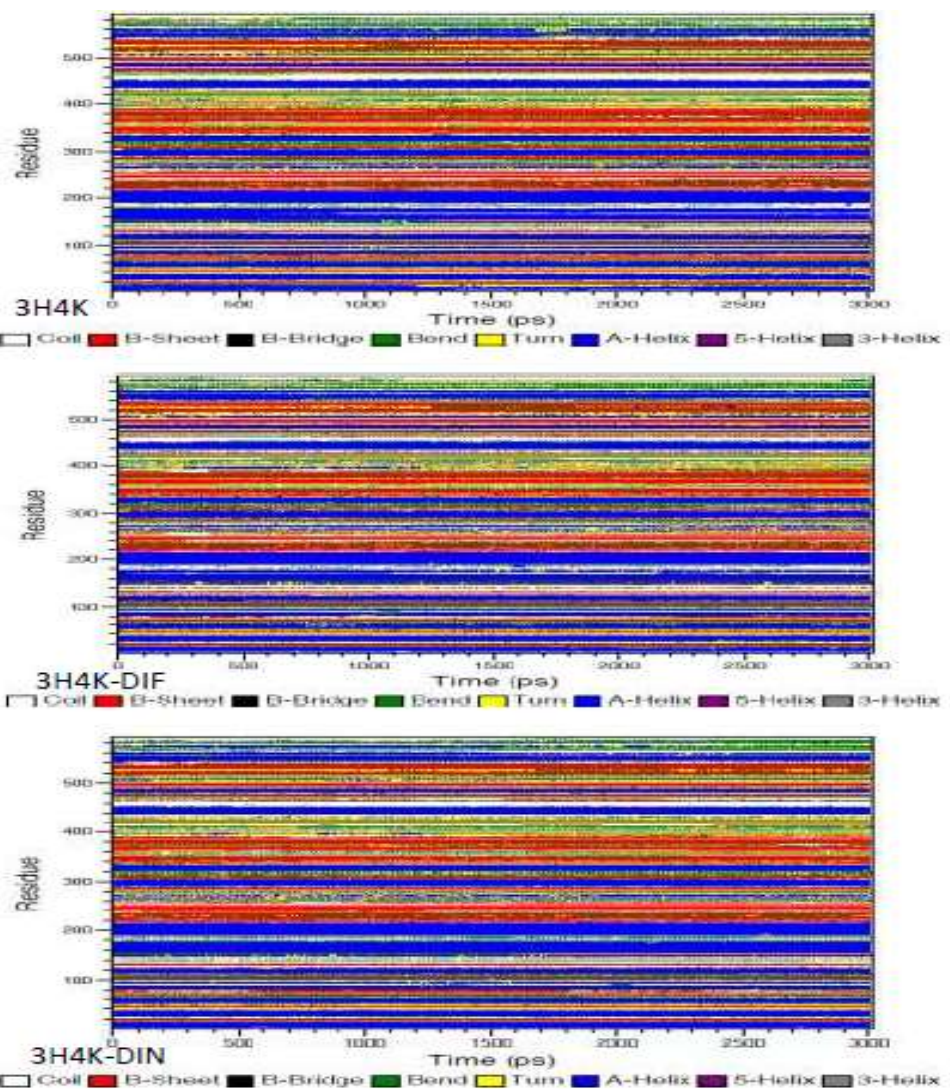


Figure 4.16b: Secondary structure changes in thioredoxin glutathione reductase observed during the 3000 ps MD simulation of thioredoxin glutathione reductase (3H4K) and its ligand complexes. AUR = auranofin, DIF=diflunisal, DIN=dinesterol and TOL=tolmetin.

Hydrogen bond/polar interaction profile

At 0.0 ps of the oxamniquine bound sulfotransferase MD simulation, oxygen atom (OD1) at the side chain of Asn233 formed hydrogen bond with a hydrogen atom (H16) at the amine functional group in oxamniquine (*Asn233 – OD1 H16 – Oxa*) (Figure 4.17). Then, during MD simulations involving diflunisal and dinesterol, oxygen atom (OD2) at the carboxylic side chain of Asp96 formed hydrogen bond with hydrogen atoms (H3 and 1H18) at the hydroxyl functional groups in diflunisal (*Asp96 – OD2 H3 – Dif*) and dinesterol (*Asp96 – OD2 1H18 – Din*) respectively (Figure 4.17). Again, a hydrogen atoms (2HD2 and HG1) at the side chains of Asn233 and Thr242 in schistosomal sulfotransterase formed hydrogen bonds with oxygen atoms (O1 and O2) at carboxyl functional groups in diflunisal (*Asn233 – 2HD2 O1 – Dif*) and tolmetin (*Thr – HG1 O2 – Tol*) respectively (Figure 4.17). Also, a hydrogen atom (1HH1) at the side chain of Arg19 formed hydrogen bond with oxygen atoms (O1 and O2) at the carboxylic functional group in diflunisal (*Arg19 – 1HH1 O1 – Dif , Arg19 – 1HH1 O2 – Dif*) (Figure 4.17).

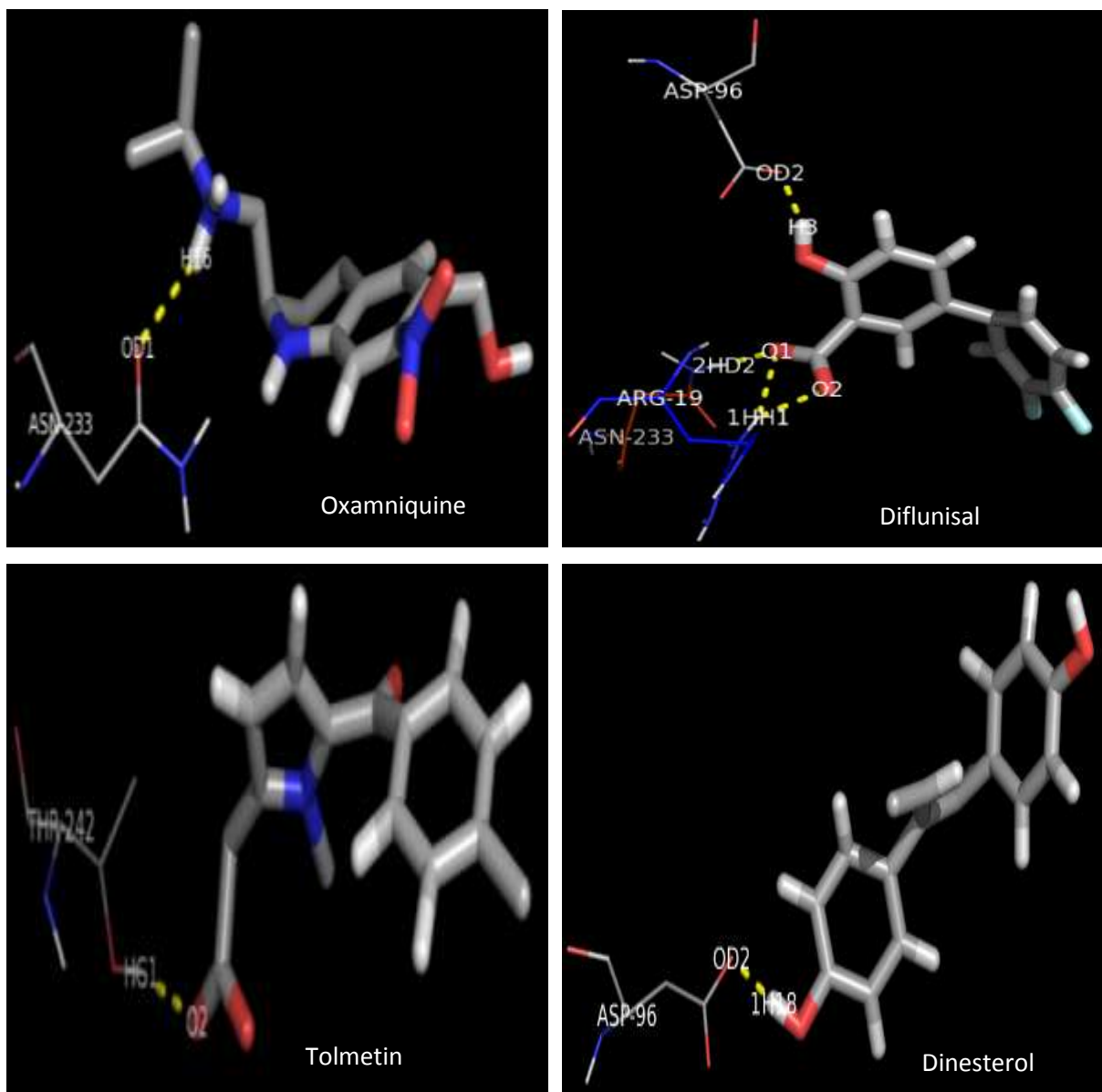


Figure 4.17: The polar contacts/hydrogen bond formation in sulfotransferase-ligand complexes at 0 ps of MD simulations. The ligands (oxamniquine, dilunisal, tolmetin and dinesterol) are represented as sticks while amino acids that show direct contact with the ligands are represented as lines. Both ligands and the amino acids are colored according the atoms. Red is oxygen, white is hydrogen, blue is nitrogen and grey is carbon atoms. The atoms that show direct contacts are labeled.

The *Asn233 – OD1**H16 – Oxa* interaction observed at 0.0 ps during sulfotransferase-oxamniquine MD simulation was not maintained at 480 ps (Figure 4.18) while *Asn233 – 2HD2**O1 – Dif*, *Arg19 – 1HH1**O1 – Dif* and *Asp96 – OD2**H3 – Dif* interactions observed at 0.0 ps during sulfotransferase-diflunisal MD simulation are maintained (Figure 4.18). Also, hydrogen bond was formed between amide hydrogen atom (H) in Arg19 and oxygen atom (OD2) at carboxylic functional group in diflunisal (*Arg19 – H**O2 – Dif*).

Again, *Thr – HG1**O2 – Tol* interaction disappeared at 480 ps of sulfotransferase-tolmetin MD simulation with formation of hydrogen bonds between hydrogen atom (2HD2) at the side chain of Asn233 with oxygen atoms (O2 and O3) at carboxylic functional group in tolmetin (*Asn233 – 2HD2**O2 – Tol*, *Asn233 – 2HD2**O3 – Tol*) (Figure 4.18).

In addition to *Asp96 – OD2**1H18 – Din* interaction, hydrogen bond was formed between the amide hydrogen (H) in Arg19 and oxygen atom (O2) at hydroxyl functional group in dinesterol (*Asp19 – H**O2 – Din*) (Figure 4.18) at 480 ps of the sulfotransferase-dinesterol MD simulation. Also, oxygen atom (OD1) at the carboxylic side chain of Asp149 formed a hydrogen bond with hydrogen atom (1H13) at the hydroxyl functional group in dinesterol (*Asp149 – OD1**1H13 – Din*) (Figure 4.18).

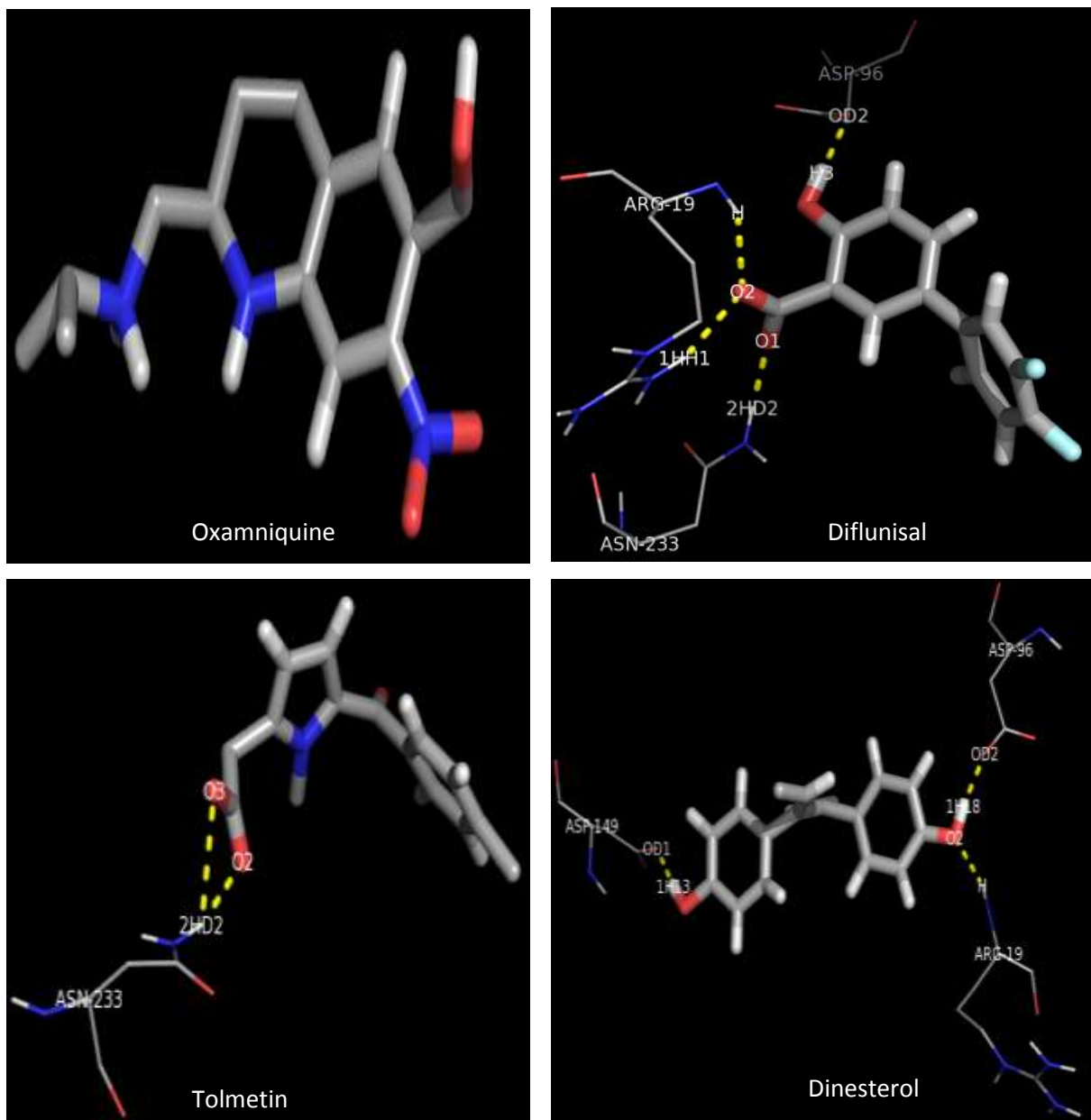


Figure 4.18: The polar contacts/hydrogen bond formation in sulfotransferase-ligand complexes at 480 ps of MD simulations. The ligands (oxamniquine, dilunisal, tolmetin and dinesterol) are represented as sticks while amino acids that show direct contact with the ligands are represented as lines. Both ligands and the amino acids are colored according to the atoms. Red is oxygen, white is hydrogen, blue is nitrogen and grey is carbon atoms. The atoms that show direct contacts are labeled.

At 2800 ps of the sulfotransferase- oxamniquine MD simulation, oxygen atom (OD1) at the side chain of Asn46 formed a polar contact with oxygen atom (O1) at nitroaromatic functional group in oxamniquine (*Asn46 – OD1 O1 – Oxa*) (Figure 4.19). Also, C_{α} oxygen atom (O) in Leu261 formed a polar contact with oxygen atom (O2) at nitroaromatic functional group in oxamniquine (Figure 4.19). At 2800 ps of the sulfotransferase-diflunisal MD simulation, all the interactions observed at 0.0 ps were restored with the exception of *Arg19 – 1HH1 O1 – Dif*. Again, at 2800 ps of sulfotransferase-tolmetin MD simulation, *Asn233 – 2HD2 O2 – Tol* interaction disappeared while that of *Asn233 – 2HD2 O3 – Tol* was maintained (Figure 4.19). Also, formation of additional hydrogen bond between hydrogen atom (HZ3) at the side chain of Lys23 and oxygen atom (O3) at carboxylic functional group in tolmetin was observed (*Lys23 – HZ3 O3 – Tol* (Figure 4.19). At 2800 ps of the sulfotransferase-dinesterol MD simulation, *Asp19 – H O2 – Din* interaction was maintained while *Asp149 – OD1 1H13 – Din* interaction was replaced by *Asp96 – OD1 1H18 – Din* (Figure 4.19). Also, hydrogen atom (2HD2) at the side chain of Asn233 formed hydrogen bond with oxygen atom (O1) at hydroxyl functional group in dinesterol (*Asn233 – 2HD2 O1 – Din*) (Figure 4.19).

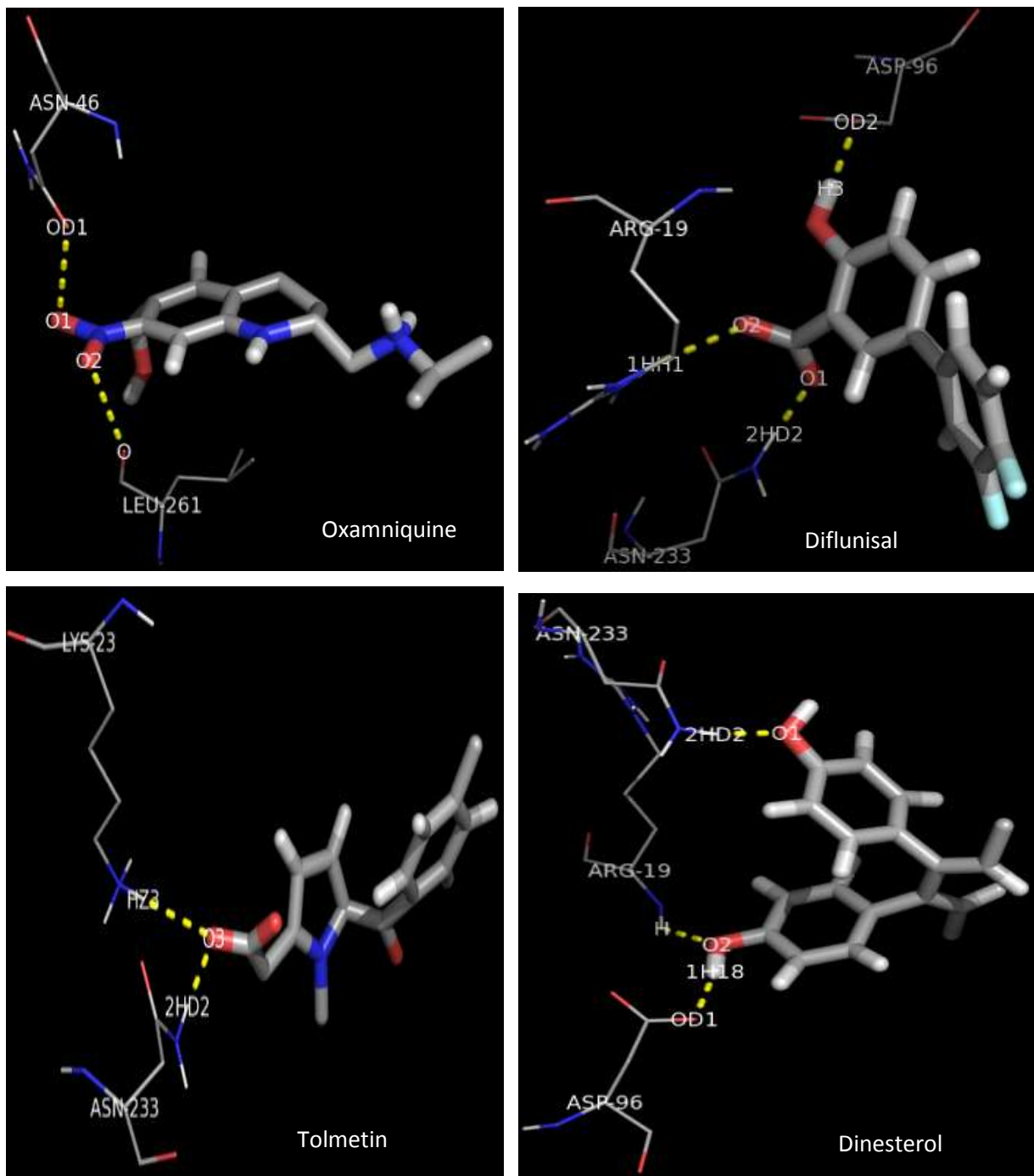


Figure 4.19: The polar contacts/hydrogen bond in sulfotransferase-ligand complexes at 2800 ps of MD simulations. The ligands (oxamniquine, dilunisal, tolmetin and dinesterol) are represented as sticks while amino acids that show direct contact with the ligands are represented as lines. Both ligands and the amino acids are colored according the atoms. Red is oxygen, white is hydrogen, blue is nitrogen and grey is carbon atoms. The atoms that show direct contacts are labeled.

The various amino acids that have direct/polar contact with the ligands (Figure 4.17 to 4.19) are in turn connected to other amino acid(s) (Figure 4.20). For example, it can be observed from figure 4.20 that Pro18 is connected to Arg19 and Asp96 is connected to Leu97.

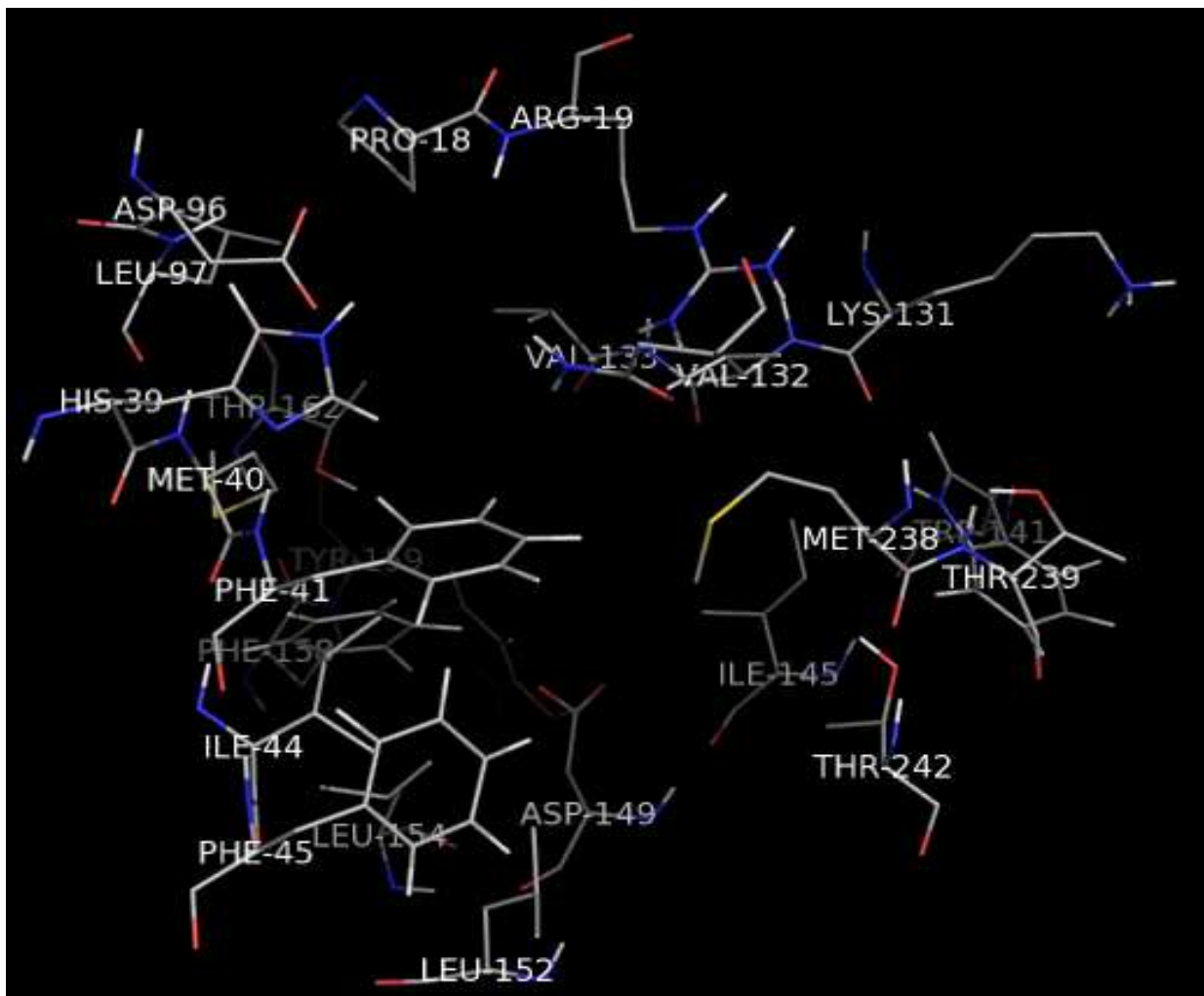


Figure 4.20 Amino acids in sulfotransferase that interacts with the ligands from the MD simulations

At 0.0 ps and in site 1 of auranofin bound thioredoxin glutathione reductase MD simulation, hydrogen atom (HZ3) at the side chain of Lys162 and amide hydrogen atom (H) in Thr442 formed hydrogen bonds with oxygen atoms (O9 and O3) at ester functional groups in auranofin (*Lys162 – HZ3 O9 – Aur, (Thr442 – H O3 – Aur)*) respectively (Figure 4.21). Also, a presence of covalent bond was estimated between oxygen atom (OD2) at the carboxylic side chain of Asp433 and hydrogen atom (1H11) at the sulphurhydryl (–SH) functional group in auranofin (*Asp433 – OD2 _____ 1H11 – Aur*) (Figure 4.21).

Again, at 0.0 ps and in site 2 of auranofin bound thioredoxin glutathione reductase MD simulation, hydrogen atom (2HD2) at the side chain of Asn543 and (HE1) at the side chain of Trp510 formed hydrogen bonds with oxygen atoms (O7 and O5) at ester functional groups in auranofin (*Asn543 – 2HD2 O7 – Aur, Trp510 – HE1 O5 – Aur*) respectively (Figure 4.21). It is important to note that hydrogen bond was observed in site 3 of thioredoxin glutathione reductase between an amide hydrogen in Gln440 and oxygen atom (O9) in the ester functional group in auranofin (*Gln440 – H O9 – Aur*) at 0.0 ps (Figure 4.21).

At 0.0 ps and in site 1 of diflunisal bound thioredoxin glutathione reductase MD simulation, amide hydrogen (H) in Cys154 and hydrogen atom (HG1) at the hydroxyl side chain of Thr442 formed hydrogen bonds with oxygen atoms (O1 and O2) at carboxylic functional groups in diflunisal (*Cys154 – H O1 – Dif, Thr442 – HG1 O2 – Dif*) respectively (Figure 4.21). Also at 0.0 ps and site 1, oxygen atom (OD1) at the carboxylic side chain of Asp433 formed a hydrogen bond with hydrogen atom (H7) at hydroxyl functional group in diflunisal (*Thr433 – OD1 H7 – Dif*) (Figure 4.21).

At 0.0 ps and in site 2 of diflunisal bound thioredoxin glutathione reductase MD simulation, a hydrogen atom (HE1) at the side chain of Trp510 formed hydrogen bond with oxygen atom (O2) at the carboxylic functional group in diflunisal (*Trp510 – HE1 O2 – Dif*) (Figure 4.21).

This hydrogen bond was maintained at 480 ps but disappeared at 2800 ps to formation of zero polar contact (Figure 4.21).

At 0.0 ps and in site 3 of diflunisal bound thioredoxin gluthathione reductase MD simulation, amide hydrogen (H) and C_{α} oxygen (O) in Gly483 formed hydrogen bond/polar contact with oxygen atom (O3) at hydroxyl functional group in diflunisal ($Gly483 - H \dots O3 - Dif$, $Gly483 - O \dots O3 - Dif$) (Figure 4.21). Again in site 3 and at 0.0 ps, amide hydrogen atom (H) in Asp325 and hydrogen atom (HH) at the hydroxyl group of Tyr479 side chain formed hydrogen bonds with oxygen atom (O1) at carboxylic functional group in diflunisal ($Tyr479 - HH \dots O1 - Dif$, $Asp325 - H \dots O1 - Dif$) (Figure 4.21). Also, a hydrogen atom (HE2) at the side chain of His538 formed hydrogen bond with oxygen atom (O2) in carboxylic functional group in diflunisal ($His538 - HE2 \dots O2 - Dif$).

At 0.0 ps and in site 1 of tolmetin bound thioredoxin gluthathione reductase MD simulation, amide hydrogen atom (H) in Cys159 and Thr472 formed hydrogen bonds with oxygen atoms (O1and O2) at ketone and carboxylic functional groups in tolmetin ($Cys159 - H \dots O1 - Tol$, $Thr472 - H \dots O2 - Tol$)respectively (Figure 4.21).

During 0.0 ps at site 2 of the tolmetin bound thioredoxin gluthathione reductase MD simulation, hydrogen atoms (2HD2 and 2HE2) at side chain of Asn543 and Gln167 respectively formed hydrogen bonds with oxygen atoms (O1 and O2) at the ketone and carboxylic functional groups in tolmetin ($Asn543 - 2HD2 \dots O1 - Tol$, $Gln167 - 2HE2 \dots O2 - Tol$) respectively (Figure 4.21).

At 0.0 ps and in site 3 of tolmetin bound thioredoxin gluthathione reductase MD simulation, hydrogen atoms at the hydroxyl side chain of Tyr479 (HH) and HE2 at the side chain of His538 formed hydrogen bonds with oxygen atoms (O2 and O3) at the carboxylic functional group in tolmetin ($Tyr479 - HH \dots O2 - Tol$, $His538 - HE2 \dots O2 - Tol$) respectively (Figure

4.21). Again, amide hydrogen atom (H) in Asp325 formed hydrogen bond with oxygen atom (O2) at the carboxylic functional group in tolmetin (*Asp325 – H O2 – Tol*) (Figure 4.21).

At 0.0 ps and in site 2 of dinesterol bound thioredoxin gluthathione reductase MD simulation, hydrogen atom (HH) at the hydroxyl side chain of Tyr335 formed hydrogen bond with an oxygen atom (O2) at the hydroxyl functional group in dinesterol (*Asp335 – HH O2 – Din*) at site 2 (Figure 4.21). Also, nitrogen atom (ND1) at the imidazole side chain of His173 formed hydrogen bond with a hydrogen atom (1H18) at functional group in dinesterol (*His173 – ND1 1H18 – Din*) (Figure 4.21). Polar interaction was not observed in site 3 during dinesterol bound thioredoxin gluthathione reductase MD simulation (Figure 4.21).

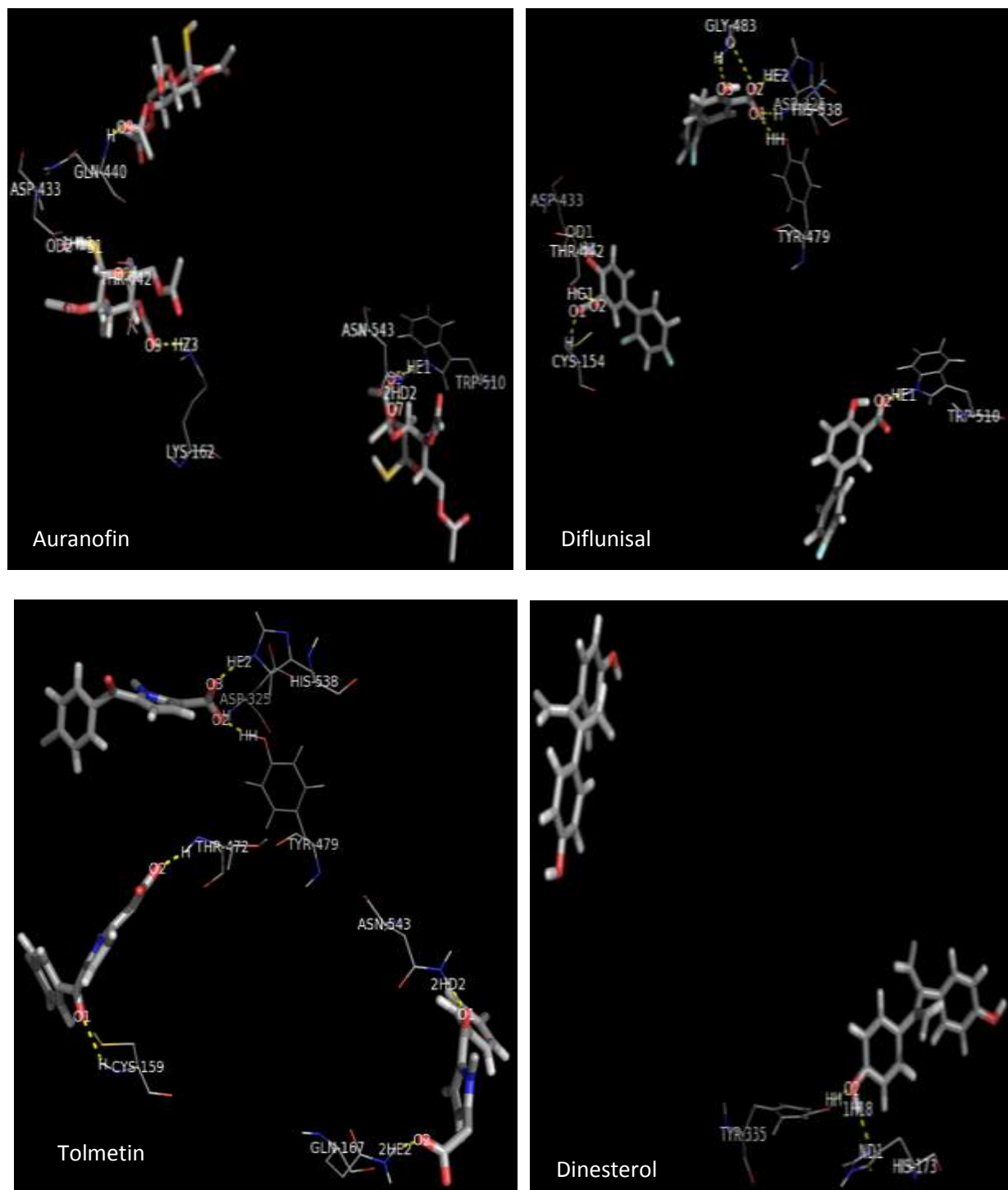


Figure 4.21: The polar contacts/hydrogen bond formation in thioredoxin glutathione reductase-ligand complex at 0 ps of MD simulations. The ligands (auranofin, dilunisal, tolmetin and dinesterol) are represented as sticks while amino acids that show direct contact with the ligands are represented as lines. Both ligands and the amino acids are colored according to the atoms. Red is oxygen, white is hydrogen, blue is nitrogen and grey is carbon atoms. The atoms that show direct contacts are labeled.

At 480 ps and in site 1 of auranofin bound thioredoxin gluthathione reductase MD simulation, *Thr442 – H O3 – Aur* interaction observed at 0.0 ps disappeared with formation of hydrogen bonds between hydrogen atoms (HG1 and HG) at the hydroxyl side chain of Thr442 and Ser117 with oxygen atoms (O1 and O5) at ether and ester functional groups in auranofin (*Thr442 – HG1 O1 – Aur, Ser117 – HG O5 – Aur*) respectively (Figure 4.22). Again, oxygen atom (OE1) at the carboxylic side chain of Glu259 and hydrogen atom at the side chain of Arg393 formed hydrogen bond/polar interaction with oxygen atom (O7) at ester functional group in auranofin (*Glu259 – OE1 O7 – Aur, Arg393 – HE O7 – Aur*). It is important to note that at 480 ps and in site 1, a covalent interaction (*Asp433 – OD2____1H11 – Aur*) estimated at 0.0 ps was maintained with formation of additional polar interaction between oxygen atom (OD1) at the carboxylic side chain of Asp433 and oxygen atom (O5) at the ester functional group in auranofin (*Asp433 – OD1 O5 – Aur*) (Figure 4.22). Polar interaction was not observed in site 2 at 480 ps during of auranofin bound thioredoxin gluthathione reductase MD simulation (Figure 4.22).

It is important to note that the *Gln440 – H O9 – Aur* interaction observed in site 3 at 0.0 ps (Figure 4.22) was maintained at 480 ps and 2800 ps of the simulation (Figure 4.22). However, at 480 ps the following additional interactions were observed. First, C_{α} oxygen (O) in Gly323 and Gln440 formed hydrogen bond/polar interaction with oxygen atoms (O5 and O9) ester functional groups in auranofin (*Gly323 – O O5 – Aur, Gln440 – O O9 – Aur*) respectively (Figure 4.22). Secondly, hydrogen atom (HG) at the hydroxyl side chain of Ser485 formed hydrogen bond with oxygen atom (O5) at ester functional group in auranofin (*Ser485 – HG O5 – Aur*) (Figure 4.22).

At 480 ps and in site 1 of diflunisal bound thioredoxin gluthathione reductase MD simulation, amide hydrogen atom (H) in Cys159 formed hydrogen bond with two oxygen atoms (O1 and O2) at the carboxylic functional group in diflunisal (*Cys159 – H O1 – Dif, Cys159 –*

$H \dots O2 - Dif$) (Figure 4.22). Again, at 480 ps, amide hydrogen (H) in Thr442 and C_α oxygen (O) in Gln440 formed hydrogen bonds with oxygen atom (O3) and hydrogen atom (H7) at hydroxyl functional group in diflunisal ($Thr442 - H \dots O3 - Dif$, $Gln440 - O \dots H7 - Dif$) respectively (Figure 4.22). Also at 480 ps and in site 1, hydrogen atom (HZ2) at the side chain of Lys162 formed hydrogen bond with oxygen atom (O2) at carboxylic functional group in diflunisal ($Lys162 - HZ2 \dots O2 - Dif$) (Figure 4.22).

It is important to note that $Trp510 - HE1 \dots O2 - Dif$ interaction observed at 0.0 ps of the diflunisal bound thioredoxin gluthathione reductase MD simulation was maintained at 480 ps (Figure 4.21 and 4.22).

At 480 ps and in site 1 of tolmetin bound thioredoxin gluthathione reductase MD simulation, $Cys159 - H \dots O1 - Tol$ and $Thr472 - H \dots O2 - Tol$ interactions (Figure 4.21) observed at 0.0 ps were lost to the formation of possible covalent bond between hydrogen atom (HG) at the sulphurhydryl side chain of Cys159 with an oxygen atom at the carboxylic functional group of tolmetin ($Cys159 - HG \dots O3 - Tol$) (Figure 4.22). Also in site 1 and at 480 ps, hydrogen atom (HG1) at the hydroxyl side chain of Thr442 formed hydrogen bond with oxygen atom (O2) at the carboxylic acid functional group in tolmetin ($Thr442 - HG1 \dots O2 - Tol$) (Figure 4.22).

At 480 ps and site 2 of the tolmetin bound thioredoxin gluthathione reductase MD simulation, the $Gln167 - 2HE2 \dots O2 - Tol$ interaction observed at 0.0 ps (Figure 4.21) persisted but that of $Asn543 - 2HD2 \dots O1 - Tol$ disappeared (Figure 4.22).

At site 3 and 480 ps of tolmetin bound thioredoxin gluthathione reductase MD simulation, the interactions observed at 0.0 ps were maintained (Figure 4.21 and 4.22). However, additional hydrogen bonds were formed between amide hydrogen atoms (H) in Val469 and Gly483 with oxygen atom (O1) in the ketone functional group in tolmetin ($Val469 - H \dots O1 - Tol$, $Gly483 - H \dots O1 - Tol$) (Figure 4.22). Again, C_α oxygen atom (O) in Asp325 formed a polar

interaction with oxygen atom (O1) at the ketone functional group in tolmetin (*Asp*325 – *O* *O1* – *Tol*) (Figure 4.22).

At 480 ps and site 2 of dinesterol bound thioredoxin glutathione reductase MD simulation, *His*173 – *ND*1 *1H*18 – *Din* interaction observed at 0.0 ps (Figure 4.21 and 4.22) was maintained while that of *Asp*335 – *HH* *O2* – *Din* disappeared (Figure 4.22). Again, polar contact was not observed in site 3 at 480 ps of the MD simulation (Figure 4.22).

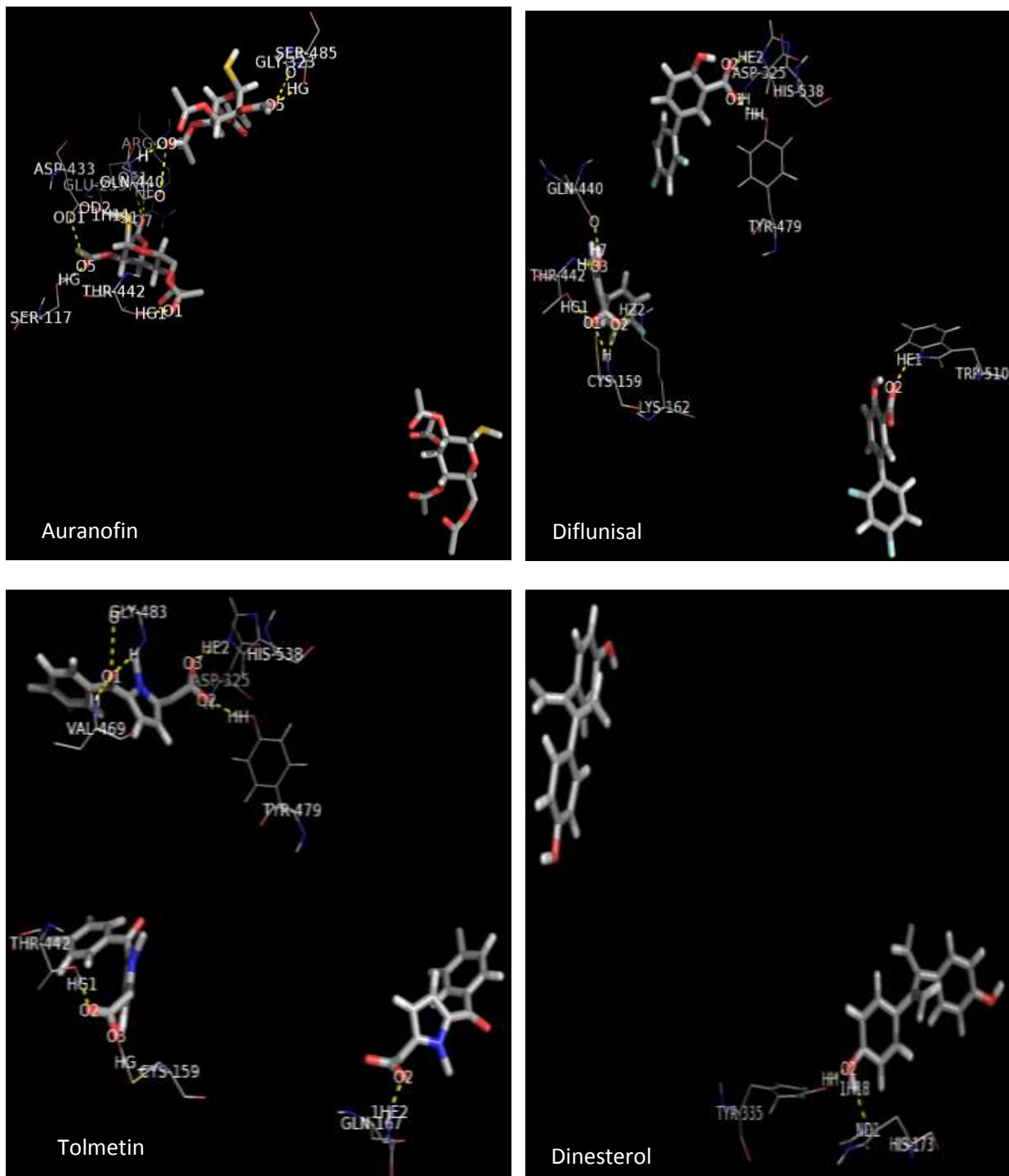


Figure 4.22: The polar contacts/hydrogen bond formation in thioredoxin glutathione reductase-ligand complex at 480 ps of MD simulations. The ligands (auranofin, dilunisal, tolmetin and dinesterol) are represented as sticks while amino acids that show direct contact with the ligands are represented as lines. Both ligands and the amino acids are colored according the atoms. Red is oxygen, white is hydrogen, blue is nitrogen and grey is carbon atoms. The atoms that show direct contacts are labeled.

At site 1 and 2800 ps of auranofin bound thioredoxin gluthathione reductase MD simulation, the *Ser117 – HG* *O5 – Aur* interaction observed at 480 ps was maintained (Figure 4.22 and - 4.23). However, *Thr442 – H* *O3 – Aur* interaction observed at 0.0 ps was replaced by *Thr442 – H* *O2 – Aur* (Figure 4.23). In addition, a polar interaction was formed between C_{α} oxygen atom (O) in Cys154 and oxygen atom (O9) at ester functional group in auranofin (*Cys154 – O* *O9 – Aur*) (Figure 4.23). Polar interaction was not observed in site 2 at 480 ps of the auranofin bound thioredoxin gluthathione reductase MD simulation (Figure 4.23). However, at 2800 ps hydrogen atom (1HD2) attached to $-NH_3$ in the side chain of Asn543 formed hydrogen bond with oxygen atom (O9) at ester functional group in auranofin (*Asn543 – 1HD2* *O9 – Aur*) (Figure 4.23). Also at 2800 ps and in site 3, *Gln440 – H* *O9 – Aur* interaction observed at 0.0 and 480 ps was maintained (Figure 4.22 and 4.23). However, additional polar interaction was established between C_{α} oxygen atom (O) in Arg322 and oxygen atom (O1) at ether functional group in auranofin (*Arg322 – O* *O1 – Aur*) (Figure 4.23).

At site 1 of diflunisal bound thioredoxin gluthathione reductase MD simulation, *Cys159 – H* *O1 – Dif*, *Cys159 – H* *O2 – Dif* and *Gln440 – O* *H7 – Dif* interactions observed at 480 ps were maintained at 2800 ps. However, a covalent bond was estimated between hydrogen atom (HG) at the sulphhydryl side chain of Cys159 and oxygen atom (O1) at the carboxylic functional group in diflunisal (*Cys159 – H* *O1 – Dif*) (Figure 4.23). In addition, *162 – HZ2* *O2 – Dif* , *Thr442 – H* *O3 – Dif* interactions observed at 480 ps were replaced by *Lys162 – HZ1* *O2 – Dif* , *Thr442 – HG1* *O1 – Dif* interactions respectively (Figure 4.23).

Polar interaction was not observed at site 2 in the diflunisal bound thioredoxin gluthathione reductase MD simulation (Figure 4.23) but *Tyr479 – HH* *O1 – Dif* , *Asp325 – H* *O1 – Dif* and *His538 – HE2* *O2 – Dif* interactions observed in site 3 at 0.0 ps

persisted at 480 ps and 2800 ps of the diflunisal bound thioredoxin glutathione reductase MD simulation (Figure 4.23).

At 2800 ps and site 1 of tolmetin bound thioredoxin glutathione reductase MD simulation, hydrogen atom (HG) at the sulphurhydryl side chain of Cys154 formed covalent bond with oxygen atom (O2) at the carboxylic functional group in tolmetin (*Cys154 – HG O2 – Tol*) (Figure 4.23) while hydrogen atom (HG1) at hydroxyl side chain of Thr442 formed hydrogen bond with oxygen atom (O3) at the carboxylic functional group in tolmetin (*Thr442 – HG1 O3 – Tol*) (Figure 4.23). Then, at 2800 ps and site 2, the hydrogen atom (1HE2) attached to $-NH_2$ at side chain of Gln167 formed hydrogen bond with oxygen atom (O3) at the carboxylic functional group in tolmetin (*Gln167 – 1HE2 O3 – Tol*) (Figure 4.23).

In site 3 and at 2800 ps of tolmetin bound thioredoxin glutathione reductase MD simulation, it is important to mention that the hydrogen bond formed between hydrogen atom (HE2) attached to the imidazole side chain of His538 and oxygen atom (O3) at the carboxylic functional group of tolmetin at 0..0 ps was maintained throughout the simulation time (Figure 4.21 to 4.23).

Again at 2800 ps of dinesterol bound thioredoxin glutathione reductase MD simulation, *His173 – ND1 1H18 – Din* interaction observed at 0.0 ps and 480 ps persisted up to 2800 ps with reestablishment of *Asp335 – HH O2 – Din* interaction at site 2 (Figure 4.23). Again, in site 3, hydrogen bond was formed between amide hydrogen (H) in Tyr296 and oxygen atom (O2) at the hydroxyl functional group in dinesterol (*Tyr296 – H O2 – Din*) (Figure 4.23).

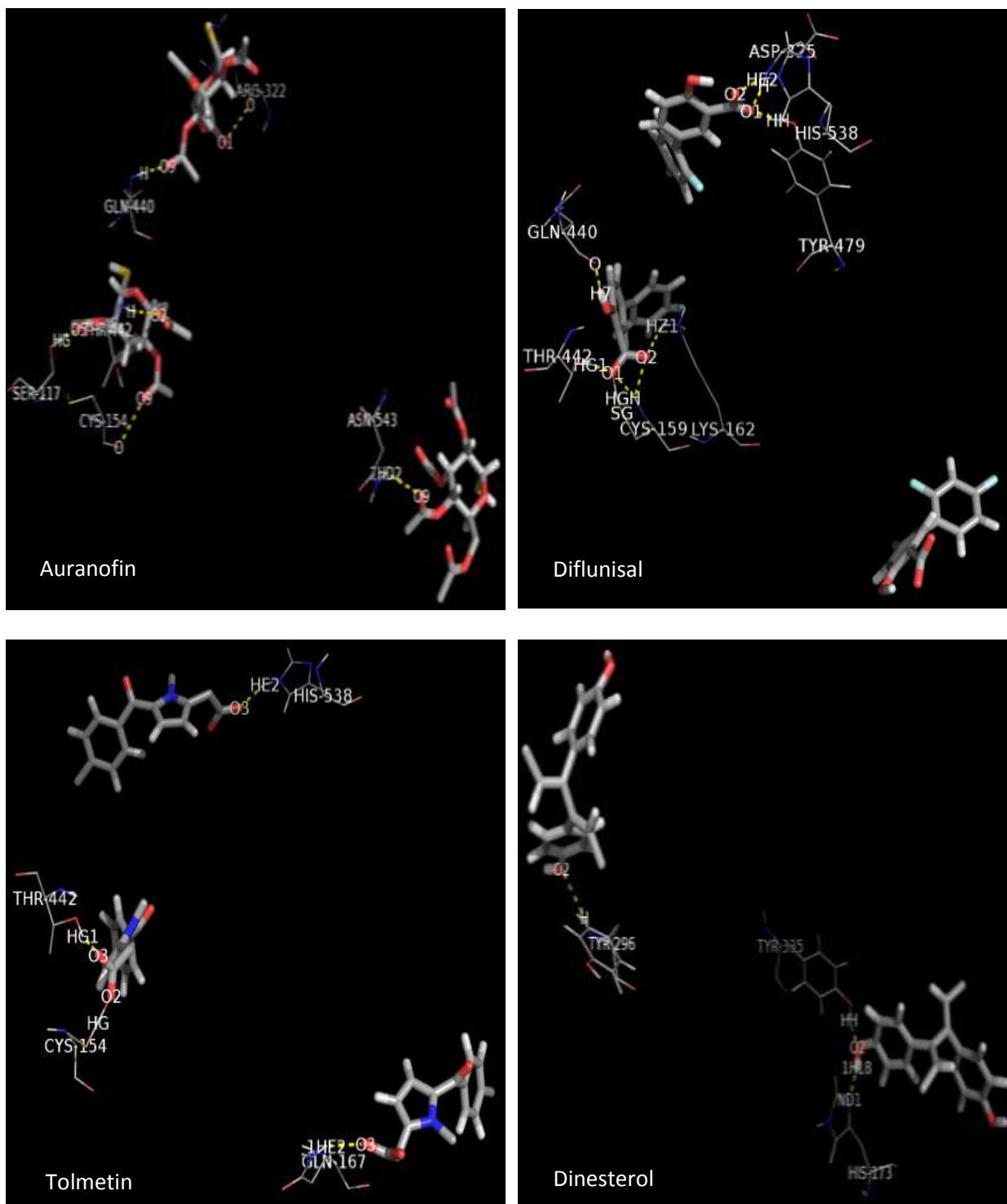


Figure 4.23: The polar contacts/hydrogen bond formation in thioredoxin glutathione reductase-ligand complex at 2800 ps of MD simulations. The ligands (auranofin, dilunisal, tolmetin and dinesterol) are represented as sticks while amino acids that show direct contact with the ligands are represented as lines. Both ligands and the amino acids are colored according to the atoms. Red is oxygen, white is hydrogen, blue is nitrogen and grey is carbon atoms. The atoms that show direct contacts are labeled.

The various amino acids that have direct/polar contact with the ligands (Figure 4.21 to 4.23) are in turn connected to other amino acid(s) (Figure 4.24). For example, it can be observed from figure 4.24 that Cys159 is connected to Gly158, Gln440 is connected to Leu441 and His173 is connected to Ala174.

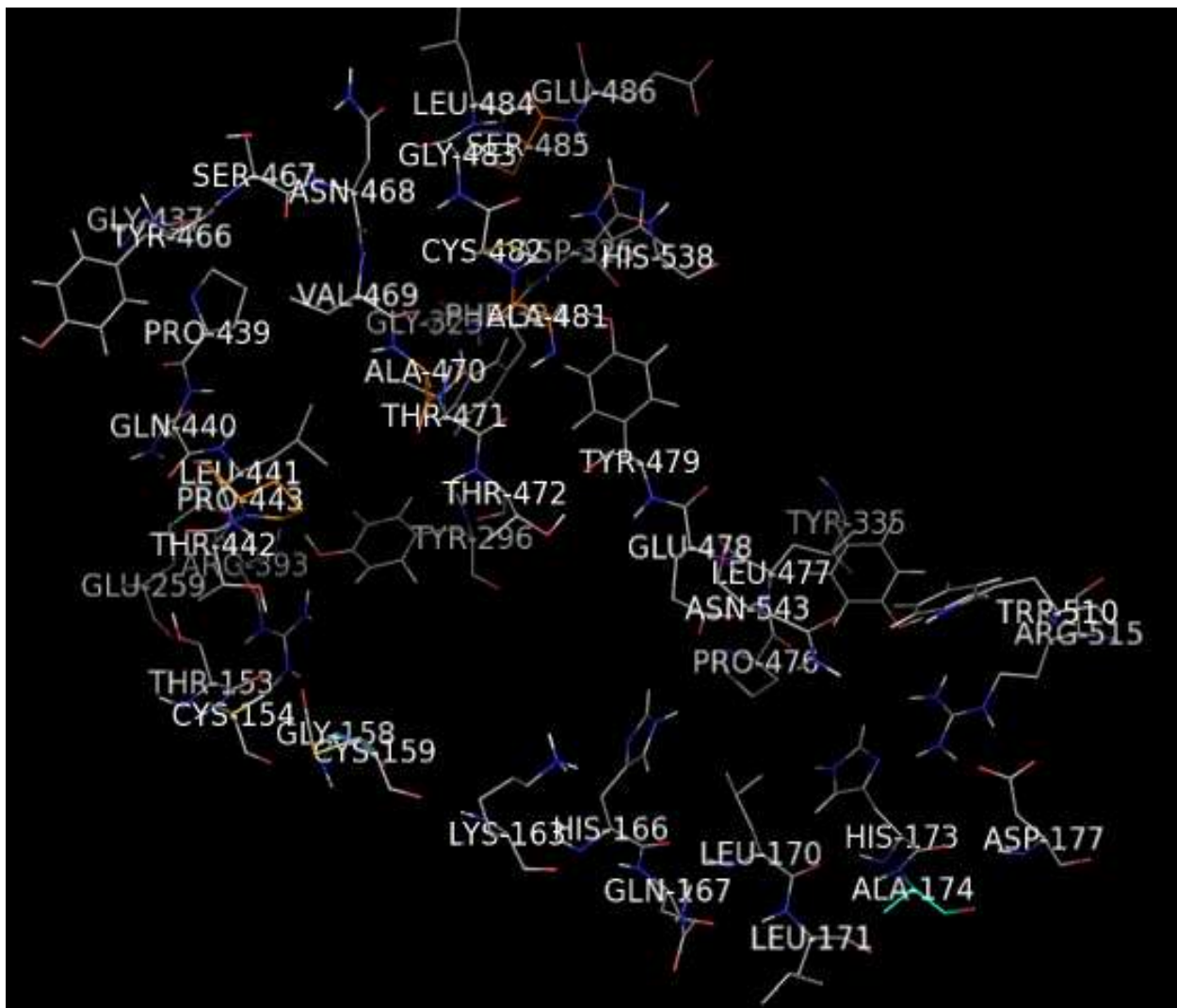


Figure 4.24 Amino acids in thioredoxin glutathione reductase that interacts with the ligands from the MD simulation.

Bond distance/stretching

To get information about bond formation and breakage of bonds in the target-ligand interactions, the distance of the various interactions (hydrogen bonds, possible covalent bonds etc) were monitored as a function of time and presented in figure 4.25 and figures 4.27 to 4.29. Also, the average distances were computed and presented in Appendix 17. Figure 4.25 is suggestive of breakage of *Asn233: OD1/H16: Oxa*, *Thr242: HG1/O2: Tol* and *Asp149: OD1/1H13: Din* hydrogen bonds during the auranofin, tolmetin and dinesterol bound sulfotransferase MD simulations respectively. It is important to note that *Asn233: OD1/H16: Oxa*, *Thr242: HG1/O2: Tol* and *Asp149: OD1/1H13: Din* showed average distance of 0.88295 ± 0.23768 nm, 1.13370 ± 0.21481 nm and 0.73031 ± 0.51959 nm respectively (Appendix 17). Also, figure 4.25 indicates that breakage of *Asn233: OD1/H16: Oxa*, *Thr242: HG1/O2: Tol* and *Asp149: OD1/1H13* hydrogen bonds are accompanied with formation of *Asn46: OD1/O1: Oxa*, *Lys23: HZ3/O3: Tol* and *Asn233: 2HD2/O1: Din* hydrogen bonds at different time points in the MD simulations (Figure 4.25).

It is important to note that *Asp96: OD2/H3: Dif* hydrogen bond distance was very stable with average length of 0.18731 ± 0.01838 nm during the diflunisal bound sulfotransferase MD simulation while *Asn233: 2HD2/O1: Dif*, *Arg19: 1HH1/O1: Dif* and *Arg19: 1HH1/O2: Dif* showed fluctuations with average bond distances of 0.24947 ± 0.06941 nm, 0.30253 ± 0.07492 nm and 0.28327 ± 0.07125 nm respectively (Appendix 17).

Again, *Asp96: OD2/1H18: Din*, *Asp96: OD1/1H18: Din* and *Arg19: H/O2: Din* hydrogen bond distances were stable during the dinesterol bound sulfotransferase MD simulation (Figure 4.25) with average distances of 0.20057 ± 0.04480 nm, 0.25229 ± 0.0619 nm and 0.21943 ± 0.03613 nm respectively (Appendix 17).

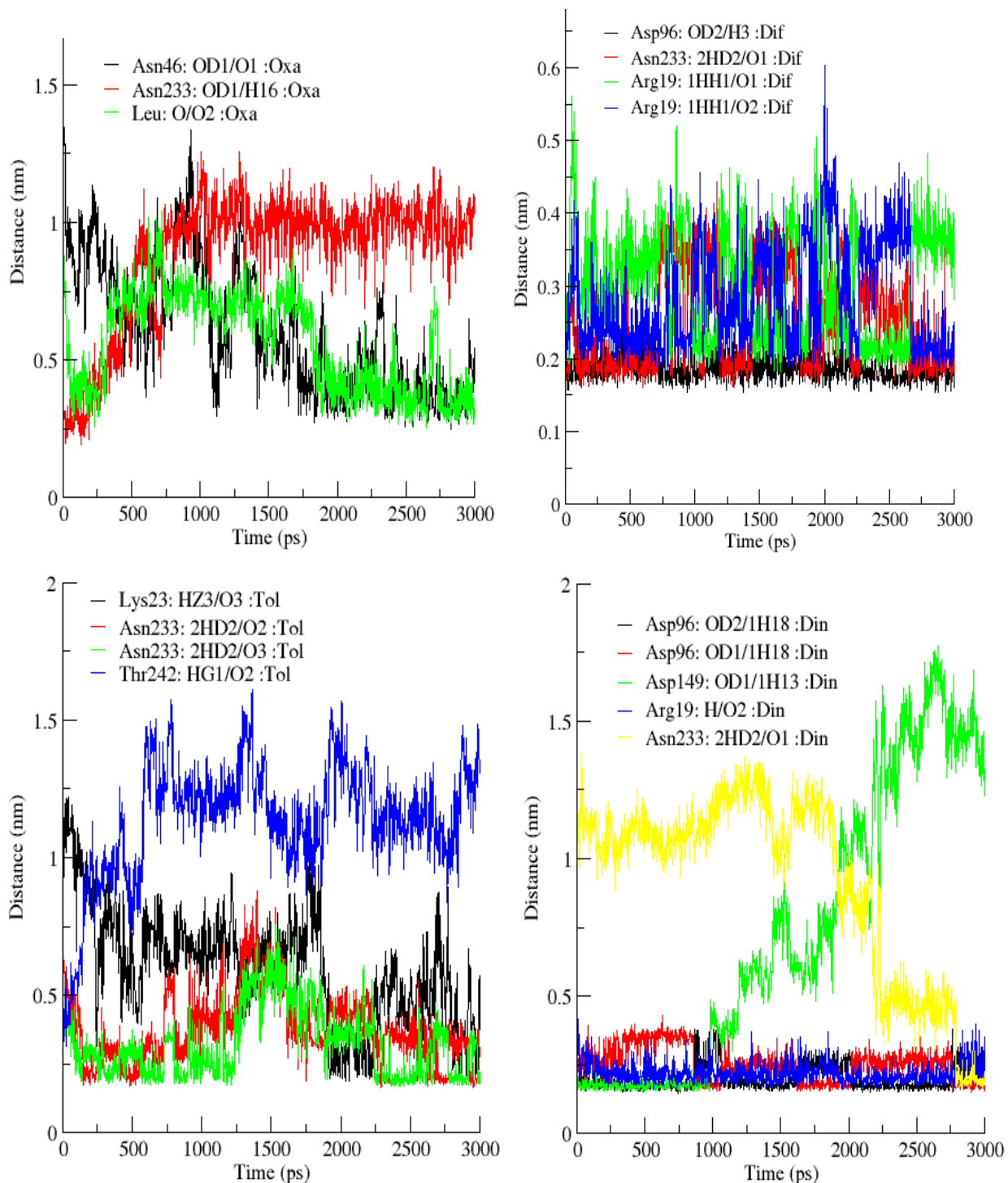


Figure 4.25: Distance of hydrogen bonds in sulfotransferase-ligand complexes during MD simulations. OXA = oxamniquine, DIF=diflunisal, DIN=dinesterol and TOL=tolmetin.

Figure 4.26 shows the structure of thioredoxin glutathione reductase with the locations of the three binding sites for the ligands as well as FAD cofactor. The bond distances between atoms in its amino acid residues that showed direct interaction with the ligands (auranofin, diflunisal, tolmetin and dinesterol) as well as the minimum distances between the ligands and the FAD were computed and presented in figures 4.27 to 4.29, figure 4.30 respectively and appendix 17.

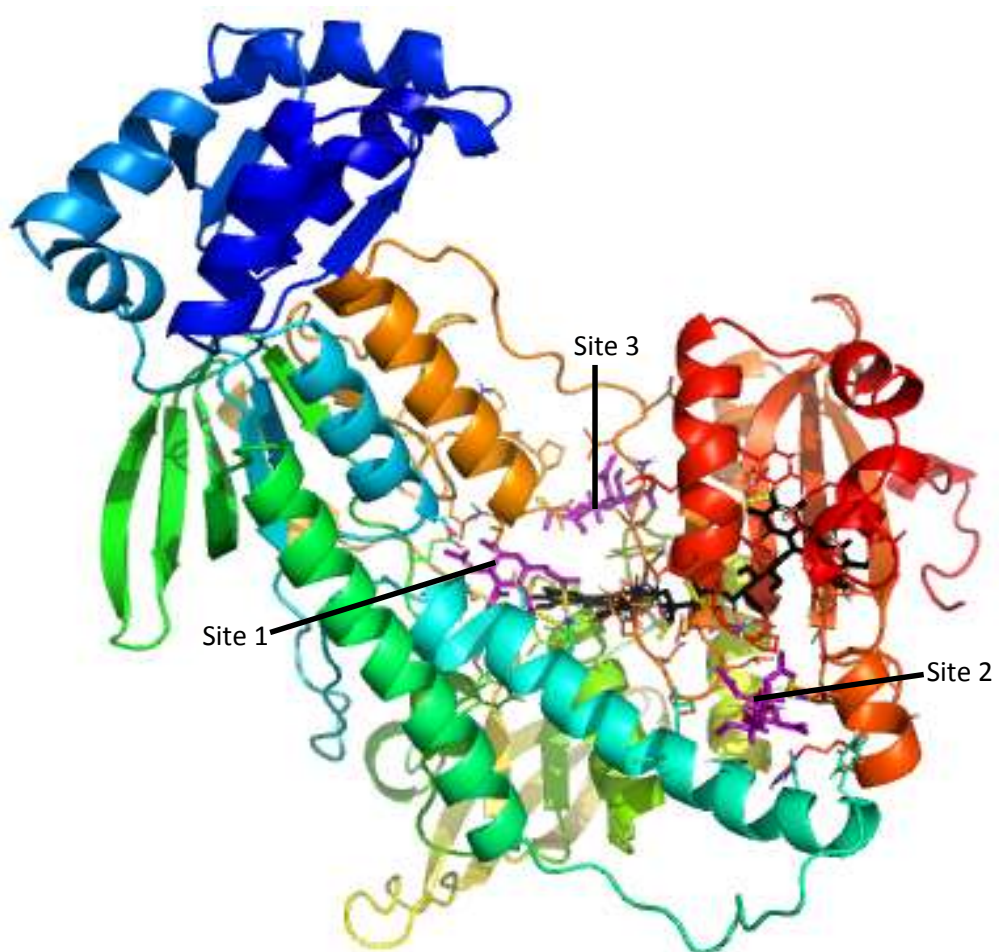


Figure 4.26: The three-dimensional structure of schistosomal thioredoxin glutathione reductase showing the three binding sites for ligands. Black stick representation is FAD while purple are the ligands.

Figure 4.27 is suggestive of formation of weak hydrogen bond (*Lys162: HZ3/O9: Aur*) as auranoxin bound thioredoxin glutathione reductase MD simulation progressed. Figure 4.27 suggests breakage and formation of *Asp433: OD1/H7: Dif* interaction with average distance of 0.69924 ± 0.10775 nm (Appendix 17). Figure 4.27 suggests breakage of *Thr472: H/O2: Tol* and *Cys159: H/O1: Tol* bonds with corresponding formation of potential covalent bond (*Cys159: HG/O3: Tol*) with estimated average distance of 0.28618 ± 0.14979 nm (Appendix 17). It is important to note that *Asp433: OD2/1H11: Aur*, *Cys159: HG/O1: Dif* and *Cys159: HG/O3: Tol* potential covalent bonds were observed in the auranoxin, diflunisal and tolmetin bound thioredoxin glutathione reductase MD simulations (Figure 4.27) with estimated average lengths of 0.14282 ± 0.04108 nm, 0.15324 ± 0.02388 nm and 0.28618 ± 0.14979 nm respectively (appendix 17).

Also, the various hydrogen bond distances involving amide hydrogen in the different amino acids and the ligands are stable during the MD simulations (Figure 4.27) and are comparable to the distances of the potential covalent bonds (Appendix 17). It is important to mention that dinosterol did not bind to site 1 even from the molecular docking simulation experiments (Figure 4.4 B). Other bonds observed in site 1 are either stable or fluctuated around a particular value for the entire ligand bound thioredoxin glutathione reductase MD simulations (Figure 4.27 and appendix 17).

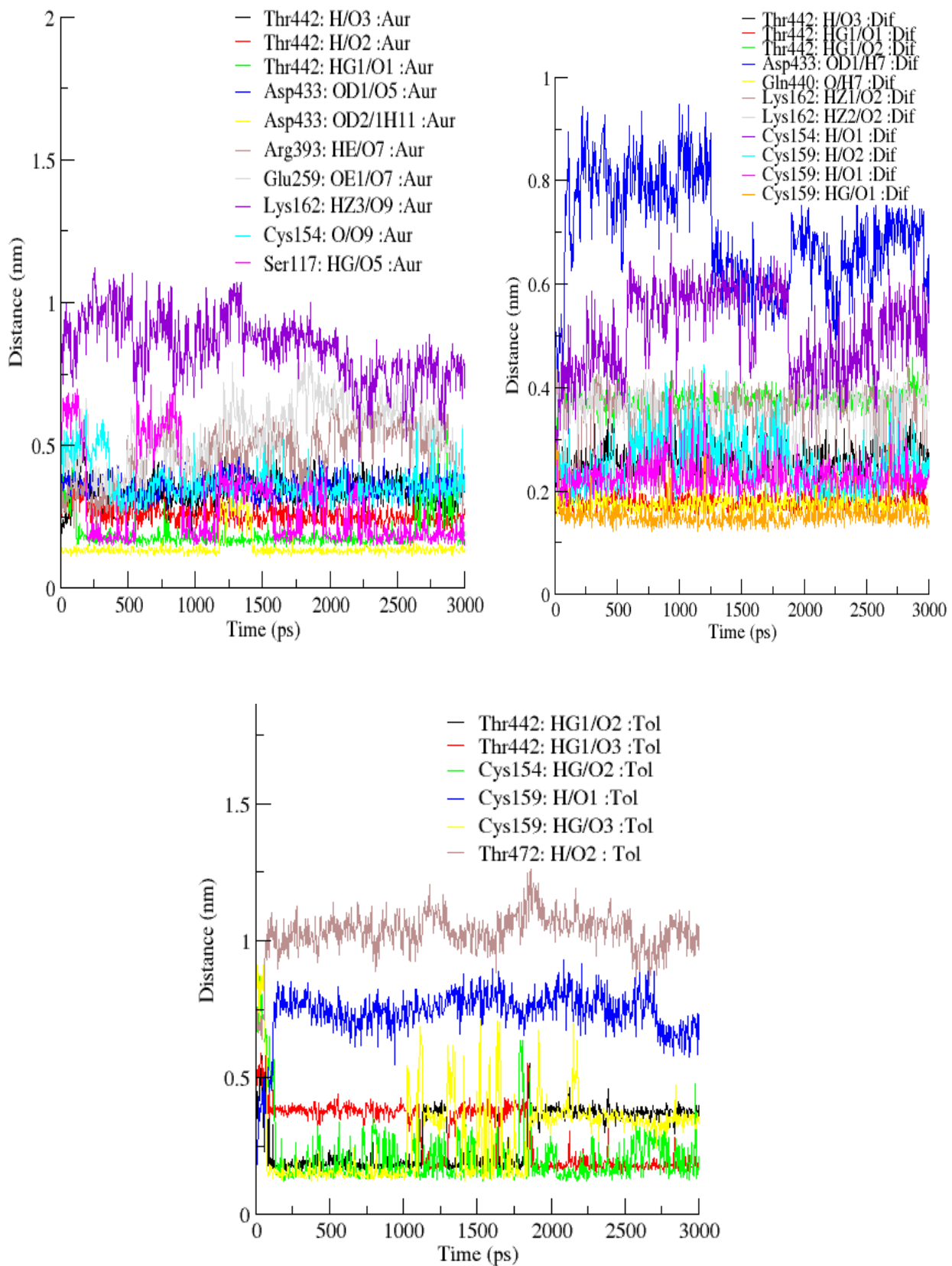


Figure 4.27: Distance of hydrogen bonds at site 1 in ligand bound thioredoxin glutathione reductase complexes during MD simulations. AUR = auranofin, DIF=diflunisal and TOL=tolmetin.

Figure 4.28 suggests breakage and formation of Asn543: 1HD2/09: Aur and Asn543: 2HD2/07: Aur hydrogen bonds at different time points in the auranoxin bound thioredoxin glutathione reductase MD simulation. This is in contrast with Trp510: HE1/05: Aur interaction distance that was fairly stable with average length of 0.37562 ± 0.09109 nm (Figure 4.28 and appendix 17).

During diflunisal bound thioredoxin glutathione reductase MD simulation, Trp510: HE1/02: Dif bond was broken at about 750 ps of the simulation (Figure 4.28). Then during tolmetin bound thioredoxin glutathione reductase MD simulation, there was breakage and reformation of Asn543: 2HD2/01: Tol interacton (Figure 4.28) with average bond distances presented in appendix 17.

Also, during dinesterol bound thioredoxin glutathione reductase MD simulation, Tyr335: HH/02: Din hydrogen bond distance was more stable compared with that of His173: ND1/1H18: Din (Figure 4.28). They showed average bond length of 0.21841 ± 0.07857 nm and 0.34062 ± 0.12007 nm respectively (Appendix 17).

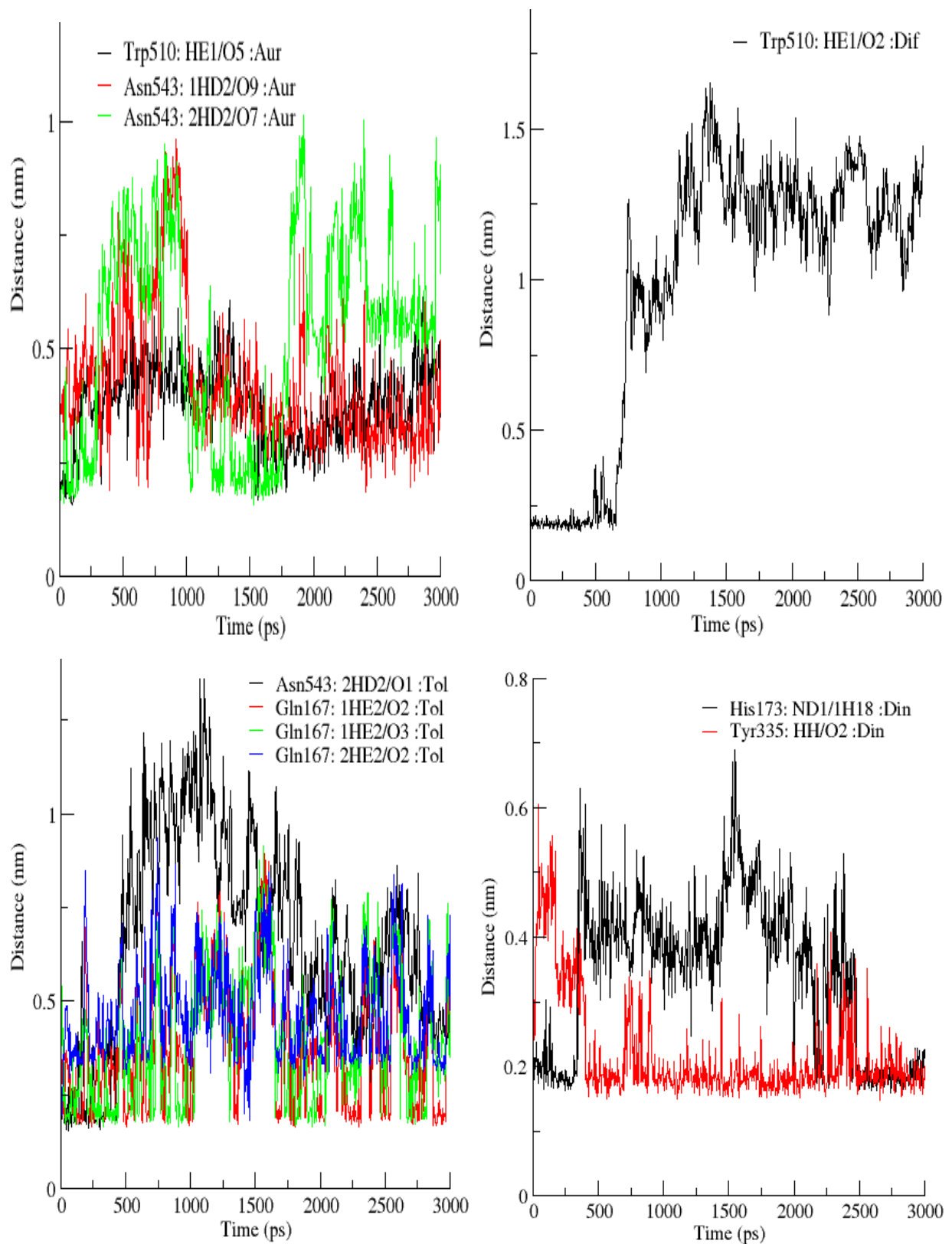


Figure 4.28: Distance of hydrogen bonds at site 2 in ligand bound thioredoxin glutathione reductase complexes during MD simulations. AUR = auranofin, DIF=diflunisal, DIN=dinesterol and TOL=tolmetin.

Figure 4.29 showed that Gln440: H/09: *Aur* bond distance at site 3 during the auranofin bound thioredoxin glutathione reductase MD simulation was more stable with average bond distance of 0.19398 ± 0.02337 nm when compared with Ser485: HG/05: *Aur* , Gln440: O/09: *Aur* , Gly323: O/05: *Aur* and Arg322: O/01: *Aur* bonds (Figure 2.29 and appendix 17). Similarly, diflunisal bound thioredoxin glutathione reductase MD simulation indicate that His538: HE2/ O2: *Dif*, Asp325: H/01: *Dif* and Tyr479: HH/01: *Dif* hydrogen bond distances are more stable with average bond lengths of 0.20095 ± 0.02103 nm, 0.20808 ± 0.02870 nm and 0.18199 ± 0.02668 nm when compared with Gly483: H/03: *Dif* and Gly483: O/03: *Dif* bond distances (Figure 4.29 and appendix 17). Again, tolmetin bound thioredoxin glutathione reductase MD simulation indicate that His538: HE2/O3: *Tol* bond distance was more stable with average bond length of 0.19364 ± 0.04288 nm when compared with Gly483: H/01: *Tol* , Tyr479: HH/02: *Tol* , Val469: H/01: *Tol* and Asp325: H/02: *Tol* bond distances (Figure 4.29 and appendix 17). Finally at site 3 of the dinesterol bound thioredoxin glutathione reductase MD simulation indicate that Tyr292: H/02: *Din* hydrogen bond distance attained a shorter distance between 2000 to 3000 ps of the simulation (Figure 4.29) with average bond distance of 0.40766 ± 0.11964 nm (appendix 17).

Also the minimum distance between the ligand (auranofin, diflunisal, tolmetin, dienestrol) in site 1, 2 and 3 with FAD in thioredoxin glutathione reductase were calculated and presented in Figure 4.30 and Appendix 18.

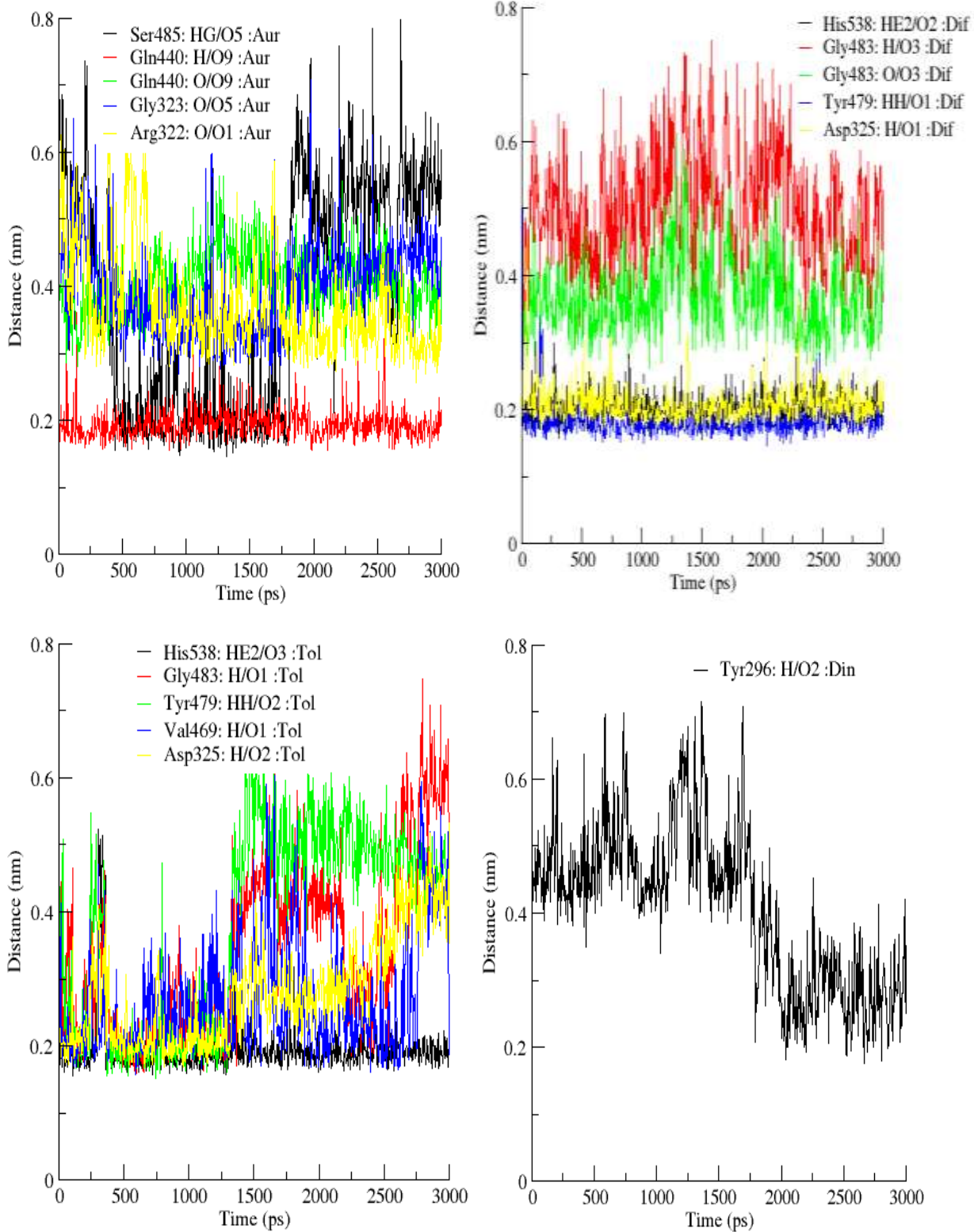


Figure 4.29: Distance of hydrogen bonds at site 3 in ligand bound thioredoxin glutathione reductase complexes during MD simulations. AUR = auranofin, DIF=diflunisal, DIN=dinesterol and TOL=tolmetin.

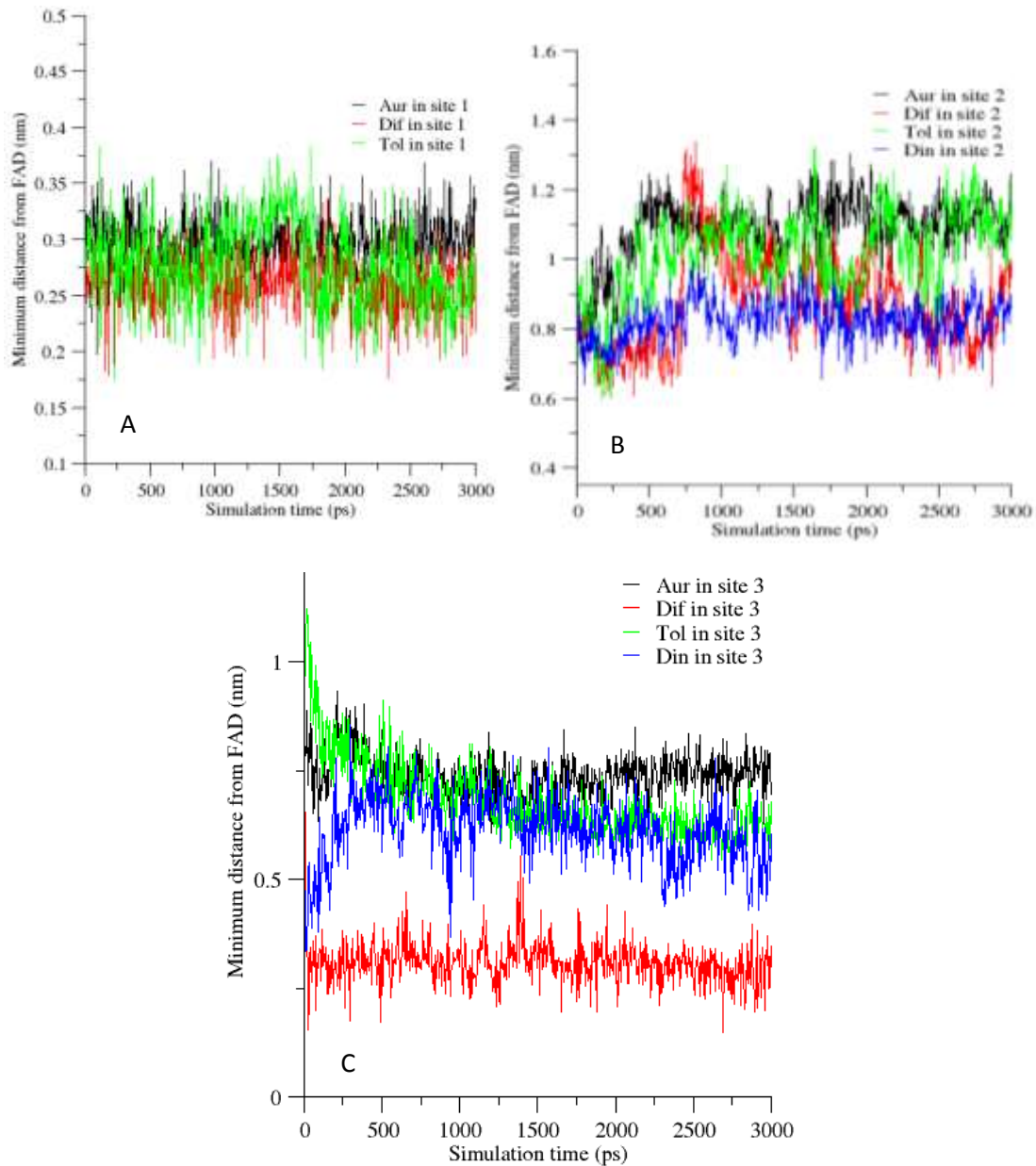


Figure 4.30: Minimum distance between FAD and fronrunners (Auranofin, Diflunisal, Tolmetin, and Dienestrol) in site 1, 2 and 3 and FAD in thioredoxin glutathione reductase. (A), (B) and (C) are distances between FAD and fronrunner at spite 1, 2 and 3 respectively.

Conformational Sampling

Inorder to detect populated conformations sampled by the MD siulations of free and ligand bound sulfotransferase and TGR, clustering analysis wad conducted with clustering cutoff of 1.5 Å. It can be seen from appendix 19 that the distributions of cluster size of free and ligand bound sulfotransferase and TGR were markedly different. Free sulfotransferase showed 21 clusters compared to 23, 23, 22 and 25 clusters due to interactions with oxamniquine, diflunisal, tolmetin and dinesterol respectively (Appendix 19). Also, free TGR showed 35 clusters compared to 27, 29, 30 and 30 clusters due to influence of auranofin, diflunisal, tolmetin and dinesterol respectively (appendix 19). The percentage of the clusters had also been calculated as illustrated in figure 4.31 and appendix 19. The seven most populated clusters in free sulfotransferase typically encompassed up to 77.34843438 % of the total structure populations compared with 71.28580946 %, 74.61692205 %, 74.81678881 % and 66.95536309 % due to interactions with oxamniquine, diflunisal, tolmetin and dinesterol repectively. Again, the seven most populated clusters in free TGR typically encompassed up to 42.21038615 % of the total structure populations compared with 56.99067909 %, 50.19973369 %, 49.80026631 % and 49.26764314 % due to interactions with auranofin, diflunisal, tolmetin and dinesterol respectively. As reflected in figure 4.32 to 4.35, cluster 1 in the whole trajectories verified that there were conformational changes leading to different atom prefernces for the ligand target interactions.

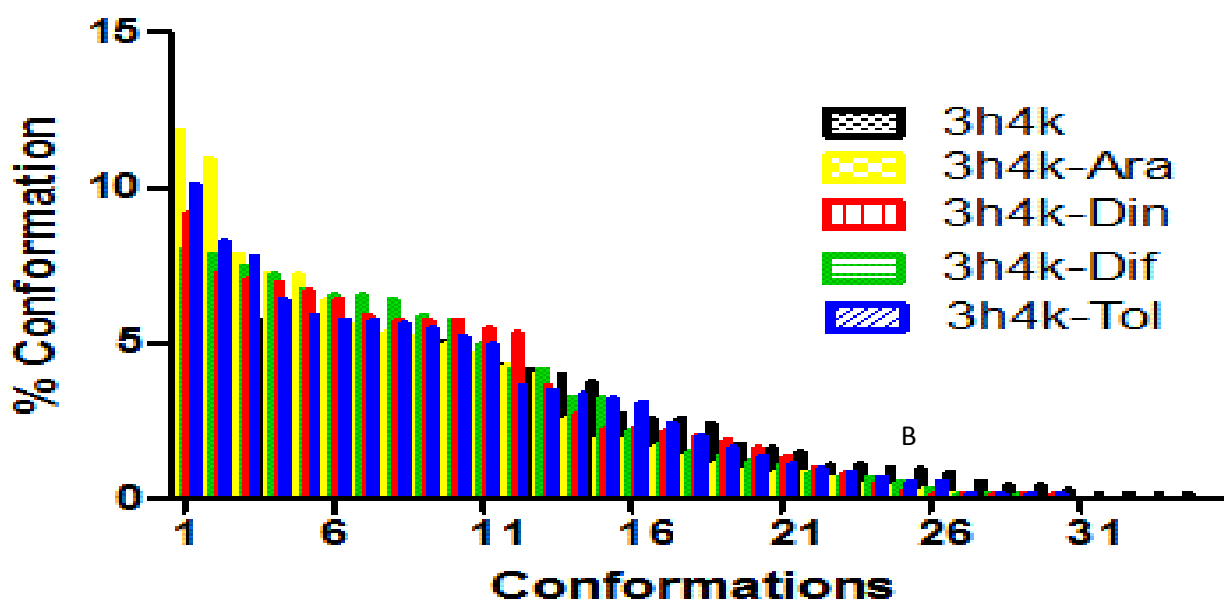
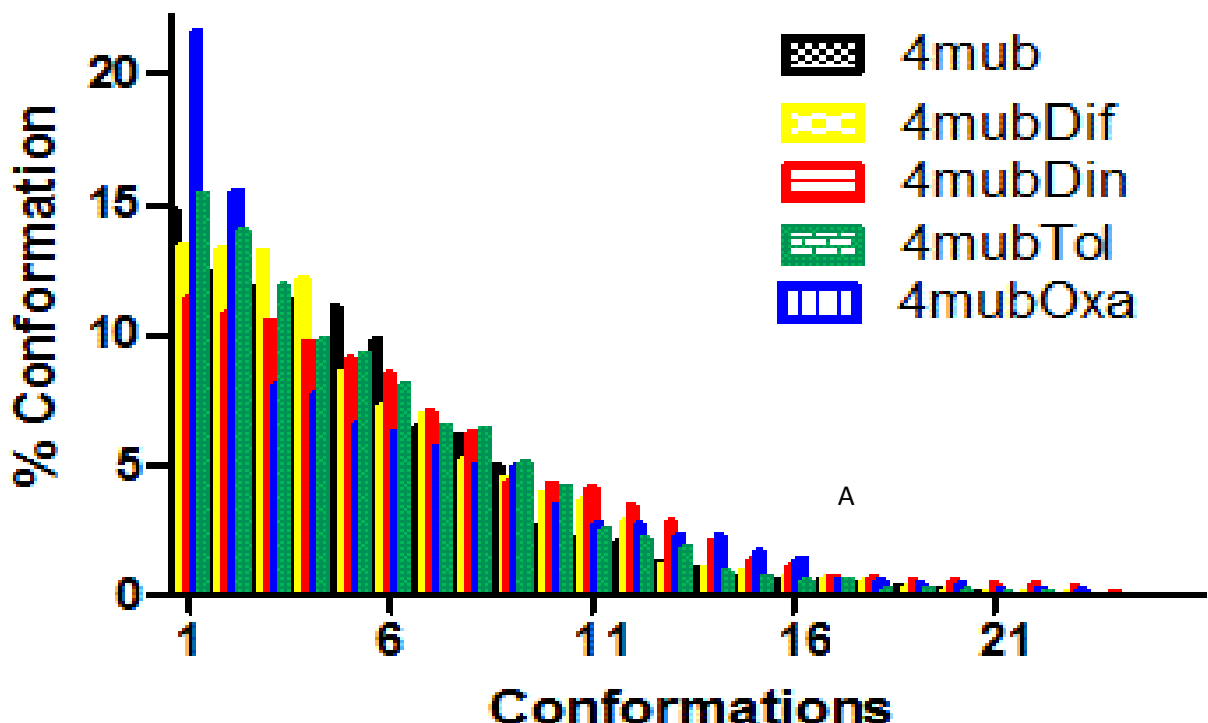


Figure 4.31: Conformational sampling of free and frontrunner bound sulfotransferase (4MUB) and thioredoxin glutathione reductase (3H4K) at clustering cutoff of 1.5 Å. AUR = auranofin, OXA=oxamniquine, DIF=diflunisal, DIN=dinesterol and TOL=tolmetin.

Conformational remodeling due to interaction with ligands

Representative structures from conformational sampling of free and ligand bound sulfotransferase are presented in Figure 4.32 to 4.33. Atoms in amino acids in the sulfotransferase especially those at the binding sites and/or close to them showed marked rearrangement in presence of ligands when compared with same in absence of ligands (Figure: 4.32). For example, it can be observed from figure 4.32 that carboxylic acid and hydroxyl functional groups in diflunisal showed more preference of interaction with oxygen and hydrogen atoms in sulfotransferase than the rest of the ligands while their respective benzoic groups showed more interaction with the carbon atoms. Benzoic rings in dinesterol had preference for carbon atoms.

Close observation showed that the preferences for different atomic interactions brought about conformational changes in the secondary structure of sulfotransferase as shown in Figure 4.33.

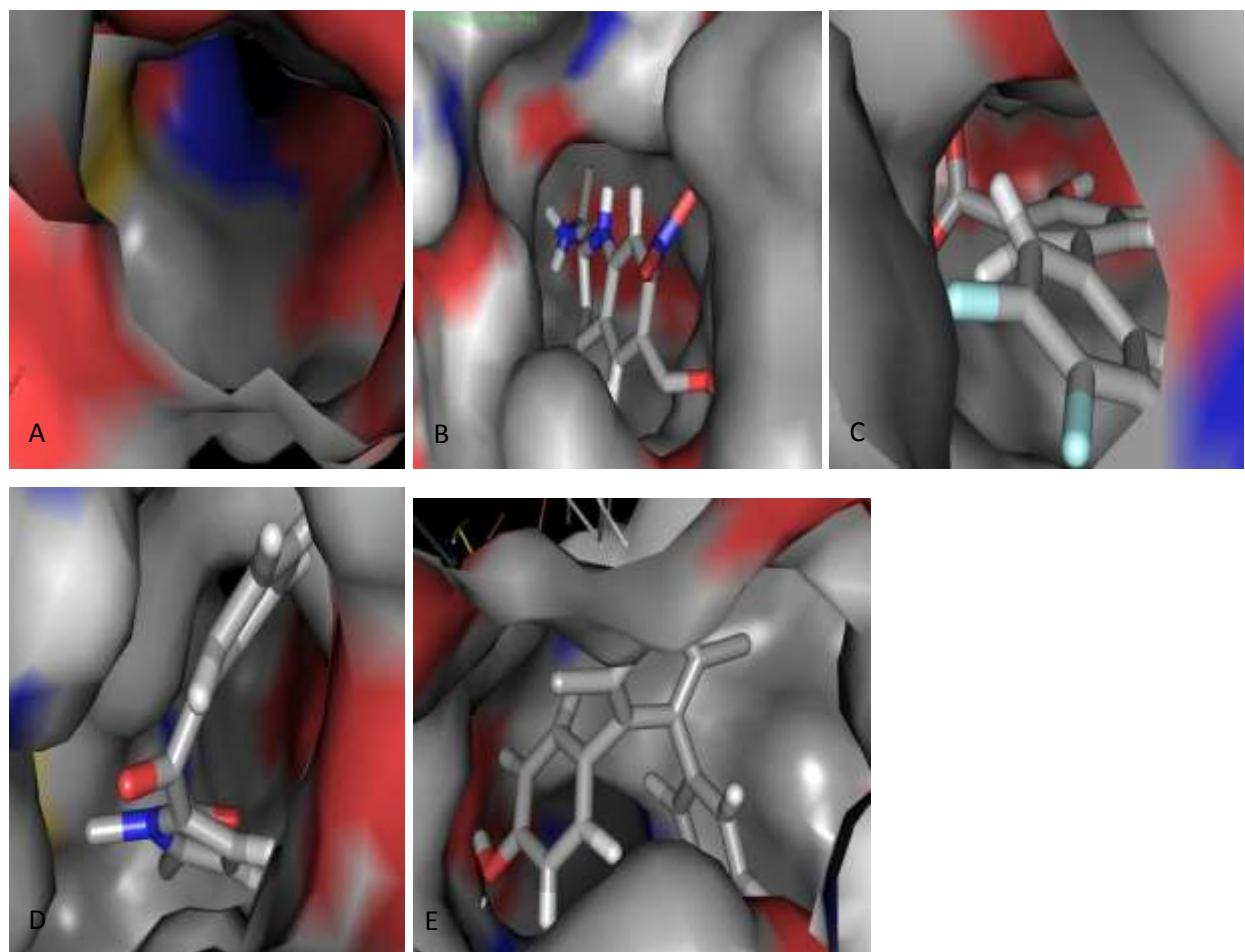


Figure 4.32: Amino acids remodeling/readjustment due to ligand and sulfotransferase interactions. (A) sulfotransferase without frontrunner, (B) Oxamniqine interaction with sulfotransferase, (C) Diflunisal interaction with sulfotransferase, (D) Tolmetin interaction with sulfotransferase and (E) Dinesterol interaction with sulfotransferase. Both targets and frontrunners are coloured by atomic representations, red is oxygen, blue is nitrogen, white is hydrogen, yellow is sulphur and grey is carbon atoms

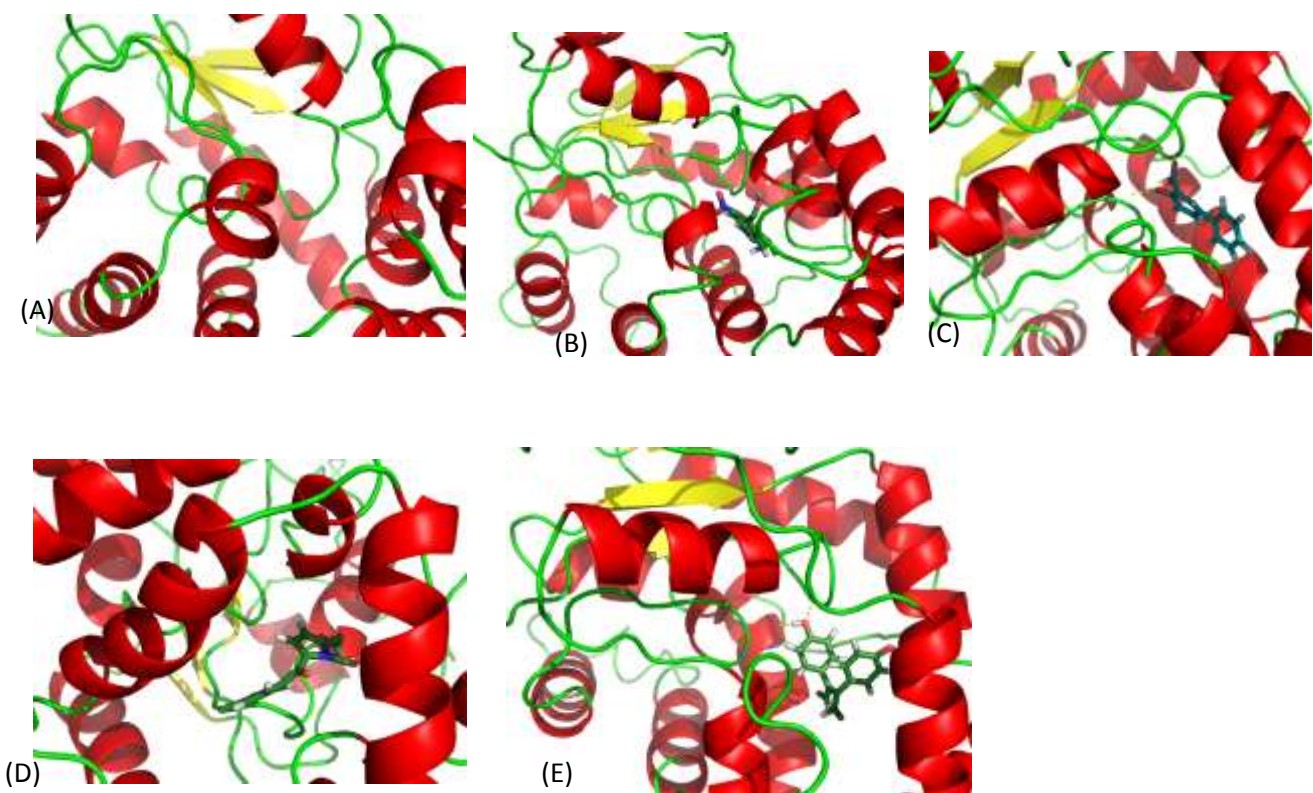


Figure 4.33: Conformational changes due to ligand and sulfotransferase interactions. (A) sulfotransferase without fronrunner, (B) Oxamniqine interaction with sulfotransferase, (C) Diflunisal interaction with sulfotransferase, (D) Tolmetin interaction with sulfotransferase and (E) Dinesterol interaction with sulfotransferase. Fronrunners are represented as sticks and coloured by atomic representation while sulfotransferase is represented as cartoon with helix coloured as red, sheets as yellow and loop as green.

Representative structures from conformational sampling of free and ligand bound thioredoxin glutathione reductase are presented in Figure 4.34 to 4.35. Atoms in amino acids in the thioredoxin glutathione reductase especially those at the binding sites and/or close to them showed marked rearrangement. For example, it can be observed from figure 4.34 that more widening of site 2 was observed due to interaction with auranofin and diflunisal than the rest of the ligands.

Also, close observation showed that the amino acids remodeling/rearrangement brought about conformational changes in the thioredoxin glutathione reductase secondary structures especially at the loops as shown in Figure 4.35.

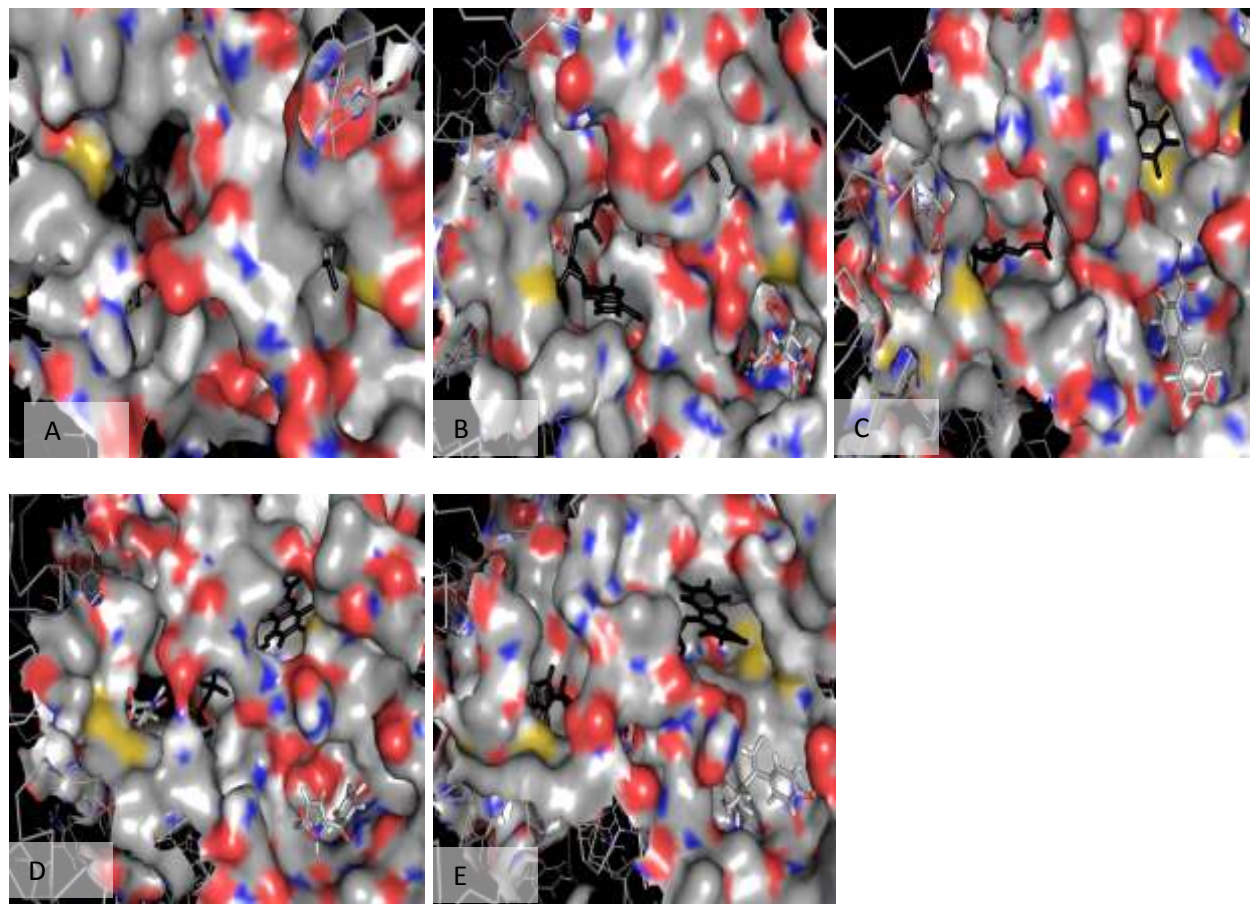


Figure 4.34: Amino acids remodeling/readjustment due to ligand and thioredoxin glutathione reductase interactions. (A) thioredoxin glutathione reductase without fronrunner, (B) auranofin interaction with thioredoxin glutathione reductase, (C) Diflunisal interaction with thioredoxin glutathione reductase, (D) Tolmetin interaction with thioredoxin glutathione reductase and (E) Dinesterol interaction with thioredoxin glutathione reductase. The target is represented as surface while auranofin, diflunisal, tolmetin, dinesterol and FAD are represented as sticks respectively. Both targets and fronrunners are coloured by atomic representations but FAD is coloured black, red is oxygen, blue is nitrogen, white is hydrogen, yellow is sulphur and grey is carbon atoms.

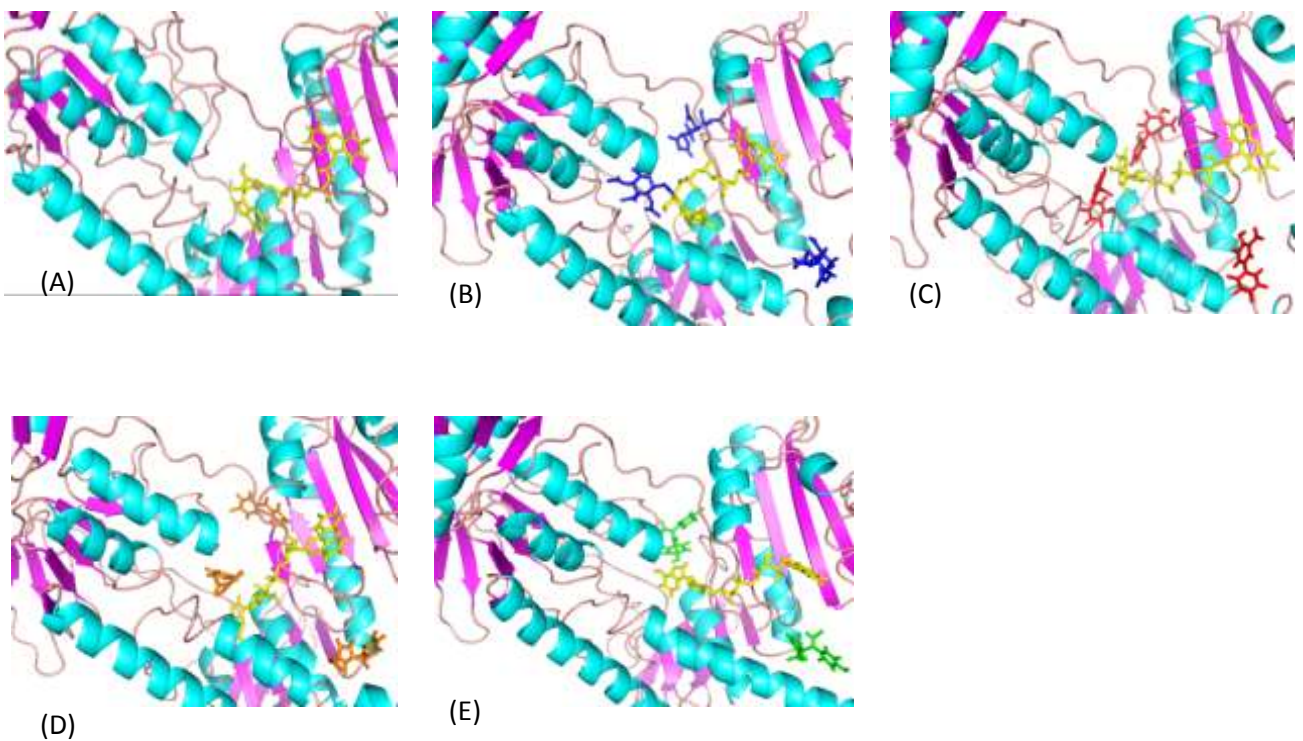


Figure 4.35: Conformational changes due to ligand and thioredoxin glutathione reductase interactions. (A) thioredoxin glutathione reductase without frontrunner, (B) auranofin interaction with thioredoxin glutathione reductase, (C) Diflunisal interaction with thioredoxin glutathione reductase, (D) Tolmetin interaction with thioredoxin glutathione reductase and (E) Dinesterol interaction with thioredoxin glutathione reductase. The target is represented as cartoon (helix are colourd, sky blue, sheets are coloured purple while loops are coloured light orange) while auranofin, diflunisal, tolmetin, dinesterol and FAD are represented as blue, red, orange, green and yellow sticks respectively.

Solvent Accessible Surface Area

Solvent accessible surface area (SASA) analysis measures the interaction between complexes and solvents. Relatively stable SASA indicate no significant changes in the protein structure. To get information about the behaviour of the protein surface during the dynamics, total hydrophobic and hydrophilic accessible surface areas were calculated and presented in figure 4.36 and appendix 20. Reduction in total, hydrophobic and hydrophilic accessible surface areas were observed when averaged over time (Appendix 20). Diflunisal, tolmetin or dinesterol interaction with sulfotransferase or TGR caused reduction in total, hydrophobic and hydrophilic accessible surface areas of the targets (Appendix 20).

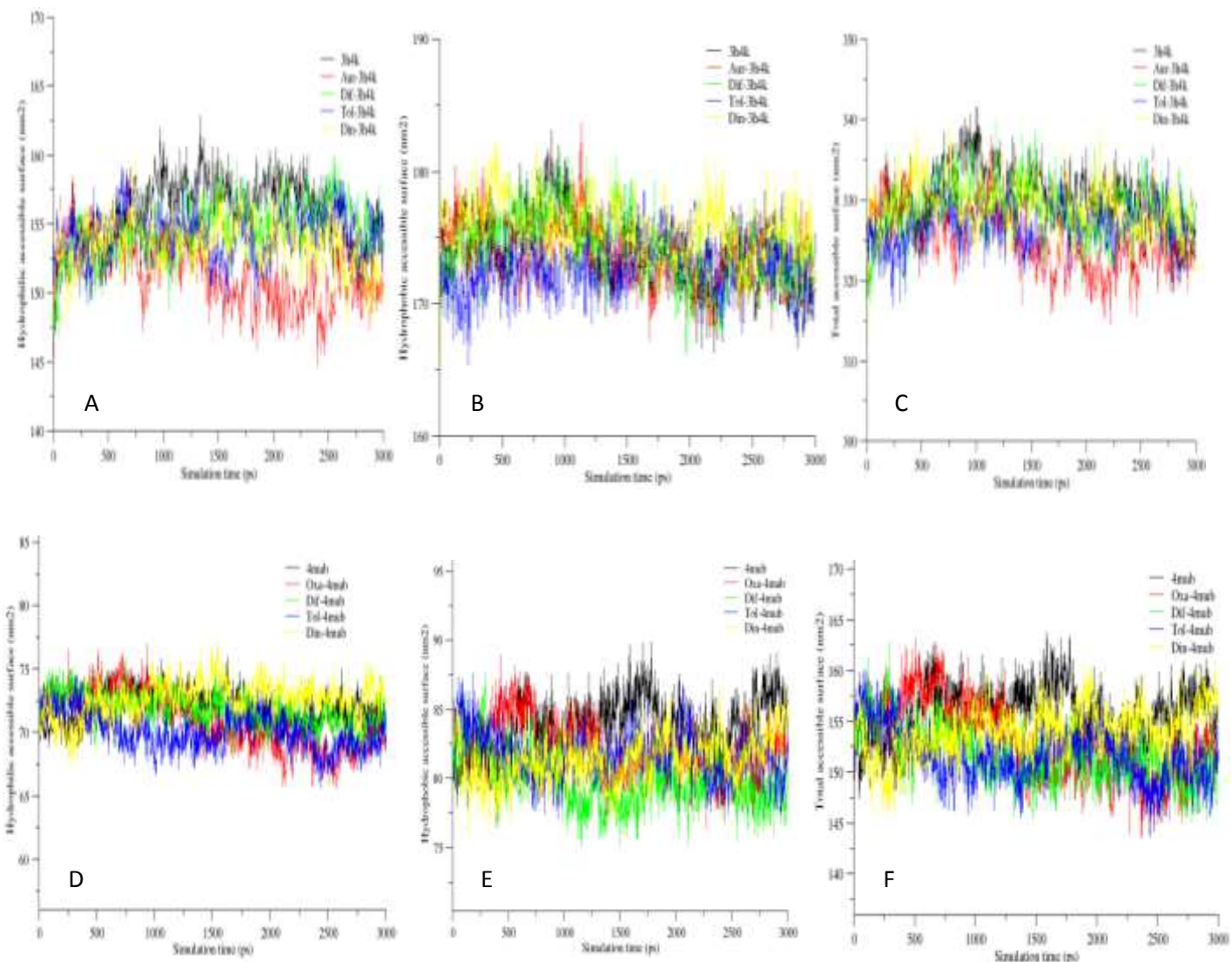


Figure 4.36: Accessible Surface Areas of free and frontrunner bound sulfotransferase and thioredoxin glutathione reductase interactions. (A) and (D) is hydrophilic accessible surface area (B) and (E) is hydrophobic accessible surface area, and (C) and (F) total accessible surface area. AUR = auranofin, OXA=oxamniquine, DIF=diflunisal, DIN=dinesterol and TOL=tolmetin.

4.1.6.5 Binding energy computation results

The binding energy of a drug for a receptor describes how avidly the drug binds to the receptor. Drug-receptor binding determines pharmacological response and size of that response. Sulfotransferase-tolmetin and thioredoxin glutathione reductase-tolmetin interactions showed the highest binding energies of -231.064 ± 18.55 KJ/mol and -338.636 ± 36.90 KJ/mol respectively (Table 4.5) compared with other studied approved drugs. Also presented in table 4.5 are values for solvent accessible surface area (SASA) energy, Polar salvation, electrostatic and van der Waal energies. Van der Waal energy appears to play more significant role in the interaction of all the drugs (oxamniquine, auranofin, tolmetin, diflunisal and dinesterol) with sulfotransferase and thioredoxin glutathione reductase.

Table 4.5: Binding energies between schistosomal drug targets and some approved drugs

Target-drug complex	Binding energy (KJ/mol)	SASA energy (KJ/mol)	Polar salvation energy (KJ/mol)	Electrostatic energy (KJ/mol)	Van der waal energy (KJ/mol)
4mub-Oxa	-130.091±8.800	-16.276±1.113	38.924±6.305	2.123±4.360	-154.861±9.412
4mub-Din	-80.087±11.096	-17.384±0.878	129.111±14.686	-64.724±10.153	-127.090±11.48
4mub-Dif	-168.641±20.37	-14.603±0.753	-22.395±28.179	-21.118±19.152	-110.525±11.78
4mub-Tol	-231.064±18.55	-15.519±0.950	-249.793±33.81	158.135±23.462	-123.888±10.27
3h4k-Aur	-114.420±26.73	-48.410±1.769	561.949±32.348	-188.742±23.290	-439.217±21.15
3h4k-Din	-84.454±23.217	-29.815±1.317	232.942±31.586	-53.994±20.656	-233.587±15.40
3h4k-Dif	-290.117±43.80	-36.636±1.717	-49.285±89.104	49.698±60.611	-253.893±21.62
3h4k-Tol	-338.636±36.90	-37.682±1.874	-151.604±75.659	145.230±57.551	-294.580±22.10

Key: Sulfotransferase (4mub), thioredoxin glutathione reductase (3h4k), oxamniquine (Oxa), Dinesterol (Din), Tolmetin (Tol), Auranofin (Aur), solvent accessible surface area (SASA)

The binding energies as a function of time and the residue wise contribution of binding energy in ligand bound sulfotransferase and thioredoxin glutathione reductase are presented in Figure 4.37.

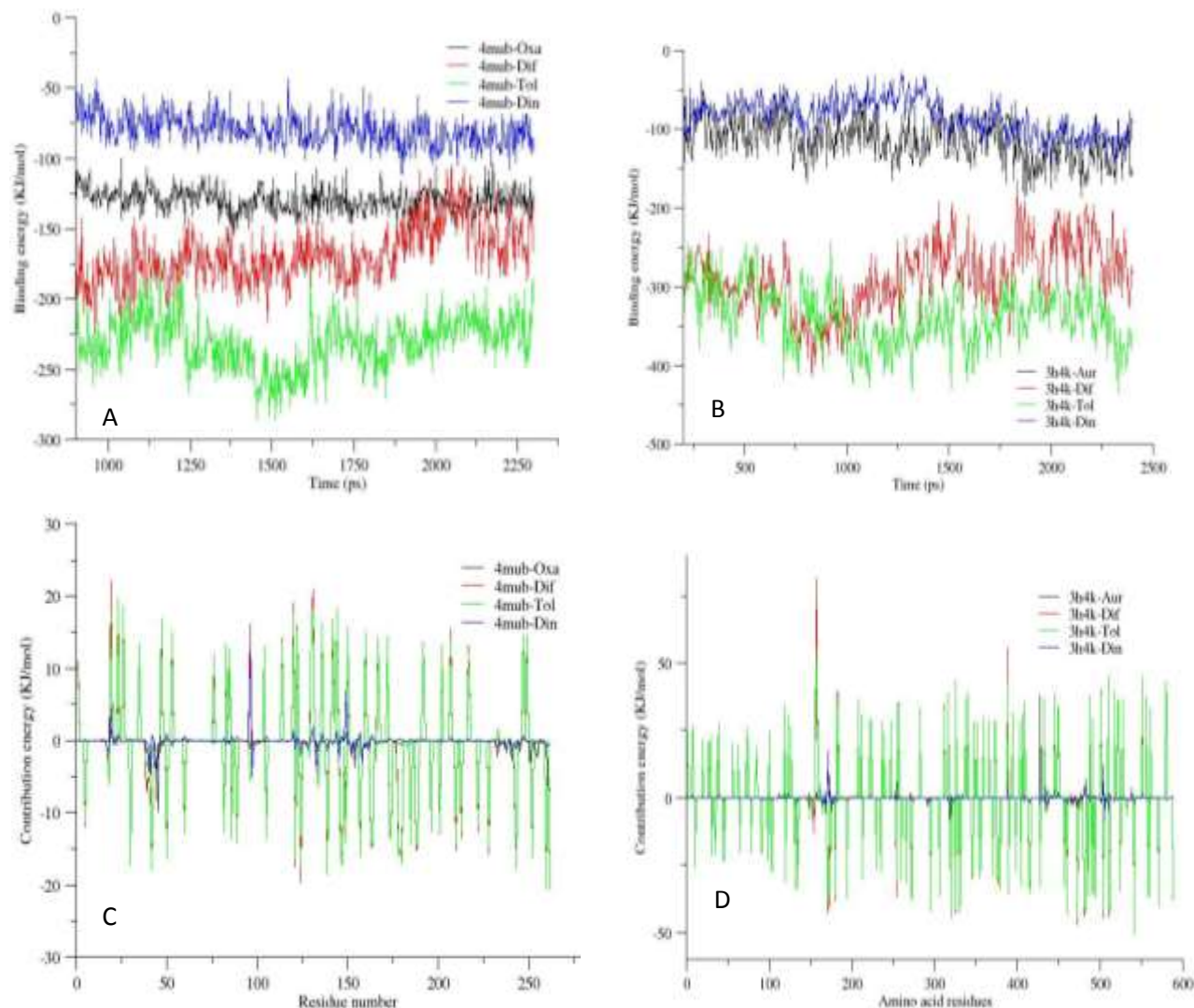


Figure 4.37: Binding energies and their amino acid residues contribution (A) and (C) are binding energies of sulfotransferase-fronrunner interactions and their amino acid residues contribution respectively. (B) and (D) are binding energies of thioredoxin glutathione reductase- fronrunner interactions and their amino acid residues contribution respectively. AUR = auranofin, OXA=oxamniquine, DIF=diflunisal, DIN=dinesterol and TOL=tolmetin.

Polar and Non-polar Energies

Polar and non-polar energies involved in ligand bound sulfotransferase and TGR interactions were calculated and presented in Figure 4.38. Auranofin showed the highest non-polar interaction energy with TGR while dinesterol showed highest for sulfotransferase when compared with the rest of the ligands (Figure 4.38 A and B). Also, tometin showed the highest polar energy of interaction with sulfotransferase and TGR when compared with diflunisal, oxamniquine and dinesterol (Figure 4.38 C and D).

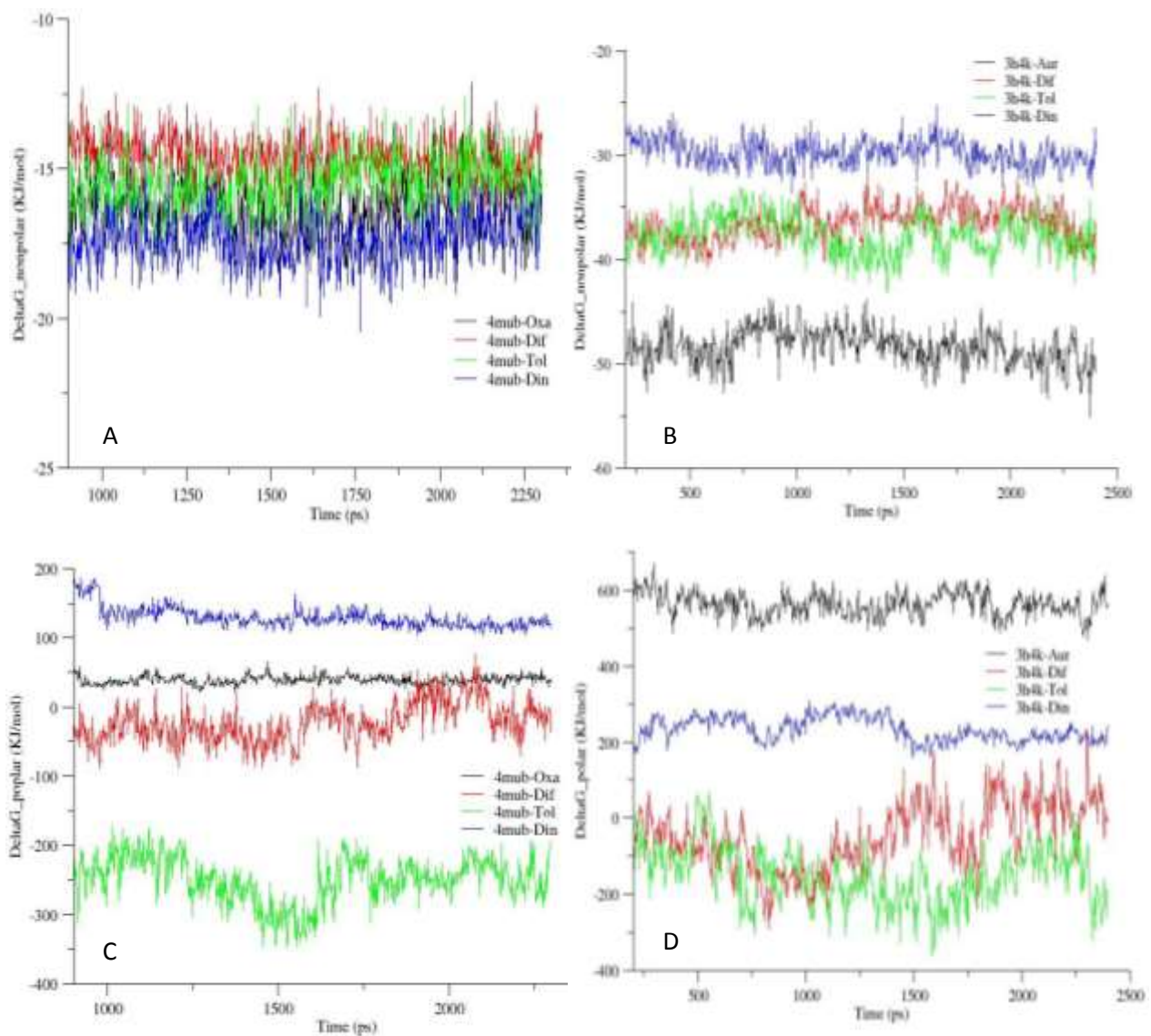


Figure 4.38: Polar and non-polar energies involved in sulfotransferase-fronrunner and thioredoxin glutathione reductase-fronrunner interactions. (A) and (B) are non-polar energies of sulfotransferase-fronrunner and thioredoxin glutathione reductase-fronrunner interactions respectively while (C) and (D) are for polar energies. AUR = auranofin, OXA=oxamniquine, DIF=diflunisal, DIN=dinesterol and TOL=tolmetin.

4.1.7 Molecular descriptors and bioactivities of some predicted drugs

The bioactivities and some molecular descriptors of the predicted drugs were calculated and presented in table 4.6. A relative common trend exists between the enzyme inhibition activities and GPCR activities of the predicted drugs with the reference drugs compared with other bioactivities. In addition, vildagliptin showed protease inhibitor activity of 0.87 while diflunisal and dinesterol showed higher nuclear receptor ligand inhibitor activities of 0.26 and 0.25 compared with others (Table 4.6). Oxytetracycline showed the highest tPSA of 206 and lowest xlogP of -2.2 compared with the rest of the drugs in table 4.6.

Table 4.6: Molecular descriptors and bioactivities of some predicted antischistosomal drugs

S/N	Compounds	Mwt (g/mol)	tPSA	xLogP	GPCR	ICM	KI	PI	EI	NRL
1	Praziquantel	312.413	41	2.74	0.25	-0.01	-0.48	0.07	-0.08	-0.46
2	Oxamniquine	280.348	95	2.62	0.07	0.11	-0.21	0.02	-0.03	-0.31
3	Auranofin	364.372	114	0.69	0.01	-0.16	-0.31	-0.02	0.28	-0.16
4	Diflunisal	249.192	60	3.9	0.01	0.15	0.05	-0.14	0.22	0.26
5	Tolmetin	256.281	62	2.73	0.15	-0.07	-0.26	-0.38	0.22	0.0
6	Dinesterol	266.34	40	3.82	0.02	0.09	-0.09	-0.11	0.13	0.25
7	Oxytetracycline	459.431	206	-2.2	-0.03	-0.05	-0.40	0.04	0.53	0.12
8	Vidagliptin	288.415	61	2.55	0.31	-0.13	-0.40	0.87	0.03	-0.37
9	Haloperidol	376.879	42	4.5	0.30	0.14	-0.12	-0.04	0.14	0.01

4.1.8 Results of conservation of drug targets and human liver enzymes in drosophila

The results of conservation of drug targets and human liver enzymes in *D. melanogaster* are presented 4.1.7.1 to 4.1.7.2 below.

4.1.8.1 Results on conservation of schistosomal targets in drosophila

BLAST search of glutathione s-transferase (1gtb), and sulfotransferase (4mub) against molecular targets of *Drosophila melanogaster* in flybase showed that the schistosomal enzymes are not conserved in *Drosophila melanogaster* (Figure 4.39 A and B). Sequence alignment of the schistosome targets (query) and drosophila proteins (subjects) is presented in Figure 4.39 C and D with the highest sequence identity of 22.5 %.

BLAST search of thioredoxin glutathione reductase (3h4k) and cathepsin B1 (3qsd) against molecular targets of *D. melanogaster* in flybase show that the schistosomal enzymes are conserved in *D. melanogaster* (Figure 4.40 A and B). Sequence alignment of the schistosome targets (query) and drosophila proteins (subjects) is presented in Figure 4.40 C and D with the highest sequence identity of 57.9 %.

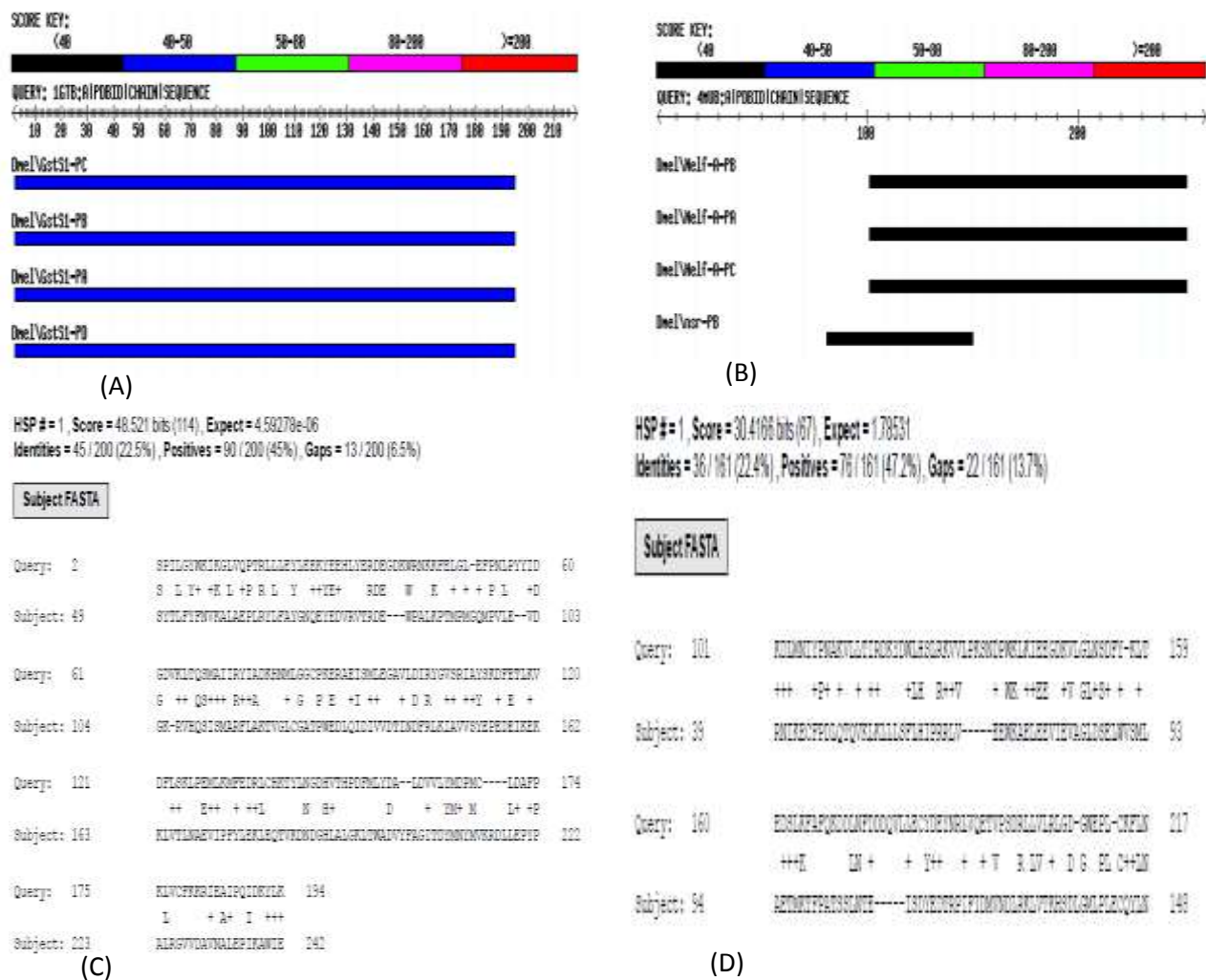


Figure 4.39: Molecular targets (1GTB and 4MUB) of schistosome that are not conserved in *drosophila melanogaster*. (A) and (B) are score key summary BLAST serach of 1GTB and 4MUB respectivley while (C) and (D) are sequence alignment of the schistosome targets (query) and *drosophila* proteins (subjects). Red indicate the highest level of sequence identity between query and subject.

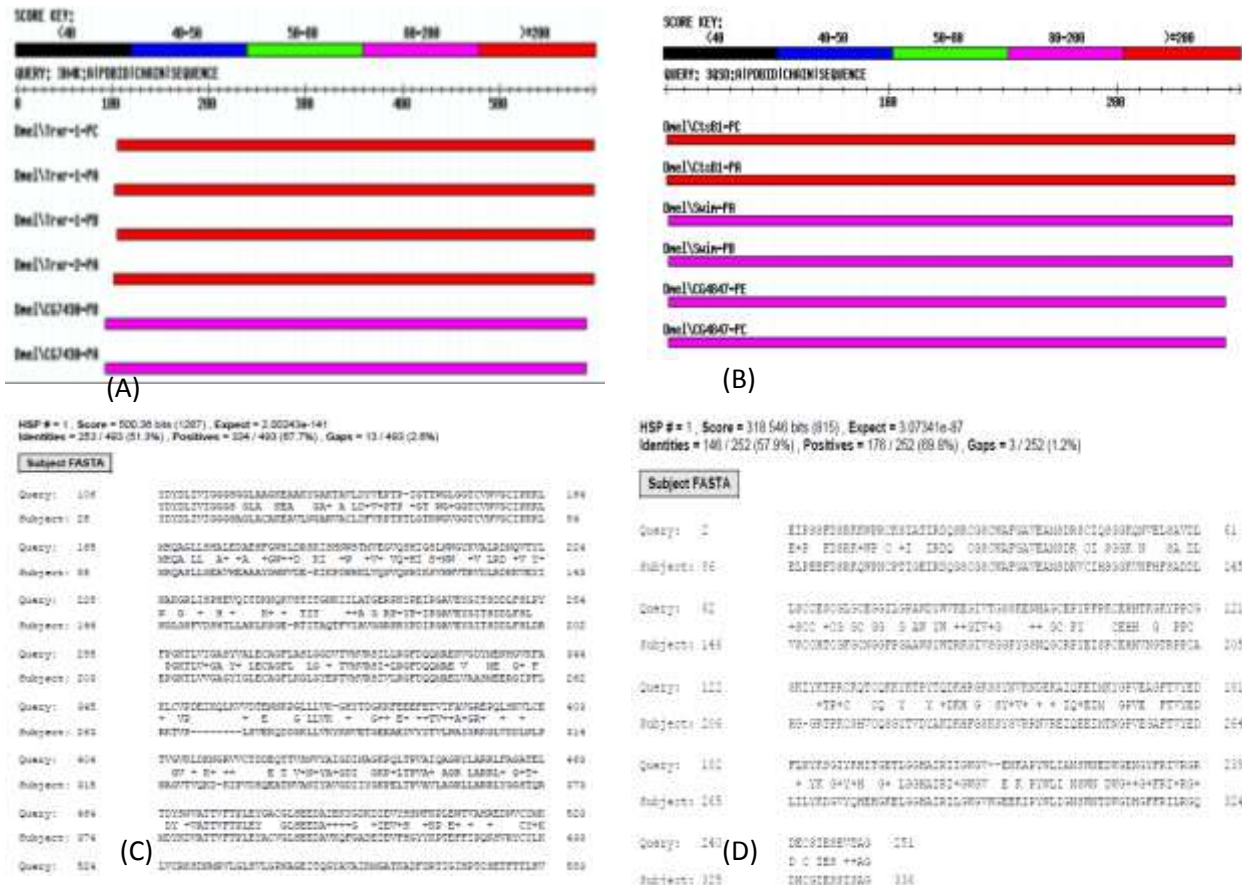


Figure 4.40: Schistosomal thioredoxin glutathione reductase and cathepsin B1 are conserved in *D. melanogaster*. (A) and (B) are score key summary BLAST serach of TGR and cathepsin B1 respectivley while (C) and (D) are sequence alignment of the schistosome targets (query) and drosophila proteins (subjects). Red indicate the highest level of sequence identity between query and subject.

4.1.8.2 Results of conservation of human liver enzymes in drosophila

BLAST search of human liver enzymes [(aspartate aminotransferase (3WZF) and alkaline phosphatase (2GLQ)] against *D. melanogaster* proteins in flybase show that they are conserved in *D. melanogaster* (Figure 4.41 A and B). Sequence alignment of the human liver enzymes (query) and drosophila proteins (subjects) is presented in Figure 4.41 C and D with the highest sequence identity of 56.4 %.

BLAST search of human liver alanine aminotransferase (5F9S) against *D. melanogaster* show that human liver alanine aminotransferase is conserved in *D. melanogaster* (Figure 4.42). Sequence alignment of the human enzyme (query) and drosophila proteins (subjects) is presented in Figure 4.42 B with the highest sequence identity of 62.8 %.



Figure 4.41: Liver biomarkers [aspartate aminotransferase (3WZF) and alkaline phosphatase (2GLQ)] of humans are conserved in *Drosophila melanogaster*. (A) and (B) are score key summary BLAST serach of 3WZF and 2GLQ respectivley while (C) and (D) are sequence alignment of the biomarkers (query) and drosophila proteins (subjects). Red indicate the highest level of sequence identity between query and subject

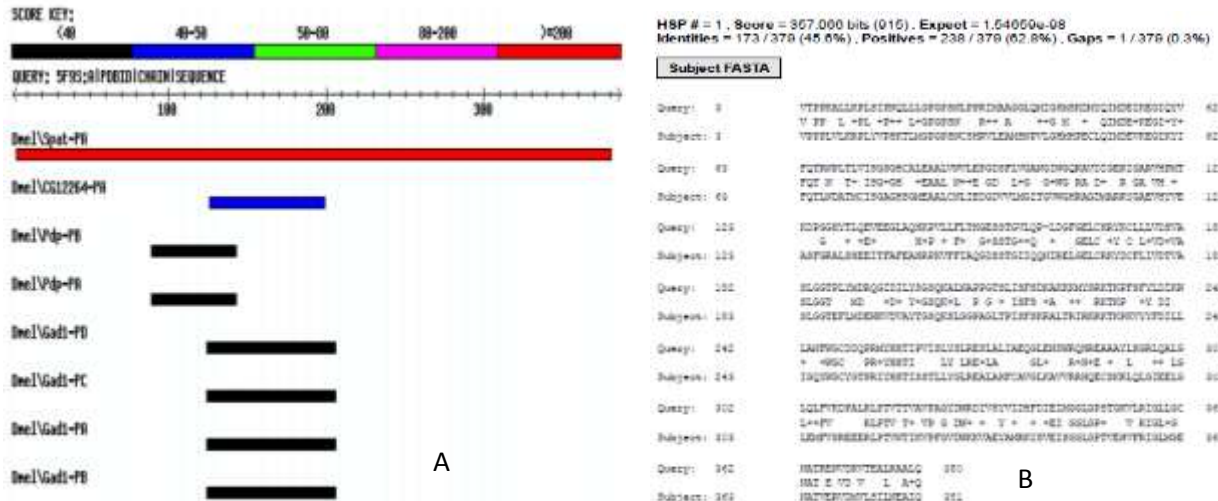


Figure 4.42: Human liver alanine aminotransferase (5F9S) is conserved in *Drosophila melanogaster*. (A) is a score key summary BLAST search of 5F9S while (B) is sequence alignment of the biomarkers (query) and drosophila proteins (subjects). Red indicate the highest level of sequence identity between query and subject.

4.1.9 Results of survival rates and longevity of *D. melanogaster* in some of the drugs

4.1.9.1 Survival and longevity of *D. melanogaster* on PZQ –treated food

Survival of male and female *D. melanogaster* in presence of different doses of praziquantel is presented in Figure 4.43. It was observed that praziquantel altered survival of male and female *D. melanogaster* up to 50 % after 9 and 13 days (Figure 4.44) of exposure respectively which was not observed after 4 days of exposure at 0.6 mg dose (Figure 4.43 C and D, Figure 4.44).

Longevity profile of male and female *Drosophila melanogaster* is also presented in Figure 4.44. It is evident from figure 4.44 that male flies had longevity period of 24 days while female flies had 25 days in different doses of praziquantel.

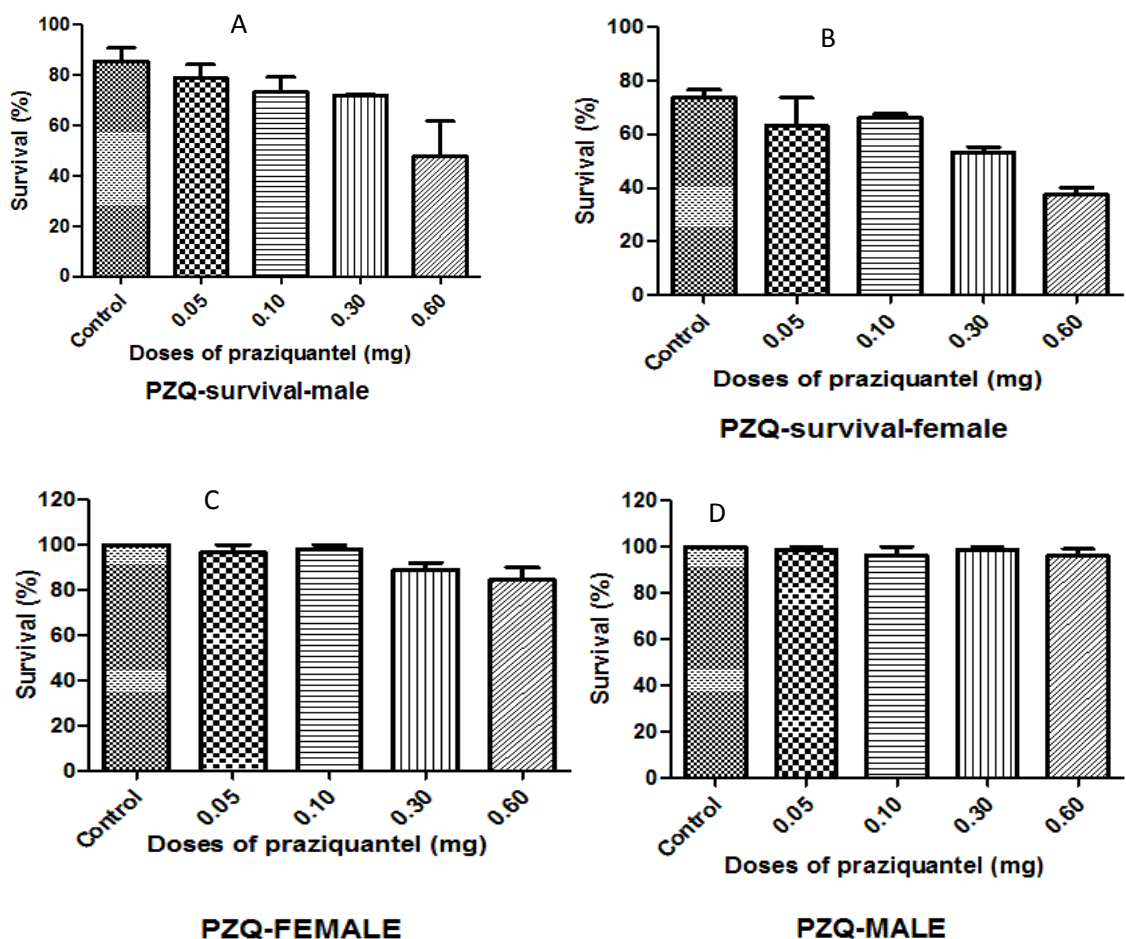


Figure 4.43: Survival of male and female *D. melanogaster* presence of different doses of praziquantel. Praziquantel altered survival of male (A) and female (B) *D. melanogaster* up to 50 % after 9 and 13 days of exposure at 0.6 mg respectively but did not alter their survival after 4 days of exposure to (C) male and (D) female flies.

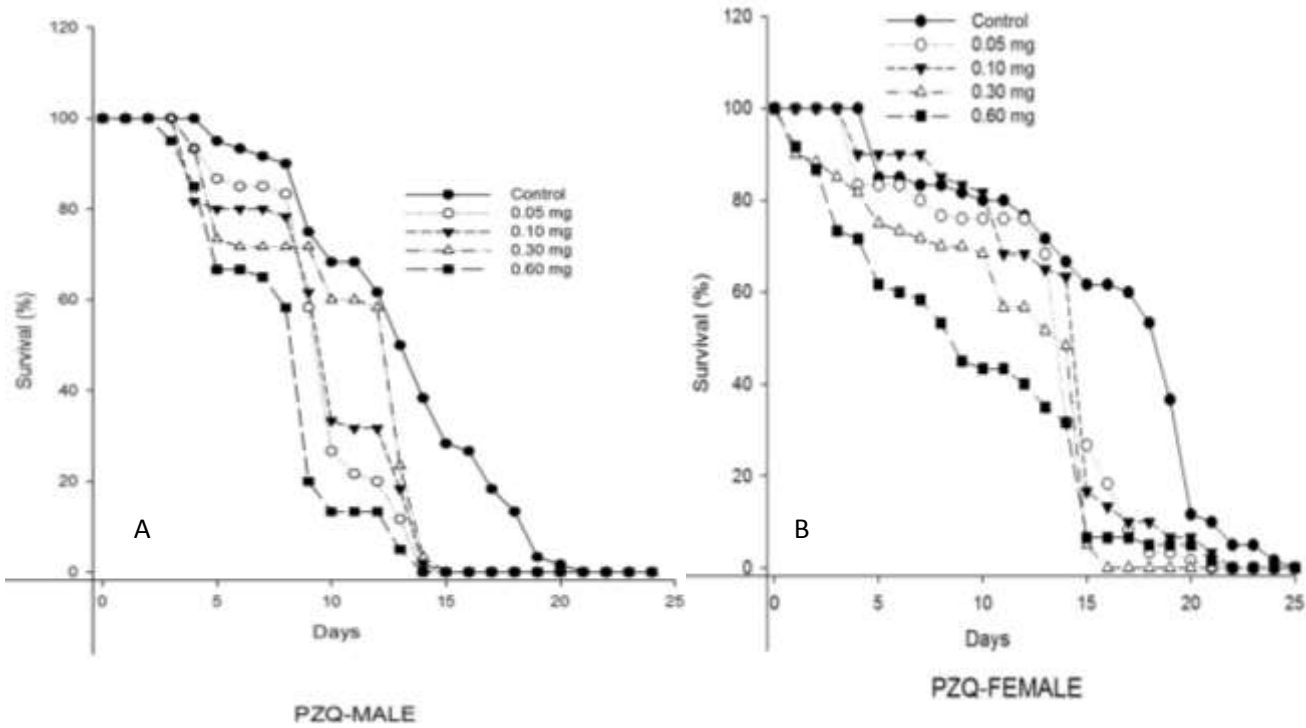


Figure 4.44: Praziquantel reduced survival rates of *D. melanogaster*. (A) 24 days survival of male flies treated with praziquantel and (B) 25 days survival of female flies treated with Praziquantel. Data are presented as mean \pm SD of three independent biological replicates carried out in duplicates. Each assay was carried out in three independent experiments.

4.1.9.2 Survival and longevity of *D. melanogaster* on oxytetracycline treated food

Survival of male and female *D. melanogaster* in presence of different doses of oxytetracycline is presented in Figure 4.45. It was observed that oxytetracycline enhanced the survival of male and female *D. melanogaster*. However, at 0.5 mg, oxytetracycline reduced the survival of male flies up to 50 % after 16 days (Figure 4.46) of exposure which was not observed in females. Seven days exposure of *D. melanogaster* to oxytetracycline at 0.5 g dose did not reduce the survival up to 50 % (Figure 4.45 C and D, Figure 4.46).

Longevity profile of male and female *Drosophila melanogaster* in presence of different doses of oxytetracycline is also presented in Figure 4.46. It is evident from Figure 4.46 male flies had longevity period of 24 days while female flies had 29 days in different doses of oxytetracycline.

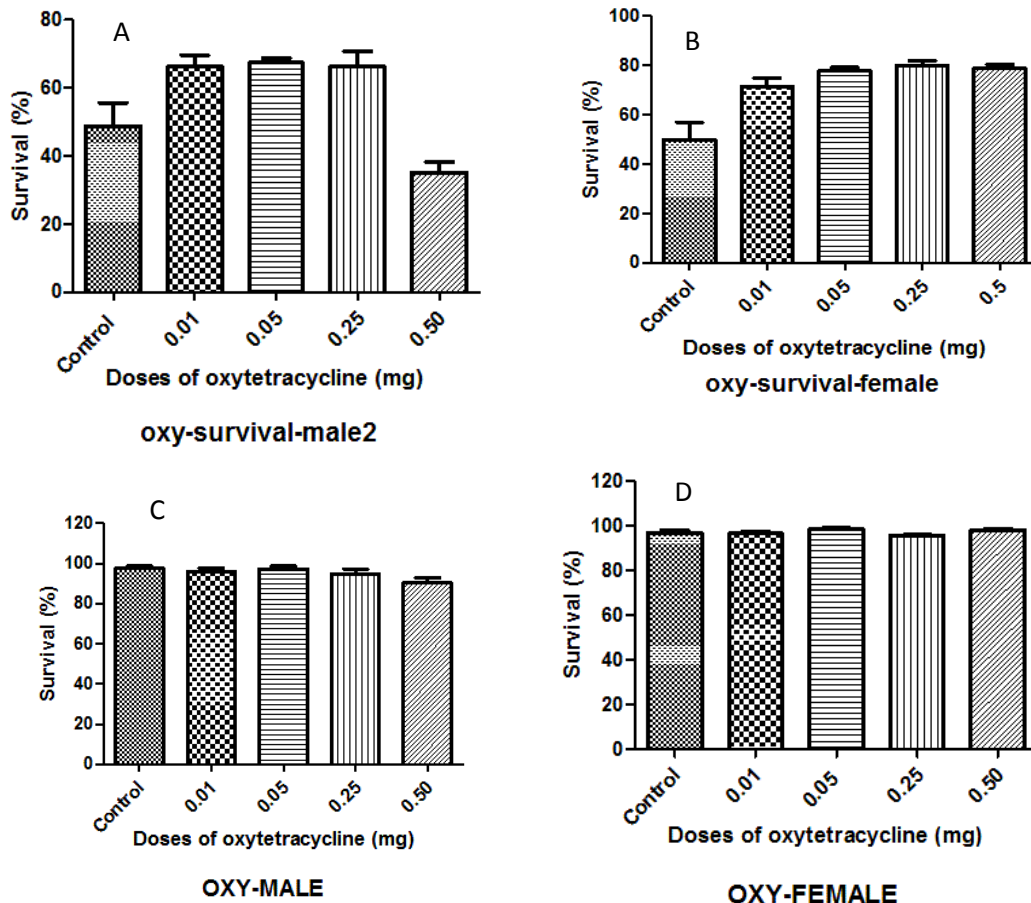


Figure 4.45: Survival of male and female *D. melanogaster* in presence of different doses of oxytetracycline. Oxytetracycline increased survival of male (A) and female (B) *D. melanogaster*. Also, oxytetracycline did not significantly alter their survival after 7 days of exposure to (C) male and (D) female flies at 0.5 mg dose.

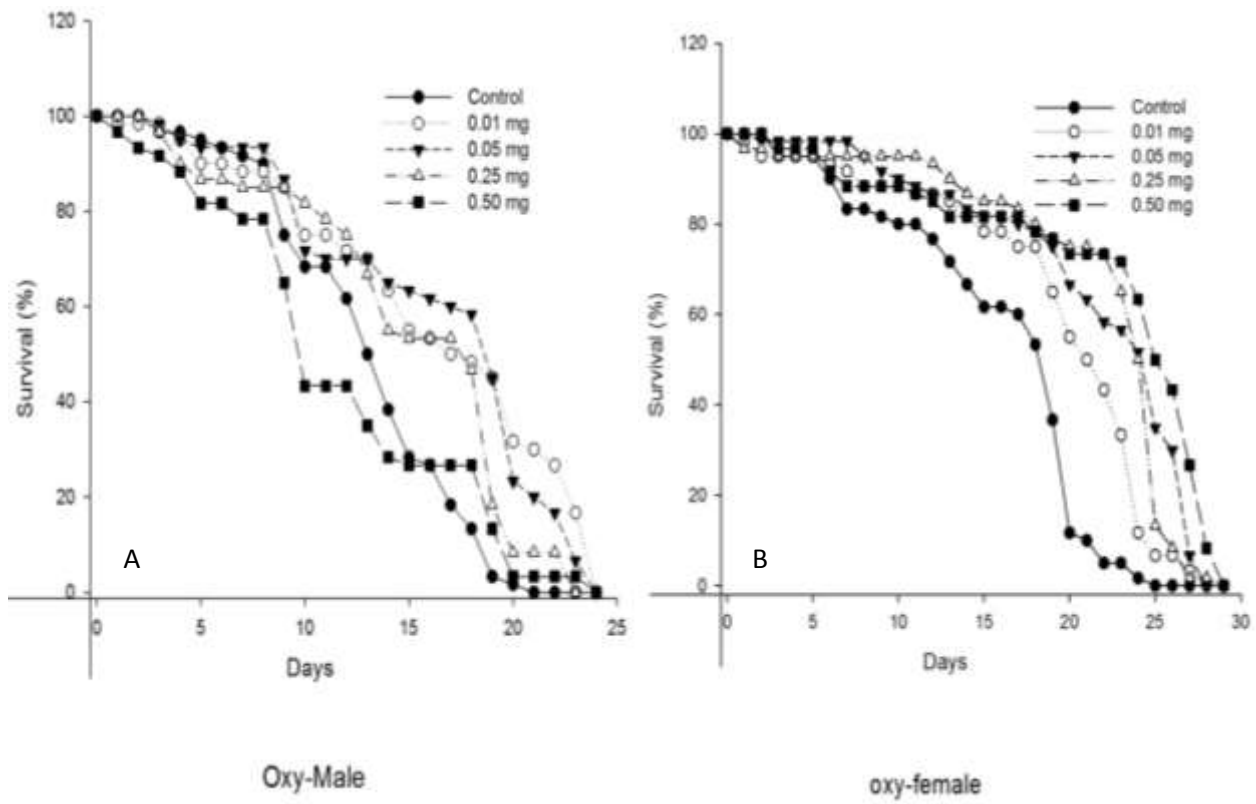


Figure 4.46: Oxytetracycline increased survival rates of *Drosophila melanogaster*. (A) 24 days survival of male flies treated with oxytetracycline and (B) 29 days survival of female flies treated with oxytetracycline. Each assay was carried out in three independent experiments.

4.1.9.3 Survival and longevity of *D. melanogaster* on haloperidol treated food

Survival of male and female *D. melanogaster* in presence of different doses of haloperidol is presented in Figure 4.47. It was observed that haloperidol altered survival of male and female *D. melanogaster* up to 50 % after 9 and 13 days of exposure respectively which was not observed after 4 days of exposure at the studied doses of haloperidol. Four days exposure of *D. melanogaster* to haloperidol at 0.002 mg dose did not reduce the survival up to 50 % (Figure 4.47 C and D, Figure 4.48).

Longevity profile of male and female *Drosophila melanogaster* in presence of different doses of haloperidol is also presented in Figure 4.48. It is evident from figure 4.48 that male flies had longevity period of 25 days in different doses of haloperidol and conditions of the experiments.

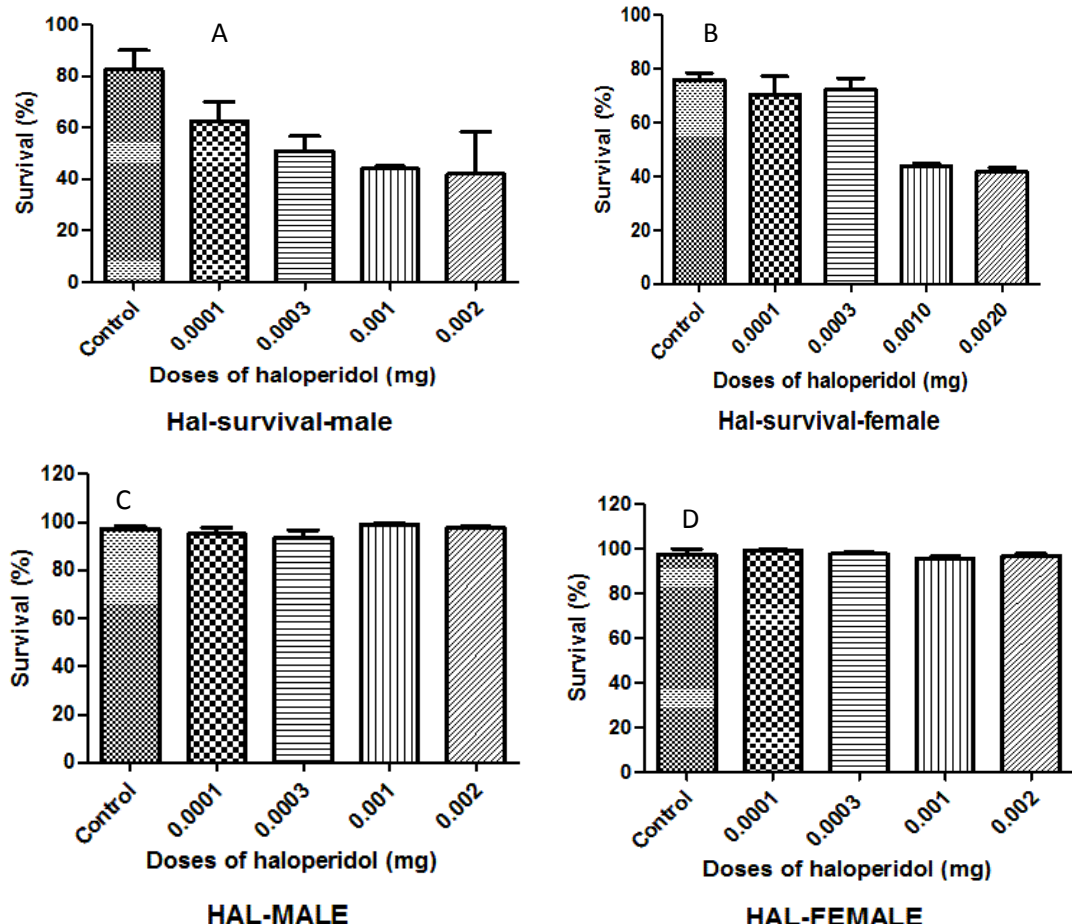


Figure 4.47: Survival of male and female *D. melanogaster* presence of different doses of haloperidol. Haloperidol altered survival of male (A) and female (B) *D. melanogaster* up to 50 % after 9 and 13 days of exposure respectively but did not alter their survival after 6 days of exposure to (C) male and (D) female flies at 0.002 mg dose.

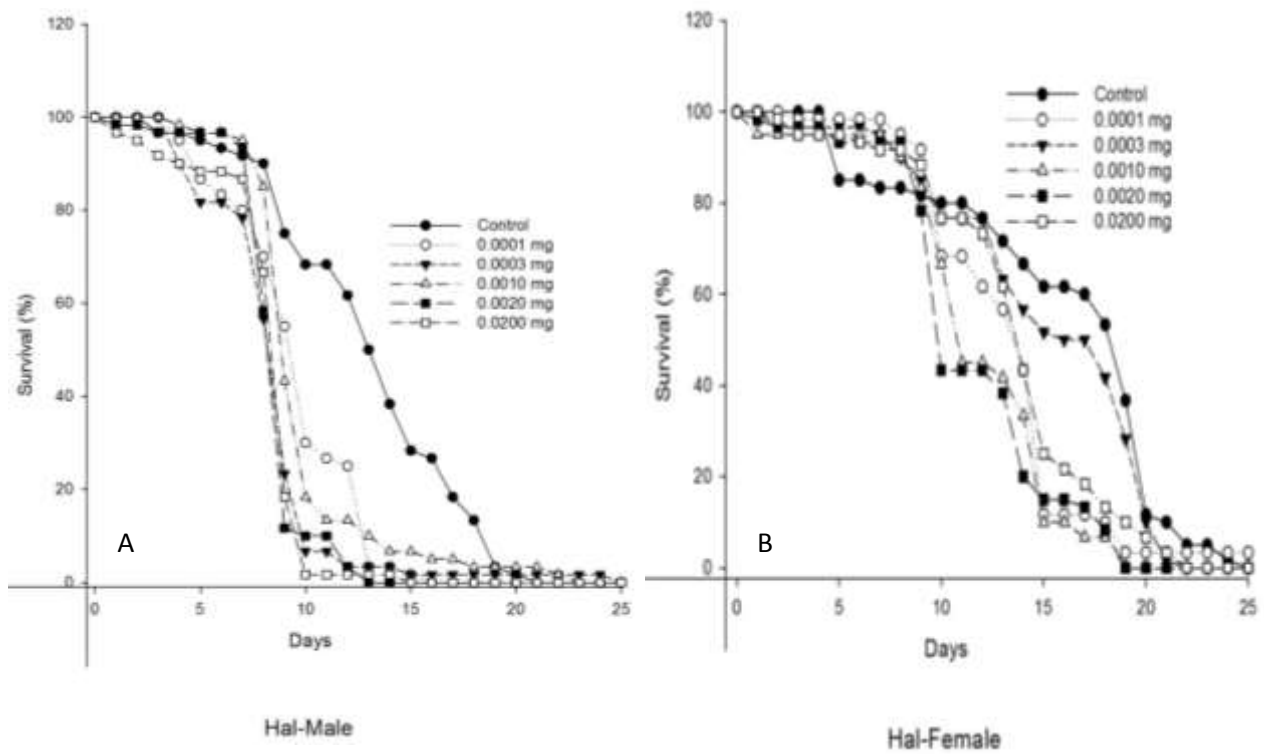


Figure 4.48: Haloperidol increased survival rates of *Drosophila melanogaster*. (A) 25 days survival of male flies treated with haloperidol and (B) 25 days survival of female flies treated with haloperidol. Each assay was carried out in three independent experiments.

4.1.9.4 Survival and longevity of *D. melanogaster* on vildagliptin treated food

Survival of male and female *D. melanogaster* in presence of different doses of vildagliptin is presented in Figure 4.49. It was observed that vildagliptin altered survival of male and female *D. melanogaster* up to 50 % after 7 and 13 days of exposure respectively which was not observed after 4 days of exposure at the studied doses of vildagliptin. Four days exposure of *D. melanogaster* to vildagliptin at 0.014 mg dose did not reduce the survival up to 50 % (Figure 4.49 C and D, Figure 4.50).

Longevity profile of male and female *D. melanogaster* in presence of different doses of vildagliptin is also presented in Figure 4.50. It is evident from Figure 4.50 that male flies had longevity period of 21 days in different doses of vildagliptin.

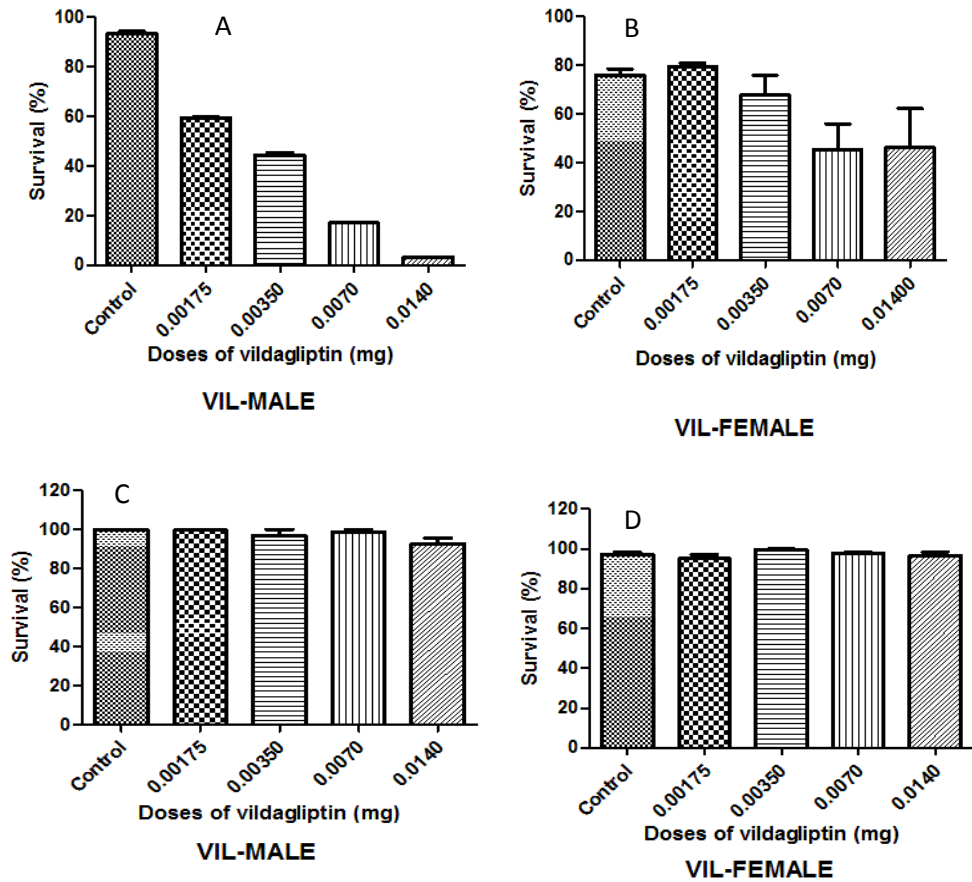


Figure 4.49: Survival of male and female *D. melanogaster* presence of different doses of vildagliptin. Vildagliptin altered survival of male (A) and female (B) *D. melanogaster* up to 50 % after 7 and 13 days of exposure respectively but did not alter their survival after 4 days of exposure to (C) male and (D) female flies.

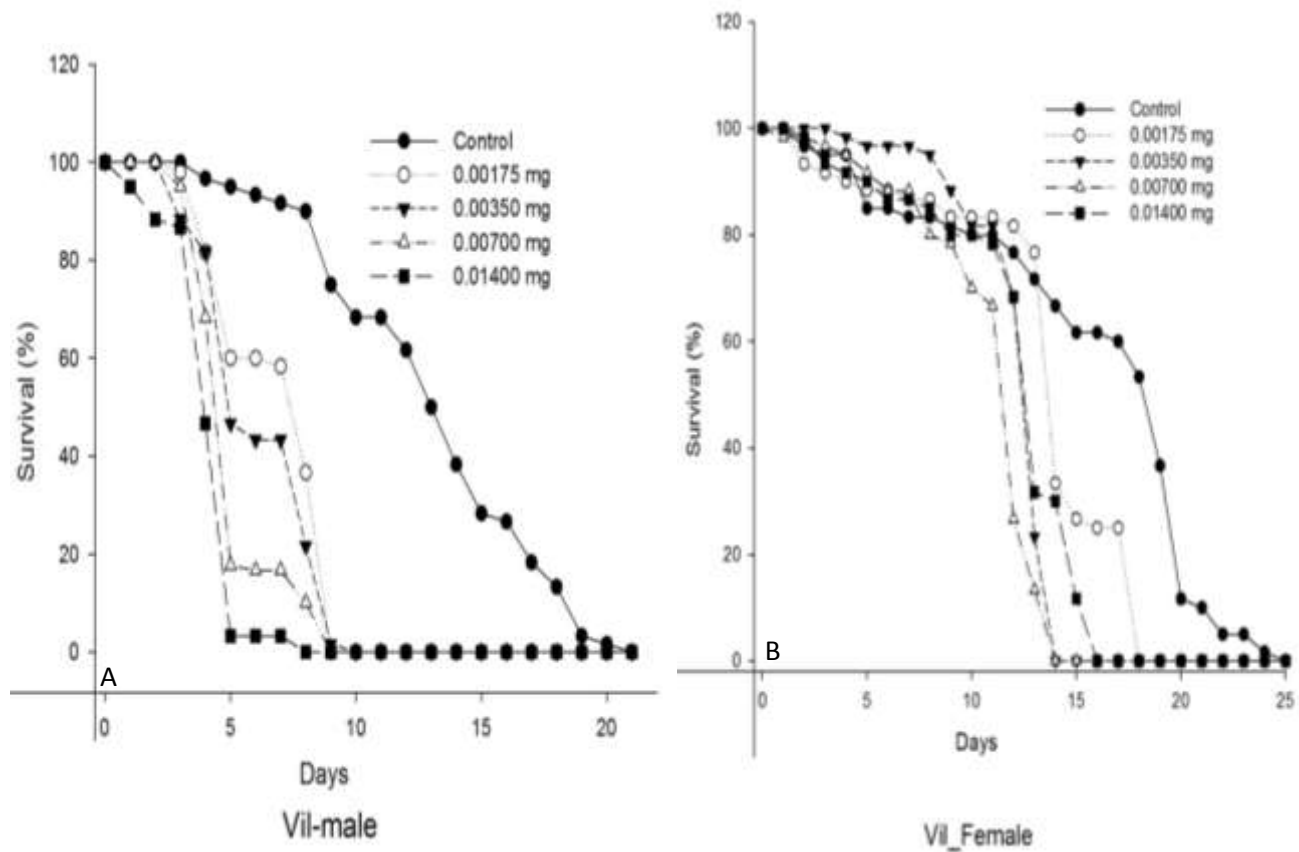


Figure 4.50: Vildagliptin increased survival rates of *D. melanogaster*. (A) 21 days survival of male flies treated with vildagliptin and (B) 25 days survival of female flies treated with vildagliptin. Each assay was carried out in three independent experiments.

4.2 Discussions

Four (4) schistosomal drug targets (glutathione s-transferase, thioredoxin glutathione reductase, cathepsin B1, and sulfotransferase) with bound reference compounds (praziquantel, oxamniquine, auranofin and [propylamino-3-hydroxy-buta-1,4-dionyl]-isoleucylproline respectively) were identified with bioinformatics mining (Table 4.1, 4.2 and 4.3) of TDR database and/or PDB. The identified targets were obtained from PDB and used for the molecular docking and dynamics simulations. The missing amino acid residues (Pro65, Pro66 and Pro67) in between -N and -C terminals in schistosomal sulfotransferase were successfully modeled from the starting structure and the model was sufficiently reliable with 98.8 % sequence identity. Arnold *et al.*, (2006) have reported template and target sequence identity of more than 50 % as reliable model. The missing amino acid residues are in the loop region of sulfotransferase (Figure 4.1). The flexibility of sulfotransferase and TGR were modulated by the ligands (Figure 4.13). The observed reductions in target flexibilities (Figure 4.13) were associated with stability and conformational changes in the targets which could lead to their inhibition by the ligands.

A total of 612 drugs including their isomers were selected for the molecular docking simulations and targets experimental complexes from PDB were successfully reproduced *in silico* (Figure 4.3) before the molecular docking simulations. The molecuar docking simulations showed three approved drugs (diflunisal, tolmetin and dinesterol) with possible multi-target inhibitory activities against schistosoma drug targets (Table 4.4). They showed higher and concurrent binding affinities than PZQ and oxamniquine for two schistosome targets suggesting that they may produce better pharmacological response. Diflunisal and tolmetin are non-steroidal anti-inflammatory drugs (NSAIDs) and it has been reported that other drugs like salicylate, metformin or Gleevec™, affect many drug targets simultaneously (Csermely *et al.*, 2005). Also, few others were identified as potential uni-target anti-schistosomal agents from the molecular docking simulations (Appendix 12). In line with drug repurposing approach, it has been reported by Li *et*

al., (2013) that dihydroartemisinin exhibited good activity against the schistosomula of *S. mansoni*. Also, ferroquine- an organometallic compound, showed moderate *in vitro* and low *in vivo* activities against larval and adult stages of *S. mansoni* (Keiser *et al.*, 2014). It is important to note that auranofin - an approved drug for treatment of rheumatoid arthritis, is being investigated for potential therapeutic application in many other diseases including schistosomiasis and bacterial infections (Roder and Thomson, 2015). On the other hand, Keiser *et al.*, (2014b) reported that addition of mefloquine or mefloquine-artesunate does not increase the efficacy of praziquantel against chronic *S. haematobium* infection. To large extent, molecular docking simulations predicted anti-schistosomal agents are in line with the reports of previous studies (Li *et al.*, 2013; Keiser *et al.*, 2014; Roder and Thomson, 2015). The predicted approved drugs bind and exploit the same binding site on sulfotransferase and thioredoxin glutathione reductase (Figure 4.4).

The energy minimization and position restrained dynamics steps in the molecular dynamics simulations of solvated targets and target-ligand complexes successfully removed restraining forces in the starting molecular coordinates of the molecular systems (target, target-frontrunner complexes) and brought the systems to global energy minima (Figure 4.6 and 4.7) thus, allowed the molecular systems to be properly soaked in explicit SPC water model (Figure 4.5). This permitted production run and analysis of its trajectories to obtain results like C_α RMSD, radius of gyration, non-covalent interactions etc.

The C_α RMSD of the simulated protein over time is a reliable parameter to analyze the stability of the system. The targets showed the most stable C_α RMSD of $0.188255739 \pm 0.018454801$ nm and $0.217006693 \pm 0.031973524$ nm (Appendix 14) due to sulfotransferase and TGR interactions with diflunisal and tolmetin respectively. Structural transition of diflunisal from stable to unstable state with high RMSD was observed during diflunisal bound MD simulation (Figure 4.9). The transition in diflunisal was due to its interaction with amide hydrogen in Arg19 of schistosomal sulfotransferase (Figure 4.18). Also, structural transition to unstable state occurred

in dinesterol (Figure 4.9) which was due to compactness of the structure (Figure 4.12). Stability of targets can be due to its compactness as a result of interactions with ligands.

Radius of gyration (R_g) enables one to assess the compactness changes of a ligand-target complex (Liao *et al.*, 2014). It is one of the important parameters that provide quantitative descriptions of changes in the tertiary structure of the simulated protein. However, fluctuations in R_g of the targets (Figure 4.11) and that of ligand (Figure 4.12) were recorded for simulations involving sulfotransferase, TGR suggesting loss/gain of compactness in the structures. This is in agreement with Liao *et al.*, (2014) who reported that when radius of gyration of target due to ligand binding is higher, the compactness of ligand-target complex becomes lower causing the interactions between ligand and target to be weak. It is important to note that the extent of interaction between a ligand and drug target can be quantified in terms of binding energy. Molecular dynamics simulation is a better predictor of binding energy of molecular interactions than molecular docking simulations which gave binding energy between -29.9156 to -35.9824 KJ/mol (Table 4.4 and 4.5).

Two approved drugs (diflunisal and tolmetin) from the MD simulations formed better stable complexes, showed higher and concurrent binding energies than auranofin and oxamniquine for two schistosomal drug targets (sufotransferase and thioredoxin glutathione reductase) suggesting possible better pharmacological response. Their binding energies ranged from -168.641 ± 20.37 to -231.064 ± 18.55 KJ/mol and -290.117 ± 43.80 to -338.636 ± 36.90 KJ/mol for MD simulations involving sufotransferase and thioredoxin glutathione reductase respectively (Table 4.5). The energy computation experiments showed that van der Waals interactions were the major driving forces for interactions between the two schistosomal drug targets and the ligands (Table 4.5). SASA energy had minimal contribution while polar solvation and electrostatic energies had different degrees of driving forces for the target-ligand interactions (Table 4.5). The positive polar solvation and electrostatic energies in some of the MD simulations (Table 4.5) suggests net repulsion with respect to the polar solvation or electrostatic terms. However, there are negative

van der Waal and SASA energies that offset the positive values such that the binding energies were negative (Table 4.5). We also observed repulsive O....O interactions mainly in MD simulations that showed positive polar and/or solvation energies (Figure 4.19, 4.21 and 4.23) and Bissantz *et al.*, (2010) have associated O....O interactions to loss of affinity. This may also contribute to the observed low binding energies in molecular systems with positive polar solvation and/or electrostatic energies in the MD simulations. This could also be due to loss in configurational entropy of the binding partners as pointed out by Kar *et al.*, (2013) or solvation-driven differences as a result of different solvation properties of the ligands in water as pointed out by Mobley and Dill, (2009) and can be inferred from SASA binding energies in the present study. Kar *et al.*, (2013) also reported with computational mutagenesis experiments that increased polar solvation free energy contributes to drug resistance. This may be the case for oxamniquine resistance since Cioli *et al.*, (1993) reported that resistance to oxamniquine is controlled by a single autosomal recessive gene and the study showed polar solvation energy due to oxamniquine interaction with sulfotransferase as 38.924 ± 6.305 KJ/mol. However, this has to be tested experimentally.

It was observed that breakage of some hydrogen or polar bond at different time points in the MD simulations were accompanied by formation of another hydrogen bond/polar bond (Figure 4.25 and Figure 4.27 to 4.29). This explains why some hydrogen/polar bonds observed at different time points could not be seen at other time points in the MD simulations (Figure 4.17 to 4.19 and Figure 4.21 to 4.23). Some amino acids in sulfotransferase and TGR that formed hydrogen bond at 0.0 ps (Figure 4.17 and 4.19) but disappeared as the simulation progressed were assigned a functional role of ligand binding only. Also, amino acids that were not involved in any form of hydrogen/polar bond with the ligands at 0.0 ps but established hydrogen, polar and/or perceived covalent bond after 0.0 ps (Figure 4.25, 4.27 to 4.29) were assigned a functional role of inhibition while those that maintained hydrogen, polar and/or suspected covalent bonds with the ligands throughout the MD simulations (Figure 4.17 to 4.19, Figure 4.21 to 4.23, Figure 4.25

and Figure 4.27 to 4.29) were assigned a functional role of both binding and inhibition or activation.

The ligands cause changes in secondary structure mostly because of formation of hydrogen bonds with oxygen and/or hydrogen atoms from the main chain (backbone) of the targets (including suspected covalent bonds with TGR). The decrease in α -helix composition in schistosomal sulfotransferase (Appendix 16) and disappearance of 5-helix (Figure 4.15a) were attributed to formation of hydrogen bonds between oxygen or hydrogen atoms from the main chain of sulfotransferase. These findings are similar to that of Khrustalev *et al.*, (2017) who associated decrease in 3/10 helices to formation of hydrogen bonds between ethanol and oxygen and nitrogen atoms from main chain of protein. However, increase in beta-sheet, 3-helix and turn compositions in sulfotransferase were observed due to interactions with the ligands. Again, decrease in alpha-helix and increase in 5-helix compositions were observed in TGR due to interaction with the ligands (Appendix 16). These conformational changes may be important for molecular recognition, specificity and inhibition of schistosomal sulfotransferase and TGR or activation of ligands (tolmetin and diflunisal) by schistosomal sulfotransferase. This is in agreement with report of Liu *et al.*, (2016) that conformational dynamics play distinct and fundamental roles in tuning the affinity and specificity of molecular interactions. Khrustalev *et al.*, (2017) also reported that binding of ligands to regions of target not involved in catalytic activity or binding of other substrates will not cause any significant changes in the function of the targets while binding to functionally important region may cause structural changes which can be explained by local dehydration, delocalization of electron density, altered flexibility, resulting in the modification of hydrogen bond pattern. The altered flexibility and modification of hydrogen bonds observed (Figure 4.13, Figure 4.17 to 4.19 and Figure 4.21 to 4.23) are in agreement with the report of Khrustalev *et al.*, (2017). In particular, the reduction in the target flexibilities (Figure 4.13) may be important for inhibition of schistosomal TGR or activation of ligands (tolmetin and diflunisal) by schistosomal sulfotransferase.

The amino acids that have direct contacts with auranofin, oxamniquine, diflunisal, toletin or dinesterol (Figure 4.17 to 4.19 and Figure 4.21 to 4.23) and those that did not (Figure 4.20 and 4.24) showed different preference for secondary structure formation (Figure 4.15b and 4.16b). So, the study suggests that the discovered preferences for secondary structure motifs include some useful information on makers of auranofin, diflunisal tolmetin or dinesterol binding site in schistosomal sulfotransferase and TGR. Khrustalev *et al.*, (2017) have reported similar findings for ethanol binding sites on proteins.

The hydrogen bonds observed in the sulfotransferase and oxamniquine, diflunisal, tolmetin or dinesterol or TGR and auranofin, diflunisal, tolmetin or dinesterol (Figure 4.17 to 4.19 and 4.21 to 4.23) are suggested to be responsible for the specificities and molecular recognition of the interactions. Previous study has reported that hydrogen bonds are the most important specific interactions in biological recognition processes (Bissantz *et al.*, 2010). Again, Nil *et al.*, (2013) showed that additional hydrogen bond can dramatically reduce catalytic activity of *Bacillus subtilis* lipase A. The distance between atoms involved in hydrogen bonds from the MD simulations (Figure 4.25 and figure 4.27 to 4.29) suggests formations and breakages of some hydrogen bonds due to influence of the drugs. However, some of the calculated distances are stable throughout the MD simulations and maintained average distances within the range of hydrogen bond distances reported elsewhere (Bissantz *et al.*, 2010) for different types of hydrogen bonds. Data from the present study is also in agreement with the report of Jeffrey (1997) who categorized hydrogen bonds into “strong, mostly covalent”, “moderate, and mostly electrostatic” and “weak, electrostatic” with donor-acceptor distances of 0.22 to 0.25 nm, 0.25 to 0.32 nm and 0.32 to 0.40 nm respectively. Amino acid residues that formed short hydrogen bonds distances (0.17470 ± 0.07403 to 0.25719 ± 0.05321 nm) are mostly in backbone, side chain or different secondary structural regions such as helices, strands and turns which is in agreement with the report of Rajagopal and Vishveshwara, (2005). Also, Rajagopal and Vishveshwara, (2005) reported that short hydrogen bonds are found in the active site of enzymes and aid

enzyme catalysis. Therefore, the observed short hydrogen bonds may interfere with catalysis and suggests their involvement in competitive inhibition.

The study suggests that hydrogen bonds observed between amide hydrogens and oxygen atoms in auranofin, oxamniquine, diflunisal, tolmetin or dinesterol (Figure 4.18 to 4.19 and Figure 4.21 to 4.23) are not localized to specific binding site but are spread throughout the structure via a network of intramolecular interactions. Similar observation has been made elsewhere (Polshakov *et al.*, 2006). The study also observed repulsive $O \dots O$ interactions (Figure 4.19) which has been associated to loss of affinity Bissantz *et al.*, (2010). The protonated aliphatic amine functional group in oxamniquine that formed hydrogen bond with carbonyl oxygen atom at the side chain of Asn233 (Figure 4.17) may have implication for DNA alkylation and oxamniquine toxicity. da Silva *et al.*, (2017) pointed out that the aliphatic amine may probably contributes to strong interaction between oxamniquine and DNA through electrostatic bond with negatively charged phosphodiester group of DNA.

Involvement of potential covalent bond in the interactions as can be inferred from average distances of 0.14282 ± 0.04108 nm between hydrogen atom in $-SH$ from auranofin and oxygen atom in $-COOH$ of Asp433 and 0.153241 ± 0.02388 nm between hydrogen atom in $-SH$ of Cys159 and oxygen atom in $-COOH$ of diflunisal. The distance computations suggest presence of potential covalent bonds between TGR and auranofin, diflunisal or tolmetin (Figure 4.27). The average distances of the suspected covalent bonds suggest that diflunisal and tolmetin maybe targeted covalent inhibitors of TGR. Awoonor-Williams *et al.*, (2017) reported that targeted covalent inhibitors achieve high selectivity for targets by the combination of selective non-covalent interactions and the additional strength of covalent interaction between the warhead and complementary amino acid. Some FDA approved drugs (e.g saxagliptin, boceprevir, afatinib, nexium, telaprevir, clopidogrel, lansoprazole, esomeprazole, aspirin, osimertinib, ibrutinib etc) have been reported as covalent inhibitors (De Cesco *et al.*, 2017; Wang *et al.*, 2017). Both covalent and non-covalent interactions have been implicated in detoxification of cobra

phospholipase A2 by persimmon tannin (Zhang *et al.*, 2017). Selective covalent quinazoline inhibitors of KRAS G12C have been reported (Zeng *et al.*, 2017). Irreversible covalent bond formation between haloperidol derivatives and dopamine D2 receptor have been reported (Schwalbe *et al.*, 2017).

The study predicted that carboxylic functional group in diflunisal and tolmetin may interact covalently with $-SH$ group of Cys159 in schistosomal TGR (Figure 4.21 to 4.22 and Appendix 17) with high binding energies (Table 4.5). Previous study has reported that binding of covalently bound state of covalent inhibitor drugs results from both covalent and non-covalent interactions (Awoonor-Williams *et al.*, 2017). This may explain the high binding energy of diflunisal and tolmetin for TGR than sulfotransfase. However, the covalent bonds were only estimates from the distances of hydrogen atom in $-SH$ of Cys159 and oxygen atom in $-COOH$ of diflunisal and tolmetin as direct connection with sulfur atom was not observed in our classical molecular dynamics simulations. Confirmation of the covalent interaction requires modeling of reactivity using density functional theory approaches or QM/MM molecular dynamics simulations. However, Gissinger *et al.*, (2017) has reported modeling of chemical reactions in classical molecular dynamics simulations using reactive force field. Reversible and irreversible covalent binding of drugs to target have been reported (Awoonor-Williams *et al.*, 2017) and different functional groups involved in reversible and irreversible covalent inhibition and their mechanisms have been reported (De Cesco *et al.*, 2017). The thiol group in Cys159 of TGR and auranofin may serve as nucleophile for formation of the suspected covalent bonds (Figure 4.22). Lagoutte *et al.*, (2017) reported that cysteine's thio is endowed with enhanced reactivity, making it the nucleophile of choice for covalent engagement with a ligand aligning an electrophilic trap with a cysteine residue in a target of interest. Study has also shown that covalent modifiers of cysteine residues often feature acrylamide or other electron-deficient alkenes, which can undergo Michael additions to cysteine residue to form thioether adducts (Awoonor-Williams *et al.*, 2017) and rate of covalent engagement varies depending on the nucleophilicity of the targeted residue

and the type of electrophile (Lagoutte *et al.*, 2017). The study showed that electrophiles in diflunisal and tolmetin that may take part in covalent bond formation is their carboxylic ($-COOH$) functional groups while that for auranofin may come from carboxylic side chain of Asp433 (appendix 17). Thus, they can undergo Michael addition with Cys159 in TGR to form thioether adducts. Macegoniuk *et al.*, (2017) has identified reversible covalent interaction between thiol functional group in Cys322 of bacterial urase and acetyleneddicarboxylic acid while Martin-Gago *et al.*, (2017) reported selective covalent targeting of binding site carboxylic acids of aspartate in whole proteome. This may be the case for interaction of tolmetin or diflunisal with schistosomal TGR. Also, recent demonstration that a lysine's amide can also be engaged covalently with a mild electrophile extends the potential of covalent inhibitors (Lagoutte *et al.*, 2017).

Diflunisal, tolmetin or dinesterol interaction with sulfotransferase or TGR caused reduction in total, hydrophobic and hydrophilic accessible surface area of the targets (Appendix 20). It has been reported that residues lose part of their solvent-accessible surface due to folding (Lins *et al.*, 2003). Study has also shown significant decrease in hydrophobic surface (Eisenhaber and Argos, 1996). Therefore, the study attributed the reductions in accessible surface areas to protein stability due to folding as a result of burial of residues to the protein core. The reduction in radius of gyration of the targets due to influence of auranofin, oxamniquine, diflunisal, tolmetin or dinesterol relative to their unliganded states (Figure 4.11 and Appendix 14) supports this assertion. Also, number of hydrogen bonds increases with decreasing solvent accessibility (Bissantz *et al.*, 2010) and higher number of hydrogen bonds were observed in diflunisal or tolmetin bound MD simulations relative to dinesterol (Figure 4.17 to 4.19 and Figure 4.21 to 4.23).

The average minimum distances between the ligands (auranofin, dinesterol, tolmetin) at site 1 in TGR is smaller compared with their distances at site 2 and 3 (Appendix 18). This suggests stronger interaction at site 1 when compared with site 2 and 3. Also, distances between the

ligands at sites 2 and 3 of TGR and FAD in TGR (Figure 4.30) are suggestive of dynamical system with initial rearrangement of close interacting components (i.e Ligands and FAD). The initial rearrangements may be important for inhibition. Also, the observed close distance of ligands at site 1 to FAD (Appendix 18) might be implicated in charge transfer complex which may interfere with charge transfer complex in Cys154-Cys159 couple and FAD as speculated elsewhere (Angelucci *et al.*, 2010). Again, diflunisal and dinesterol showed lower minimum distance from sulfotransferase when compared with that of oxaniquine (Appendix 18). This suggests stronger interaction than tolmetin. However, only minimum distance cannot be used to measure extent of interaction between protein and ligand.

The nanosecond scale explicit solvent MD simulations performed on the sulfotransferase and thioredoxin glutathione reductase best describes an advanced stage conformational remodeling that binding site amino acid residues undergo in order to accommodate the ligand. One would expect this remodeling to be an important determinant of substrate selectivity. As reflected in figure 4.31 to 4.35, the major cluster in the whole trajectories verified that there were conformational changes and atom preferences for ligand interactions. Similar observations have been made by Zhao *et al.*, (2017) for binding of HIV-1 regulatory protein to grapheme. Olubiyi *et al.*, (2016) reported that highly selective binding site is expected to undergo limited conformational remodeling as opposed to a promiscuous binding site.

The sequence conservation analysis results showed that schistosomal glutathione s-transferase and sulfotransferase are not conserved in *D. melanogaster* while cathepsin B1 and TGR are conserved (Figure 4.39 and 4.40). Again, human liver alkaline phosphatase, alanine aminotransferase and aspartate aminotransferase are conserved in *D. melanogaster* (Figure 4.41 and 4.42). This implies that *D. melanogaster* will serve as a good model organism for testing compounds targeting schistosomal glutathione s-transferase and/or sulfotransferase. However, previous studies have reported TGR as a good drug target for development of new anti-

schistosomal drugs (Angelucci *et al.*, 2009, 2010). The conservation of human liver enzymes in the fly implies that it can serve as a good model liver function tests.

The longevity and survival rates of *D. melanogaster* fed with different doses of the approved drugs were expressed as percentage of live flies. It was observed that praziquantel and haloperidol reduced the survival rate of male and female *D. melanogaster* up to 50 % after 9 and 13 days of exposure respectively (Figure 4.43 and 4.47). Similar results were observed when they were fed with different doses of vildagliptin (Figure 4.49). Also, male flies showed lower longevity compared to females in the presence of the drugs (Figure 4.44, 4.48, 4.50) On the other hand, oxytetracycline enhanced survival rate and longevity of male and female flies (Figure 4.45 and 4.46). However, from the 16 th day of treatment survival rate of male flies was reduced by 50%. The female flies were not affected similarly. The results indicate that praziquantel, oxytetracycline, haloperidol or vildagliptin may be successfully used for treatment within one week.

CHAPTER FIVE

5.0 SUMMARY, CONCLUSION AND RECOMMENDATION

5.1 Summary of Findings

The following summary were drawn from the research:

- 1) Molecular docking simulations identified three approved drugs (diflunisal, tolmetin and dinesterol) with possible multi-target anti-schistosomal activities. Few others (e.g oxytetracycline, haloperidol) were also predicted as potential uni-target anti-schistosomal agents.
- 2) Two approved drugs (diflunisal and tolmetin) from the MD simulations formed better stable complexes, showed higher and concurrent binding energies than auranofin and oxamniquine for two schistosomal proteins (sulfotransferase and thioredoxin glutathione reductase) suggesting possible better pharmacological response. Tolmetin was predicted as potential multi-target antischistosomal drug with binding energies of -231.064 ± 18.55 and -338.636 ± 36.90 KJ/mol for sulfotransferase and thioredoxin glutathione reductase (TGR) respectively. Also diflunisal was predicted as potential multi-target antischistosomal drug with binding energies of -168.641 ± 20.37 and -290.117 ± 43.80 KJ/mol for sulfotransferase and TGR respectively.
- 3) Molecular dynamics simulation is a better predictor of binding energy of molecular interactions than molecular docking simulations which gave binding energy between -29.9156 to -35.9824 KJ/mol

- 4) The study predicted that carboxylic functional groups in diflunisal and tolmetin may interact covalently with $-SH$ side chain of Cys159 in schistosomal TGR. Therefore, the study proposed that diflunisal and/or tolmetin may be targeted covalent inhibitors of schistosomal TGR
- 5) The sequence conservation analysis results showed that schistosomal glutathione s-transferase and sulfotransferase are not conserved in *D. melanogaster* while cathepsn B1 and TGR are conserved.
- 6) Again, human liver alkaline phosphatase, alanine aminotransferase and aspartate aminotransferase are conserved in *D. melanogaster*
- 7) Longevity and survival rate experiments using *D. melanogaster* indicate that praziquantel, oxytetracycline, haloperidol or vildagliptin are safe for *D. melanogaster* within one week of administration.

5.2 Conclusion

The following conclusions were made from the research:

- 1) Two drugs (diflunisal and tolmetin) previously indicated as non-steroidal anti-inflammatory drugs were predicted as potential antischistosomal drugs with possible multi-target inhibitory activities against schistosoma species. They were projected to be safer than oxamniquine due to presence of carboxylic and hydroxyl functional groups and absence of nitroaromatic and amine functional groups which were present in oxamniquine.
- 2) Non-covalent interactions and conformational changes were responsible for molecular recognition and specificities of the interactions between the targets (sulfotransferase and thioredoxin glutathione reductase) and diflunisal or tolmetin.

- 3) Schistosomal glutathione s-transferase and sulfotransferase are not conserved in *D. melanogaster*. This implies that it can serve as a good model organism for testing compounds targeting schistosomal glutathione s-transferase and/or sulfotransferase.
- 4) Human liver alkaline phosphatase, alanine aminotransferase and aspartate aminotransferase are conserved in *D. melanogaster*. This implies that it can be used as model for liver function tests.
- 5) Longevity and survival rate experiments using *D. melanogaster* indicate that praziquantel, oxytetracycline, haloperidol or vildagliptin are safe for the flies within one week of administration.

5.3 Recommendations for further research

The following recommendations were drawn from the research:

- 1) There is need for confirmation of existence of covalent bond between Cys159 in schistosomal thioredoxin glutathione reductase and carboxylic functional group in diflunisal and tolmetin using density functional theory approaches and/or QM/MM molecular dynamics simulations.
- 2) There is need to perform structural optimization of tolmetin and diflunisal for schistosomal activity.
- 3) There is need to perform computational and/or wet laboratory mutagenesis experiments to confirm the role of critical amino acid residues involved in target (sulfotransferase and thioredoxin glutathione reductase) and ligand (diflunisal and tolmetin) interactions.
- 4) There is need for pre-clinical and clinical validations of the predicted multi-targets approved drugs (tolmetin and diflunisal) against schistosomiasis.

5.4 Contribution to knowledge

- 1) The study identified two approved drugs (diflunisal and tolmetin) previously indicated as non-steroidal anti-inflammatory drugs as potential antischistosomal drugs with possible multi-target inhibitory activities.
- 2) The study also identified few other drugs (such as oxytetracycline, haloperidol etc) as potential antischistosomal drugs
- 3) Praziquantel, oxytetracycline, haloperidol and vildagliptin are safe for *D. melanogaster* within one week of administration.

Limitations of the study

- 1) Antischistosomal activities of the predicted drugs were not carried out because efforts to obtain schistosome infected snails locally were not successful. Also, efforts to obtain same from BEI Resources of the National Institute of Allergy and Infectious Diseases (NIAID) at National Institute of Health (NIH) were not successful due to inability to meet up with biosafety cabinet certification requirement of class 2 laboratory (See appendix 22).
- 2) Longevity and survival rate experiments was carried out with praziquantel, oxytetracycline, haloperidol and vildagliptin instead of tolmetin and diflunisal because tolmetin and diflunisal were not available in Nigerian drug market as at the time of the investigation

References

- Abdulkadir, A., Ahmed, M., Abubakar, B.M., Suleiman, I.E., Yusuf, I., Imam, I.M. Sule, A.A., Tela, U.M., Dogo, H.M., Yakasai, A.M. and Musa B.M. (2017) Prevalence of urinary schistosomiasis in Nigeria, 1994–2015: Systematic review and meta-analysis. *African Journal of Urology* (2017) xxx, xxx–xxx
- Abdulla, M.H.; Ruelas, D.S.; Wolff, B.; Snedecor, J.; Lim, K.C.; Xu, F.; Renslo, A.R.; Williams, J.; Mckerrow, J.H. & Caffrey, CR. (2009). Drug discovery for schistosomiasis: hit and lead compounds identified in a library of known drugs by mediumthroughput phenotypic screening. *PLoS Neglected Tropical Disease*, **3**. e478
- Abolaji, A.O., Jean Paul Kamdem, J.P., Lugokenski, T.H., Nascimento, T.K., Waczuk, E.P., Farombi, E.O., Loreto, E.L.D and Rocha, J.B.T (2014) Involvement of oxidative stress in 4-vinylcyclohexene-induced toxicity in *Drosophila melanogaster* *Free Radical Biology and Medicine* **71** (2014) 99–108
- Abolaji, A.O., Kamdem J.P., Farombi E.O and Rocha J.B.T (2013) *Drosophila melanogaster* as a Promising Model Organism in Toxicological Studies *Arch. Bas. App. Med.* **1** (2013) 33 – 38
- Adenowo, A.F., Oyinloye, B.E., Ogunyinka, B.I and Kappo, A.P (2015) Impact of human schistosomiasis in sub-Saharan Africa *Braz J Infect Dis.* **1** 9(2). 196–205
<http://dx.doi.org/10.1016/j.bjid.2014.11.004>
- Alonso, H., Bliznyuk, A.A., and Gready, J.E (2006) Combining Docking andMolecular Dynamic Simulations in Drug Design *Medicinal Research Reviews*, **26** (5). 531-568, DOI 10.1002/med.20067
- Altschul, S.F., Madden, T.L., Schaffer, A.A., Zhang, J., Zhang, Z., Miller, W. and Lipman, D.J. (1997) Gapped BLAST and PSI-BLAST: a new generation of protein database search programs. *Nucleic Acids Res*, **25**. 3389-3402.
- Angelucci, F., Ahmed A. S., Williams, D. L., Boumis, G., Brunori, M., Dimastrogiovanni, D., Miele, A. E., Pauly, F and Bellelli, A (2009) Inhibition of *Schistosoma mansoni* Thioredoxin-glutathione Reductase by Auranofin Structural And Kinetic Aspects *The Journal Of Biological Chemistry* **284**: (42) 28977–28985
- Angelucci, F., Dimastrogiovanni, D., Boumis, G., Brunori, M., Miele, A. E., Saccoccia, F and Bellelli, A (2010) Mapping the Catalytic Cycle of *Schistosoma mansoni* Thioredoxin Glutathione Reductase by X-ray Crystallography *The Journal Of Biological Chemistry* **285** (42). 32557–32567

Arnold, K., Bordoli L., Kopp J and Schwede T (2006) The SWISS-MODEL Workspace: A webbased environment for protein structure homology modelling. *Bioinformatics* **22**. 195-201

Ashburn, T.T and Thor K.B (2004) Drug repositioning: identifying and developing new uses for existing drugs *Nature reviews / drug discovery* **3**. 673 - 683 doi:10.1038/nrd1468

Awoonor-Williams, E., Walsh, A.G and Rowley, C.N (2017) Modeling covalent-modifier drugs* *BBA - Proteins and Proteomics* **1865**. 1664–1675.
<http://dx.doi.org/10.1016/j.bbapap.2017.05.009>

Aziz, I.N., Yacoub, M., Rashid, L and Solieman, A (2015) Malondialdehyde; Lipid peroxidation plasma biomarker correlated with hepatic fibrosis in human *Schistosoma mansoni* infection *Acta Parasitologica*. **60**(4). 735–742; DOI: 10.1515/ap-2015-0105

Benkert, P., Biasini, M. and Schwede, T. (2011) Toward the estimation of the absolute quality of individual protein structure models. *Bioinformatics*, **27**. 343-350.

Berendsen, H. J. C., Postma, J. P. M., van Gunsteren,W. F., Hermans, J. (1981) Interaction models for water in relation to protein hydration. In: Intermolecular Forces. Pullman, B. ed. .D.Reidel Publishing Company Dordrecht 1981. 331–342

Berman, H.M., Westbrook, J., Feng, Z., Gilliland, G., Bhat, T.N., Weissig, H., Shindyalov, I.N., and Bourne P.E. (2000) The Protein Data Bank *Nucleic Acids Research*, **28**. 235-242.
www.rcsb.org

Bin Dajem, S.M and Mostafa, O.M.S (2007) Scanning Electron Microscopical Studies on *Schistosoma mansoni* cercariae Exposed to Ultraviolet Irradiation *Australian Journal of Basic and Applied Sciences*, **1**(4): 776-784, 2007

Bissantz, C., Kuhn, B and Stahl, M (2010) A Medicinal Chemist's Guide to Molecular Interactions. *J. Med. Chem.* **53**. 5061–5084 5061 DOI: 10.1021/jm100112j

Boehr, D.D., Nussinov, R and Wright, P.E (2009) The role of dynamic conformational ensembles in biomolecular recognition. *Nat. Chem. Biol.* **5**. 789–796

Boran, A.D and Iyengar R (2010) Systems approaches to polypharmacology and drug discovery. *Curr Opin Drug Discov Devel* **13**. 297–309.

Bordoli, L and Schwede, T (2012) Automated Protein Structure Modeling with SWISS-MODEL Workspace and the Protein Model Portal in *Homology Modeling: Methods and Protocols*, Methods in Molecular Biology, Andrew J.W. Orry and Ruben Abagyan (eds.), **857**, DOI 10.1007/978-1-61779-588-6_5, © Springer Science+Business Media, LLC

Borhani, D.W., Shaw, D. E (2012).The future of molecular dynamics simulations in drug discovery. *J. Comput.-Aided Mol. Des* **26**. 15–26.

- Bryantsev, A.L and Cripps, R.M (2009) Cardiac gene regulatory networks in Drosophila *Biochim Biophys. Acta* **1789**. 343–353.
- Bussi, G., Donadio, D., Parrinello, M (2007) Canonical sampling through velocity rescaling. *J.Chem. Phys.* **126**:014101
- Capron, A., Dessaint, J.P., Capron, M., Ouma, J.H and Butterworth, A.E (1987) Immunity to schistosomes: Progress toward vaccine *Science* **238**. 1065-1072
- Caffrey, C.R., Rohwer, A., Oellien, F., Marhofer, R., Braschi, S., Oliveira, G., McKerrow, J.H and Seizer, P.M (2009) A comparative chemogenomics strategy to predict potential drug targets in the metazoan pathogen, *Schistosoma mansoni* *PLoS One* **4**(2). e4413. doi:10.1371/journal.pone.0004413
- Chandramouli R, Kumar, P.P., and Bibhishan, K. V (2010) Analytical Method Development and Validation for Pre-Clinical Analysis *J. Pharm. Sci. & Res.* **2** (12). 795-803
- Changeux, J.P., Edelstein, S. (2011). Conformational selection or induced fit 50 years of debate resolved. *F1000 Biol. Rep.* **3**, 19
- Chauhan, V and Chauhan, A. (2016) Effects of methylmercury and alcohol exposure in Drosophila melanogaster: Potential risks in neurodevelopmental disorders *Int. J. Devl Neuroscience* **51**. 36–41
- Chiyaka, E T., Magombedze, G and Mutimbu, L (2010) Modelling within host parasite dynamics of schistosomiasis *Computational and Mathematical Methods in Medicine* **11** (3): 255–280
- Cioli, D., Pica-Mattoccia, L and Archer, S (1993) Drug resistance in schistosomes *Parasitol Today* **9**:162–166.
- Corbett, A., Williams, G and Ballard, C (2013) Drug Repositioning: An Opportunity to Develop Novel Treatments for Alzheimer's Disease *Pharmaceuticals* 2013 (6): 1304-1321; doi:10.3390/ph6101304
- Croset, S.C.J (2014) Drug repositioning and indication discovery using description logics A thesis submitted in Darwin College, University of Cambridge for Degree of Doctor of Philosophy
- Csermely, P., Agoston, V and Pongor S (2005) The efficiency of multi-target drugs: the network approach might help drug design. *Trends Pharmacol Sci* 26: 178– 182
- da Silva, V.B.R., Campos, B.R.K., de Oliveira, J.F., Decout, J and de Lima, M.d (2017) Medicinal chemistry of antischistosomal drugs: Praziquantel and Oxamniquine. *Bioorganic and Medicinal Chemistry* **25** (2017). 3259–3277. <http://dx.doi.org/10.1016/j.bmc.2017.04.031>
- Darden, T., York, D., Pedersen, L. (1993) Particle mesh Ewald: An N_log(N) method for Ewaldsums in large systems. *J. Chem. Phys.* **98**:10089–10092

Daura, X., Gademann, K., Jaun, B., Seebach, D and van Gunsteren (1999) W The β -peptide hairpin in solution: conformational study of a β -hexapeptide in methanol by NMR spectroscopy and MD Simulation. *Angew. Chem. Int. Ed.*, **38**. 236-240

Dawaki, S., Hesham M. Al-Mekhlafi1, H.M., Ithoi, I., Ibrahim, J., Abdulsalam, A.M., Ahmed, A., Sady, H., Nasr, N.A., and Atroosh W.M (2015) The Menace of Schistosomiasis in Nigeria: Knowledge, Attitude, and Practices Regarding Schistosomiasis among Rural Communities in Kano State. *PLoS ONE* **10**(11): e0143667. doi:10.1371/journal.pone.0143667

De Cesco, S., Kurian, J., Dufresne, C., Mittermaier, A.K., and Moitessier, N (2017) Covalent inhibitors design and discovery. *European Journal of Medicinal Chemistry* **138** 96e114
<http://dx.doi.org/10.1016/j.ejmech.2017.06.019>

de Moraes, J (2012) Antischistosomal Natural Compounds: Present Challenges for New Drug Screens Current Topics in Tropical Medicine (Ed) Alfonso Rodriguez-Morales Pp 333 – 358

De Vivo, M., Masetti, M., Bottegoni, G and Cavalli, A (2016) Role of Molecular Dynamics and Related Methods in Drug. *J. Med. Chem.* **59**. 4035–4061 DOI: 10.1021/acs.jmedchem.5b01684

Doenhoff, M. J., Cioli, D and Utzinger, J (2008) Praziquantel: mechanisms of action, resistance and new derivatives for schistosomiasis *Current Opinion in Infectious Diseases* **21**:659– 667

Durrant, J and McCammon, J. A (2011) Molecular dynamics simulations and drug discovery *BMC Biol.* **9**, 71.

Eisenhaber, F and Argos, P (1996) Hydrophobic regions on protein surfaces: definition based on hydration shell structure and a quick method for their computation *Protein Engineering* **9** (12). 1121-1133

El-Lakkany, N.M., Hammam, O.A., El-Maadawy, W.H., Badawy, A.A., Ain-Shoka, A.A and Ebeid, F.A (2012) Anti-inflammatory/anti-fibrotic effects of the hepatoprotective silymarin and the schistosomicide praziquantel against *Schistosoma mansoni*-induced liver fibrosis Parasites and Vectors 2012, 5:9

Essmann, U., Perera, L., Berkowitz, M. L., Darden, T., Lee, H., Pedersen, L. G.A (1995) smooth particle meshe wald potential. *J. Chem. Phys.* **103**. 8577–8592

Fenwick, A., Rollinson, D and Southgate V (2006) Implementation of human schistosomiasis control: challenges and prospects. *Adv. Parasitol.* **61**. 567–622.

Ferreira, L.G., dos Santos, R.N., Oliva, G., and Andricopulo, A.D (2015) Molecular Docking and Structure-Based Drug Design Strategies *Molecules* **20**. 13384-13421; doi:10.3390/molecules200713384

Fischer, M., Coleman, R. G., Fraser, J. S., Shoichet, B. K. (2014) Incorporation of protein flexibility and conformational energy penalties in docking screens to improve ligand discovery. *Nat. Chem.* **6**. 575–583.

Fortini, M.E., and Bonini, N.M (2000) Modeling human neurodegenerative diseases in Drosophila: on a wing and a prayer. *Trends Genet.* **16**. 161–167.

Fortini, M.E., M.P. Skupski, M.S. Boguski, and I.K. Hariharan (2000) A survey of human disease gene counterparts in the Drosophila genome *J. Cell Biol.* **150**. F23–30.

Foster R. A (1987) review of clinical experience with oxamniquine *Trans R Soc Trop Med Hyg* **81**. 55–59.

Gissinger, J.R., Jensen, B.D and Wise, K.E (2017) Modeling chemical reactions in classical molecular dynamics Simulations Polymer **128**. 211e217
<https://doi.org/10.1016/j.polymer.2017.09.038>

Gordon A (2015) Government of Nigeria Releases New Data on the Prevalence of Schistosomiasis and Intestinal Worms.
<http://endtheneglect.org/2015/06/governmentofnigeriareleasesnewdataontheprevalenceofschistosomiasisandintestinalworms/>. Retrieved on 4/13/2017

Greenberg, R. M. (2005) Are Ca₂C channels targets of praziquantel action? *International Journal for Parasitology* **35**: 1–9

Grimes, J.E.T., Croll, D., Harrison, W.E., Utzinger, J., Freeman, M.C and Templeton, M.R (2015) The roles of water, sanitation, and hygiene in reducing schistosomiasis: a review. *Parasites and Vectors* **8**. 156. DOI: 10.1186/s13071-015-0766-9

Gryseels, B., Polman, K., Clerinx, J., and Kestens, L. (2006) Human schistosomiasis *Lancet* **368**. 1106–1118.

Guedes, I.A., de Magalhães, C.S and Dardenne L.E (2014) Receptor-Ligand Molecular Docking *Biophysical Reviews* DOI: 10.1007/s12551-013-0130-2

Guex, N. and Peitsch, M.C. (1997) SWISS-MODEL and the Swiss-PdbViewer: an environment for comparative protein modeling. *Electrophoresis*, **18**. 2714-2723.

Harvey, M.J and De Fabritiis, G (2012) High-throughput molecular dynamics: the powerful new tool for drug discovery *Drug Discovery Today* **17**. 1059–1062.

Heimburg, T., Chakrabarti, A., Lancelot, J., Marek, M., Melesina, J., Hauser, A., Shaik, T.B., Duclaud, S., Robaa, D., Erdmann, F., Schmidt, M., Romier, C., Pierce, R.J., Jung, M., and Sippl W (2016) Structure-Based Design and Synthesis of Novel Inhibitors Targeting HDAC8 from *Schistosoma mansoni* for the Treatment of Schistosomiasis *J. Med. Chem.* **59**. 2423–2435 DOI: 10.1021/acs.jmedchem.5b01478

Hess, B. (2007) P-LINCS: A parallel linear constraint solver for molecular simulation. *J. Chem.Theory Comp.* **4**. 116–122

Hess, B., Kutzner, C., Van der Spoel, D. and Lindahl, E. (2008) Gromacs 4: Algorithms for highly efficient, load-balanced, and scalable molecular simulation, *J. Chem. Theory Comput.*, **4** (3): 435–447.

Hirth F. (2010) *Drosophila melanogaster* in the study of human neurodegeneration *CNS and Neurological Disorders - Drug Targets* **9**. 504-523

Huang, H., Rigouin, C., and Williams, D.L. (2012) The Redox Biology of Schistosome Parasites and Applications for Drug Development *Curr Pharm Des.* **18**(24): 3595–3611.

Huang, S.Y and Zou, X (2010) Advances and challenges in protein-ligand docking. *Int. J. Mol. Sci.* **11**. 3016–3034.

Humphery, W., Dalke, A and Schulten, K (1996) VMD –Visual Molecular Dynamics *J. Molec. Graphics* **14**. 33 – 38.

Iman, M., Saadabadi, A and Davood, A (2015) Molecular docking analysis and molecular dynamics simulation study of ameltolide analogous as a sodium channel blocker *Turk J Chem* **39**. 306 doi:10.3906/kim-1402-37

Irwin, J.J., Sterling, T., Mysinger, M.M., Bolstad, E.S., Coleman, R.G. (2012) ZINC: A Free Tool to Discover Chemistry for Biology *Journal of Chemical Information and Modeling* **52**. 1757–1768

Ismail, M., Botros, S., Metwally, A., William, S., Farghally, A., Tao, L., Day, T. A. and Bennet, J. A. (1999) Resistance to praziquantel: direct evidence from *Schistosoma mansoni* isolated from Egyptian villagers, *Am, J. Trop. Med. Hyg.* **60**(6). 932-935.

Jeffrey, G.A (1997) An introduction to hydrogen bonding, oxford university press. Pp 12 – 14

Jones, I., Sokolow, S and Rickards, C (2015) Tanzania. Stanford University. Upstream Alliance

Kanwai, S., Ndams, I.S., Kogi, E., Abdulkadir, J.S., Gyam, Z.G and Bechemagbor. A (2011) Cofactors influencing prevalence and intensity of Schistosoma haematobium infection in sedentary Fulani settlements of Dumbi, Igabi LGA, Kaduna State, Nigeria. *Sci World J.* **6**:159.

Kar, P., Lipowsky, R and Knecht, V (2013) Importance of polar solvation and configurational entropy for design of antiretroviral drugs targeting HIV-1 protease. *J Phys. Chem. B* **117**: 5793 – 5805. dx.doi.org/10.1021/jp30852921

Keiser, J. (2010). *In vitro* and *in vivo* trematode models for chemotherapeutic studies. *Parasitology*, **137**. 589-603

Keiser, J., Silue, K. D., Adiossan, L. K., Guessan, N.A. N., Monsan, N, Utzinger, J., N'Goran, E. K. (2014b) Praziquantel, Mefloquine-Praziquantel, and Mefloquine-Artesunate-Praziquantel against Schistosoma haematobium: A Randomized, Exploratory, Open-Label Trial. *PLoS Negl Trop Dis* **8**(7): e2975. doi:10.1371/journal.pntd.0002975

Keiser, J., Vargas, M., Rubbiani, R., Gasser, G., and Biot, C. (2014a) In vitro and in vivo antischistosomal activity of ferroquine derivatives *Parasites & Vectors* **7**:424 doi:10.1186/1756-3305-7-424

Khrustalev, V.V., Khrustaleva, T.A and Lelevich, S.V (2017) Ethanol binding sites on proteins *Journal of Molecular Graphics and Modelling* **78**. 187–194. <https://doi.org/10.1016/j.jmgm.2017.10.017>

King, C.H., Muchiri, E.M., and Ouma, J.H (2000) Evidence Against Rapid Emergence of Praziquantel Resistance in Schistosoma haematobium, Kenya *Emerging Infectious Diseases* **6** (6): 585-594

Koutsoukasa, A., Simmsb, B., Kirchmair, J., Bonda, P.J., Whitmorec, A.V., Zimmerc, S., Young, M.P., Jenkins, J.L., Glick, M., Glen, R.C and Bender, A (2011) From in silico target prediction to multi-target drug design: Current databases, methods and applications, *J Prot.* doi:10.1016/j.jprot.2011.05.011

Kubinyi, H. (2003) Drug research: myths, hype and reality. *Nat. Rev. Drug Discov.* **2**, 665–668

Kuklinski NJ, Berglund EC, and Ewing AG (2010) Micellar capillary electrophoresis—electrochemical detection of neurochemicals from *Drosophila* *J Sep Sci* **33**. 388 –393

Kumari, R., Kumar, R., Open Source Drug Discovery Consortium, Lynn, A (2014). g_mmpbsa A GROMACS Tool for High-Throughput MM-PBSA Calculations. *J. Chem. Inf. Model.* XXXX, XXX, XXX–XXX dx.doi.org/10.1021/ci500020m

Kuntz, A.N., Davioud-Charvet, E., Sayed, A.A., Califf, L.L., Dessolin, J., Elias S. J., Arné, r5., Williams, D. L. (2007) Thioredoxin glutathione reductase from *Schistosoma mansoni*: An essential parasite enzyme and a key drug target. *PLoS Med* 4(6): e206. doi:10.1371/journal.pmed.0040206

Lagoutte, R., Patouret, R and Winssinger, N (2017) Covalent inhibitors: an opportunity for rational target selectivity. *Current Opinion in Chemical Biology* 39. 54–63. <http://dx.doi.org/10.1016/j.cbpa.2017.05.008>

Li, H, Wang, W., Li, Y., Qu, G., Xing, Y., Qian, K., Jia, Y., Yang, Z., Qian, Y., Dai, J and Liang, Y (2013) *In vivo* activity of dihydroartemisinin against *schistosoma mansoni* schistosomula in mice *Southeast Asian J Trop Med Public Health* 44 (3): 379 – 387

Liao, K.H., Chen, K., Lee, W., Sun, M., Lee, C and Chen C.Y (2014) Ligand-Based and Structure-Based Investigation for Alzheimer's Disease from Traditional Chinese Medicine. *Evidence-Based Complementary and Alternative Medicine* Article ID 364819, 16 pages <http://dx.doi.org/10.1155/2014/364819>

Lim, K., Ho, J.X., keeling, K., Gilliland, G.L., ji, X., Ruker, F., and Carter, D.C (1994) Three-dimensional structure of *Schistosoma japonicum* glutathione S-transferase fused with a six-amino acid conserved neutralizing epitope of gp41 from HIV *Protein Science*, 3:2233-2244.

Lins, L., Thomas, A., and Brasseur, R (2003) Analysis of accessible surface of residues in proteins *Protein Science* 12:1406–1417

Liu, J., Dyer, D., Wang, J., Wang, S., Du, X., Xu, B., Zhang, H., Wang, X., Hu, W (2013) 3-Oxoacyl-ACP Reductase from *Schistosoma japonicum*: Integrated In Silico-In Vitro Strategy for Discovering Antischistosomal Lead Compounds *PLoS ONE* 8(6): e64984. doi:10.1371/journal.pone.0064984

López-Vallejo, F., Caulfield, T., Martínez-Mayorga, K., Giulianotti, M.A., Houghten, R.A., Nefzi, A and Medina-Franco, J.L. (2011) Integrating virtual screening and combinatorial chemistry for accelerated drug discovery. *Comb. Chem. High Throughput Screen.* 14: 475–487

Lu, J.J., Pan, W., Hu, Y.J and Wang, Y.T (2012) Multi-Target Drugs: The Trend of Drug Research and Development. *PLoS ONE* 7(6): e40262. doi:10.1371/journal.pone.0040262

Macegoniuk, K., Kowalczyk, R., Rudzin'ska, A., Psurski, M., Wietrzyk, J and Berlicki, L (2017) Potent covalent inhibitors of bacterial urease identified by activity-reactivity profiling *Bioorganic and Medicinal Chemistry Letters* **27**: 1346–1350 <http://dx.doi.org/10.1016/j.bmcl.2017.02.022>

Mafud, A.C., Ferreira, L.G., Mascarenhas, Y.P., Andricopulo, A.D and de Moraes, J (2016) Discovery of Novel Antischistosomal Agents by Molecular Modeling Approaches *Trends in Parasitology*, **32** (11): 874 – 886 <http://dx.doi.org/10.1016/j.pt.2016.08.002>

Makos, M.A., Kuklinski, N.J., Berglund, E.C., Heien, M.L and Ewing, A.G (2009) Chemical measurements in *Drosophila* *Trends Analyt Chem.* **28**(11): 1223–1234. doi:10.1016/j.trac.2009.08.005

Malde, A.K., Zuo, L., Breeze, M., Stroet, M., Poger, D., Nair, P.C, Oostenbrink, C., Mark, A.E. (2011) An Automated force field Topology Builder (ATB) and repository version 1.0. *Journal of Chemical Theory and Computation*, **7**(12), 4026-4037. <http://pubs.acs.org/doi/abs/10.1021/ct200196m>

Mantawy, M.M., Hanan Farouk Ali, H.F and Rizk, M.Z (2011) Therapeutic effects of *Allium sativum* and *Allium cepa* IN *Schistosoma mansoni* experimental infection *Rev. Inst. Med. Trop. Sao Paulo* **53**(3):155-163, doi: 10.1590/S0036-46652011000300007

Martí'n-Gago, P., Fansa, E.K., Winzker, M., Murarka, S., Janning, P., Schultz-Fademrecht, C., Baumann, M., Wittinghofe, A and Waldmann, H (2017) Covalent Protein Labeling at Glutamic Acids *Cell Chemical Biology* **24**: 589–597.e1–e5, <http://dx.doi.org/10.1016/j.chembiol.2017.03.015>

Mayer F, Mayer N, Chinn L, Pinsonneault RL, Kroetz D, and Bainton RJ (2009) Evolutionary conservation of vertebrate blood-brain barrier chemoprotective mechanisms in *Drosophila*. *J Neurosci* **29**:3538 –3550

McManus, D. P and Loukas, A (2008) Current Status of Vaccines for Schistosomiasis *Clinical Microbiology Reviews* 2008: 225–242

McTigue, M.A., Williams, D.R., Tainer, J.A (1995) Crystal structures of a schistosomal drug and vaccine target: glutathione S-transferase from *Schistosoma japonica* and its complex with the leading antischistosomal drug praziquantel. *J.Mol.Biol.* **246**: 21-27

Michel, F.S (1999) Python: A Programming Language for Software Integration and Development. *J. Mol. Graphics Mod.* **17**:57-61.

Mobley, D.L and Dill, K.A (2009) Binding of small-molecule ligands to proteins: “what you see” is not always “what you get” *Structure* **17** (4): 489-498. doi:10.1016/j.str.2009.010

Mølgaard, P., Nielsen, S.B., Rasmussen, D.E., Drummond, R.B., Makaza, N., and Andreassen, J. (2001) Anthelmintic screening of Zimbabwean plants traditionally used against schistosomiasis. *Journal of Ethnopharmacology*, **74**: 257-264

Morris, G.M., Huey, R., Lindstrom, W., Sanner, M.F., Belew, R.K., Goodsell, D.S., Olson, A.J (2009) Autodock4 and AutoDockTools4: automated docking with selective receptor flexibility. *J. Comp. Chem.* **16**: 2785-91.

Mortier, J., Rakers, C., Bermudez, M., Murgueitio, M.S., Riniker, S and Wolber, G (2015) The impact of molecular dynamics on drug design: applications for the characterization of ligand-macromolecule complexes *Drug Discovery Today* **20** (6) 686 – 702
<http://dx.doi.org/10.1016/j.drudis.2015.01.003>

Nair P.C, Malde A.K, Drinkwater N, Mark A.E (2012) Missing fragments: detecting cooperative binding in fragment-based drug design. *ACS Med Chem Lett* **3**:322–326

Nair P.C, Malde A.K, Mark A.E (2011) Using theory to reconcile experiment: the structural and thermodynamic basis of ligand recognition by Phenylethanolamine N-Methyl Transferase (PNMT). *J Chem Theory Comput* **7**:1458–1468

Nair, P.C and Miners, J.O (2014) Molecular dynamics simulations: from structure function relationships to drug discovery. *In Silico Pharmacology* 2014 2:4. doi:10.1186/s40203-014-0004-8

Naylor, S and Schonfeld, J. M (2014) Therapeutic Drug Repurposing, Repositioning and Rescue Part 1: Overview *Drug Discovery World Winter* **15**: 49 – 62

Ni, Z., Jin, R., Chen, H and Lin, X Lin (2013) Just an additional hydrogen bond can dramatically reduce the catalytic activity of *Bacillus subtilis* lipase A I12T mutant: An integration of computational modeling and experimental analysis. *Computers in Biology and Medicine* **43** 1882–1888 <http://dx.doi.org/10.1016/j.combiomed.2013.08.018>

O’Boyle, N.M., Banck, M., James, C. A., Morley, C., Vandermeersch, T. and Hutchison, G. R. (2011).Open Babel: An open chemical toolbox.*Journal of Cheminformatics*; **3**:33.

Olubiyi1, O.O., Olagunju, M .O and Obisesan, A.O (2016) Computational Analysis of Physicochemical Factors Driving CYP2D6 Ligand Interaction *Current Computer-Aided Drug Design*, **12**: 000-000 DOI: 10.2174/1573409912666160909092600

Olveda, D.U., Li, Y., Olveda, R.M., Lam, A.K., Chau, T.N.P., Harn, D.A., Williams, G.M., Gray, D.J and Ross, A.G.P (2013) Bilharzia: Pathology, Diagnosis, Management and Control. *Trop Med Surg* **1**: 135. doi:10.4172/2329-9088.1000135

Oostenbrink, C., Villa, A., Mark, A. E., Van Gunsteren, W. F. A (2004) Biomolecular force fieldbased on the free enthalpy of hydration and solvation: The GROMOS force-field parametersets 53A5 and 53A6. *Journal of Computational Chemistry* **25**(13):1656–1676

Ouedraogo, H., Drabo, F., Zongo, D., Bagayan, M., Bamba, I., Pima, T., Yago-Wienne, F., Toubalie, E., and Zhang, Y (2016) Schistosomiasis in school-age children in Burkina Faso after a decade of preventive chemotherapy *Bull World Health Organ* **94**:37–45. doi: <http://dx.doi.org/10.2471/BLT.15.161885>

Pandey, U.B. and Nichols, C.D (2011) Human disease models in *Drosophila melanogaster* and the role of the fly in therapeutic drug discovery *Pharmacol Rev.* **63**: 411–436

Peak, E. Chalmers, I.W and Hoffmann, K.F. (2010) Development and validation of a quantitative, high-throughput, fluorescent-based bioassay to detect schistosoma viability, *PLoS Neglected Tropical Disease*, **4**: e759

Perrimon, N., Friedman, A., Mathey-Prevot B and Eggert, U.S (2007) Drug-target identification in *Drosophila* cells: combining high-throughout RNAi and small-molecule screens *Drug Discovery Today* **12** (1/2)

Pessetto, Z.Y., Weir, S.J, Sethi, G., Broward, M.A, Godwin, A.K. (2013) Drug repurposing for gastrointestinal stromal tumor. *Mol Cancer Ther.* **12**(7): 1299–309. doi:10.1158/1535-7163.mct-12-0968.

Petrelli, A and Giordano S (2008) From single- to multi-target drugs in cancer therapy: when aspecificity becomes an advantage. *Curr Med Chem* **15**: 422– 432

Pettersen, E.F., Goddard, T.D., Huang, C.C, Couch, G.S, Greenblatt, D.M, Meng, E.C, Ferrin, T.E. (2004) UCSF Chimera: A visualization system for exploratory research and analysis. *J Comput Chem.* **25**(13):1605-12.

Pica-Mattoccia, L., Carlini, D., Guidi, A., Cimica, V., Vigorosi, F., and Cioli, D (2006) The schistosome enzyme that activates oxamniquine has the characteristics of a sulfotransferase *Mem Inst Oswaldo Cruz*, Rio de Janeiro, **101**(Suppl. I): 307-312

Poddighe S, K.M. Bhat, M.D. Setzu, P. Solla, A.M. Angioy, R. Marotta, R. Ruffilli, F. Marrosu, and A Liscia (2013) Impaired sense of smell in a *Drosophila* Parkinson's model. *PLoS One* **29**(8):e73156.

Polshakov, V.I., Birdsall, B and Feeney, J (2006) Effects of Co-operative Ligand Binding on Protein Amide NH Hydrogen Exchange *J. Mol. Biol.* **356**: 886–903 doi:10.1016/j.jmb.2005.11.084

Prast-Nielsen, S., Huang, H and Williams, D.L (2012) Thioredoxin glutathione reductase: its role in redox biology and potential as a target for drugs against neglected diseases *Biochim Biophys Acta* **1810**(12): 1262–1271. doi:10.1016/j.bbagen.2011.06.024.

Pronk, S., Páll, S., Schulz, R., Larsson, P., Bjelkmar, P., Apostolov, R., Shirts, M. R., Smith, J. C., Kasson, P. M., van der Spoel, D., Hess, B., and Lindahl, E. (2013) GROMACS 4.5: a high-throughput and highly parallel open source molecular simulation toolkit, *Bioinformatics*, **29**: 845–854.

Prüßing, K., Voigt, A and Schulz, J.B (2013) *Drosophila melanogaster* as a model organism for Alzheimer's disease *Molecular Neurodegeneration* **8** (35): 1-11

Rajagopal, S and Vishveshwara, S (2005) Short hydrogen bonds in proteins *FEBS Journal* **272** 1819–1832 doi:10.1111/j.1742-4658.2005.04604.x

Ramirez, B., Bickle, Q., Yousif, F., Fakorede, F., Mouries, M.A and Nwaka, S (2007) Schistosomes: Challenges in compound screening *Expert Opinion on Drug Discovery*, **2**: 53-61

Reim, I and Frasch, M (2010) Genetic and genomic dissection of cardiogenesis in the *Drosophila* model *Pediatr. Cardiol.* **31**:325–33

Reiter, L.T., L., Potocki, S., Chien, M., Gribskov, and Bier E. (2001) A systematic analysis of human diseaseassociated gene sequences in *Drosophila melanogaster*. *Genome Res.* **11**:1114–1125.

Remmert, M., Biegert, A., Hauser, A. and Soding, J. (2011) HHblits: lightning-fast iterative protein sequence searching by HMM-HMM alignment. *Nat Methods*, **9**: 173-175.

Roder, C and Thomson M. J. (2015) Auranofin: Repurposing an Old Drug for a Golden New Age Drugs R D **15**:13–20 DOI 10.1007/s40268-015-0083-y

Ross, F., Hernández, P., Porcal, W., Lo'pez, G V., Cerecetto, H., González, M., Basika,T., Carmona, C., Flo', M., Maggioli, G., Bonilla, M., Gladyshev, V. N., Boiani, M., Salinas, G (2012) Identification of Thioredoxin Glutathione Reductase Inhibitors That Kill Cestode and Trematode Parasites *PLoS ONE* **7**(4): e35033. doi:10.1371/journal.pone.0035033

Salinas, G, Selkirk, M.E, Chalar, C., Maizels, R.M., and Fernandez C (2004) Linked thioredoxin-glutathione systems in platyhelminths *Trends Parasitol.* **20**:340–346.

Salvador-Recatalà V, Greenberg R.M (2012) Calcium channels of schistosomes: unresolved questions and unexpected answers. *Wiley Interdiscip Rev Membr Transp Signal* **1**: 85-93.

Schüttelkopf, A.W and van Aalten, D.M (2004) PRODRG: a tool for hightthroughput crystallography of proteinligand complexes. *Acta Crystallogr D Biol Crystallogr* **60**(Pt 8):1355 - 63.

Schwalbe, T., Kaindl, J., Hübner, H and Gmeiner, P (2017) Potent haloperidol derivatives covalently binding to the dopamine D2 Receptor *Bioorganic and Medicinal Chemistry* **25** 5084–5094 <http://dx.doi.org/10.1016/j.bmc.2017.06.034>

Sher, A., James, S.L, Correa-Oliveira, R., Hieny, S and Pearce, E. (1989) Schistosome vaccines: Current progress and future prospects. *Parasitology* **98**:S61-568.

Skelly, P.J., Tielens, A.G.M and Shoemaker, C.B. (1998) Glucose Transport and Metabolism in Mammalian-stage Schistosomes *Parasitology Today* **14**: (10) 402 – 406

Smout, M.J., Kotze, A.C., McCarthy, J.S and Loukas, A. (2010) A novel high throughput assay for anthelmintic drug screening and resistance diagnosis by real-time monitoring of parasite motility. *PLoS Neglected Tropical Disease* **4**: e885

Song, L., Li, J., Xie, S., Qian, C., Wang, J., Zhang, W., Yin, X., Hua, Z., Yu, C (2012) Thioredoxin Glutathione Reductase as a Novel Drug Target: Evidence from *Schistosoma japonicum* *PLoS ONE* **7**(2): e31456. doi:10.1371/journal.pone.0031456

Stork, T., Engelen, D., Krudewig, A., Silies, M., Bainton, R. J. and KI'ambt, C. (2008) Organization and function of the blood-brain barrier in Drosophila *J. Neurosci* **28**(3), 587–597

Taylor, A. B., Pica-Mattoccia, L., Polcaro, C. M., Donati, E., Cao, X., Basso, A., Guidi, A., Rugel, A. R., Holloway, S. P., Anderson, T. J. C., Hart, P. J., Cioli, D., LoVerde, P.T. (2015) Structural and Functional Characterization of the Enantiomers of the Antischistosomal Drug Oxamniquine. *PLoS Negl Trop Dis* **9**(10): e0004132 doi:10.1371/journal. pntd.0004132

Trainor-Moss, S and Mutapi, F. (2016) Schistosomiasis therapeutics: whats in the pipeline?, *Expert Review of Clinical Pharmacology*, **9**:2, 157-160, DOI: 10.1586/17512433.2015.1102051

Trott, O. and Olson, A. J. (2010) AutoDockVina: improving the speed and accuracy of docking with a new scoring function, efficient optimization andmulti-threading. *Journal of Computational Chemistry*; **31**: 455-461.

Valentim, C.L., Cioli, D., Chevalier, F.D., Cao, X., Taylor, A.B., Holloway, S.P., Pica-Mattoccia, L., Guidi, A., Basso, A., Tsai, I.J., Berriman, M., Carvalho-Queiroz, C., Almeida, M., Aguilar, H., Frantz, D.E., Hart, P.J., LoVerde, P.T., Anderson, T.J. (2013) Genetic and molecular basis of drug resistance and species-specific drug action in schistosome parasites. *Science* **342**: 1385-1389 DOI: 10.1126/science.1243106

Vogt, A.D and Di Cera, E (2012) Conformational selection or induced fit? A critical appraisal of the kinetic mechanism *Biochemistry*, **51**: 5894–5902

Volkamer, A., Kuhn, D., Rippmann, F and Rarey, M (2012) DoGSiteScorer: A web-server for automatic binding site prediction, analysis, and druggability assessment Oxford University Press Pp 1 -2 <http://dogsitem.zbh.uni-hamburg.de>

Walker, A. J (2011) Insights into the functional biology of schistosomes *Parasites and Vectors* **4**:203 1 – 6

Wang, H. L. W., Li, Y., Qu, G., Xing, Y., Qian, K., Jia, Y., Yang, Z., Qian, Y., Dai, J., and Liang, Y (2013) *In Vivo Activity Of Dihydroartemisinin Against Schistosoma Mansoni Schistosomula In Mice Southeast Asian J Trop MedPublic Health* **44** (3): 379 – 387

Wang, L., Zhao, J., Yao, Y., Wang, C., Zhang, J., Shu, X., Sun X., Li, Y., Liu K., Yuan, H and Ma, X (2017) Covalent binding design strategy: A prospective method for discovery of potent targeted anticancer agents *European Journal of Medicinal Chemistry* **142** 493e505. <https://doi.org/10.1016/j.ejmech.2017.09.024>

Weber, W., Hunenbeger, P. H and McCammon, J.A (2000) Molecular dynamics simulations of a polyalanineoctapeptide under Ewald boundary conditions: Influence of artificial periodicity on peptide conformation, *J. Phys. Chem., B* **104**: 3575 – 3668.

WHO (2012) Schistosomiasis: progress report 2001-2011 and strategic plan 2012-2020. Geneva: World Health Organization; 2012.

WHO, (2003) Manual of basic techniques for a health laboratory (second edition) Malta Pp 125 – 146

WHO, (1989) WHO Drug Information. Genève: WHO

Yousif, F.; Hifnawy, M.S.; Soliman, G.; Boulos, L.; Labib, T.; Mahmoud, S.; Ramzy, F.; Yousif M.; Hassan, I.; Mahmoud, K.; El-Hallouty, S.M.; El-Gendy, M.; Gohar, L.; El-Manawaty, M.; Fayyad, W. & El-Menshawi, B.S. (2007) Large-scale *in vitro* screening of Egyptian native and cultivated plants for schistosomicidal activity. *Pharmaceutical Biology*, **45**: 501–510

Zeng, M., Lu, J., Li, L., Feru, F., Quan, C., Gero, T.W., Ficarro, S.B., Xiong, Y., Ambrogio, C., Paranal, R.M., Catalano, M., Shao, J., Wong , K., Marto, J.A., Fischer, E.S., J€anne, P.A., Scott, D.A., Westover, K.D and Gray N.S (2017) Potent and Selective Covalent Quinazoline Inhibitors of KRAS G12C. *Cell Chemical Biology* **24**: 1005–1016.e1–e3, <http://dx.doi.org/10.1016/j.chembiol.2017.06.017>

Zhang, S and Coulter, K. A (2013) Identification of plumbagin and sanguinarine as effective chemotherapeutic agents for treatment of schistosomiasis *International Journal for Parasitology: Drugs and Drug Resistance* **3** (2013) 28–34

Zhao, D., Li, L., He, D and Zhou, J (2016) Molecular dynamics simulations of conformation changes of HIV-1 regulatory protein on grapheme *Applied Surface Science* **377**: 324–334. <http://dx.doi.org/10.1016/j.apsusc.2016.03.177>

Zheng, H., Fridkin, M and Youdim M (2014) From Single Target to Multitarget/Network Therapeutics in Alzheimer's Therapy *Pharmaceuticals* **7**: 113-135; doi:10.3390/ph7020113

Zimmermann, G. R., Leha, J. and Keith, C. T. (2007) Multi-target therapeutics: when the whole is greater than the sum of the parts *Drug Discovery Today* **12**, (1/2): 34 – 42

APPENDICES

Appendix 1: Morphological features of schistosome

Species of schistosoma	Egg						
	Place found	Size (µm)	Shape	Spine	Shell	Colour	content
<i>Schistosoma haematobium</i>	Urine and occasionally in stools.	110–150	oval, with one well-rounded pole.	Smooth, very thin.		grey or pale yellow	A well-formed broad ciliated embryo surrounded by a membrane (internal shell).
<i>Schistosoma intercalatum</i>	Similar in appearance to <i>S. haematobium</i> , but found in stools.	140–180	spindle-shaped; less broad than <i>S. haematobium</i> (sides particularly flattened towards the rounded pole).	Terminal spine; longer and more tapered than <i>S. haematobium</i> .		grey or pale yellow	a ciliated embryo surrounded by a membrane with two depressions or indentations, one on each side near the middle.
<i>Schistosoma japonicum</i>		70–100	Oval, almost round.	Difficult to see, lateral and very small; may be hidden by small granules often found on the surface of the egg		Transparent or pale yellow.	a broad ciliated embryo
<i>Schistosoma mansoni</i>		110–180	oval, with one well-rounded pole and one conical pole	lateral, near the rounded pole; large and triangular	smooth, very thin	pale yellow	a broad ciliated embryo, surrounded by a membrane (internal shell) as in all <i>Schistosoma</i> spp.

Source: WHO, (2003)

Appendix 2: Drugs approved for new indications after being subjected to drug repurposing

DRUG NAME	ORIGINAL INDICATION	NEW INDICATION	YEAR	PHARMA COMPANY
Amitriptyline	Antidepressant	Neuropathic pain	2005	AstraZeneca
Amphotericin B	Antifungal	Leishmaniasis	1997	NeXstar Pharma
Aspirin	Inflammation, Pain	Anti-platelet, heart attack, stroke	Various	Various
Azathioprine	Rheumatoid Arthritis (RA)	IBD, MS, organ transplants	Various	Various
Bimatoprost	Glaucoma	Eyelash growth	2008	Allergan
Bleomycin	Antibiotic	Cancer	1973	Kayaku/BMS
Bromocriptine	Parkinson's Disease	Type II diabetes	2009	Novartis
Buprenorphine	Pain	Drug treatment	2002	Reckitt-Benckiser
Bupropion	Antidepressant	Smoking cessation	1997	GSK
Canakinumab	Rheumatoid Arthritis (RA)	Weight-loss (combi-therapy)	2014	Orexigen/Takeda
Clofazime	Tuberculosis	Muckle-Wells Syndrome	2009	Novartis
Colchicine	Gout	Leprosy	1986	Geigy
Colesevelam	LDL-lowering	Familial mediterranean fever	2009	URL Pharma
Crizotinib	Lymphoma	Type II diabetes	2008	Daiichi-Sankyo
Cycloserine	Tuberculosis	NSCLC	2011	Pfizer
Cyclosporine	Organ transplant rejection	CNS disorders	Various	Various
Dapoxetine	Antidepressant	Psoriasis, RA	1997	Novartis
Dimethyl Fumarate	Psoriasis	Premature ejaculation	2004	J&J
Donepezil	Alzheimer's Disease	MS	2013	Biogen IDEC
Doxepin	Antidepressant	Dementia	2006	Eisai/Pfizer
Duloxetine	Depression & GAD	Atopic dermatitis	2003	Various
		Stress urinary incontinence	2004	Lilly
		Fibromyalgia	2008	Lilly
		Pain	2010	Lilly
Eflornithine	Cancer	Hirsutism	2000	Gillette
		Sleeping sickness	1990	Aventis
Etanercept	Rheumatoid Arthritis (RA)	Plaque psoriasis	2004	Amgen/Pfizer
Everolimus	Organ rejection	Various cancers	Various	Novartis
Finasteride	Hypertension	Benign prostate hyperplasia	1992	Merck
Fluoxetine	Antidepressant	Male pattern baldness	1997	Merck
Gabapentin	Seizure	PMDD	2002	Lilly
Galantamine	Chronic fatigue syndrome	Postherpetic neuralgia	2004	Parke Davis
Gemcitabine	Anti-viral	Alzheimer's Disease	2001	Various
Glycopyrronium	Anti-ulcer	Various cancers	Various	Lilly
Histrellin	Prostate cancer	COPD	2005	Sosei/Novartis
Hydroxychloroquine	Malaria	Precocious puberty	2007	Endo Pharma
Ibuprofen	Inflammation, pain	Lupus, rheumatoid	Various	Various
Imatinib	CML	OA, RA, headache, migraine	Various	Novartis
Imflitiximab	Autoimmune diseases	GIST	2012	Novartis
Iproniazid	Tuberculosis	ALL	2013	Janssen
Lomitapide	Hypercholesterolemia	Crohn's Disease	1998	Various
Methotrexate	Cancer	Antidepressant	1958	Aegerion Pharma
Minoxidil	Hypertension	HoFH	2012	Barr Labs
Milnacipran	Antidepressant	Psoriasis, RA	2001	Upjohn
Miltefosine	Cancer	Hair Loss	1988	Forest Pharma
Naltrexone	Opioid/alcohol addiction	Fibromyalgia	2009	Zentaris
Onabotulinumtoxin	Facial spasm	Leishmaniasis	2014	Orexigen/Takeda
		Weight-loss (combi-therapy)	2014	Allergan
		Cervical dystonia	2000	Allergan
		Chronic migraine	2010	Allergan
		Facial cosmetics	2012	Allergan
		Stent restenosis prevention	Various	Various
Paclitaxel	Various cancers	Menopausal hot flashes	2013	GSK
Paroxetine	Antidepressant	HER-2 + breast cancer	2013	Genetech
Pertuzumab	Various cancers	Lymphoma & multiple myeloma	2008	Genzyme
Plertixafor	AIDS/HIV	Restless leg syndrome	2006	Boehringer
Pramipexole	Parkinson's Disease	Fibromyalgia	2007	Pfizer
Pregabalin	Anticonvulsant, neuropathic pain	Migraine, angina, tremors	Various	Various
Pregabalin	Hypertension	Acute myeloid leukaemia	1995	Hoffman La Roche
Propranolol	Acne	Breast cancer	2007	Lilly
Retinoic Acid	Osteoporosis	Rheumatoid Arthritis	2004	IDEC
Raloxifene	Various cancers	Restless leg syndrome	2005	GSK
Rituximab	Parkinson's Disease	Erectile dysfunction	1998	Pfizer
Ropinirole	Angina	PAH	2005	Pfizer
Sildenafil		Pancreatic tumors	2010	Pfizer
Sunitinib	GIST and RCC	Leprosy	1998	Celgene
Thalidomide	Anti-nausea	Multiple myeloma	2006	Celgene
Zidovudine	Cancer	HIV/AIDS	1987	Burroughs

Source: Naylor and Schonfeld (2014)

Appendix 3: Information on drugs used for survival and longevity experiments on *D. melanogaster*

Drug	Form	Dosage	Solubility in:	Taste
Praziquantel (600 mg)	Tablet	60 mg/kg/day in 2 or 3 divided doses Or 40 mg/kg/day in 1 or 2 divided doses	Water: 250 µg/ml or 400 mg/L DMSO: 100 mg/ml Ethanol: 750 g/L	Bitter
Haloperidol hydrochloride (5.0 mg)	Tablet	For nausea/vomiting: 1 – 5 mg for every 4 to 6 hours For psychosis: 0.5 – 5 mg/day in 2 – 3 divided doses Maintenance dose: 5 – 10 mg/day Resistant schizophrenia: up to 30 mg/day	Water: 3.0 mg/ ml Ethanol: 5.14 mg/ml	Tasteless
Oxytetracycline hydrochloride (250 mg)	Capsule	250 mg for every 6 hours, initial dose of 500 mg may be given. For severe infection: 500 mg for every 6 hours may be recommended by a doctor	Water: 1.0g/ml	Slightly bitter
Vildagliptin (50 mg)	Tablet	100 mg/day (i.e 50 mg in the morning and 50 mg in the evening). Dose greater than 100 mg are not recommended	PBS, pH 7.2: 10 mg/ml Ethanol: 16 mg/ml	Bitter

Appendix 4: Configuration files and script used for the validation of docking protocol and the docking simulation

Configuration files

receptor	=	1gtb.pdbqt
center_x	=	26.12
center_y	=	43.942
center_z	=	35.452
size_x	=	15
size_y	=	15
size_z	=	15

receptor	=	3h4k.pdbqt
center_x	=	56.865
center_y	=	-5.892
center_z	=	18.188
size_x	=	32
size_y	=	25
size_z	=	30

receptor	=	3qsd.pdbqt
center_x	=	18.203
center_y	=	15.035
center_z	=	20.002
size_x	=	13
size_y	=	20
size_z	=	13

receptor	=	4mub.pdbqt
center_x	=	108.616
center_y	=	8.676
center_z	=	15.452
size_x	=	15
size_y	=	15
size_z	=	15

Script used for validation of docking protocol and local molecular docking simulation using autodock vina®

```
#!/bin/bash

for f in zinc_*.pdbqt; do
    b=`basename $f .pdbqt`
    echo Processing ligand $b
    mkdir -p $b
    vina --config conf.txt --ligand $f --out ${b}/out.pdbqt -log \
    ${b}/log.txt
done
```

Appendix 5: ATB codes for the topologies of drugs used for MD simulation

Drug	Binding mode	ATB code
Topologies of drugs from molecular docking with sulfotransferase		
Dilunisal	1	33322
Tolmetin	1	33323
Dinesterol	1	33324
Topologies of drugs from molecular docking with TGR		
Auranofin	1	33762
	2	33763
	9	33764
Dinesterol	1	33766
	3	33767
	7	33769
Diflunisal	1	33770
	4	33771
	5	33772
Tolmetin	1	33773
	2	33774
	6	33323

Note: The topologies of oxamniquine and FAD were generated with PRODRG online tool because getting them with ATB failed.

Appendix 6: basic steps in the MD simulations and the molecular dynamics parameter files used

MD SIMULATION OF PROTEIN

1. Inspect your receptor for missing residues
 - i. Less receptor.pdb
 - ii. /
 - iii. MISSING + enter
2. Extract the protein from other things like comments remarks etc. in pdb file.
 - (i) grep "ATOM" protein.pdb > rec.pdb ; this was not used for target with eg, cofactor
 - (ii) editconf -f rec.pdb -o rec.pdb
3. Generate gromacs topdogy file for your protein
 - (i) pdb2gmx -f rec.pdb -p protein.top -i posre.itp -o conf.pdb
 - (ii) less protein.top
 - (iii) vmd conf.pdb or pymol conf.pdb
4. Generate a simulation box for your system
 - i. editconf -f conf.pdb -o box.pdb -bt cubic -d 1.5
 - ii. vmd box.pdb
 - iii. Click on Extentions and type pbc box: use s and r keys to view the box if need be.
5. Perform *in vacuo* energy minimization on your system.

- i. grompp -f minmdp -c box.pdb -p protein.top -o min.tpr
 - ii. mdrun -v -deffnm min
 - iii. Make and visualise movie of the minimization. vmd box.pdb min.trr. Representations, colour by atom type, choose molecule d contrast.
6. Solvate your molecular system
- i. genbox -cp min.gro -cs spc216.gro -o solvated.gro -p protein.top
 - ii. vmd solvated.gro
 - iii. vmd solvated.gro min.trr
7. Neutralize your system if need be
- i. grompp -f minmdp -c solvated.gro -p protein.top -o ion.tpr
 - ii. genion -s ion.tpr -p protein.top -o ionized.gro -neutral -conc 0.154
8. Run energy minimization on the solvated and ionized system
- i. grompp -f minmdp -c ionized.gro -p protein.top -o minionized.tpr (-maxwarn 1)
 - ii. mdrun -v -deffnm minionized
 - iii. You can analyze the energy of the minimized system.
 - ❖ g_energy -f minionized.edr -o potential.xvg
 - ❖ xmgrace potential.xvg
 - iv. View the dynamics of the minimization
 - ❖ vmd minionized.gro minionized.trr
 - ❖ Manipulate with vmd to view the dynamics of a given subsystem.
9. Perform position restrain dynamics on your system.
- i. View, create or edit pr.mdp.less pr.mdp
 - ii. vim pr.mdp, gedit pr.mdp
 - iii. grompp -f pr.mdp -c minionized.gro -p protein.top -o pr.tpr -maxwarn 1
 - iv. mdrun -v -deffnm pr
 - v. vmd pr.gro pr.trr
 - vi. g_energy -f pr.edr -o potential.xvg
10. Perform production run
- i. View, create or edit md.mdp: less md.mdp; gedit md.mdp
 - ii. grompp -f md.mdp -c pr.gro -p protein.top -o md.tpr
 - iii. mdrun -v -deffnm md

MD SIMULATION OF TARGET – LIGAND COMPLEX

1. Make directory for your MD simulation and examine your receptor for missing residues
 - i) less protein.pdb
 - ii) /
 - iii) MISSING + enter
2. Generate .itp file for your protein (using pdb2gmx) and ligand (use ATB or prodrug)

- i. pdb2gmx -f protein.pdb -p protein-top -i posire.itp -o gmxprotein.pdb
 - ii. cp protein.top protein.itp
4. Manual generation of complex topology carcase. See complex.top
5. Generate complex.pdb i.e concatenate protein and ligand
- i. cat protein.pdb ligand.pdb > complex.pdb
 - ii. editconf -f complex.pdb -o complex.pdb -resnr 1
6. Generate simulation box for your system
- i. editconf -f complex.pdb -o box.pdb -bt cubic -d 1.5
7. Perform in vacuo energy minimization
- i. grompp -f minmdp -c box.pdb -p complex.top -o min.tpr
 - ii. mdrun -v -deffnm min
8. Solvate your molecular system
- i. genbox -cp min.gro -cs spc216.gro -o solvated.gro -p complex.top
 - ii. vmd solvated.gro
9. Neutralize your molecular system if need be
- i. grompp -f minmdp -c solvated.gro -p complex.top -o ion.tpr
 - ii. genion -s ion.tpr -p complex.top -neutral -o ionized.gro -conc 0.154
10. Perform energy minimization on the solvated and ionized system.
- i) grompp -f minmdp -c ionized.gro -p complex.top -o minionized.tpr
 - ii) mdrun -v -deffnm minionized
 - iii) g_energy -f minionized.edr -o potential.xvg
 - iv) vmd minionized.gro minionized.trr
11. Perform position restrained dynamics
- i. less pr.mdp; edit pr.mdp if need be
 - ii. grompp -f pr.mdp -c minionized.gro -p complex.top -o pr.tpr -maxwarn 1
 - iii. mdrun -v -deffnm pr
11. Perform production run
- i. Less md.mdp; edit md.mdp if need be
 - ii. grompp -f md.mdp -c pr.gro -p complex.top -o md.tpr
 - iii. mdrun -v -deffnm md
13. Analysis of md simulation results

NB: restarting a crashed run/continuing run: mdrun -v -deffnm md -append -cpi md.cpt

MOLECULAR DYNAMICS PARAMETER FILES USED

Energy minimization parameters i.e min.mdp

```
cpp      = /usr/bin/cpp
define   = -DFLEX_SPC
constraints = none
integrator = steep
nsteps    = 1000
;
; Energy minimizing stuff
;
emtol    = 20
emstep   = 0.01
nstxout  = 1
nstvout  = 1
nstfout  = 0
nstlog   = 0
nstenergy = 10
nstlist   = 10

nstcomm  = 1
ns_type  = grid
rlist    = 1.0
rcoulomb = 1.0
rvdw     = 1.0
Tcoupl   = no
Pcoupl   = no
gen_vel  = no
```

Position restrain MD Simulation parameters i.e pr.mdp

```
define   = -DPOSRES
constraints = all-bonds
integrator = md
dt       = 0.002 ; ps !
nsteps   = 25000 ; total 50 ps.
nstcomm  = 1
nstxout  = 500
nstvout  = 0
nstfout  = 0
nstlog   = 500
nstenergy = 500
nstlist  = 10
ns_type  = grid
rlist    = 1.5
rcoulomb = 1.5
rvdw     = 1.5
```

```

; Berendsen temperature coupling is on in two groups
Tcoupl      = berendsen
tc-grps     = system
tau_t       = 0.1
ref_t       = 300 ; reference temperature in K
; Energy monitoring
energygrps  = system
; Pressure coupling is not on
Pcoupl      = berendsen
tau_p       = 0.5
compressibility = 4.5e-5
ref_p       = 1.0 ; reference pressure in atm
coulombtype = pme
pbc         = xyz

; Generate velocities is on at 300 K.
gen_vel     = yes
gen_temp    = 300.0
gen_seed    = 173529

```

Production MD simulation parameters i.e mdmdp

```

constraints   = all-bonds
integrator   = md
dt           = 0.002 ; ps !
nsteps       = 1500000 ; total 3000 ps.
nstcomm      = 1
nstxout      = 1000
nstvout      = 0
nstfout      = 0
nstlog       = 1000 ; this is 2000 in the case of 3H4K MD simulations
nstenergy    = 1000 ; this is 2000 in the case of 3H4K MD simulations
nstlist      = 10
ns_type      = grid
rlist        = 1.2
rcoulomb    = 1.2
rvdw         = 1.2
; v-rescale temperature coupling is on in two groups
Tcoupl      = v-rescale
tc-grps     = System
tau_t       = 0.1
ref_t       = 300
; Energy monitoring
energygrps  = System
; Isotropic pressure coupling is now on
Pcoupl      = parrinello-rahman
Pcoupltype  = isotropic
tau_p       = 0.5
compressibility = 4.5e-5

```

```

ref_p      = 1.0
coulombtype = pme
pbc       = xyz

; Generate velocities is on at 300 K.
gen_vel    = yes
gen_temp   = 300.0
gen_seed   = 173529

```

Example of topology carcase for the target-ligand md simulations i.e complex.top

```

; File 'topol.top' was generated
; By user: Ezebuo (3000)
; On host: ezebuo
; At date: Mon Nov 24 12:24:41 2016
;
; This is a standalone topology file
;
; It was generated using program:
; pdb2gmx - VERSION 4.5.5
;
; Topology file manually created for ligand bound to protein
; Force field was read from the standard Gromacs share directory.
;

; Include forcefield parameters
#include "gromos53a6.ff/forcefield.itp"

; Include chain topologies
#include "protein.itp"
#include "Tol.itp"

; Include water topology
#include "gromos53a6.ff/spc.itp"

#ifndef POSRES_WATER
; Position restraint for each water oxygen
[ position_restraints ]
; i funct    fcx     fcy     fcz
  1 1      1000    1000    1000
#endif

; Include Position restraint file
#ifndef POSRES
#ifndef posre.itp
#ifndef posreligand.itp
#endif
#endif

```

```
; Include topology for ions
#include "gromos53a6.ff/ions.itp"
```

```
[ system ]
; Name
Sulfotransferase-TOL complex in water
```

```
[ molecules ]
; Compound      #mols
Protein_chain_A    1
TOL                  1
```

Appendix 7: Doses of the drugs used for survival and longevity experiments and their preparations

Drug	Dose (mg)	Stock solution of drug (mg/ml)	Volume of stock solution of drug (ml)
Praziquantel	0.00	0.0	0.00
	0.05	1.0	0.05
	0.10	1.0	0.10
	0.30	1.0	0.30
	0.60	1.0	0.60
Oxytetracycline	0.00	0.0	0.00
	0.01	0.1	0.10
	0.05	0.1	0.50
	0.25	1.0	0.25
	0.50	1.0	0.50
Haloperidol	0.0000	0.000	0.00
	0.0001	0.001	0.10
	0.0003	0.001	0.30
	0.0010	0.010	0.10
	0.0020	0.010	0.20
	0.0200	0.100	0.20
Vildagliptin	0.00000	0.00	0.00
	0.00175	0.01	0.10
	0.00350	0.01	0.30
	0.00700	0.01	0.10
	0.01400	0.10	0.20

Appendix 8: Administration of the drugs (paraziquantel, oxytetracycline, haloperidol and vildagliptin) to the *Drosophila melanogaster*



Appendix 9: Druggability index, pockets and descriptors of schistosome targets

Pocket descriptor table for 3H4K:

Name	Volume [Å³]	Surface [Å²]	Lipo surface [Å²]	Depth [Å]	Drug Score
P0	2830.59	2944.89	1847.26	41.28	0.81
P1	368.08	676.33	353.77	17.38	0.72
P2	331.17	414.18	265.57	11.50	0.53
P3	312.35	590.75	309.59	12.20	0.52
P4	310.82	373.86	308.69	11.34	0.54
P5	301.59	401.52	254.03	9.76	0.44
P6	282.07	461.60	294.45	12.08	0.52
P7	261.36	528.12	354.63	10.46	0.43
P8	242.43	428.57	365.86	10.04	0.41

Name	Volume [Å³]	Surface [Å²]	Lipo surface [Å²]	Depth [Å]	Drug Score
P9	237.11	321.30	230.87	10.45	0.43
P10	223.62	283.03	142.53	11.95	0.47
P11	216.40	311.74	198.65	11.89	0.46
P12	204.69	362.43	218.05	7.05	0.27
P13	194.27	302.37	158.70	13.54	0.51
P14	177.24	234.01	126.06	8.49	0.29
P15	149.79	387.80	292.50	9.69	0.32
P16	139.73	250.84	156.90	8.19	0.25
P17	120.56	259.74	193.25	8.13	0.24
P18	103.53	242.50	189.28	7.41	0.19

Subpocket descriptor for 3h4k

Name	Volume [Å³]	Surface [Å²]	Lipo surface [Å²]	Depth [Å]	Drug Score
P0SP0	1228.71	1246.29	798.14	16.21	0.81
P0SP1	235.80	366.26	241.15	10.30	0.40
P0SP2	200.43	418.36	249.81	10.69	0.10
P0SP3	191.44	368.95	297.19	10.13	0.21
P0SP4	191.08	285.16	135.51	9.43	0.11
P0SP5	143.16	352.60	232.15	11.02	0.15
P0SP6	135.24	217.22	151.24	0.49	0.30
P0SP7	125.65	216.16	119.09	7.48	0.28
P0SP8	109.44	204.13	131.01	2.86	0.25
P0SP9	90.63	236.37	148.28	0.98	0.19
P0SP10	67.80	176.36	86.82	6.17	0.03
P0SP11	58.92	78.69	58.91	0.00	0.29
P0SP12	52.30	165.75	71.82	6.17	0.18
P1SP0	147.90	361.74	157.36	9.04	0.05
P1SP1	140.32	287.58	164.84	8.90	0.13
P1SP2	79.86	198.02	131.71	6.84	0.25
P3SP0	124.71	357.97	214.64	9.79	0.15
P3SP1	106.01	222.99	133.23	9.18	0.22
P3SP2	81.64	208.80	66.82	7.49	0.13
P6SP0	202.20	373.01	228.43	9.39	0.37
P6SP1	79.86	174.81	128.48	6.40	0.43
P7SP0	154.40	381.12	242.67	7.78	0.24
P7SP1	106.96	247.86	157.59	6.33	0.09
P8SP0	136.30	330.66	293.08	7.54	0.30
P8SP1	106.13	197.14	164.44	8.40	0.46

Name	Volume [Å³]	Surface [Å²]	Lipo surface [Å²]	Depth [Å]	Drug Score
P10SP0	134.64	160.26	71.92	10.12	0.09
P10SP1	88.97	167.61	102.10	7.87	0.09
P11SP0	132.63	211.16	126.98	8.86	0.35
P11SP1	83.77	149.49	103.00	6.60	0.14
P13SP0	153.81	256.58	118.40	7.78	0.25
P13SP1	40.46	62.92	53.50	1.77	0.45
P15SP0	81.99	224.17	138.15	6.48	0.07
P15SP1	67.80	246.03	223.03	6.33	0.35

legend: undruggable => druggable



Pocket descriptor table for 1BDG:

Name	Volume [Å³]	Surface [Å²]	Lipo surface [Å²]	Depth [Å]	Drug Score
P0	1490.69	1680.87	1017.06	23.43	0.79
P1	411.14	461.44	323.52	18.00	0.77
P2	300.35	485.69	308.87	14.65	0.59
P3	267.84	373.04	204.27	14.89	0.62
P4	255.36	394.83	259.41	10.22	0.43
P5	250.94	389.09	270.68	12.35	0.49
P6	167.30	328.91	125.02	8.21	0.25
P7	136.83	260.28	147.07	8.13	0.19
P8	116.93	178.15	110.51	7.33	0.19
P9	112.58	293.08	146.29	9.80	0.30
P10	107.78	257.68	175.03	7.98	0.20
P11	106.82	382.95	298.24	6.86	0.21
P12	106.11	252.54	182.58	8.26	0.20
P13	105.34	246.90	157.45	8.93	0.22

Subpocket descriptor table for 1BDG:

Name	Volume [Å³]	Surface [Å²]	Lipo surface [Å²]	Depth [Å]	Drug Score
POSP0	577.09	575.53	259.25	18.02	0.26

Name	Volume [Å³]	Surface [Å²]	Lipo surface [Å²]	Depth [Å]	Drug Score
P0SP1	365.12	661.02	368.74	14.33	0.21
P0SP2	221.25	337.06	264.88	8.66	0.14
P0SP3	144.06	295.76	183.75	9.56	0.23
P0SP4	122.56	250.15	172.61	9.94	0.30
P0SP5	60.61	85.91	34.21	0.89	0.22
P1SP0	195.90	344.47	247.76	9.55	0.25
P1SP1	166.27	121.94	76.70	1.60	0.37
P1SP2	48.96	80.84	67.42	0.00	0.36
P2SP0	142.78	238.65	169.74	9.20	0.34
P2SP1	96.45	247.19	167.77	8.77	0.08
P2SP2	61.12	172.01	78.38	0.80	0.09
P3SP0	221.89	355.51	188.41	9.69	0.22
P3SP1	45.95	59.31	36.47	1.60	0.54
P9SP0	62.14	212.03	123.28	4.63	0.07
P9SP1	50.43	123.31	41.42	4.98	0.06

legend: undruggable => druggable



Pocket descriptor table for 2XBI:

Name	Volume [Å³]	Surface [Å²]	Lipo surface [Å²]	Depth [Å]	Drug Score
P0	216.70	361.90	266.37	14.16	0.53
P1	150.14	270.86	216.34	11.36	0.39
P2	135.49	299.67	195.04	7.01	0.22
P3	124.16	449.95	232.66	9.87	0.26
P4	101.06	339.18	196.12	7.98	0.21

Subpocket descriptor table for 2XBI:

Name	Volume [Å³]	Surface [Å²]	Lipo surface [Å²]	Depth [Å]	Drug Score
P0SP0	122.30	234.29	181.11	10.51	0.38
P0SP1	94.40	274.74	203.35	7.22	0.32
P3SP0	62.53	258.87	93.89	5.81	0.05
P3SP1	61.63	241.78	151.32	6.51	0.15

legend: undruggable => druggable



Pocket descriptor table for 3HXG:

Name	Volume [Å³]	Surface [Å²]	Lipo surface [Å²]	Depth [Å]	Drug Score
P0	672.70	770.78	426.65	23.03	0.85
P1	298.94	652.40	386.37	16.65	0.68
P2	228.93	419.17	229.99	13.25	0.53
P3	174.98	359.41	261.62	12.09	0.43
P4	145.34	310.84	156.97	13.31	0.44
P5	138.37	225.50	176.98	8.19	0.24
P6	125.50	353.22	170.03	12.98	0.38
P7	121.66	112.00	47.43	12.56	0.42

Subpocket descriptor table for 3HXG:

Name	Volume [Å³]	Surface [Å²]	Lipo surface [Å²]	Depth [Å]	Drug Score
P0SP0	303.55	416.29	229.57	14.20	0.23
P0SP1	299.20	441.02	210.55	12.17	0.14
P0SP2	69.95	67.40	44.26	0.40	0.26
P1SP0	183.17	452.13	258.77	13.89	0.22
P1SP1	115.78	294.47	182.64	7.44	0.30
P3SP0	96.51	239.57	193.19	8.36	0.30
P3SP1	78.46	180.85	107.20	5.35	0.06
P4SP0	102.21	175.39	111.64	2.15	0.27
P4SP1	43.14	188.52	85.40	4.96	0.08
P6SP0	69.95	232.95	116.32	5.89	0.10
P6SP1	55.55	147.09	80.53	6.27	0.10

legend: undruggable => druggable



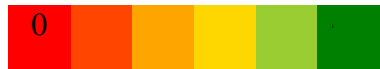
Pocket descriptor table for 2V1M:

Name	Volume [Å³]	Surface [Å²]	Lipo surface [Å²]	Depth [Å]	Drug Score
P0	246.34	581.19	388.63	12.62	0.50
P1	229.31	424.75	197.43	13.46	0.54
P2	213.70	300.72	183.43	14.18	0.54
P3	124.61	246.72	128.62	11.94	0.39

Subpocket descriptor table 2V1M:

Name	Volume [Å³]	Surface [Å²]	Lipo surface [Å²]	Depth [Å]	Drug Score
P0SP0	164.61	350.84	252.64	9.51	0.39
P0SP1	81.73	355.97	245.94	7.40	0.22
P2SP0	166.14	289.21	179.97	11.27	0.26
P2SP1	47.55	27.36	19.30	2.00	0.45

legend: undruggable => druggable



Appendix 10: BLAST search results of the schistosome targets against humans

Representatives of the BLAST results of the schistosome targets

Query ID: 3hxg (eukaryotic translation initiation factor 4e)

Sequence id (in a database)	Score (bits)	E value	Identities (%)	Positives (%)	Gaps (%)
Gb AAC39871.1	89.4	1e-20	29	55	5
Gb AAH12611.1	124	6e-34	34	52	3
Ref NP_001124150.1	126	3e-34	35	52	3
Gb EAX06080.1	125	2e-34	35	52	3
Ref NP_001959.1	125	2e-34	35	52	3

QUERY ID: 1BDG (HEXOKINASE)

Sequence id (in a database)	Score (bits)	E value	Identities (%)	Positives (%)	Gaps (%)
Gb AAA52646.1 (Range 1)	377	1e-119	46	62	3
Gb AAA52646.1 (Range 2)	344	3e-107	42	60	4
Emb CAA47379.1 (Range 1)	377	9e-123	46	62	3
Emb CAA47379.1 (Range 2)	116	6e-27	42	56	8
Em CAA86476.2 (Range 1)	381	2e-121	48	63	3
Em CAA86476.2 (Range 1)	351	5e-110	44	62	3
Pdb 2NZT A (Range 1)	385	4e-123	48	63	3
Pdb 2NZT A (Range 2)	352	2e-110	44	62	3

Representatives of the sequence alignment from BLAST results of the schistosome targets

3H4K:

thioredoxin reductase 3 [Homo sapiens]

Sequence ID: [gb|AAD39929.1|AF133519_1](#) Length: 577 Number of Matches: 1

Range 1: 2 to 577 GenPept Graphics			Next Match	Previous Match	
Score	Expect	Method	Identities	Positives	Gaps
609 bits(1571)	0.0	Compositional matrix adjust.	312/582(54%)	408/582(70%)	9/582(1%)
Query 20	VILFSKTTCPYCKVKDVLAEEKIKHATIELDQLSNGSAIQKCLASF SKIETVPQM FVRGKFIGDSQTVLKYY SNDELAGIVNES-KYDY	108			
Sbjct 2	.VI...SY..HSTR..ELFSSLGVECNVL...VDD.ARV.EV.SEITNQK..NI..NKVHV.GCDQTFOA.QSGL.QKLLQ.DLA...	91			
Query 109	DLIVIGGGSGGLAAGKEAAKYGAKTAVLDYWEPTPIGTTWGLGGTCVNVG CIPKKLMHQAGLISHALEDAEHF GWSLRSKISKHNSTMV	198			
Sbjct 92	...I.....SCA....IL.K.VM...F.V.S.Q.S.....A.GQ..C.SRK...EYNQ-QVR...E..T	180			
Query 199	EGVQSHIGSLNWNGYKV ALRDQNQV TYLN AGR LISPHEV QITDKNQ KV STITGNK II LATGERP KPY EIPGA VEV GITSDDL FSPY FPGK	288			
Sbjct 181	KAI.N..S.....RLS..EKA.A.V.SY.EFVEH.KIKA.N.KQGETYY.AAQFVI.....R.LG.Q.DK.C.....C...	270			
Query 289	TLVIGASVVALECA GFLASLG GDVT VMVRSILLRGFDQQMAEKVG DYMENHGVFKFAKLCVPDEIKQLKVVDTENNKPGLLLVKGHYTDGK	378			
Sbjct 271	P..V.....GF.L.....E.....S..Q.....LRKFI.VMVQ...----.KGS..K.K.LAKS.E.T	355			
Query 379	K-FEEEFETVIFAVGREPQLSKVLCETVGVKL-DKNGRVVCTDDEQTTVS NVAIG DINAGKPQLTPVAIQAG RYLARRLFAGATEL TDY	466			
Sbjct 356	ETI.GVYN..LL.I..DSCTR.IGL.KI...INE.S.KIPVN.V..N.PY..V..LED..E.....S.KL..Q..CASL.RC..	445			
Query 467	SNVATTVFTPLEY GAC GLSEED AIE KYGD KDI EY HSNFK PLEW TIAHRED NV CYMKLV CRK SDNM RV LGLH VLPN AGE ITQGYAVA IK	556			
Sbjct 446	I..P.....C.....K..V.KKENL.I..TL.W.....G..N.T..A.II.N.F.HD..I.F.I.....V..F.A.M.	535			
Query 557	MGATKADFDRTIGHPTCSETFTLHVTKSGVSPIVSGCCG	598			
Sbjct 536	C.L..QLL.D.....G.V..EI..S..LDITQK..U	577			

Chain A, The Structure Of Dimeric Human Glutaredoxin 2

Sequence ID: [pdb|2HT9|A](#) Length: 146 Number of Matches: 1

[See 1 more title\(s\)](#)

Range 1: 42 to 134 GenPept Graphics			Next Match	Previous Match	
Score	Expect	Method	Identities	Positives	Gaps
62.0 bits(149)	4e-10	Compositional matrix adjust.	28/93(30%)	51/93(54%)	0/93(0%)
Query 11	LRKTVDSA AVILFSKTTCPYCKVKDVLAEEKIKHATIELDQLSNGSAIQKCLASF SKIETVPQM FVRGKFIGDSQTVLKYY SNDELAGI	100			
Sbjct 42	IQE.ISDNC.VI....S.S..TMA.KLFHD MNVN YKVV...L.EY.NQF.DA.YKMTGER...RI..N.T...GATDTH RLHKEGK.LPL	131			
Query 101	VNE 103				
Sbjct 132	.HQ 134				

Chain A, Crystal Structure Of Glutaredoxin Domain Of Human Thioredoxin Reductase 3

Sequence ID: [pdb|3H8Q|A](#) Length: 114 Number of Matches: 1

[See 1 more title\(s\)](#)

Range 1: 14 to 107 GenPept Graphics			Next Match	Previous Match	
Score	Expect	Method	Identities	Positives	Gaps
58.9 bits(141)	3e-09	Composition-based stats.	26/94(28%)	54/94(57%)	1/94(1%)
Query 15	VDSAAVILFSKTTCPYCKVKDVLAEEKIKHATIELDQLSNGSAIQKCLASF SKIETVPQM FVRGKFIGDSQTVLKYY SNDELAGIVNES	104			
Sbjct 14	IERSR.VI...SY..HSTR..ELFSSLGVECNVL...VDD.ARV.EV.SEITNQK..NI..NKVHV.GCDQTFOA.QSGL.QKLLQ.D	103			
Query 105	-KYD 107				
Sbjct 104	LA.. 107				

glutathione reductase [Homo sapiens]

Sequence ID: [emb|CAA38367.1](#) Length: 230 Number of Matches: 1

Range 1: 26 to 227 GenPept Graphics						Next Match	Previous Match
Score	Expect	Method	Identities	Positives	Gaps		
68.2 bits(165)	9e-12	Compositional matrix adjust.	59/215(27%)	105/215(48%)	28/215(13%)		
Query 217	RDNQVTYLNAKGRLISPHEVQITDKNQKVST-----ITGNKI----ILATGERPKYP---EIPGAVEYGITSDDLFSLPYFPGKTLVIG	293					
Sbjct 26	..A.Y.SR...IYQNLTKSHIE.IRGHAFTSDKPTIEVS.K.YTAPH..IA.GM.ST.HESQ....-SL...-GF.Q.EEL..RSVIV.	113					
Query 294	ASYVALECAGFLASLGGDVTVMVRSLILLRGFDQQMAEKVGDYMNENHGVKFAKLCPDEIKQLKVVVDTE--NNKPGLLLVKGHYTDGKKFE	381					
Sbjct 114	..-I.V.M..I.SA..SKTSLRHDKV..S..SMISTNCTE-L..A..EVL.FSQVK.V.T.SGLEVSMVTAV..R.P.-----TMI	193					
Query 382	EEFETVIFAVGREPQLSKVLCEITVGVKLDKNGRVV 416						
Sbjct 194	PDVDCLLW.I..V.N-TDLSLNKL.IQT.DK.HII 227						

thioredoxin reductase 1 [Homo sapiens]

Sequence ID: [gb|AAQ62469.1](#) Length: 64 Number of Matches: 1

Range 1: 11 to 64 GenPept Graphics						Next Match	Previous Match
Score	Expect	Method	Identities	Positives	Gaps		
65.5 bits(158)	8e-12	Compositional matrix adjust.	43/54(80%)	47/54(87%)	0/54(0%)		
Query 106	YDYDLIVIGGGSGGLAAGKEAAKYGAKTAVALDYVEPTPIGTTWGLGGTCVNVC 159						
Sbjct 11I.....A.....Q..K.VM...F.T...LE.R..... 64						

Chain A, Crystal Structure Of Human Thioredoxin Reductase 1

Sequence ID: [pdb|2CFY|A](#) Length: 521 Number of Matches: 1

[See 5 more title\(s\)](#)

Range 1: 33 to 521 GenPept Graphics						Next Match	Previous Match
Score	Expect	Method	Identities	Positives	Gaps		
597 bits(1539)	0.0	Compositional matrix adjust.	301/495(61%)	376/495(75%)	8/495(1%)		
Query 106	YDYDLIVIGGGSGGLAAGKEAAKYGAKTAVALDYVEPTPIGTTWGLGGTCVNVC 195						
Sbjct 33I.....A.....Q..K.VM...F.T...L.R.....A.GQ..Q.SRNY..RVEET-VK.D.D 121						
Query 196	TMVEGVQSHIGSLNWGYKVALRDQNQVTYLNAKGRLISPHEVQITDKNQKVSTITGNKIIILATGERPKYPEIPGAVEYGITSDDLFSLPYF 285						
Sbjct 122	R.I.A..N..R..EKK.V.E..Y.Q.F.G..RIKA.NNKG.EKIYSAERFLI..R.LG..DK..C.S.....C 211						
Query 286	PGKTLIVGASYVALECAGFLASLGGDVTVMVRSLILLRGFDQQMAEKVGDYMNENHGVKFAKLCPDEIKQLKVVDTENNKPGLLLVKHYT 375						
Sbjct 212V.....GI.L.....D..N.I.EH..E..I..IRQF..IRVE.I----AGT..R.R.VAQ.S. 296						
Query 376	DGKKF-EEEFETVIFAVGREPQLSKVLCEITVGVKL-DKNGRVVCTDDEQTTVSNVYAIGDINAGKPLTPVAIQAGRYLARRLFAGATEL 463						
Sbjct 297	NSEEII.G.YN..ML.I..DACTR.IGL.....INE.T.KIPV..E..N.PYI.....LED.VE.....L.Q..Y..S.VK 386						
Query 464	TDYSNVATTVFTPLEYGACGLSEEDAIEKYGDKDIEVYHSNFKPLEWTVAHREDNVYCIMKLVCRKSDNMVRVLHVLGPNAEGITQGYAV 553						
Sbjct 387	C..E..P.....K.V..F.EEN.....Y.W.....IPS.DN.K..A.II.NTK..E..V.F.....V..F.A 476						
Query 554	AIKMGATKADFDRTIGIHPCTSETFTLHVTKKSGVSPIVSGCCG 598						
Sbjct 477	.L.C.L..KQJ.S.....V.A.V..S..R..A.IQQA..G. 521						

Chain A, X-Ray Structure Of Human Thioredoxin Reductase 1

Sequence ID: [pdb|2J3N|A](#) Length: 519 Number of Matches: 1

[See 5 more title\(s\)](#)

Range 1: 31 to 519 GenPept Graphics					Next Match	Previous Match
Score	Expect	Method	Identities	Positives	Gaps	
600 bits(1547)	0.0	Compositional matrix adjust.	302/495(61%)	377/495(76%)	8/495(1%)	
Query 106	YDYDLIVIGGGSGGLAAGKEAAKYGAKTAVLDYVEPTPIGTTWGLGGTCNVGCIPKKLMHQAGLLSHALEDAEFGWSLDRSKISHNW	195				
Sbjct 31I.....A.....Q.....K.V.M.....F.T.....L.R.....A.GQ.....Q.SRNY.....RVEET-VK.D.D	119				
Query 196	TMVEGVQSHIGSLNNGYKVALRDNQVITYLNKGRLLSPHEVQITDKNQKVSTITGNKIIILATGERPKYPEIPGAVEYGITSSDLFSLPYF	285				
Sbjct 120	R.I.A..N.....R.....EKK.V.E..Y.QF.G..RIKA.NNKG.EKIYSAERFLI.....R.LG..DK..C.S.....C	209				
Query 286	PGKTLVIGASYVALECAAGFLASLGDDVTVMVRSSILLRGFDQQMAEKVGVDYMEHGVKFAKLCVPDEIKQLKVVDTENNKPGLLVKGHYT	375				
Sbjct 210V.....GI.L.....D..N.I.EH..E..I..IRQF..IKVE.I----.AGT..R.R.VAQS.	294				
Query 376	DGKKF-EEEFETVIFAVGREGPQLSKVLCETVGVLK-DKNGRVVCTDD-EQTTVSNVYAIIDINAGKPQLTPVAIQAGRYLARRLFAGATEL	463				
Sbjct 295	NSEEII.G.YN..ML.I..DACTR.IGL.....INE.T.KIPV..E..N.PYI.....LED.VE.....L.Q..Y..S.VK	384				
Query 464	TDYSNVATTVFITLEYGAACGLSEDAIEKYGDKDIEVYHSNFKPLEWTVAHREDNVCYMKLVCRKSDNMRLVGLHVLGPNAEGITQGYAV	553				
Sbjct 385	C..E..P.....K.V..F.EEN.....Y.W.....IPS.DN.K..A.II.NTK..E..V.F.....V..F.A	474				
Query 554	AIKMGATKADFRTIGIHPCTSETFTLHVTKSGVSPIVSGCCG	598				
Sbjct 475	L.C.L..RQL.S.....V.A.V....S..R..A.ILOA....	519				

thioredoxin reductase [Homo sapiens]

Sequence ID: [gb|AAD25167.1|AF044212_1](#) Length: 521 Number of Matches: 1

Range 1: 34 to 521 GenPept Graphics					Next Match	Previous Match
Score	Expect	Method	Identities	Positives	Gaps	
510 bits(1313)	6e-174	Compositional matrix adjust.	261/496(53%)	349/496(70%)	10/496(2%)	
Query 105	KYDYDLIVIGGGSGGLAAGKEAAKYGAKTAVLDYVEPTPIGTTWGLGGTCNVGCIPKKLMHQAGLLSHALEDAEFGWSLDRSKISHNW	194				
Sbjct 34	QR.....L.V.....CA.....Q.L.R.V.V.....S.Q.R.....A.GGLIQ.....PNY.EVAQP-VP.D.	122				
Query 195	STMVEGVQSHIGSLNNGYKVALRDNQVITYLNKGRLLSPHEVQITDKNQKVSTITGNKIIILATGERPKYP-EIPGAVEYGITSSDLFSLP	283				
Sbjct 123	RK.A.A..N.VK.....HR.Q.Q.RK.K.E.IASFVDE.T.CGVA.GG.EILLSADH..I..G..R..TH.E..L.....I.W.K	212				
Query 284	YFPGKTLVIGASYVALECAAGFLASLGDDVTVMVRSSILLRGFDQQMAEKVGVDYMEHGVKFAKLCVPDEIKQLKVVDTENNKPGLLVKGH	373				
Sbjct 213	ES.....V.....TGI.L.T.I.M..P.....SSM.IEH.AS..TR.LRG.A.SRVRR.P--.GQ----.QVTWED	295				
Query 374	YTDGKKFEEEFETVIFAVGREGPQLSKVLCETVGVLKDNGRVCCTDD-EQTTVSNVYAIIDINAGKPQLTPVAIQAGRYLARRLFAGATE	462				
Sbjct 296	S.T..EDGT.G..LW.I..V.DTRSLSNL.KA..DTSPDTQKTLV.SR.A.S.PHI.....VBE.R.E..I..M..L.VQ..G.SSD	385				
Query 463	LTDYSNVATTVFITLEYGAACGLSEDAIEKYGDKDIEVYHSNFKPLEWTVAHREDNVCYMKLVCRKSDNMRLVGLHVLGPNAEGITQGYA	552				
Sbjct 386	M..D..P.....CV.....E.VARH.QBEV..AHY..F..G.DASQ..V.M..LREPPQL.....F.....V..F.	475				
Query 553	VAIKMGATKADFRTIGIHPCTSETFTLHVTKSGVSPIVSGCCG	598				
Sbjct 476	LG..C..SY.QM..V.....EVVK.RIS.R..LD.T.T..U.	521				

Chain A, Crystal Structure Of Human Thioredoxin Reductase I (Secys 498 Cys)

Sequence ID: [pdb|2ZZ0|A](#) Length: 513 Number of Matches: 1

[See 11 more title\(s\)](#)

Range 1: 25 to 513 GenPept Graphics					Next Match	Previous Match
Score	Expect	Method	Identities	Positives	Gaps	
601 bits(1550)	0.0	Compositional matrix adjust.	302/495(61%)	377/495(76%)	8/495(1%)	
Query 106	YDYDLIVIGGGSGGLAAGKEAAKYGAKTAVLDYVEPTPIGTTWGLGGTCNVGCIPKKLMHQAGLLSHALEDAEFGWSLDRSKISHNW	195				
Sbjct 25I.....A.....Q.....K.V.M.....F.T.....L.R.....A.GQ.....Q.SRNY.....RVEET-VK.D.D	113				
Query 196	TMVEGVQSHIGSLNNGYKVALRDNQVITYLNKGRLLSPHEVQITDKNQKVSTITGNKIIILATGERPKYP-EIPGAVEYGITSSDLFSLPYF	285				
Sbjct 114	R.I.A..N.....R.....EKK.V.E..Y.QF.G..RIKA.NNKG.EKIYSAERFLI.....R.LG..DK..C.S.....C	203				
Query 286	PGKTLVIGASYVALECAAGFLASLGDDVTVMVRSSILLRGFDQQMAEKVGVDYMEHGVKFAKLCVPDEIKQLKVVDTENNKPGLLVKGHYT	375				
Sbjct 204V.....GI.L.....D..N.I.EH..E..I..IRQF..IKVE.I----.AGT..R.R.VAQS.	288				
Query 376	DGKKF-EEEFETVIFAVGREGPQLSKVLCETVGVLK-DKNGRVVCTDD-EQTTVSNVYAIIDINAGKPQLTPVAIQAGRYLARRLFAGATEL	463				
Sbjct 289	NSEEII.G.YN..ML.I..DACTR.IGL.....INE.T.KIPV..E..N.PYI.....LED.VE.....L.Q..Y..S.VK	378				
Query 464	LTDYSNVATTVFITLEYGAACGLSEDAIEKYGDKDIEVYHSNFKPLEWTVAHREDNVCYMKLVCRKSDNMRLVGLHVLGPNAEGITQGYA	553				
Sbjct 379	M..D..P.....CV.....E.VARH.QBEV..AHY..F..G.DASQ..V.M..LREPPQL.....F.....V..F.	468				
Query 554	AIKMGATKADFRTIGIHPCTSETFTLHVTKSGVSPIVSGCCG	598				
Sbjct 469	LG..C..SY.QM..V.....EVVK.RIS.R..LD.T.T..U.	513				

thioredoxin reductase TR2 [Homo sapiens]

Sequence ID: [gb|AAD51325.1|AF171055_1](#) Length: 579 Number of Matches: 1

Range 1: 4 to 579 GenPept Graphics					Next Match	Previous Match
Score	Expect	Method	Identities	Positives	Gaps	
612 bits(1578)	0.0	Compositional matrix adjust.	313/582(54%)	409/582(70%)	9/582(1%)	
Query 20	VILFSKTTCPYCKVKDVLAEEKIKHATIELDQLSNGSAIQKCLASF SKIETVPQM FVRGKFIGDSQTVLKYY S NDELAGIVNES-KYDY					108
Sbjct 4	.VI...SY..HSTR..ELFSSLGVECNVL...VDD.ARV.EV.SEITMQK..NI..NKVHV.GCDQTPQA.QSGL.QKLQ.DLA...					93
Query 109	DLIVIGGGSGGLAAGKEAAKYGAKTAVLDYVEPTPIGTTWGLGGTCVNVCIPKKLMHQAGLLSHALEDAEHFGWSLDRSKISHNWSTMV					198
Sbjct 94	...I.....SCA...IL.K.VM...F.V.S.Q.S.....A..GQ..C.SRK...EYNQ-QVR...E..T					182
Query 199	EGVQSHIGSLNNGYKVVALRDNQVTYLNALKRGLISPHEVQITDKNQKVSTITGNKIIILATGERPKYPEIPGAVEYGITSDLFSLPYFPKG					288
Sbjct 183	KAI.N..S.....RLS..EKA.A.V.SY.EFVEH.RIKA.N.KQGETYY.AAQFVI.....R.LG.Q.DK..C.....C...					272
Query 289	TIVIGASVVALECA GFLASLGGDVTVMVR SILLRGFDQQMAEKVG DYMENHGVFAKLCVPDEIKQLKVVDTENNKPGLLLVKGHYTDGK					378
Sbjct 273	...V.....GF.L.....E.....S..Q.....LRKFI.VMVQ...---.KGS..K.K.LAKS.E.T					357
Query 379	K-FEEE FETVIFAVG REPQLSKVL CETVG VKL-DKN GRV VCTD DEQTT VSNV AIGDIN AGK PQL TPVAI QAG RYLARR LFAGATE LDY					466
Sbjct 358	BTI.GV/N..LL.I..DSCTR.IGL.KI..INE.S.KIPVN.V..N.PY..V..LED..E.....S.KL..Q..GASL.KC..					447
Query 467	SNVATT VFTPLEY GAC GLSEED AEI KYGD KDI E VYHSNF KPLEW TVAHRED NV CYMKLVCRKSDNMRV LGLHV LGPNAGE ITQGYAVA IK					556
Sbjct 448	I..P.....C.....K..V.KKENL.I..TL.W.....G..N.T..A.II.N.F.HD..I.F.I.....V..F.A.M.					537
Query 557	MGATKADFDRTIGIHPTCSETFTTLHVT KSGVSPIVSGCCG	598				
Sbjct 538	C.L..QLL.D.....G.V..EI..S..LDITQK..U.	579				

thioredoxin reductase 1 [Homo sapiens]

Sequence ID: [gb|AAL15432.1|](#) Length: 647 Number of Matches: 1

Range 1: 59 to 647 GenPept Graphics					Next Match	Previous Match
Score	Expect	Method	Identities	Positives	Gaps	
635 bits(1638)	0.0	Compositional matrix adjust.	325/595(55%)	423/595(71%)	15/595(2%)	
Query 11	LRKTVDSA AVILFSKTTCPYCKVKDVLAEEKIKHATIELDQLSNGSAIQKCLASF SKIETVPQM FVRGKFIGDSQTVLKYY S NDELAGI					100
Sbjct 59	.QAYI.GHS.VI..RS..TR..TE..KLFKSLCVPYFV..TED.R.LEGT.SELAAETDL.WV..RJRK..GHGPT..A.QEGR.QKL					148
Query 101	VNES-----KYDYDLIVIGGGSGGLAAGKEAAKYGAKTAVLDYVEPTPIGTTWGLGGTCVNVCIPKKLMHQAGLLSHALEDAEHFGW					183
Sbjct 149	LKINGPEDI LPKS.....I.....A....Q..K.VM..F.T..L.R.....A..GQ..Q.SRNY..					238
Query 184	SLDRSKISHNWSTMV EG VQSHIGSLN WGYKVVALRDNQVTYLNALKRGLISPHEVQITDKNQKVSTITGNKIIILATGERPKYPEIPGAVEY G					273
Sbjct 239	KVEET-VK.D.DR.I.A.N.....R..EKK.V.E..Y.QF.G..RIKA.NNKG.EKIYSABSFLI.....R.LG..DK..C					327
Query 274	ITSDDLFSLPYFPGKTLVIGASVVALECA GFLASLGGDVTVMVR SILLRGFDQQMAEKVG DYMENHGVFAKLCVPDEIKQLKVVDTENN					363
Sbjct 328	.S.....C.....V.....GI.LG.....D..N.I.EH..E..I..IRQF..IKVE.I----.AG					412
Query 364	KPGLLL VKGHYTDGKKF-EEEFETVIFAVG REPQLSKVL CETVG VKL-DKN GRV VCTD DEQTT VSNV AIGDIN AGK PQL TPVAI QAG RY					451
Sbjct 413	T..R.R.VAQS.NSEEII.G.YN..ML.I..DACTR.IGL.....INE.T.KIPV..E..N.PYI.....LED.VE.....L					502
Query 452	LARR LFAGATE LTDY SVATT VFTPLEY GAC GLSEED AEI KYGD KDI E VYHSNF KPLEW TVAHRED NV CYMKLVCRKSDNMRV LGLHV LG					541
Sbjct 503	.Q..Y..S.VKC..E..P.....K.V..F.EEN.....Y.W.....IPS.DN.K..A.II.NTK..E..V.F....					592
Query 542	PNA GEITQGYAVA IKMGATKADFDRTIGIHPTCSETFTTLHVT KSGVSPIVSGC	596				
Sbjct 593V..F.A.L.C.L..QKL.S.....V.A.V....S..R..A.IUQA..	647				

Hexokinase of schistosome against human hexokinase

Chain A, Crystal Structure Of Human Hexokinase Ii

Sequence ID: [pdb1NZTIA](#) Length: 902 Number of Matches: 2

[► See 1 more title\(s\)](#)

Range 1: 460 to 896 GenPept Graphics						▼ Next Match	▲ Previous Match
Score	Expect	Method	Identities	Positives	Gaps		
385 bits(990)	4e-123	Compositional matrix adjust.	213/443(48%)	283/443(63%)	15/443(3%)		
Query 16	LKPFDSLVDVYEEICDRMGE S MRLGLQKSTNEKSSIKMFP S VTKTPNGTETGNFLALDLGGTN Y RVL S T L E-GK K SPRIQERTYCIP	104					
Sbjct 460	.EHLQ..HDQLL.VKR..KVE.ER..S.E.HASAPV..L.T..CA..D..K.D.....F...L.RVRN..WGGVEMENKI.A..		549				
Query 105	AEKMSGSGTELFKYIAETLADFLENNGMKDKKF D LGFTFS F PCVQKGLTHATLVRWT K GFSADGVEGHNV A ELLQTEL D KRE-LNVKCVA	193					
Sbjct 550	Q.V.H.T.D..DH.Q C I..YM..GVS L P.....Q.NS.DESI.LK.....K.S.C..ED.VT..KEAIHR..EF D LDV..	639					
Query 194	VVNDITVGT L ASCALEDPKCAVG L IVG T G T INVAYIEDSSK V ELMDGV K PEPEVV V INTEWGAF G E K GELDCWR T QFDKSMID I SLHPGKQLYE	283					
Sbjct 640MMT.GF..H.E.....S.AC.M.EMRN..VE..E.GRMCV.M.....DN.C..DF..E..VAV.EL..N....RF..	728					
Query 284	KMVSGMYLGE V R H IVYLV E Q K ILFRGDL P ERLKVRNS L TRYLT D VERDPAHLLYN T HM L DDLHVP V EPIDNR-IVRYACEMVK	372					
Sbjct 729I..N..LIDFTKRG LRIS....T.GIFE.KF.SQI.S.CLA..QVRAIL---Q.LGLESTC.DSI..KEV.TV.AR	814					
Query 373	RAAYLAGAGIACILRR I --NRS---EVTVGDGS L YK H PKFC E RM T DMV D KL K PK N TR C LR I SE D GSGKGAAAIAASCTR	449					
Sbjct 815Q.C...M.AV D .RE..GLDALK.....T...L..H.AKV.HET.RD.A..CDVS F .Q-.....L.T.VAC.	896					

Range 2: 2 to 448 GenPept Graphics						▼ Next Match	▲ Previous Match	▲ First Match
Score	Expect	Method	Identities	Positives	Gaps			
352 bits(903)	2e-110	Compositional matrix adjust.	200/455(44%)	284/455(62%)	17/455(3%)			
Query 4	SDQQLFEKVV E ILKPF D LSVV D YEEICDRMGE S MRLGLQKSTNEKSSIKMFP S VTKTPNGTETGNFLALDLGGTN Y RVL S T L E-GK K SPRIQERTYCIP	92						
Sbjct 2-VQ..DQY.YHMR..DETLL..SK.FRKE.EK..GAT.HPTAAV..L.TF.RS..D..H.E.....F...W.RVTDN.LQ	89						
Query 93	SPRIQERTYCIP A EKMSGSGTELFKYIAETLADFLENNGMKDKKF D LGFTFS F PCVQKGLTHATLVRWT K GFSADGVEGHNV A ELLQTEL	182						
Sbjct 90	KVEMENQI.A..EDI.R..Q..DH..C..N.MDKLQI..LP.....H.TK.DESF..S.....KSS..RD.VA.IRKAI	179						
Query 183	DKR-ELNVKCVAVVNDTVGT L ASCALEDPKCAVG L IVG T G T INVAYIEDSSK V ELMDGV K PEPEVV V INTEWGAF G E K GELDCWR T QFDKSM D	271						
Sbjct 180	QR.GDFDIDI.....MMT.GYD.HN.EI.....S.AC.M.EMRHIDM V .-D.GRM C .M.....DD.S.NDI..E.QEI.	268						
Query 272	IDSLHPGKQLYEKMVSGMYLGE V R H IVYLV E Q K ILFRGDL P ERLKVRNS L TRYLT D VERDPAHLLYN T HM L DDLHVP V EPIDNR	361						
Sbjct 269	MG..N....F..I..M....L.L.RMAKEEL..G.K.SPE.LNTGR F .KD I .I.GEKDGIRKAREVLMRLG.D-.TQ.--.CV	355						
Query 362	IVRYACEMVKVRAAYLAGAGIACILRR I ----RSEVTVGVDGS L YK H PKFC E RM T DMV D KL K PK-NTR C LR I SE D GSGKGAAAIA	444						
Sbjct 356	ATHRI.QI.ST.S.S.CA.TL.AV.Q..KENKGEE.LRS.I.....V..K..H.AK.LHRT.RR.V.GCDV..--.....MVT	443						
Query 445	ASCTR 449							
Sbjct 444	.VAY. 448							

hexokinase II [Homo sapiens]

Sequence ID: [emb|CAA86476.2](#) Length: 916 Number of Matches: 2

Range 1: 474 to 909 GenPept Graphics			▼ Next Match ▲ Previous Match		
Score	Expect	Method	Identities	Positives	Gaps
381 bits(979)	2e-121	Compositional matrix adjust.	213/443(48%)	283/443(63%)	16/443(3%)
Query 16	LKPFDSLSSVVDYEEICDRMGESMRGLQKSTNEKSSIKMFPSSYVTKTPNGTETGNFLALDLGGTNYRVLSVTLE-GKGKSPRIERTYCIP	104			
Sbjct 474	.EHLQ..HDQLL.VKR..KVE.ER..S.E.HASAPV..L.T..CA..D..K.D.....F..L.RVRN..WGGVEMHNKI.A..				563
Query 105	AEKMSGSGTTELKYIAETLADFLENNGMKDKKFDLGFTFSFPCVQKGLTHATLVRWTKGFSADGVEGHNVAEELLQTELDKRE-LNVKVA	193			
Sbjct 564	Q.V.H.T.D..DH.VQCI....YM..GVSLP.....Q.NS.DESI.LK....K.S.C..ED..VT..KAIHR..EFIDLV..				653
Query 194	VVNDTVGTLASCALEDPKCAVGLIVGTGTNVAYIEDSSKVELMDGVKEPEVVINTEWGAFFGEKGELDCWRQFDKSMIDDSLHPGKQLYE	283			
Sbjct 654MMT.GF..H.E.....S.AC.M.EMRN..VE.-E.GRMV.C.M.....DN.C..DF..E..VAV.EL..N...RF.				742
Query 284	KMWSGMYLGEVLVRHIIVYLVQKILFRGDLPERLKVRNSLLTRYLTDDVERPAHLLYNTHMLTDLHVPPVEPIDNR-IVRYACEMVK	372			
Sbjct 743	.I.....I..N.LIDFTKRG...RIS...T.GIFE.KF.SQI.S.CLA..QVRAIL---Q.LGLESTC.DSI..KEV.TV.AR				828
Query 373	RAAYLAGAGIACILRR--NRS---EVITVGVDGSLYKFHFKFCERMTDMVDKLKPKNTRFCLRLSEDGSGKGAIAAASCTR	449			
Sbjct 829	...Q.C..M.AVVD..RE..GLDALK.....T..L..-.AKV.HET.KD.A..CDVSF.Q-.....L.T.VAC.				909

Range 2: 20 to 462 GenPept Graphics			▼ Next Match ▲ Previous Match ▲ First Match		
Score	Expect	Method	Identities	Positives	Gaps
351 bits(901)	5e-110	Compositional matrix adjust.	197/449(44%)	281/449(62%)	15/449(3%)
Query 10	EKVVEILKPFDSLSSVVDYEEICDRMGESMRGLQKSTNEKSSIKMFPSSYVTKTPNGTETGNFLALDLGGTNYRVLSVTLEGKG-KSPRIQE	98			
Sbjct 20	Q..DQY.YHMR..DETLL..SK.FRKE.EK..GAT.HPTAAV..L.TF.RS..D..H.E.....P..W.KVTDN.LQVMEN				109
Query 99	RTYCIPAEKMSGSGTTELKYIAETLADFLENNGMKDKKFDLGFTFSFPCVQKGLTHATLVRWTKGFSADGVEGHNVAEELLQTELDKRE-EL	187			
Sbjct 110	QI.A..EDI.R...Q..DH..C..N.MDKLHI....LP.....H.TK.DESF..S....KSS....RD.VA.IRKAIQR.GDF				199
Query 188	NVKCVAVVNDTVGTLASCALEDPKCAVGLIVGTGTNVAYIEDSSKVELMDGVKEPEVVINTEWGAFFGEKGELDCWRQFDKSMIDDSLHP	277			
Sbjct 200	DIDI.....MMT.GYD.HN.EI.....S.AC.M.EMRHIDME.-D.GRM..M.....DD.S.NDI..E..QEI.MG..N.				288
Query 278	GKQLYEKMVSGMYLGEVLVRHIIVYLVQKILFRGDLPERLKVRNSLLTRYLTDDVERPAHLLYNTHMLTDLHVPPVEPIDNRIVRYAC	367			
Sbjct 289F..I..M.....L.L.KMAKEEL..G.K.SPE.LNTGRFE.KDIS.I.GEKDGIRKAREVLMRLG.D..TQ.--.CVATHRI.				375
Query 368	EMVVKRAAYLAGAGIACILRRIN----RSEVITVGVDGSLYKFHFKFCERMTDMVDKLKP-NTRFCLRLSEDGSGKGAIAAASCTR	449			
Sbjct 376	QI.ST.S.S.CA.TL.AV.Q..KENKGE..LRS.I.....V..K..H.AK.LHKT.RR.V.GCDV.--.MVT.VAY.				462

hexokinase 1 [Homo sapiens]

Sequence ID: [gb|AAA52646.1](#) Length: 917 Number of Matches: 2

Range 1: 469 to 910 GenPept Graphics			▼ Next Match ▲ Previous Match		
Score	Expect	Method	Identities	Positives	Gaps
377 bits(967)	1e-119	Compositional matrix adjust.	205/448(46%)	282/448(62%)	15/448(3%)
Query 11	KVVEILKPFDSLSSVVDYEEICDRMGESMRGLQKSTNEKSSIKMFPSSYVTKTPNGTETGNFLALDLGGTNYRVLSVTLEGKG-KSPRIQE	99			
Sbjct 469	QIE.T.AH.H.TKDMLL.VKK..RAE.E..R.Q.HNNAVV..L..F..RR..D..N.D.....F..L.KIRS..KRTVEMHNK				558
Query 100	TYCIPAEKMSGSGTTELKYIAETLADFLENNGMKDKKFDLGFTFSFPCVQKGLTHATLVRWTKGFSADGVEGHNVAEELLQTELDKRE-LN	188			
Sbjct 559	I..A..I..I.Q.T.E..DH.VSCIS..DYM.I.GPRMP.....Q.TS.DAGI.IT....K.TDCV..D.VT..RDAIKR..EFD				648
Query 189	VVKCVAVVNDTVGTLASCALEDPKCAVGLIVGTGTNVAYIEDSSKVELMDGVKEPEVVINTEWGAFFGEKGELDCWRQFDKSMIDDSLHP	278			
Sbjct 649	LDV.....MMT..Y.E.T.E.....S.AC.M.EMRN..HVE..DQGQMC..M.....DN.C..DI..HY.RLVINEY..NA.				737
Query 279	KQLYEKMVSGMYLGEVLVRHIIVYLVQKILFRGDLPERLKVRNSLLTRYLTDDVERPAHLLYNTHMLTDLHVPPVEPIDNRIVRYAC	368			
Sbjct 738	..F..I..M.....I..N.LIDFTKGF...QIS.TM.T.GIFE.KF.SQI.S.RLA..QVRAILQQLG.NSTCDDS.--L.KTV.G				824
Query 369	MVVKRAAYLAGAGIACIL----RINRSEVITVGVDGSLYKFHFKFCERMTDMVDKLKP-NTRFCLRLSEDGSGKGAIAAASCTR	449			
Sbjct 825	V..SR..Q.C..M.AVVDKIREN.GLD.LN.....T..L..H.SRI.HQT.KE.S..C.VS.L--.....L.T.VGV.				910

Range 2: 14 to 462 GenPept Graphics			▼ Next Match ▲ Previous Match ▲ First Match		
Score	Expect	Method	Identities	Positives	Gaps
344 bits(882)	3e-107	Compositional matrix adjust.	194/458(42%)	279/458(60%)	20/458(4%)
Query 3	FSDQQLFEKVVEILKPFDSLSSVVDYEEICDRMGESMRGLQKSTNEKSSIKMFPSSYVTKTPNGTETGNFLALDLGGTNYRVLSVTLEGKG	91			
Sbjct 14	LK.D..V.K.IDKY.YAMR..DETLL..MT.FRKE.KN..SRDF.PTATV..L.TF.RSI.D..S.K.D.I.....SSF.I.R.QVNHE.N				102
Query 92	KSPRIERTYCIPAEKMSGSGTTELKYIAETLADFLENNGMKDKKFDLGFTFSFPCVQKGLTHATLVRWTKGFSADGVEGHNVAEELLQTE	181			
Sbjct 103	QNVHMESEV.DT.ENIVH..SQ..DHV..C.G..M.KRKI..LPV.....Q.SKIDE.I.IT..R.K.S..AD.VK..NKA				192
Query 182	LDKR-ELNVKCVAVVNDTVGTLASCALEDPKCAVGLIVGTGTNVAYIEDSSKVELMDGVKEPEVVINTEWGAFFGEKGELDCWRQFDKSM	270			
Sbjct 193	IK..GDYDANI.....MMT.GYD.QH.E..I..AC.M.ELRHID.VE.-D.GRM..DD.S.EDI..E..REI				281
Query 271	DIDSLHPGKQLYEKMVSGMYLGEVLVRHIIVYLVQKILFRGDLPERLKVRNSLLTRYLTDDVERPAHLLYNTHMLTDLHVPPVEPIDN	360			
Sbjct 282	.RG..N..F.....L..L.KMAKEGL..E.RITPE.LT.GKFN.SDVSIA.IKREG..H.AKEI..R---LG..S.D				366
Query 361	RI--VRYACEMVVKRAAYLAGAGIACILRRIN----RSEVITVGVDGSLYKFHFKFCERMTDMVDKLKP-KNTRFCLRLSEDGSGKGA	441			
Sbjct 367	DCVS.QHV.TI.SF.S.N.VA.TLGA..N.LRDNKGTP.LRT.....T..QYSR.FHKTLLR.V.DSDV..L--..S.....				454
Query 442	AIAASCTR 449				
Sbjct 455	MVT.VAY. 462				

Schistosome translation initiation factor against human translation initiation factor

eukaryotic translation initiation factor 4E isoform 1 [Homo sapiens]

Sequence ID: [ref|NP_001959.1|](#) Length: 217 Number of Matches: 1

[► See 24 more title\(s\)](#)

Range 1: 28 to 217 GenPept Graphics			▼ Next Match ▲ Previous Match		
Score	Expect	Method	Identities	Positives	Gaps
125 bits(315)	2e-34	Compositional matrix adjust.	67/192(35%)	100/192(52%)	7/192(3%)
Query 3	LGSPE--FPHPLQDSWSYYLFQFRKALDWDECLEKVATFSTIEDFWSVLHTVPRREITYGKDLYMFKSDIMPWKEDPKNENGGRWLINV	90			
Sbjct 28	VAN..HYIK....NR.ALWF.KND.SKT.QAN.RLISK.D.V....ALYN.IQLSSNLMP.C.YSL..DG.E.M...E..KR.....TL	117			
Query 91	TARQ---DVDFLWDELLMLLIGSDWDTDEEDRQICGAVFQPRSRGSKLSVWLTSNEEETILSIGRRRIKERLELEDTIYFQPVSDQRSQT	177			
Sbjct 118	NKQ.RRS.L.RF.L.T.LC...ESF.DYSD.--V....VIV.AK.D.IAI.T.ECENR.AVTH...VY...G.PPK.VIGYQ.HADTA.	205			
Query 178	RGSDICTGKYEI 189				
Sbjct 206	KSGSTTKNRFVV 217				

Eukaryotic translation initiation factor 4E [Homo sapiens]

Sequence ID: [gb|AAH12611.1|](#) Length: 217 Number of Matches: 1

Range 1: 28 to 217 GenPept Graphics			▼ Next Match ▲ Previous Match		
Score	Expect	Method	Identities	Positives	Gaps
124 bits(312)	6e-34	Compositional matrix adjust.	66/192(34%)	100/192(52%)	7/192(3%)
Query 3	LGSPE--FPHPLQDSWSYYLFQFRKALDWDECLEKVATFSTIEDFWSVLHTVPRREITYGKDLYMFKSDIMPWKEDPKNENGGRWLINV	90			
Sbjct 28	VAN..HYIK....NR.ALWF.KND.SKT.QAN.RLISK.D.V....ALYN.IQLSSNLMP.C.YSL..DG.E.M...E..KR.....TL	117			
Query 91	TARQ---DVDFLWDELLMLLIGSDWDTDEEDRQICGAVFQPRSRGSKLSVWLTSNEEETILSIGRRRIKERLELEDTIYFQPVSDQRSQT	177			
Sbjct 118	NKQ.RRS.L.NRF.L.T.LC...ESF.DYSD.--V....VIV.AK.D.IAI.T.ECENR.AVTH...VY...G.PPK.VIGYQ.HADTA.	205			
Query 178	RGSDICTGKYEI 189				
Sbjct 206	KSGSTTKNRFVV 217				

Appendix 11: selected drugs with different reference compounds (Praziquantel, oxamniquine, auranofin, and 074) used the molecular docking simulations

Praziquantel

Drugs	GPCR ligand	Protease inhibitor
Fexofenadine 1	0.4	0.1
Fexofenadine 2	0.4	0.1
LACTULOSE3977952	0.4	0.1
Fosaprepitant	0.4	0.05
Indacaterol	0.38	0.11
Vacuronium	0.38	0.09
Escitalopram 2	0.37	0.09
Fluvastatin 3	0.37	0.05
Escitalopram 1	0.36	0.07
Ponatinib	0.36	0.04
Diphenidol	0.35	0.12
Hydroxychloroquine 1	0.35	0.12
Hydroxychloroquine 2	0.35	0.12
Homatropine methylbromide 3	0.35	0.11
promethazine2	0.34	0.11
tafluprostx3	0.34	0.11
Capecitabine	0.34	0.09
Ethinyl estradiol	0.33	0.03
LEVOMETHADYL ACETATE1530967	0.32	0.08
METHADYL ACETATE1530967	0.32	0.08
METHADYL ACETATE2007678	0.32	0.08
METHADYL ACETATE2007680	0.32	0.08
METHADYL ACETATE2007682	0.32	0.08
Chloroquine	0.32	0.05
Anileridine	0.31	0.08
Epinastine 1	0.31	0.08
Epinastine 2	0.31	0.08
METHADONE1530706	0.31	0.05
METHADONE1530707	0.31	0.05
Dextropropoxyphene 1	0.3	0.12
Dextropropoxyphene 2	0.3	0.12
Vilazodone	0.3	0.07

LORAZEPAM431	0.29	0.09
LORAZEPAM896595	0.29	0.09
Bethanidine	0.28	0.12
PAROXETINE527386	0.28	0.11
Ritodrine	<u>0.28</u>	0.04
Alfacalcidol	0.26	0.12
Avanafil	0.26	0.12
Sotalol	0.26	0.1
sotalol2	0.26	0.1
Halopeadol 3	0.26	0.07
Haloperidol 2	0.26	0.07
praziquantel x2	0.25	0.07
propericiazine	<u>0.25</u>	0.07
Alogliptin	0.24	0.12
LABETALOL64348909	0.24	0.05
LABETALOL64348912	0.24	0.05
Verapamil	0.24	0.05
salbutamolx2	0.23	0.07
LANSOPRAZOLE21985533	0.23	0.05
<u>Aprindine</u>	0.22	0.07
Sparfloxacin	0.22	0.06
sparfloxacin3	0.22	0.06
Donepezil 2	0.22	0.03
Cholecalciferol	0.21	0.12
Tazarotene	0.21	0.06
Thioridazine	0.21	0.05
Ergocalciferol 1	0.21	0.04
Ergocalciferol 2	0.21	0.04
Ergocalciferol 3	0.21	0.04
Ergocalciferol 4	0.21	0.04
MIRABEGRON1996784	0.2	0.08
Dihydrotachysterol 4	0.2	0.06
Dihydrotachysterol 5	0.2	0.06
Dihydrotachysterol 6	0.2	0.06
Dihydrotachysterol 1	0.2	0.05
Dihydrotachysterol 2	0.2	0.05
Dihydrotachysterol 3	0.2	0.05
Formestane 9	0.2	0.05
voriconazole 2	0.2	0.04
Etoposide 1	0.18	0.12

Etoposide 2	0.18	0.12
Etoposide 3	0.18	0.12
Etoposide 4	0.18	0.12
Sorafenib	0.18	0.11
Bezafibrate	0.16	0.12
Plerixafor	<u>0.16</u>	0.1
Dronedarone	0.16	0.09
Encainide 1	0.16	0.09
Encainide 2	0.16	0.09
Esmolol 2	0.16	0.09
Icosapent ethyl	0.16	0.08
Dicyclomine	0.16	0.04
Esmolol 1	0.15	0.09
Carteolol	0.15	0.05
Dapagliflozin	0.15	0.05
Iohexol11525622	0.14	0.09
Iohexol11525623	0.14	0.09
Iohexol8214413	0.14	0.09
L-HISTIDINE18274816	0.14	0.09
OUABAIN8143614	0.14	0.09
OUABAIN8214757	0.14	0.09
OUABAIN8214758	0.14	0.09
OUABAIN8214759	0.14	0.09
Repaglinide	0.14	0.07
Atenolol	0.13	0.08
Falbamate	0.12	0.11
OXAPROZIN1863	0.12	0.1
L-TRYPTOPHAN95878046	0.12	0.07
L-TRYPTOPHAN95878048	0.12	0.07
Estrone 1	0.12	0.05
Estrone 2	0.12	0.05

Negative control for praziquantel

Drugs	GPCR ligand	Protease inhibitor
METHIMAZOLE1187543	-4.49	-4.72
Fomepizole	-4.01	-4.51
Chlorpropamide	-4.08	-4.02
acetic acid	-4.11	-3.82
hydrogen carbonate	-4.11	-3.82
LITHIUM6827693	-4.11	-3.82

sodium bicarbntc	-4.11	-3.82
sevelamer	-4.51	-3.61
pyruvic acid	-4.04	-3.23

Selected drugs using oxamniquine

Drugs	GPCR ligand	Ion channel modulator
PETHIDINE1681	0.12	0.18
LACTULOSE12494320	0.12	0.11
LACTULOSE4556763	0.12	0.11
LACTULOSE4556765	0.12	0.11
LACTULOSE4556766	0.12	0.11
OSELTAMIVIR3874568	0.12	0.1
OSELTAMIVIR3874569	0.12	0.1
OSELTAMIVIR3874570	0.12	0.1
OSELTAMIVIR3874571	0.12	0.1
OSELTAMIVIR3929508	0.12	0.1
propranololx2	0.12	0.06
pindolol2	0.12	0.05
Isoetarine401	0.11	0.14
Isoetarine402979	0.11	0.14
Isoetarine402980	0.11	0.14
Isoetarine402981	0.11	0.14
Edetic acid (EDTA)	0.1	0.07
Flurbiprofen 1	0.09	0.2
Flurbiprofen 2	0.09	0.2
PHENOL167812	0.09	0.13
Ketoprofen2272	0.09	0.07
Ketoprofen5560	0.09	0.07
METOPROLOL1530717	0.09	0.03
METOPROLOL1530718	0.09	0.03
NANDROLONE		
PHENPROPIONATE3881613	0.08	0.03
Dexfenfluramine 1	0.07	0.2
Dexfenfluramine 2	0.07	0.2
Dexmedetomidine 2	0.07	0.2
AMSACRINE	0.07	0.12
Isotretinoin71789533	0.07	0.12

OXAMNIQUINE570	0.07	0.11
OXAMNIQUINE896836	0.07	0.11
Chlorcyclizine	0.07	0.08
MITOXANTRONE3794794	0.07	0.05
METHOCARBAMOL57340	0.06	0.13
METHOCARBAMOL57341	0.06	0.13
triamcinolone	0.06	0.12
METHYLDOPA125025	0.06	0.08
METHYLDOPA20255	0.06	0.08
<u>Bromfenac</u>	0.06	0.06
NANDROLONE DECANOATE8214619	0.06	0.03
Chlorphenesin	0.05	0.19
phentolamine2	<u>0.05</u>	0.09
Epoprostenol 2	0.05	0.08
<u>Benzphetamine</u>	0.05	0.04
Cyclizine	0.04	0.09
NIFLUMIC ACID125031	0.04	0.04
PAPAVERINE56555	0.04	0.04
NEPAFENAC5162311	0.04	0.03
MASOPROCOL12342	0.03	0.11
Dienestrol 1	0.02	0.09
METYROSINE693	0.02	0.09
cerulenin	0.02	0.08
<u>Bedaquiline</u>	0.02	0.06
Dydrogesterone 1	0.02	0.05
Dydrogesterone 2	0.02	0.05
Dydrogesterone 3	0.02	0.05
Dydrogesterone 4	0.02	0.05
Dydrogesterone 5	0.02	0.05
tolmetin 2	0.02	0.04
EFLORINITHINE	0.01	0.19
eflornithine	0.01	0.19
Diflunisal 1	0.01	0.15
Brimonidine	0.01	0.09
Buclizine	0.01	0.06

Negative control for oxamniqiune

Drugs	GPCR ligand	Ion channel modulator
-------	-------------	-----------------------

sevelamer	-4.51	-4.89
METHIMAZOLE1187543	-4.49	-4.36
acetic acid	-4.11	-4.05
Cysteamine	-4.1	-4.3
Chlorpropamide	-4.08	-4.52
Chlorhexidine	-3.93	-4.08
acetohydroxamic acid	-3.9	-4.99
Hydroxyurea	-3.84	-4.33
Fluticasone propionate	-3.66	-4.22
Halobetasol Propionate	-3.66	-4.22
MAGNESIUM SULFATE6827621	-3.07	-4

Selected drugs using 074

Drugs	GPCR ligand	Protease inhibitor
LISINOPRIL3812863	0.6	0.91
LISINOPRIL9212370	0.6	0.91
Fosphenytoin	0.59	0.54
MARIMASTAT1544157	0.58	1.52
LISINOPRIL71789805	0.58	0.88
Argatroban	0.54	1.05
Zanamivir	0.54	0.71
Peramivir X2	0.53	0.9
Eletriptan	0.52	0.57
NETILMICIN52981502	0.51	0.78
NETILMICIN64622556	0.51	0.78
Boceprevir	0.5	1.41
Saxagliptin	0.49	1.56
saxagliptin 2	0.49	1.56
Argatroban	0.49	0.98
LISDEXAMFETAMINE11680943	0.49	0.61
Efavirenz 1	0.48	0.53
Favirenz 2	0.48	0.53
Aspartame	0.47	0.77
Relenza	0.47	0.55
Ligand (074)	0.46	0.94
Ritonavir 2	0.45	0.92
Fosinopril 1	0.44	1.03
Fosinopril 2	0.44	1.03

Enalapril 2	0.44	0.78
Enalapril 3	0.44	0.78
Enalapril 4	0.44	0.78
Enalapril 5	0.44	0.78
MEROPENEM21984184	0.43	1.41
MEROPENEM29401570	0.43	1.41
MEROPENEM34071989	0.43	1.41
MEROPENEM3808779	0.43	1.41
MEROPENEM4657633	0.43	1.41
MEROPENEM8585152	0.43	1.41
MEROPENEM8602603	0.43	1.41
MEROPENEM8602605	0.43	1.41
Glutathione 1	0.43	1.13
Tirofiban	0.43	0.63
Conjugated Estrogens	0.42	0.62
Estropipate 2	0.42	0.62
Estropipate 3	0.42	0.62
Estropipate 4	0.42	0.62
Estropipate 5	0.42	0.62
Benzylpenicilloyl Polylysine	0.4	0.93
vildagliptin 2	0.4	0.83
LEUCOVORIN15894357	0.4	0.49
LEUCOVORIN15894358	0.4	0.49
LEUCOVORIN15894718	0.4	0.49
LEUCOVORIN15894719	0.4	0.49
MITOTANE3874923	0.39	0.82
L-Arginine1532525	0.39	0.79
spaglumic acid	0.39	0.59
ORLISTAT8101159	0.39	0.51
ORLISTAT8101161	0.39	0.51
ORLISTAT8214635	0.39	0.51

Negative Control for 074

Drugs	GPCR ligand	Protease inhibitor
Sevelamer	-4.51	-3.61
METHIMAZOLE1187543	-4.49	-4.72
acetic acid	-4.11	-3.82
hydrogen carbonate	-4.11	-3.82
LITHIUM6827693	-4.11	-3.82
sodium bicarbnte	-4.11	-3.82
Chlorpropamide	-4.08	-4.02

pyruvic acid	-4.04	-3.23
Fomepizole	-4.01	-4.51

Selected drugs using auranofin

Drugs	GPCR ligand	Enzyme inhibitor
Flurbiprofen 1	0.09	0.28
Flurbiprofen 2	0.09	0.28
Ketoprofen2272	0.09	0.27
Ketoprofen5560	0.09	0.27
Aminoglutethimide	0.09	0.22
PHENOL167812	0.09	0.2
L-CYSTEINE1532673	0.08	0.36
L-CYSTINE1529198	0.08	0.36
L-CYSTINE1532673	0.08	0.36
PAZOPANIB11617039	0.08	0.35
ACITRETIN	0.08	0.32
Dutasteride 1	0.08	0.31
Dutasteride 2	0.08	0.31
Dutasteride 3	0.08	0.31
Dutasteride 4	0.08	0.31
pivmecillinam3x	0.08	0.28
Dasatinib 2	0.08	0.13
Cefepime	0.07	0.39
PANTOPRAZOLE4099200	0.07	0.37
PANTOPRAZOLE4676424	0.07	0.37
PANTOPRAZOLE96337083	0.07	0.37
Ixabepilone3993846	0.07	0.36
Ixabepilone52245489	0.07	0.36
AMOXICILLINE	0.07	0.27
MITOXANTRONE3794794	0.07	0.2
LINEZOLID1622	0.07	0.12
LINEZOLID2008866	0.07	0.12
Amsacrine	0.07	0.1

Famotidine 1	0.06	0.38
Bromfenac	0.06	0.31
Bendroflumethiazide	0.06	0.17
METHOCARBAMOL57340	0.06	0.17
METHOCARBAMOL57341	0.06	0.17
Carbenicillin	0.05	0.3
N-ACETYL-D-GLUCOSAMINE9915679	0.05	0.28
N-ACETYL-D-GLUCOSAMINE9915680	0.05	0.28
Butoconazole	0.05	0.27
Chlorphenesin	0.05	0.14
sulfathiazole 2	0.05	0.1
Carglumic Acid	0.04	0.35
Droxidopa 1	0.04	0.26
Droxidopa 2	0.04	0.26
Droxidopa 3	0.04	0.26
Droxidopa 4	0.04	0.26
Ampicillin sodium	0.04	0.25
Ampicillin sodium	0.04	0.25
NEPAFENAC5162311	0.04	0.24
PAPAVERINE56555	0.04	0.21
Hesperetin 1	0.04	0.16
Hesperetin 2	0.04	0.16
OXICONAZOLE3873295	0.04	0.13
OXICONAZOLE3873296	0.04	0.13
NIFLUMIC ACID125031	0.04	0.11
probucol	0.04	0.11
lutein	0.03	0.28
lutein	0.03	0.28
ticarcillin x3	0.03	0.26
Dactinomycin	0.03	0.19
Ezogabine	0.03	0.18
Chlorambucil	0.03	0.17
NIZATIDINE1530736	0.03	0.17
Ibudilast	0.03	0.13

MASOPROCOL12342	0.03	0.13
vismodegib	0.03	0.11
MIFEPRISTONE27644954	0.02	0.32
MIFEPRISTONE27644962	0.02	0.32
MIFEPRISTONE27644968	0.02	0.32
MIFEPRISTONE27644974	0.02	0.32
MIFEPRISTONE3831128	0.02	0.32
MIFEPRISTONE45789044	0.02	0.32
MIFEPRISTONE45789047	0.02	0.32
LYMECTYCLINE33359852	0.02	0.3
LYMECTYCLINE33359853	0.02	0.3
cefaclor	0.02	0.29
Hetacillin	0.02	0.29
Drospirenone 5	0.02	0.22
Drospirenone 1	0.02	0.22
Drospirenone 2	0.02	0.22
Drospirenone 3	0.02	0.22
Drospirenone 4	0.02	0.22
Drospirenone 6	0.02	0.22
pivampicillin	0.02	0.2
Cyclandelate	0.02	0.16
tolmetin 2	0.02	0.15
Dienestrol 1	0.02	0.13
Azlocillin	0.02	0.12
Azidocillin	0.01	0.4
topotecan 2	0.01	0.39
Glutathione 2	0.01	0.38
Benzylpenicillin	0.01	0.3
Auranofin	0.01	0.28
Bacampicillin	0.01	0.28
becampicilin	0.01	0.28
Carbamazepine	0.01	0.24
Diflunisal 1	0.01	0.22
eflornithine	0.01	0.14

LULICONAZOLE38339093	0.01	0.14
LULICONAZOLE38339095	0.01	0.14
LULICONAZOLE38339097	0.01	0.14
LULICONAZOLE38339099	0.01	0.14
OXYTETRACYCLINE71789632	0	0.36
OXYTETRACYCLINE71789641	0	0.36
Colchicine	0	0.14
sulfamoxole	0	0.14
piperacillin2x	0	0.12
sulfasalazine 2	0	0.1

Negative control for auranofin

Drugs	GPCR ligand	Enzyme inhibitor
Chlorpropamide	-4.08	-4.57
Fomepizole	-4.01	-3.96
acetic acid	-4.11	-3.81
Guanidine 1	-3.44	-3.69
piperazine	-3.59	-3.65
<u>Atracurium</u>	-3.38	-3.63
sevelamer	-4.51	-3.62

Appendix 12: amino acids at the binding sites of the docked and wet lab experimental complexes

4mub-oxa	1gtb-pzq	3qsd-074	3h4k-aur
Pro16	Gln67	Gln94	Site 1
Thr20	Leu100	Ser95	Ser117
His37	Asp101	Arg96	Val155
Met38	Tyr104	Cys97	Thr442
Phe39	Ser107	Cys100	Cys154
Ile42	Arg108	Trp101	Cys159
Asp91		Ala102	Ile160
Leu92		Cys141	Gly158
Leu93		Glu142	
Val127		Leu146	Site 2
Val128		His180	Arg393
Lys139		Ile193	Glu271
Ile140		Cys189	Gly392
Asp144		Phe245	Val391
Leu149		Val247	Ala390
Phe153		Leu252	Ser295
Thr157		Leu267	Val297
Leu236		His270	
Thr237		Ala271	Site 3
Met233		Trp292	Lys506
Leu240		Glu316	Cys520
			Phe505
			Pro507
			Cys574
			Gly541
			Pro542

The amino acids in black colour are all present at the binding site of the docked and experimental complexes; those in red are present at the binding site of the docked complexes while those in blue are present in the experimental complexes.

Appendix 13: Predicted drugs from molecular docking simulations with their binding affinities and previous indications

Praziquantel frontrunners:

DRUGS	Common name	Zinc code	Average affinity (Kcal/mol)	Previous indication(s)	Drug action	T1/2
Ergocalciferol		71618083	-7.100±0.00	Hypocalcemia	binding to a specific receptor in the mucosal cytoplasm of the intestine	19 to 48 hours
Indacaterol	Arcapta Neohale	35801098	-6.825±0.09	asthma and chronic obstructive pulmonary disease	stimulating adrenergic beta-2 receptors	45.5 to 126 hours
Etoposide		72099467	-6.650±0.10	lung cancer, lymphoma, non-lymphocytic leukemia, and glioblastoma multiforme.	Etoposide inhibits DNA topoisomerase II	4-11 hours
Estrone		3881426	-6.600±0.00	management of perimenopausal and postmenopausal symptoms	interact with estrogen receptors	19 hours
Ouabain		8214758	-6.600±0.00	treatment of atrial fibrillation and flutter and heart failure	inhibits the Na-K-ATPase membrane pump	NA
Vilazodone		1542113	-6.550±0.52	treatment of acute episodes of major depression	selective serotonin reuptake inhibitor	25.4h
Dihydrotachysterol		4544044	-6.500±0.00	Used for the prevention and treatment of rickets or osteomalacia, and to manage hypocalcemia associated with hypoparathyroidism or pseudohypoparathyroidism. Also used for the treatment of vitamin D dependent rickets, rickets or osteomalacia secondary to long-term high dose anticonvulsant therapy, early renal osteodystrophy, osteoporosis (in conjunction with calcium), and hypophosphatemia associated with Fanconi syndrome (with treatment of acidosis).	binds to the vitamin D receptor	NA
Ponatinib hydrochloride		36701290	-6.500±0.08	chronic myeloid leukemia	Bcr-Abl tyrosine kinase inhibitor	24 hours
Haloperidol		65742780	-6.475±0.05	Schizophrenia and other psychoses. It is also used in schizoaffective disorder, delusional disorders, ballism, and tourette syndrome (a drug of choice) and occasionally as adjunctive therapy in mental retardation and the chorea of huntington disease. It is a potent antiemetic and is used in the treatment of intractable hiccups. Haloperidol has been used in the prevention and control of severe nausea and vomiting.	not known. the drug appears to depress the CNS at the subcortical level of the brain, midbrain, and brain stem reticular formation	3 weeks
Fexofenadine hydrochloride	Allegra	3872566	-6.450±0.06	management of Seasonal allergic rhinitis	H1-receptor antagonist (antihistamine)	14.4 hours
Ethinyl Estradiol		3977993	-6.375±0.05	For treatment of moderate to severe vasomotor symptoms associated with the menopause, female hypogonadism, prostatic carcinoma-palliative therapy of advanced disease, breast cancer, as an oral contraceptive, and as emergency contraceptive.	binding to the estrogen receptors	36 +/- 13 hours
Praziquantel		655	-6.300±0.00	For the treatment of infections due to all species of schistosoma.	Praziquantel works by causing severe spasms and paralysis of the worms' muscles	0.8-1.5 hours

Values are expressed as mean ± SD and n = 4

Oxamniquine frontrunners:

DRUGS	Common names	Zinc code	Average affinity (Kcal/mol)	Previous indications	Drug action/class	T ½
Amsacrine		11616759	-10.000±0.00	For treatment of acute myeloid leukaemia.	potent intercalating antineoplastic agent, Amsacrine binds to DNA through intercalation and external binding	8-9 hours
Masoprolol		1539579	-9.100±0.00	Used for the treatment of actinic keratoses (precancerous skin growths that can become malignant if left untreated).	Masoprolol is a novel antineoplastic agent, It is not known exactly how masoprolol works	NA
Isotretinoin		71789533	-9.000±0.00	For the treatment of severe recalcitrant nodular acne	Isotretinoin is a retinoid, The exact mechanism of action is unknown, however it is known that it alters DNA transcription.	17-50 hours
Nandrolone phenpropionate		3881613	-8.900±0.00	For the treatment of refractory deficient red cell production anemias, breast carcinoma, hereditary angioedema, antithrombin III deficiency, fibrinogen excess, growth failure and Turner's syndrome. It is also indicated in the prophylaxis of hereditary angioedema.	Nandrolone is an androgen receptor agonist	NA
Ketoprofen		2272	-8.600±0.00	For symptomatic treatment of acute and chronic rheumatoid arthritis, osteoarthritis, ankylosing spondylitis, primary dysmenorrhea and mild to moderate pain associated with musculotendinous trauma (sprains and strains), postoperative (including dental surgery) or postpartum pain.	Ketoprofen is a nonsteroidal anti-inflammatory agent (NSAIA) with analgesic and antipyretic properties	Conventional capsules: 1.1-4 hours Extended release capsules: 5.4 hours
Triamcinolone		3977910	-8.600±0.00	For the treatment of perennial and seasonal allergic rhinitis	Triamcinolone and its derivatives are synthetic glucocorticoids	88 minutes
Diflunisal		21984653	-8.575±0.05	For symptomatic treatment of mild to moderate pain accompanied by inflammation (e.g. musculoskeletal trauma, post-dental extraction, post-episiotomy), osteoarthritis, and rheumatoid arthritis.	Diflunisal is a nonsteroidal drug with analgesic, anti-inflammatory and antipyretic properties	8 to 12 hours
Flurbiprofen		322	-8.400±0.00	Flurbiprofen tablets are indicated for the acute or long-term symptomatic treatment of rheumatoid arthritis, osteoarthritis and anklosing spondylitis. It may also be used to treat pain associated with dysmenorrhea and mild to moderate pain accompanied by inflammation (e.g. bursitis, tendonitis, soft tissue trauma).	Flurbiprofen, a nonsteroidal anti-inflammatory agent (NSAIA) of the propionic acid class	R-flurbiprofen, 4.7 hours; S-flurbiprofen, 5.7 hours
Niflumic acid		125031	-8.400±0.00	Used in the treatment of rheumatoid arthritis.	Niflumic acid, a nonsteroidal anti-inflammatory fenamate, is a Ca^{2+} -activated Cl^- channel blocker.	2.5 hours
Papaverine		56555	-8.375±0.05	For the treatment of impotence and vasospasms.	Papaverine is a nonxanthine phosphodiesterase inhibitor	0.5-2 hours
Dienestrol		1283	-8.300±0.00	For use in the treatment of atrophic vaginitis and kraurosis vulvae	Dienestrol is a synthetic, non-steroidal estrogen	NA
Bromfenac		2570817	-8.175±0.05	For the treatment of postoperative inflammation in patients who have undergone cataract extraction	Bromfenac ophthalmic solution is a sterile, topical, nonsteroidal anti-	NA

					inflammatory drug (NSAID) for ophthalmic use.	
Cyclizine		19156872	-8.175±0.05	For prevention and treatment of nausea, vomiting, and dizziness associated with motion sickness, and vertigo (dizziness caused by other medical problems).	Antihistamine, A histamine H1 antagonist	20 hours
Tolmetin	Tolectin	2191	-8.100±0.00	For the relief of signs and symptoms of rheumatoid arthritis and osteoarthritis, including the treatment of acute flares long-term management. Also for treatment of juvenile rheumatoid arthritis.	Tolmetin is a nonsteroidal anti-inflammatory agent. The mode of action of tolmetin is not known	Biphasic elimination from the plasma consisting of a rapid phase with a half-life of one to 2 hours followed by a slower phase with a half-life of about 5 hours.
Epoprostenol		12495062	-7.900±0.00	For the long-term intravenous treatment of primary pulmonary hypertension and pulmonary hypertension associated with the scleroderma spectrum of disease in NYHA Class III and Class IV patients who do not respond adequately to conventional therapy.	The major pharmacological actions of epoprostenol is ultimately inhibition of platelet aggregation.	6 minutes.
Nepafenac		5162311	-7.900±0.00	For the treatment of pain and inflammation associated with cataract surgery	non-steroidal anti-inflammatory prodrug (NSAID)	NA
Propranolol		22007352	-7.800±0.00	For the prophylaxis of migraine.	nonselective beta-blocker, beta-adrenergic receptor antagonists	4 hours
Buclizine		19364228	-7.775±0.15	For prevention and treatment of nausea, vomiting, and dizziness associated with motion sickness and vertigo (dizziness caused by other medical problems).	antihistamine used as an antivertigo/antiemetic agent	NA
Oxamniquine		570	-7.500±0.00	For treatment of Schistosomiasis caused by Schistosoma mansoni	Oxamniquine is an anthelmintic agent	1-2.5 hours

Values are expressed as mean ± SD and n = 4

Auranofin frontrunners:

DRUGS	Common names	Zinc code	Average affinity (Kcal/mol)	Previous indications	Drug action/class	T ½
Sulfasalazine		13540266	-9.275±0.05	For the treatment of Crohn's disease and rheumatoid arthritis as a second-line agent	anti-inflammatory agent	5-10 hours
Drospirenone		3927200	-9.200±0.20	For the prevention of pregnancy in women who elect an oral contraceptive	bind to the progesterone receptor	30 hours
Diflunisal		20243	-8.600±0.00	For symptomatic treatment of mild to moderate pain accompanied by inflammation (e.g. musculoskeletal trauma, post-dental extraction, post-episiotomy), osteoarthritis, and rheumatoid arthritis.	Diflunisal is a nonsteroidal drug with analgesic, anti-inflammatory and antipyretic properties	8 to 12 hours
Mifepristone		3814382	-8.575±0.05	For the medical termination of intrauterine pregnancy through 49 days' pregnancy. Also indicated to control hyperglycemia secondary to hypercortisolism in adult patients with endogenous	Competitive inhibitor of progesterone at progesterone-receptor sites	18 hours

				Cushing's syndrome who have type 2 diabetes mellitus or glucose intolerance and are not candidates for surgery or have had unsuccessful surgery.		
Oxytetracycline		95616604	-8.300±0.00	Oxytetracycline is indicated for treatment of infections caused by a variety of Gram positive and Gram negative microorganisms including <i>Mycoplasma pneumoniae</i> , <i>Pasteurella pestis</i> , <i>Escherichia coli</i> , <i>Haemophilus influenzae</i> (respiratory infections), and <i>Diplococcus pneumoniae</i> .	Oxytetracycline inhibits cell growth by inhibiting translation. It binds to the 30S ribosomal subunit and prevents the amino-acyl tRNA from binding to the A site of the ribosome.	NA
Topotecan		35572125	-8.300±0.53	For the treatment of advanced ovarian cancer in patients with disease that has recurred or progressed following therapy with platinum-based regimens. Also used as a second-line therapy for treatment-sensitive small cell lung cancer, as well as in combination with cisplatin for the treatment of stage IV-B, recurrent, or persistent cervical cancer not amenable to curative treatment with surgery and/or radiation therapy.	An antineoplastic agent. It works by inhibiting DNA topoisomerases, type I	2-3 hours
Azlocillin		3830262	-8.200±0.00	For the treatment of infections caused by <i>Pseudomonas aeruginosa</i> , <i>Escherichia coli</i> , and <i>Haemophilus influenzae</i> .	By binding to specific penicillin-binding proteins (PBPs) located inside the bacterial cell wall, azlocillin inhibits the third and last stage of bacterial cell wall synthesis.	Mean elimination half-life is 1.3 to 1.5 hours. Longer in neonates, and 2 to 6 hours in patients with renal impairment.
Bacampicillin		36385314	-7.925±0.09	For infections at the following sites: upper and lower respiratory tract; skin and soft tissue; urinary tract and acute uncomplicated gonococcal urethritis, when due to sensitive strains of the following organisms: Gram-positive: streptococci (including <i>S. faecalis</i> and <i>S. pneumoniae</i>) and nonpenicillinase-producing staphylococci; Gram-negative: <i>H. influenzae</i> , <i>N. gonorrhoeae</i> , <i>E. coli</i> , <i>P. mirabilis</i> , <i>Salmonellae</i> and <i>Shigellae</i> .	bacampicillin is hydrolyzed by esterases present in the intestinal wall. It is microbiologically active as ampicillin, and exerts a bactericidal action through the inhibition of the biosynthesis of cell wall mucopeptides.	NA
Piperacillin		3913937	-7.825±0.45	For the treatment of polymicrobial infections	Piperacillin is a penicillin beta-lactam antibiotic. Piperacillin inhibits the third and last stage of bacterial cell wall synthesis	36-72 minutes
Carbamazepine		4785	-7.800±0.00	For the treatment of epilepsy and pain associated with true trigeminal neuralgia.	Carbamazepine inhibits sustained repetitive firing by blocking use-dependent sodium channels.	Initial half-life values range from 25-65 hours, decreasing to 12-17 hours on repeated doses.
Atracurium		96006015	-7.775±0.05	For use, as an adjunct to general anesthesia, to facilitate endotracheal intubation and to provide skeletal muscle relaxation during surgery or mechanical ventilation.	Atracurium antagonizes the neurotransmitter action of acetylcholine by binding competitively with cholinergic receptor sites on the motor end-plate.	20 minutes.
Sulfamoxole		57302	-7.600±0.00	For the treatment of bacterial infection.	Sulfamoxole is a sulfonamide antibiotic	NA
Tolmetin	Tolectin	2191	-7.425±0.25	For the relief of signs and symptoms of rheumatoid arthritis and	Tolmetin is a nonsteroidal anti-	Biphasic

				osteoarthritis, including the treatment of acute flares long-term management. Also for treatment of juvenile rheumatoid arthritis.	inflammatory agent. The mode of action of tolmetin is not known	elimination from the plasma consisting of a rapid phase with a half-life of one to 2 hours followed by a slower phase with a half-life of about 5 hours.
Lymecycline		53682936	-7.425±0.77	For the treatment of infections and to treat acne. It may also be used to treat urinary tract infections, gum disease, and other bacterial infections such as gonorrhea and chlamydia. Lymecycline is also used commonly as a prophylactic treatment for infection by <i>Bacillus anthracis</i> (anthrax). It is also effective against <i>Yersinia pestis</i> and malaria and is also prescribed for the treatment of Lyme disease.	Lymecycline inhibits cell growth by inhibiting translation. It binds to the 30S ribosomal subunit and prevents the amino-acyl tRNA from binding to the A site of the ribosome	NA
Cyclandelate		968262	-7.400±0.00	Used in the treatment of various blood vessel diseases (e.g., claudication, arteriosclerosis and Raynaud's disease) and nighttime leg cramps.	vasodilators	NA
Cefaclor		43693079	-7.400±0.20	For the treatment of certain infections caused by bacteria such as pneumonia and ear, lung, skin, throat, and urinary tract infections.	Cefaclor, like the penicillins, is a beta-lactam antibiotic. By binding to specific penicillin-binding proteins (PBPs) located inside the bacterial cell wall, it inhibits the third and last stage of bacterial cell wall synthesis.	0.6-0.9 hour
Benzylpenicillin		3871699	-7.225±0.05	For use in the treatment of severe infections caused by penicillin G-susceptible microorganisms when rapid and high penicillin levels are required such as in the treatment of septicemia, meningitis, pericarditis, endocarditis and severe pneumonia.	By binding to specific penicillin-binding proteins (PBPs) located inside the bacterial cell wall, penicillin G inhibits the third and last stage of bacterial cell wall synthesis.	0.4-0.9 hours
Pivampicillin		34967244	-7.225±0.15	treatment of respiratory tract infections (including acute bronchitis, acute exacerbations of chronic bronchitis and pneumonia); ear, nose and throat infections; gynecological infections; urinary tract infections (including acute uncomplicated gonococcal urethritis) when caused by non penicillinase-producing susceptible strains of the following organisms: gram-positive organisms, e.g., streptococci, pneumococci and staphylococci; gram-negative organisms, e.g., H. influenzae, N. gonorrhoeae, E. coli, P. mirabilis.	Ampicillin (the active metabolite of pivampicillin) has a bactericidal action resulting from inhibition of cell wall mucopeptide biosynthesis	Approximately 1 hour.
Dienestrol		1283	-7.150±0.06	For use in the treatment of atrophic vaginitis and kraurosis vulvae	Dienestrol is a synthetic, non-steroidal estrogen	NA
Chlorpropamide		1530599	-6.950±0.17	treatment of non-insulin-dependent diabetes mellitus (NIDDM) in conjunction with diet and exercise.	sulfonylurea class of insulin secretagogues, which act by stimulating β cells of the pancreas to release insulin. Sulfonylureas such as chlorpropamide bind to ATP-sensitive potassium channels on the pancreatic cell surface, reducing potassium conductance and causing depolarization	Approximately 36 hours with interindividual variation ranging from 25-60 hours. Duration of effect persists

					of the membrane. Depolarization stimulates calcium ion influx through voltage-sensitive calcium channels, raising intracellular concentrations of calcium ions, which induces the secretion, or exocytosis, of insulin.	for at least 24 hours.
Luliconazole	Luzu	38339097	-6.875±0.43	Luliconazole is indicated in adults aged 18 years and older for the topical treatment of fungal infections caused by <i>Trichophyton rubrum</i> and <i>Epidermophyton floccosum</i> , specifically tinea pedis, cruris, and corporis.	The exact mechanism of action for luliconazole's anti-fungal activity is still not known, but luliconazole is thought to inhibit the enzyme lanosterol demethylase. Lanosterol demethylase is needed for the synthesis of ergosterol, which is a major component of the fungus cell membranes.	The half life of luliconazole has yet to be determined.
Piperazine		38954907	-6.825±0.05	Used as alternative treatment for ascariasis caused by <i>Ascaris lumbricoides</i> (roundworm) and enterobiasis (oxyuriasis) caused by <i>Enterobius vermicularis</i> (pinworm). It is also used to treat partial intestinal obstruction by the common roundworm, a condition primarily occurring in children.	Piperazine is an anthelmintic agent. Piperazine is a GABA receptor agonist.	NA
Azidocillin	Alocillin, Alocin or Azlocillin	8214496	-6.700±0.00	For treatment of infection (Respiratory, GI, UTI and meningitis) due to <i>E. coli</i> , <i>P. mirabilis</i> , <i>enterococci</i> , <i>Shigella</i> , <i>S. typhosa</i> and other <i>Salmonella</i> , nonpenicillinase-producing <i>N. gonorrhoeae</i> , <i>H. influenzae</i> , <i>staphylococci</i> , <i>streptococci</i> including streptoc	By binding to specific penicillin-binding proteins (PBPs) located inside the bacterial cell wall, Azidocillin inhibits the third and last stage of bacterial cell wall synthesis.	NA
Auranofin		4498297	-6.250±0.17	Used in the treatment of active, progressive or destructive forms of inflammatory arthritis, such as adult rheumatoid arthritis	Exactly how auranofin works is not well understood. It may act as an inhibitor of kappaB kinase and thioredoxin reductase which would lead to a decreased immune response and decreased free radical production, respectively	NA

Ligand_074 frontrunners:

DRUGS	Common names	Zinc code	Average affinity (Kcal/mol)	Previous indications	Drug action	Half life (T ½)
Leucovorin		18202555	-9.300±0.00	Treatment of osteosarcoma	Methotrexate Action Pathway	6.2 hours
Vildagliptin		77320042	-9.275±0.05	Reduction of hyperglycemia in type 2 diabetes mellitus	dipeptidyl peptidase-4 (DPP-4) inhibitor	90 minutes
Argatroban		12466745	-9.100±0.00	Treatment of thrombosis	selective thrombin inhibitor	39 and 51 minutes
Saxagliptin		13648755	-8.65±0.058	Treatment of type 2 diabetes mellitus	dipeptidyl peptidase-4 (DPP-4) inhibitor	2.5 hours
Estropipate		3830786	-8.600±0.00			
Fosinopril		4097309	-8.375±0.05	Treatment of mild to moderate hypertension	Angiotensin-converting enzyme (ACE) inhibitor	12 hours
Benzylpenicilloyl polylysine		12503206	-8.350±0.06	For use as a adjunct in assessing the risk of administering penicillin		
Ritonavir	Busvir,	3944422	-8.325±0.17	treatment of HIV-infection	HIV protease inhibitor	3-5 hours

	Empetus, Normune					
Fosphenytoin	Cerebyx, Fosphenytoin Sodium, Fosphenytoin	1530922	-8.300±0.00	treatment of epileptic seizures	block frequency-dependent, use-dependent and voltage-dependent neuronal sodium channels	15 minutes
Meropenem		8602605	-8.300±0.00	complicated skin and skin structure infections, complicated appendicitis and peritonitis	inhibition of cell wall synthesis	Approximately 1 hour in adults and children 2 years of age and older with normal renal function. Approximately 1.5 hours in children 3 months to 2 years of age.
Eletriptan	Apo-eletriptan	3823475	-8.025±0.05	migraine headaches	selective 5-hydroxytryptamine 1B/1D receptor agonist	4 hours
Ligand_074		-----	-8.000±0.00			

Values are expressed as mean ± SD and n = 4

Appendix 14: Values of RMSD and Radius of gyration from molecular dynamics simulation

Dynamics	RMSD (nm)	Radius of gyration (nm)
4mub	0.22567333±0.027855456	1.884123056±0.008682234
4mub-Oxa	0.24073799±0.011671517	1.867897704±0.015445051
4mub-Din	0.239163598±0.037350962	1.871080752±0.009687215
4mub-Dif	0.188255739±0.018454807	1.852820917±0.008693574
4mub-Tol	0.255235308±0.043743036	1.84842529±0.008945636
3h4k	0.310072955±0.059648152	2.87129903±0.015824005
3h4k-Aur	0.251158215±0.034970034	2.80361729±0.014827062
3h4k-Din	0.251550397±0.053459552	2.813948745±0.015664607
3h4k-Dif	0.244618624±0.042449128	2.805216448±0.012106438
3h4k-Tol	0.217006693±0.031973524	2.830938944±0.011074662

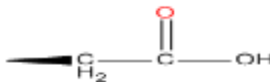
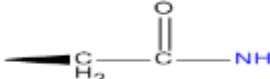
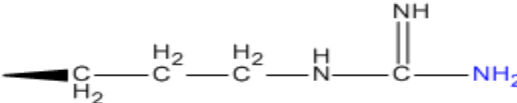
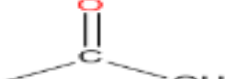
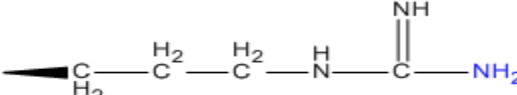
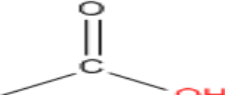
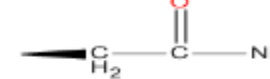
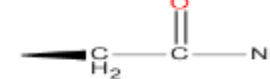
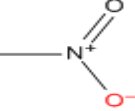
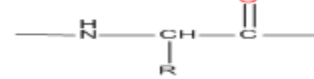
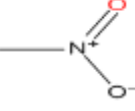
Appendix 15: Values of total energy from the molecular dynamics simulations

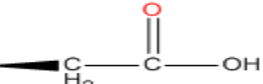
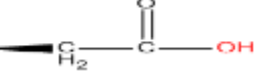
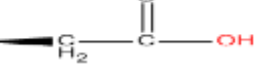
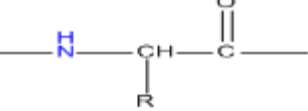
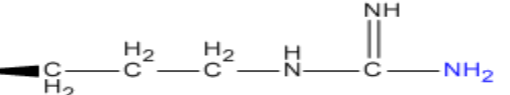
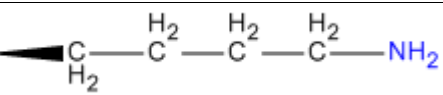
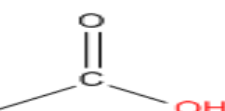
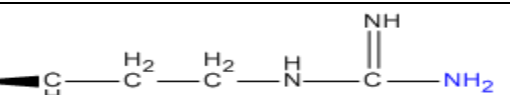
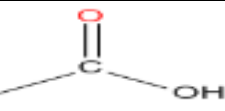
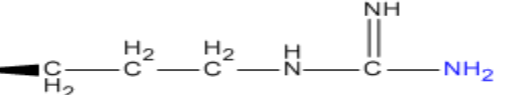
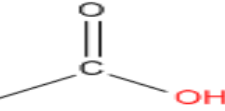
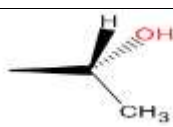
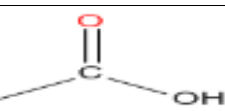
Dynamics	Total energy (KJ/mol)
4mub	-853462±47
4mub-Oxa	-852766±49
4mub-Din	-853204±18
4mub-Dif	-853643±35
4mub-Tol	-853656±23
3h4k	-2.31541 x 10 ⁶ ± 60
3h4k-Aur	-2.31383 x 10 ⁶ ± 68
3h4k-Din	-2.31487 x 10 ⁶ ± 49
3h4k-Dif	-2.317769 x 10 ⁶ ± 96
3h4k-Tol	-2.31628 x 10 ⁶ ± 62

Appendix 16: Changes in the secondary of sulfotransferase and thioredoxin glutathione reductase due to interaction with diflunisal, tolmetin, dinesterol, oxamnique or auranofin.

Secondary structure	Number of conformations (n)					Conformations of different secondary structures (%)				
	3H4K	3H4K-AUR	3H4K-DIF	3H4K-DIN	3H4K-TOL	3H4K	3H4K-AUR	3H4K-DIF	3H4K-DIN	3H4K-TOL
Coil	98681	95698	98103	95448	98964	22.34685	21.67133165	22.215957	21.61471779	22.410935
B-sheet	101884	99191	96671	100876	97230	23.07218	22.46234046	21.8916728	22.84391786	22.018261
B-bridge	7437	7256	7634	6695	7128	1.684149	1.643160593	1.72876075	1.516119097	1.6141743
Bend	47006	44617	46683	49082	46763	10.64476	10.10376188	10.5716188	11.11488537	10.589735
Turn	47845	51884	47895	45852	48626	10.83476	11.74941348	10.8460828	10.38343433	11.011622
Alpha-helix	130531	136323	136892	137199	134082	29.55945	30.87108345	30.9999366	31.06945841	30.363597
5-helix	2930	1301	2813	2395	3430	0.663514	0.294618513	0.63701912	0.542360753	0.7767421
3-helix	5274	5318	4897	4041	5365	1.194326	1.204289972	1.10895224	0.915106389	1.2149334
Total	441588	441588	441588	441588	441588	100	100	100	100	100
Secondary structure										
	4MUB	4MUB-DIF	4MUB-DIN	4MUB-OXA	4MUB-TOL	4MUB	4MUB-DIF	4MUB-DIN	4MUB-OXA	4MUB-TOL
Coil	85370	82509	81226	85881	81880	21.70817	20.98066938	20.6544238	21.83811301	20.820725
B-sheet	24716	27550	27936	27530	25968	6.284869	7.005507779	7.10366117	7.00042211	6.6032314
B-bridge	968	512	480	834	890	0.246146	0.130193103	0.12205603	0.212072359	0.2263122
Bend	45967	46525	37369	45844	40265	11.68865	11.83053537	9.50231652	11.65736837	10.238721
Turn	32336	42733	38216	31538	36301	8.222508	10.8662927	9.71769456	8.019589993	9.2307418
Alpha-helix	200831	184652	200262	192549	202157	51.06799	46.9539391	50.923303	48.96201515	51.40517
5-helix	15	0	0	0	0	0.003814	0	0	0	0
3-helix	3059	8781	7773	9086	5801	0.777853	2.23286257	1.9765449	2.310419008	1.475098
	393262	393262	393262	393262	393262	100	100	100	100	100

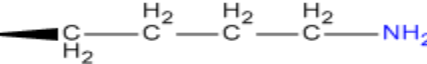
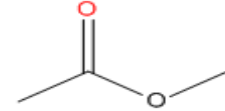
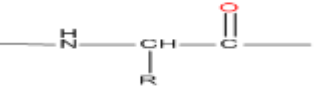
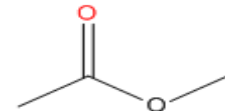
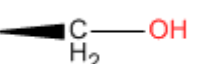
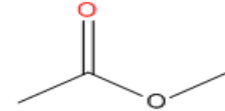
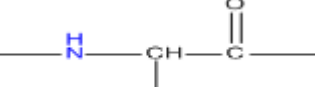
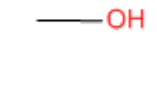
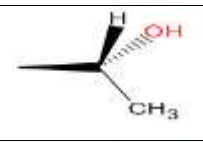
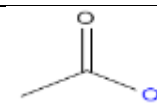
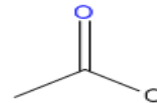
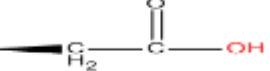
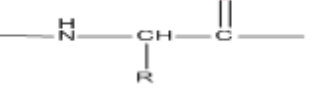
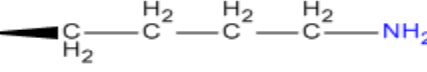
Appendix 17: Average bond distances of atoms in the amino acids and atoms in the functional groups of the ligands that show direct interaction
For Sulfotransferase MD simulations

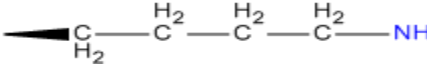
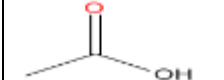
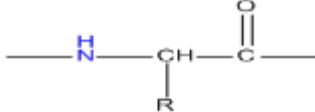
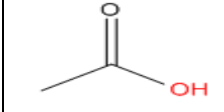
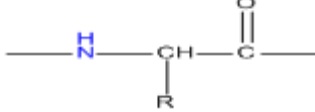
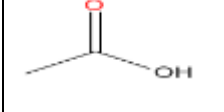
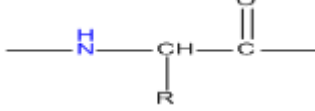
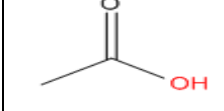
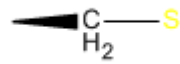
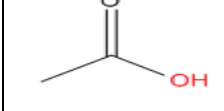
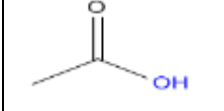
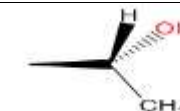
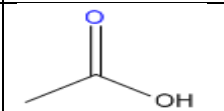
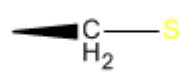
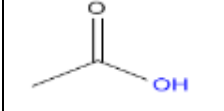
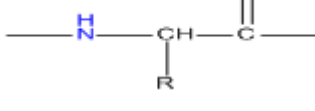
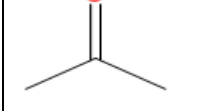
S/N	Bond	Amino acid in target showing atom involved	Ligand showing atom in its functional group involved	Average distance (nm)
1	<i>Asp96 – OD2/H3 – Dif</i>			0.18731±0.01838
2	<i>Asp233 – 2HD2/O1 – Dif</i>			0.24947±0.06941
3	<i>Arg19 – 1HH1/01 – Dif</i>			0.30253±0.07492
4	<i>Arg19 – 1HH1/02 – Dif</i>			0.28327±0.07125
5	<i>Asn233 – OD1/H16 – Oxa</i>			0.88295±0.23768
6	<i>Asn46 – OD1/O1 – Oxa</i>			0.60919±0.23570
7	<i>Leu261 – O/O2 – Oxa</i>			0.55794±0.17814

8	<i>Asp96 – OD2/1H18 – Din</i>			0.20057±0.04480
9	<i>Asp96 – OD1/1H18 – Din</i>			0.25229±0.06319
10	<i>Asp149 – OD1/1H13 – Din</i>			0.73031±0.51959
11	<i>Arg19 – H/02 – Din</i>			0.21943±0.03613
12	<i>Asn233 – 2HD2/01 – Din</i>			0.91001±0.33660
13	<i>Lys23 – HZ3/03 – Tol</i>			0.60262±0.20359
14	<i>Asn233 – 2HD2/02 – Tol</i>			0.37958±0.13050
15	<i>Asn233 – 2HD2/03 – Tol</i>			0.32398±0.12512
16	<i>Thr242 – HG1/02 – Tol</i>			1.13370±0.21481

For TGR MD simulations at site 1

S/N	Bond	Amino acid in target showing atom involved	Ligand showing atom in its functional group involved	Average distance (nm)
1	<i>Thr442 – H/03 – Aur</i>			0.34047 ± 0.05116
2	<i>Thr442 – H/02 – Aur</i>			0.25692 ± 0.03183
3	<i>Thr442 – HG1/01 – Aur</i>			0.19507 ± 0.06680
4	<i>Asp433 – OD1/05 – Aur</i>			0.35516 ± 0.03804
5	<i>Asp433 – OD2/1H11 – Aur</i>			0.14282 ± 0.04108
6	<i>Asp393 – HE/07 – Aur</i>			0.46682 ± 0.10186
7	<i>Glu259 – OE1/07 – Aur</i>			0.53811 ± 0.11288

8	<i>Lys162 – HZ3/09 – Aur</i>			0.84169±0.11564
9	<i>Cys154 – O/09 – Aur</i>			0.36686±0.06666
10	<i>Ser117 – HG/05 – Aur</i>			0.29143±0.15205
11	<i>Thr442 – H/03 – Dif</i>			0.26296±0.02694
12	<i>Thr442 – HG1/01 – Dif</i>			0.17971±0.01544
13	<i>Thr442 – HG1/02 – Dif</i>			0.37573±0.01889
14	<i>Asp433 – OD1/H7 – Dif</i>			0.69924±0.10775
15	<i>Asp440 – O/H7 – Dif</i>			0.17470±0.01612
16	<i>Lys162 – HZ1/02 – Dif</i>			0.32319±0.07403

17	<i>Lys162 – HZ2/02 – Dif</i>			0.32952±0.07229
18	<i>Cys154 – H/01 – Dif</i>			0.50844±0.08129
19	<i>Cys159 – H/02 – Dif</i>			0.25719±0.05321
20	<i>Cys159 – H/01 – Dif</i>			0.22928±0.03400
21	<i>Cys159 – HG/01 – Dif</i>			0.15324±0.02388
22	<i>Thr442 – HG1/02 – Tol</i>			0.27751±0.10311
23	<i>Thr442 – HG1/03 – Tol</i>			0.29483±0.10783
24	<i>Cys154 – HG/02 – Tol</i>			0.21473±0.11935
25	<i>Cys159 – H/01 – Tol</i>			0.73609±0.08929

26	<i>Cys159 – HG/03 – Tol</i>			0.28618±0.14979
27	<i>Thr472 – H/02 – Tol</i>			1.03080±0.08237

For TGR MD simulations at site 2

S/N	Bond	Amino acid in target showing atom involved	Ligand showing atom in its functional group involved	Average distance (nm)
1	<i>Trp510 – HE1/05 – Aur</i>			0.37562±0.09109
2	<i>Asn543 – 1HD2/09 – Aur</i>			0.41969±0.14932
3	<i>Asn543 – 2HD2/07 – Aur</i>			0.522496±0.2496
4	<i>Trp510 – HE1/02 – Dif</i>			0.97646±0.45204
5	<i>Asn543 – 2HD2/01 – Tol</i>			0.66390±0.27469

6	<i>Gln167 – 1HE2/02 – Tol</i>			0.37909±0.17151
7	<i>Gln167 – 1HE2/03 – Tol</i>			0.39824±0.17203
8	<i>Gln167 – 2HE2/02 – Tol</i>			0.46585±0.12970
9	<i>His173 – ND1/1H18 – Din</i>			0.34062±0.12007

For TGR MD simulations at site 3

S/N	Bond	Amino acid in target showing atom involved	Ligand showing atom in its functional group involved	Average distance (nm)
1	<i>Gln440 – H/09 – Aur</i>			0.19398±0.02337
2	<i>Gln440 – O/09 – Aur</i>			0.40506±0.04623
3	<i>Gly323 – 0/05 – Aur</i>			0.39696±0.06859

4	<i>Arg322 – O/01 – Aur</i>			0.37049±0.07636
5	<i>Ser485 – HG/05 – Aur</i>			0.38092±0.17160
6	<i>His538 – HE2/02 – Dif</i>			0.20095±0.02103
7	<i>Gly483 – H/03 – Dif</i>			0.50160±0.08474
8	<i>Gly483 – O/03 – Dif</i>			0.36876±0.05899
9	<i>Tyr479 – HH/01 – Dif</i>			0.18199±0.02668
10	<i>Asp325 – H/01 – Dif</i>			0.20808±0.02870
11	<i>His538 – HE2/03 – Tol</i>			0.19364±0.04288
12	<i>Gly483 – H/01 – Tol</i>			0.34633±0.12968

13	<i>Tyr479 – HH/02 – Tol</i>			0.38192±0.14672
14	<i>Val469 – H/01 – Tol</i>			0.27000±0.08805
15	<i>Asp325 – H/02 – Tol</i>			0.27904±0.07934
16	<i>Tyr335 – HH/02 – Din</i>			0.21841±0.07857
17	<i>Tyr296 – HH/02 – Din</i>			0.40766±0.11964

Appendix 18: Minimum distance of the drugs/frontrunners at different sites from FAD in 3H4K

Ligand	Distance of drugs from FAD in 3H4K (nm)		
	Site 1	Site 2	Site 3
Diflunisal	0.262635637±0.026679713	0.878458632±0.13916269	0.309250959±0.051893171
Tolmetin	0.277765448±0.039159189	1.013907354±0.120468755	0.682402586±0.089205585
Dinesterol	-	0.823746273±0.059932426	0.612924764±0.077599116
Auranofin	0.296712621±0.022190109	1.086288683±0.095942723	0.740392647±0.049087458

Appendix 19: Different conformations of 4mub from the molecular dynamics simulation and their percentages

Conforma tions	Number of conformations					Conformations (%)					
	4mub-Dif	4mub-Din	4mub	4mub-Tol	4mub- Oxa	4mub	4mub-Dif	4mub-Din	4mub-Oxa	4mub-Tol	
1	201	171	221	231	324	14.72352	13.39107262	11.39240506	21.58560959	15.38974017	
2	199	162	185	210	233	12.32512	13.25782811	10.7928048	15.52298468	13.99067288	
3	198	158	177	178	120	11.79214	13.19120586	10.52631579	7.99467022	11.85876083	
4	182	146	169	147	116	11.25916	12.12524983	9.726848767	7.728181213	9.793471019	
5	128	136	166	139	98	11.05929	8.527648235	9.060626249	6.52898068	9.260493005	
6	109	127	147	121	94	9.793471	7.26182545	8.461025983	6.262491672	8.061292472	
7	103	105	96	97	85	6.395736	6.862091939	6.995336442	5.662891406	6.462358428	
8	77	93	92	95	74	6.129247	5.129913391	6.19586942	4.930046636	6.329113924	
9	67	66	74	76	74	4.930047	4.463690873	4.397068621	4.930046636	5.063291139	
10	59	64	39	62	52	2.598268	3.930712858	4.263824117	3.464357095	4.130579614	
11	55	61	33	37	41	2.198534	3.664223851	4.063957362	2.731512325	2.465023318	
12	42	51	30	32	40	1.998668	2.798134577	3.397734843	2.664890073	2.131912059	
13	17	42	18	27	34	1.199201	1.132578281	2.798134577	2.265156562	1.798800799	
14	15	30	15	13	34	0.999334	0.999333777	1.998667555	2.265156562	0.866089274	
15	14	20	9	10	25	0.5996	0.932711526	1.332445037	1.665556296	0.666222518	
16	9	16	8	8	21	0.532978	0.599600266	1.065956029	1.399067288	0.532978015	
17	9	10	8	8	8	0.532978	0.599600266	0.666222518	0.532978015	0.532978015	
18	8	9	6	3	8	0.399734	0.532978015	0.599600266	0.532978015	0.199866755	
19	4	8	5	3	6	0.333111	0.266489007	0.532978015	0.399733511	0.199866755	
20	2	8	2	2	6	0.133245	0.133244504	0.532978015	0.399733511	0.133244504	
21	1	6	1	1	3	0.066622	0.066622252	0.399733511	0.199866755	0.066622252	
22	1	6		1	3		0.066622252	0.399733511	0.199866755	0.066622252	
23	1	4			2		0.066622252	0.266489007	0.133244504		
24		1						0.066622252			
25		1						0.066622252			

Sulfotransferase = 4MUB, OXA=oxamniquine, DIF=diflunisal, DIN=dinesterol and TOL=tolmetin.

Conformations	Number of conformations					Conformations (%)				
	3h4k-Aur	3h4k-Dif	3h4k-Din	3h4k	3h4k-Tol	3h4k	3h4k-Aur	3h4k-Dif	3h4k-Din	3h4k-Tol
1	89	60	69	56	76	7.456724368	11.85086551	7.989347537	9.187749667	10.1198402
2	82	59	54	52	62	6.924101198	10.91877497	7.856191744	7.190412783	8.25565912
3	59	56	53	47	58	6.258322237	7.856191744	7.456724368	7.057256991	7.72303595
4	54	54	52	43	48	5.725699068	7.190412783	7.190412783	6.924101198	6.39147803
5	54	50	50	40	44	5.326231691	7.190412783	6.657789614	6.657789614	5.85885486
6	48	49	48	40	43	5.326231691	6.391478029	6.524633822	6.391478029	5.72569907
7	42	49	44	39	43	5.193075899	5.592543276	6.524633822	5.85885486	5.72569907
8	40	48	43	39	42	5.193075899	5.326231691	6.391478029	5.725699068	5.59254328
9	39	44	43	39	41	5.193075899	5.193075899	5.85885486	5.725699068	5.45938748
10	37	43	43	38	39	5.059920107	4.926764314	5.725699068	5.725699068	5.1930759
11	35	37	41	33	37	4.394141145	4.66045273	4.926764314	5.459387483	4.92676431
12	32	31	40	32	27	4.260985353	4.260985353	4.127829561	5.326231691	3.59520639
13	30	31	27	31	26	4.127829561	3.994673768	4.127829561	3.595206391	3.4620506
14	19	24	20	30	25	3.994673768	2.529960053	3.195739015	2.663115846	3.32889481
15	14	24	17	28	24	3.728362184	1.864181092	3.195739015	2.263648469	3.19573901
16	14	16	17	20	23	2.663115846	1.864181092	2.130492676	2.263648469	3.06258322
17	12	13	16	19	18	2.529960053	1.597869507	1.7310253	2.130492676	2.39680426
18	10	11	15	19	15	2.529960053	1.331557923	1.464713715	1.997336884	1.99733688
19	8	10	14	18	12	2.396804261	1.065246338	1.331557923	1.864181092	1.59786951
20	7	9	12	13	10	1.7310253	0.932090546	1.19840213	1.597869507	1.33155792
21	6	8	10	12	8	1.597869507	0.798934754	1.065246338	1.331557923	1.06524634
22	6	6	7	11	7	1.464713715	0.798934754	0.798934754	0.932090546	0.93209055
23	5	5	6	8	6	1.065246338	0.665778961	0.665778961	0.798934754	0.79893475
24	3	5	3	8	5	1.065246338	0.399467377	0.665778961	0.399467377	0.66577896
25	3	4	2	7	4	0.932090546	0.399467377	0.532623169	0.266311585	0.53262317
26	2	2	1	7	4	0.932090546	0.266311585	0.266311585	0.133155792	0.53262317
27	1	1	1	6	1	0.798934754	0.133155792	0.133155792	0.133155792	0.13315579
28		1	1	4	1	0.532623169		0.133155792	0.133155792	0.13315579
29		1	1	3	1	0.399467377		0.133155792	0.133155792	0.13315579
30			1	3	1	0.399467377			0.133155792	0.13315579
31				2		0.266311585				
32				1		0.133155792				

33				1	0.133155792						
34				1	0.133155792						
35				1	0.133155792						

Thioredoxin glutathione reductase = 3H4K, AUR = auranofin, DIF=diflunisal, DIN=dinesterol and TOL=tolmetin.

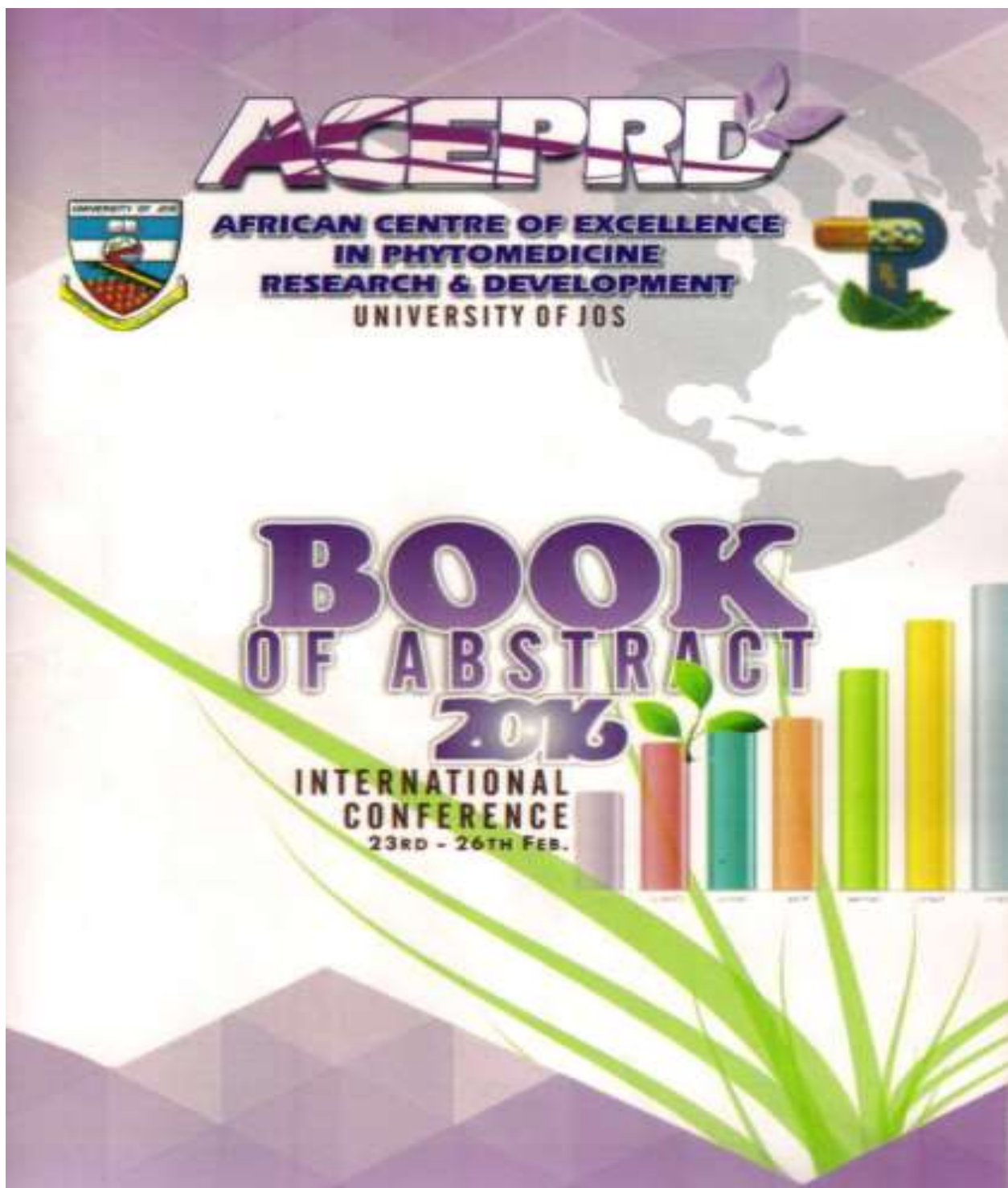
Appendix 20: Total, hydrophobic and hydrophilic accessible surface areas of 3H4K and 4MUB

Values for solvent accessible surface area calculation

Target or Target-frontrunner complex	Hydrophilic accessible surface (nm ²)	Hydrophobic accessible surface (nm ²)	Total accessible surface (nm ²)
4mub	71.95081166±1.314368932	83.74015803± 2.09126331	155.6909594±2.823638481
4mub-Oxa	70.89769247±2.172445148	82.17316949±1.959970172	153.0708594±3.698991307
4mub-Dif	71.73558787±1.319236236	79.85262725±1.959934988	151.5882105±2.689989291
4mub-Tol	70.06734157±1.508216267	81.6858465± 1.760783587	151.7531825±2.740386664
4mub-Din	72.58319014±1.437324906	81.40643571±1.828564124	153.9896143±2.579547967
3h4k	155.8128429±2.507322069	174.0488216±2.828379236	329.8616711±4.134430189
3h4k-Aur	151.4665007±2.335868929	173.7398469±2.415466188	325.2063555±4.004359029
3h4k-Dif	154.5404714±2.04309458	174.1266445±2.700768529	328.6671265±3.473374117
3h4k-Tol	154.2637643±1.843225507	172.6833928±2.110733263	326.9471691±3.01408356
3h4k-Din	153.5093755±1.918508337	175.7238349±2.390654816	329.233229±3.352458199

Sulfotransferase = 4MUB, thioredoxin glutathione reductase = 3H4K, AUR = auranofin, OXA=oxamniquine, DIF=diflunisal, DIN=dinesterol and TOL=tolmetin.

Appendix 21: Accepted/presented conference/workshop papers from the dissertation



Repurposing and Discovery of Multi-Targets Drugs For Schistosomiasis

by

Ezebuiro, Fortunatus C., and Uzochukwu, Ikemefuna, C.

*Department of Pharmaceutical and Medicinal Chemistry, Faculty of Pharmaceutical Science,
Nnamdi Azikiwe University, Awka, Nigeria*

Abstract

Schistosomiasis is a neglected disease that remains a considerable public health problem in tropical and subtropical regions. It is the most important human helminth infection in terms of morbidity and mortality and is a growing concern worldwide. Currently, treatment is based on the use of praziquantel (PZQ). However, observations from field and laboratory investigations indicate that emergence of PZQ resistance could become a serious problem. The aim of the research is to repurpose existing clinical drugs for the treatment of schistosomiasis and to elucidate their mechanism of action and synergism with PZQ and/or oxamniquine. Approved clinical drugs were selected by querying of our in-house database of approved clinical drugs using four different probes and correlation graphing techniques. The 3-D coordinates of the selected clinical drugs (1-12) including their isomers and derivatives were obtained from ZINC[®] database while four schistosome targets (PDB codes 1GTR, 3H4K, 3QSD and 4MUB) were obtained from RCSB Protein Data Bank[®]. They were prepared for docking simulation using MGLTools-1.5.6[®] and UCSF Chimera 1.9[®]. In order to validate the docking simulation protocols, the wet experimental ligand bound schistosome protein targets were reproduced *in silico*. Molecular docking simulations were performed using AutoDockVina[®] on a Linux Platform. The binding affinities were calculated and reported as mean \pm SD and docked poses were visualized with PyMol-1.4.2[®]. Three approved drugs showed higher and multi-target binding affinities than PZQ and oxamniquine for the schistosome targets suggesting that they may produce better pharmacological response. *In viv* investigations in *Drosophila melanogaster*, molecular dynamics simulations and clinical trial investigations of the multi-targeting frontrunners are recommended.

Keywords: Schistosomiasis, drug repurposing, molecular docking, praziquantel

Gmail

Compose Mail Back to Inbox Archive Report Spam Delete More Actions... Newer 15 of about 88 Older Expand all Print New window

Inbox (80) Go

Starred Sent Mail Drafts (79) All Mail Spam Bin Contacts Labels Edit labels

18th ICID - Unmoderated ePoster acceptance notification [Inbox](#)

Doris Steinbach <Doris.Steinbach@isid.org>
To: Fortunatus Ezebuo <ezebuofc@gmail.com>

[Reply](#) | [Reply to all](#) | [Forward](#) | [Print](#) | [Delete](#) | [Show original](#)

Your preliminary abstract number: 1868

Dear Fortunatus Ezebuo,

On behalf of the Scientific Committee I am pleased to inform you that your abstract
'Biomolecular Simulations of Selected Approved Drugs with Four Schistosomal Drug Targets'
was accepted for **Unmoderated ePOSTER presentation** at the '18th International Congress on Infectious Diseases/XVIII Congreso SADI' which will be held in Buenos Aires, March 1 to 5, 2018.

Please be advised of the following guidelines:

Biomolecular Simulations of Selected Approved Drugs with Four Schistosomal Drug Targets

Fortunatus C. Ezebuo^{*1,2} and Ikemefuna C. Uzochukwu¹

¹Drug Design and Informatics Group, Faculty of Pharmaceutical Sciences, Nnamdi Azikiwe University, PMB 5025 Awka 420281, Anambra State, Nigeria

²Department of Biochemistry, Faculty of Natural Sciences, Chukwuemeka Odumegwu Ojukwu University, P.M.B 02 Uli 431124, Anambra State, Nigeria

(* ezebuofc@gmail.com)

Abstract: Schistosomiasis is a neglected disease of considerable health importance in tropical and subtropical regions. It is the most important human helminth infection in terms of morbidity and mortality and is a growing concern worldwide. Currently, treatment is based on the use of praziquantel (PZQ), but long-term use results in decreased efficiency and serious concerns regarding onset of resistance. *In vitro* and animal studies have demonstrated resistance to PZQ and low cure rate has been reported elsewhere. Given the wide clinical use of PZQ, drug-resistant parasites of clinical concern may evolve. Other drugs are available, but they are more expensive, less effective, show unacceptable side effects and/or effective only on one schistosome species. Therefore, it is imperative to identify alternative drugs to ensure that PZQ resistance does not become a major health concern. Drug repurposing can provide new therapeutic options for a vast number of diseases where current therapies are failing or are inadequate. The study investigated the binding energies of selected approved drugs for four schistosomal proteins using molecular docking and dynamics simulations. Approved drugs were selected by querying an in-house database of approved drugs using four probes and correlation graphing techniques. The 3-D coordinates of the selected drugs (612) were obtained from ZINC® database while four schistosomal proteins were obtained from RCSB Protein Data Bank. They were prepared for docking simulations using MGLTools-1.5.6 and UCSF Chimera 1.9. In order to validate the docking protocols, the experimental complex were reproduced *in silico*. Molecular docking simulations were performed using AutoDockvina® while molecular dynamics simulations were performed with GROMACS-4.5.5. The binding energies were calculated using g_MMPBSA. The binding energies were reported as mean \pm SD. Two approved drugs formed better stable complexes, showed higher and concurrent binding energies than auranofin and oxamniquine for two schistosomal proteins suggesting possible better pharmacological response. Their binding energies ranged from -168.6387 ± 7.772 KJ/mol to -338.6141 ± 16.3780 KJ/mol. *In vitro* and clinical trial investigations into the anti-schistosomal activities of the drugs are recommended.

Keywords: Schistosomiasis, molecular dynamics, binding energies, Drug repurposing

DrosAfrica-ICGEB Workshop

Drosophila melanogaster in Biomedical Research: Low-Cost and Profitable.
University of Ibadan, Ibadan, Nigeria, 17 - 28 July, 2017



Effects of potential anti-schistosomiasis drugs on the longevity and survival rates of *Drosophila melanogaster*

Peregrina C Ekaebor^{1,2*} and Isacchukwu C Uchechukwu²

¹Drug Design and Informatics Group, Faculty of Pharmaceutical Sciences, Nnamdi Azikiwe University, PMB 5025 Awka 460001, Anambra State, Nigeria

²Department of Biochemistry, Faculty of Natural Sciences, Chukwuemeka Odumegwu Ojukwu University, PMB 03 138, 431138, Anambra State, Nigeria

*E-mail: cukaedebor@yahoo.com

Abstract: Schistosomiasis is a neglected disease of considerable public health importance in tropical and subtropical regions. Current treatment is based on the use of praziquantel (PZQ). However, in vitro and animal studies have demonstrated resistance to PZQ and this could become a serious problem. Some approved drugs have been predicted as potential anti-schistosomiasis drugs using computational approaches in our laboratory. The present study evaluated the effects of four potential anti-schistosomiasis drugs on the longevity and survival rates of *D. melanogaster*. Determination of conversion of the targets between drosophila and schistosomes was achieved with Python. Thirty *D. melanogaster* (Hartmann strain) of 1 to 3 days old were separated according to their sex. The flies were maintained at 25 °C and 12 h dark/light cycle. The flies were treated with different doses of each drug. The longevity and survival rates were expressed as percentages of live flies. The results showed that substituted glutathione *S*-transferase, and sulfamethoxine are not converted in *D. melanogaster* while human liver alkaline phosphatase and diaminodiphenylamine are converted in *D. melanogaster*. It was observed that praziquantel, oxytropacycline, and bupropion reduced the survival rate of male and female *D. melanogaster* up to 50 % after 9 and 13 days of exposure respectively. Also, male flies showed lower survival and longevity compared to females in the presence of the drugs. Oxytropacycline enhanced survival rate and longevity of male and female flies. From the 16th day of treatment survival rate of male flies was reduced by 50%. The female flies were not affected similarly. Liver function tests can be carried out with the fly. Praziquantel, oxytropacycline, bupropion or világaptol may be successfully used for treatment within one week.

Keywords: Schistosomiasis, substituted targets, *Drosophila melanogaster*, anti-schistosomiasis drugs, Longevity, survival rate.

Introduction

Schistosomiasis is a neglected disease of considerable public health importance in tropical and subtropical regions. It is the most important human helminth infection in terms of morbidity and mortality and is a growing concern worldwide. Currently, treatment is based on the use of praziquantel (PZQ), but long-term use of PZQ results in decreased efficiency and serious side-effects including resistance to PZQ. Other drugs are available, but they are either less effective, discontinued or affect specific life stages of the parasite species (Fleming et al., 2006; Danchin et al., 2008; Pruzanski et al., 2011). Therefore, it is imperative to identify alternative drugs to ensure that PZQ resistance does not become a major health concern since there are no schistosome drug candidates under human clinical trials (Tunney-Moss and Miltzow, 2010). Some approved drugs have been predicted as potential anti-schistosomiasis drugs using computational approaches in our previous investigation. *Drosophila melanogaster* can be used as a non-animal model for preclinical testing. It has been used for primary screens and secondary validation of biologically active compounds for therapeutic efficacy of a wide range of human diseases (Handy and Blundell, 2001; Pralling et al., 2011; Rappoport and Grigoriev, 2009; Rainey and Brady, 2010; Shattuck, 2011). The present study evaluated the longevity and survival rates of *D. melanogaster* in four potential anti-schistosomiasis drugs.

Methods

Determination of conversion

Human liver alkaline phosphatase and four substituted drug targets were obtained from protein data bank. Determination of conversion of the targets in drosophila was achieved with Python.

Drosophila melanogaster stock and culture

Drosophila melanogaster (Oregon strain) was gift from Dr. A.O. Abdej, Dosephile Laboratory, Molecular Drug Metabolism and Toxicology, Department of Pharmaceutical Sciences, College of Medicine, University of Ibadan, Ibadan, Nigeria. The flies were maintained and cultured on cornmeal medium at 25 °C, and 12 h dark/light cycle.

Preparation of doses of tested drugs

Different doses of PZQ (0.0 – 0.6 mg), oxytropacycline (0.0 – 0.5 mg), bupropion (0.0 – 0.002 mg) and világaptol (0.0 – 0.016 mg) were prepared from different stock solutions and incorporated into 0.005 kg fly food.

Drug exposure and percentage survival and longevity analyses

Twenty (20) males per gender of 1 to 3 days old were separated according to their sex and exposed to the drugs and maintained on 0.005 kg food treated with different doses of praziquantel, oxytropacycline, bupropion or világaptol at 25 °C, and 12 h dark/light cycle. The food was changed every 2 days. The longevity and survival rates were expressed as percentage of live flies and plotted with GraphPad-5.0 and SigmaPlot 11.0.



Figure 1: Human liver alkaline phosphatase and various substituted targets are converted in *D. melanogaster* (A) and (B) while substituted glutathione *S*-transferase and sulfamethoxine are not converted (C) and (D).

Conversion: Male *D. melanogaster* showed lower survival rate and longevity compared to females in praziquantel, oxytropacycline, bupropion or világaptol. Liver function tests can be carried out with the fly and the drugs may be successfully used for treatment of schistosomiasis within one week.

References

- Abdej, A.O., Ekaebor, P.C. and Kachon, J.P. (2013). *Drosophila melanogaster* as a Promising Model Organism in Toxicological Studies. *Arch. Bio. App. Med.* 1:33 – 40.
- Tunney-Moss, S. and Miltzow, F. (2010). Schistosomiasis Therapeutic: What is the pipeline? *Expert Review of Clinical Pharmacology*, 9(2), 181-180. DOI: 10.1586/ERCP.2010.102001

Results
Substituted glutathione *S*-transferase, and sulfamethoxine are not converted in *D. melanogaster* while human liver alkaline phosphatase and diaminodiphenylamine are converted in *D. melanogaster* (Figure 1). Male flies showed lower survival and longevity compared to females in the presence of the drugs. Praziquantel and bupropion reduced the survival rate of male and female *D. melanogaster* up to 50 % after 9 and 13 days of exposure which was not observed after 6 and 6 days respectively, oxytropacycline enhanced the survival rate of male and female flies (Figure 2).

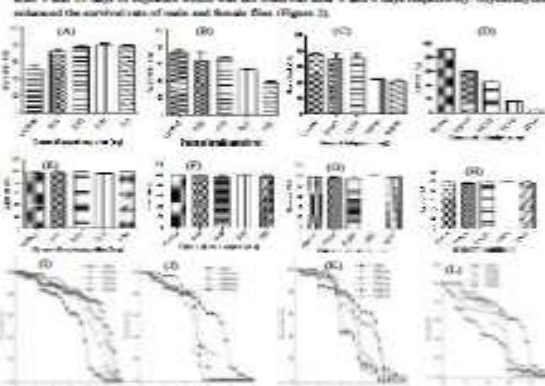


Figure 2: Survival rate of *D. melanogaster* in presence of different doses of PZQ (0.0 – 0.6 mg), oxytropacycline (0.0 – 0.5 mg), bupropion (0.0 – 0.002 mg) and világaptol (0.0 – 0.016 mg) (A to D). Longevity of *D. melanogaster* in the doses of oxytropacycline, PZQ, bupropion and világaptol are shown in (C) to (D) respectively.

Appendix 22: Efforts to obtain schistosome

Search Images Maps Play YouTube Gmail Drive Calendar More [More](#)

You are currently viewing Gmail in basic HTML. [Switch to standard view](#) | [Set basic HTML as default view](#)

ezebuofc@gmail.com | My Account | Settings | Help | Sign out

Gmail bel Search Mail Search the Web [Show search results](#) [Compose a message](#)

[Compose Mail](#) [Inbox \(11\)](#) [Starred](#) [Sent Mail](#) [Drafts \(90\)](#) [All Mail](#) [Spam \(2\)](#) [Bin](#) [Contacts](#) [Labels](#) [Subscribes](#)

[Back to Search results](#) More Actions... Go [Newest 7 of 10 Older](#)

LETTER OF ASSISTANCE/REQUEST

Ezebuo Fortunatus
McGugan, Glen (NIH/NIAID) [E] <gmcgugan@niaid.nih.gov>
To: Ezebuo Fortunatus <ezebuofc@gmail.com>
Cc: Margaret Mentink-Kane <mmentinkkane@afbr-bri.com>
[Body](#) [Replies \(1\)](#) [Forward](#) [Print](#) [Delete](#) [Show original](#)

Hi,

Thank you for your interest in the Schistosomiasis Research Reagent Resource Center that is funded by the NIAID. In order to request material, please follow the instructions at the following site:

<http://www.afbr-bri.com/schistosomiasis/>

You will be directed to fill out appropriate forms and request reagents through the web at BEI Resources (<http://www.beiresources.org/Catalog.aspx?pr=schistosomiasis>).

Should you have any questions, you may contact the Schistosomiasis Resource Center directly via Dr. Margaret Mentink-Kane (copied on this message).

Thanks,

Glen.

Glen C. McGugan, Jr., Ph.D. Program Officer
 National Institute of Allergy and Infectious Diseases
Parasitology and International Programs Branch
Division of Microbiology and Infectious Diseases
5601 Fishers Lane, Room 8A26
Rockville, MD 20852

From: Ezebuo Fortunatus <ezebuofc@gmail.com>
Date: Sunday, July 10, 2016 at 1:28 PM
To: "McGugan, Glen (NIH/NIAID) [E]" <gmcgugan@niaid.nih.gov>
Subject: LETTER OF ASSISTANCE/REQUEST
[- Show quoted text -](#)

[Reply](#) | [Reply to all](#) | [Forward](#) | [Print](#) | [Delete](#) | [Show original](#)

Margaret Mentink-Kane <mmentinkkane@afbr-bri.com>
To: "McGugan, Glen (NIH/NIAID) [E]" <gmcgugan@niaid.nih.gov>, Ezebuo Fortunatus <ezebuofc@gmail.com>
[Reply](#) | [Reply to all](#) | [Forward](#) | [Print](#) | [Delete](#) | [Show original](#)

11 July 2016 at 19:38

Thank you Glen,

We can try and help Dr Fortunatus obtain naive and pre-patent snails,

Margaret

BRI
BIOMEDICAL RESEARCH INSTITUTE

Margaret Mentink-Kane, PhD
Manager
Schistosomiasis Resource Center

9410 Key West Avenue
Rockville, MD 20850
Mobile 703-786-9262
mmentinkkane@afbr-bri.com

RE: Level 2 Registration Application Token:00008700326 [Inbox](#)

 Contact@BEIResources.org<Contact@beiresources.org>
To: Ezebui Fortunatus <ezebuofc@gmail.com>
[Reply](#) | [Reply to all](#) | [Forward](#) | [Print](#) | [Delete](#) | [Show original](#)

08 November 2016 at 17:15

Good Morning Dr. Ezebui,

Thank you for your interest in registering with BEI Resources.

We have received and are currently processing your application for Level 2 registration with BEI. During the course of the initial review, we noticed a matter that will delay the processing of your application.

On the Material Transfer Agreement (MTA), Dr. Ikemefuna Chijioke Uzochukwu signed as the "Duly Authorized Signatory for Recipient". The individual who signs this place needs to have the authority to legally bind their organization such as a: president, vice-president, dean, or provost. In other words, they need to be able to enter into a legal contract on behalf of the organization. Based upon our experiences with other registrants, other people who have this authority can be found in the Grants and Contracts office, Intellectual Properties, Tech Transfer or their equivalent within your organization.

If Dr. Ikemefuna Chijioke Uzochukwu has legal authority to bind your organization (Nnamdi Azikiwe University); then we will need a statement (an email will suffice), preferably from Dr. Ikemefuna Chijioke Uzochukwu attesting to having authority in this matter. At which point we can proceed with the processing your MTA and application for registration.

Now if it turns out that the MTA has been signed in this manner in error, then we will need a new MTA. For your convenience, I have attached a blank copy of the MTA to this email if you should have need for it. In this instance, please complete and have the proper individual sign for your organization.

The MTA can be emailed as a PDF to: Contact@beiresources.org or faxed to 1-703-365-2898.

Additionally, regarding the Biosafety Cabinet certification schedule, please let us know if it is certified annually, biannually, etc.

As soon as we have this document, we will be able to proceed with the processing of your application. We apologize for any inconvenience that this may cause you. Please let us know if you have any questions, or if we can be of further service.

Best Regards,